Human-Structure Interaction in Cantilever Grandstands

by

Jackie H H Sim

A thesis submitted for the degree of

Doctor of Philosophy

at the University of Oxford

Hilary Term 2006

ABSTRACT

Human-Structure Interaction in Cantilever Grandstands

A degree submitted for the degree of Doctor of Philosophy

Jackie Sim
Balliol College, Oxford
Hilary Term 2006

There is a risk that excessive vibration in long span cantilever grandstands can be triggered by the spectators synchronising their jumps to the music played. If the jumping frequency excites a resonance of the grandstand, large force could be generated. This thesis studies human-structure interaction in cantilever grandstands, with emphasis on modelling the passive and jumping crowds, and analysing the response of a single degree-of-freedom (SDOF) structural system.

Preliminary work on analysing a cantilever occupied by seated humans shows that it is acceptable to use a SDOF structural system for analysis which meant emphasis of later work could be placed on understanding the interaction between a passive crowd and the structure.

Human dynamic models from published biomechanics studies are used to develop a passive crowd model. A transfer function, fitted to the crowd apparent mass, is used to define the crowd model. It is found that the passive crowd can be approximated well by using a single 2DOF system. The combined passive crowd-structure system is modelled as a feedback system and a parametric study is conducted. It is found that the passive crowd adds significant mass and damping to the structure and these effects vary with the natural frequency of the structure.

Records of forces of people jumping to a beat are used to develop a probabilistic model of crowd jumping loads. Key parameters are introduced to characterise the timing and shape of the jumping impulses. An analytical function is used to approximate the impulse shape. All parameters are characterised with probability distribution functions.

Using the fitted probability distribution functions, the Monte Carlo method is used to simulate individual jumping load-time histories and to obtain the structural responses due to group jumping loads. The variations of the structural response with the natural frequency of the empty structure and the size of the active crowd are presented in charts. As expected, the worst response is found on structures with natural frequencies coinciding with the first three harmonics of the crowd jumping loads. For structures occupied by passive crowds, a significant reduction in the structural response is found at resonance excited by the second and third harmonics, due to high levels of damping provided by the passive crowds. On variation of the structural response with the crowd size, it is found that the structural response becomes asymptotic for groups larger than 16 people.

Experimental individual jumping and bobbing tests are conducted at six distinct beat frequencies to look at the variations of the impulse shape and degree of synchronisation with the beat frequency. The bobbing action is found to have a higher inherent variability between individuals compared to jumping. Jumping tests involving two people facing each other are also conducted. The results show that there is a better synchronisation when two people are jumping together compared to when jumping alone.

Acknowledgements

I would like to express my gratitude to my supervisors, Dr. Martin Williams and Dr. Anthony Blakeborough. I would like to thank them for their guidance and support. It has been a very rewarding experience to work under their supervision during my three years at Oxford.

My special thanks go to Mr. Graham Parkhouse for kindly providing the experimental data used in this thesis.

Thanks to the IStructE/ODPM/DCMS Working Group on the Dynamic Performance and Design of Stadia Structures and Seating Decks for giving me the opportunities to present my work at the group's meetings and for their valuable feedback.

Many thanks to Mr. Clive Baker for his assistance in the laboratory and to my officemates: Giang, Thanasis, Hong Rui, Felipe, Anthony, Paul, Lam and John, thank you for taking part in the experimental jumping and bobbing tests.

To my friends in Oxford, Bin, Hui, Alexi, Emily, Hsueh Ling, Alex, Jonathan, Wei Jian, Elly and Yi Ting, thank you for your friendship, care and support.

To the Oxford University Press, thank you for the Clarendon Fund Bursary provided towards supporting my study.

Lastly, I am very grateful to my parents and my sister for their support and encouragements.

TABLE OF CONTENTS

Chapter 1

1. Introduction

1.1. The Problem

Problematic levels of vibration are being reported in several stadiums around the world, especially during pop concerts and football matches, due to excitations by rhythmic crowd motions such as clapping, foot stamping, bobbing or jumping. A few examples are given here. Firstly, the Maracana football stadium in Brazil (Batista and Magluta 1993), with a capacity of 150,000 people, is a reinforced concrete structure with a cantilever stand 21 m long. The natural frequencies of the cantilever stand when empty were 4.6, 6.6 and 17.0 Hz. It was reported that high levels of acceleration and large displacements could be felt during football games. Cracks were found in the cantilever beams, most probably due to large displacements and hence over-stressing of the structure.

Another example, the Feyenoord Stadium in the Netherlands (van Staalduinen and Courage 1994), with a capacity of 61,000 people, had also experienced strong vibrations during pop concerts. The grandstand had natural frequencies of 2.3, 4.6 and 5.8 Hz. Strong vibrations were reported on the upper tier during pop concerts. To reduce the vibration level, the displacement of the stand was monitored during pop concerts and the audio system was turned down when there was excessive vibration.

The Morumbi Stadium in Brazil (Almeida and Rodrigues 1998), with a capacity of 80,000, had a few modes ranging from 2.2 to 4.0 Hz. Complaints were received

from the crowds on the vibration of the structure. Tuned mass dampers were fitted to the stadium to reduce the vibration level (GERB Vibration Control Systems 2005).

In the UK, excessive movements have been reported on several modern football stadiums during pop concerts or football matches, including Manchester United's Old Trafford Stadium (Rogers 2000), Arsenal's Highbury Stadium (Rogers 2000), Liverpool's Anfield Stadium (Rogers and Thompson, 2000) and The Millennium Stadium in Cardiff (Otlet 2004). To rectify the problem in the Old Trafford Stadium, the local authority restricted the use of the problematic tier to football match usage while for the Highbury Stadium, tuned mass dampers were fitted. Steel columns were fitted to the Anfield Stadium to raise its natural frequency while a series of temporary supports were installed at The Millennium Stadium prior to a pop concert.

All the stadiums mentioned above have large cantilever spans with natural frequencies that fall within the frequency range of human-induced loadings. In addition, they are often subjected to rhythmic human-induced loadings, especially in pop concerts in which the crowds synchronise their movements with the music played. The high flexibility of the cantilever tiers and the rhythmic crowd motion produce resonant or near-resonant dynamic behaviour which may lead to excessive vibration. This may cause human discomfort, crowd panic or at the extreme, a possible collapse of the structure.

1.2. Current approach to the problem

To tackle this problem, existing codes and guidelines, including National Building Code of Canada (1990), BS 6399 (British Standards Institution 1996) and Guide to Safety at Sports Grounds (Department of National Heritage and Scottish Office 1997) specify that a dynamic analysis should be performed for stadiums with natural frequencies below certain threshold values. However, none of these codes and guidelines provides the tools that would allow a designer to analyse the performance expected of these structures.

1.3. Human-structure interaction

Generally, the crowds on a cantilever grandstand can be classified into active and passive crowds. An active crowd moves rhythmically by jumping, bobbing or swaying, usually following a musical beat or crowd chanting. A passive crowd remains stationary by either sitting or standing on the structure. A dynamic analysis of the cantilever grandstand involves the study of how each of these two crowds interacts with the structure. The active crowd is known to exert external dynamic loads on the structure by their rhythmic motions. For the passive crowd, modal tests on several stadiums have shown that it behaves as a dynamic system added to the main structural system.

The dynamic analysis of a cantilever grandstand consists of four main tasks:

(a) Modelling the passive crowd.

(b) Defining the dynamic load induced by the active crowd.

(c) Analysing the passive crowd-structure system subjected to the dynamic load.

(d) Assessing the resultant vibration level prediction for serviceability criteria.

Current knowledge and practice are deficient in all four main areas mentioned above. Therefore, no sensible analysis has yet been conducted on a cantilever grandstand to estimate its dynamic response when subjected to a crowd rhythmic motion.

1.4. Aims of this thesis

This thesis addresses the first three areas that are identified as deficient above. For the passive crowd, the aim is to develop a simple dynamic model to represent the crowd as a system added to the main structural system. A frequency response analysis is then conducted on the joint crowd-structure system to investigate how the dynamic properties of the occupied structure are different from when the structure is empty. For the active crowd, the action of jumping, which is the most severe form of crowd-induced loading, is the subject of research in this thesis. In addition, an initial investigation on the action of bobbing is conducted. Once the passive and active crowds are defined, a dynamic analysis is conducted to calculate the response of a structure occupied by both active and passive crowds. The outcome of this thesis gives an indication on the vibration levels to be expected on cantilever grandstands when occupied by various ratios of active to passive crowds.

1.5. Thesis outline

The outline of this thesis is as follows. Firstly, a literature review is presented in Chapter 2 to discuss the nature of the vibration problem on cantilever grandstands and to review current progress in tackling the problem. The remainder of the thesis is divided into three parts: Parts I and II deal with modelling the passive and active crowds respectively. Part III deals with simulating the crowd jumping loads and calculating the resultant responses on a passive crowd-structure system.

Part I: Chapter 3 looks at the dynamics of a cantilever beam occupied by passive humans and subjected to dynamic loads. Chapter 4 investigates the effect of a passive crowd on the dynamic characteristics of a single degree-of-freedom (SDOF) structural system. The results are presented in charts which enable engineers to estimate the amount of reduction in natural frequency and structural response for an occupied structure.

Part II: Chapter 5 deals with statistical modelling of individual jumping loads which are obtained from experimental tests.

Part III: Chapter 6 deals with simulating the crowd jumping loads and calculating the resultant responses on a passive crowd-SDOF system. The results are presented in charts to allow engineers to estimate the structural responses due to various ratios of active to passive crowds. Chapter 7 reports on some experimental tests involving two subjects jumping together and a single subject bobbing.

Lastly, in Chapter 8, conclusions are drawn from Parts I, II and III.

Chapter 2

2. Literature review

In this chapter, the first two sections (2.1 and 2.2) serve to provide some background while the rest of this chapter reviews two main areas which are the focus of this thesis: modelling the passive and active crowds.

Firstly, in section 2.1, the problematic mode of vibration encountered on cantilever grandstands is identified. Then the findings from several onsite measurements of stadiums are reviewed in order to give a better understanding on the nature of the problem. This is followed by a review on the recommendations provided by existing codes and guidelines (section 2.2). The deficiencies in these codes and guidelines are identified. The rest of this chapter reviews current research work on modelling the passive (section 2.3) and active (section 2.4) crowds. For the active crowd, emphasis is placed on modelling the jumping load but a very brief review on bobbing load (section 2.5) is included. In the last section, some concluding remarks are presented, mainly to identify areas that require further research.

2.1. Vibration problem on grandstands

2.1.1. Vertical mode of vibration

In order to determine the dynamic performance of a grandstand when subjected to human-induced loads, the designer needs to identify the low-frequency modes of the proposed structure. Often, it is possible for a number of global and local modes to be excited and these modes can be classified into three directions: vertical, front-to-

back and side-to-side (Reid et al. 1997). For a grandstand with multiple tiers, the cantilever sections in the tiers above the ground level (shown by the circled section in Fig. 2.1) are most vulnerable to vibration in the vertical direction, especially for long span tiers. This thesis is concerned with this local vertical mode of vibration.

2.1.2. Onsite monitoring

Several onsite measurements have been conducted on stadiums during pop concerts and sports events. There are two main emphases in these works, one is to monitor the response of the grandstands when subjected to crowd rhythmic motions and the other is to investigate the dynamic properties of the grandstands when occupied by passive crowds.

Littler (1998, 1999) measured the performance of stadiums in the UK during pop concerts. Altogether, the responses of five large cantilever grandstands with natural frequencies between 4.64 Hz and 7.3 Hz when empty were measured. The spectators in all four concerts were quite diverse. In one concert, all the spectators consisted of 16 to 25 years olds among which two-thirds were male. At the start of each song, a large proportion of the spectators jumped to the music for 20 to 30 seconds. Another concert by an artist who has been popular for 30 years had a wide age range. Most of the spectators were standing and clapping and there was no widespread jumping. In all concerts, the motions were perceptible and several people remarked about the movements but none complained. The peak accelerations recorded were between 0.48 and 1.62 m/s^2. The frequency response spectra showed that there were significant responses due to excitations by the first three harmonics of the crowd-induced loads.

On the other hand, several modal tests and experimental studies showed that structures have different dynamic characteristics when empty compared to when occupied by passive spectators. Modal test conducted on the Twickenham Stadium (Ellis and Ji 1997), which had a natural frequency of 7.32 Hz when empty, found that there were two modes at 5.41 Hz and 7.91 Hz when occupied. Other modal tests on three cantilever grandstands (Littler 1998, 1999) showed that the natural frequencies of the empty grandstands ranged from 4 to 6 Hz and a reduction of between 0.3 Hz and 0.5 Hz was observed on all grandstands when occupied by spectators. For the Bradford Stadium which had modes between 3.28 Hz to 5.75 Hz, modal tests conducted during 20 football matches and 9 rugby matches (Reynolds et al. 2004) showed that there was a reduction in the natural frequencies when the stand was occupied by seated or standing spectators. A slightly greater reduction was observed when the spectators were standing than when seated, illustrating the effect of crowd configuration. An increase in the damping ratio was also reported. Experimental tests conducted on a SDOF platform occupied by a standing person (Harrison and Wright 2004) showed that there was a reduction in the natural frequency and an increase in the damping. However, a vibration test on an 18.68 Hz beam (Ellis and Ji 1997) showed that there was an increase in the natural frequency when a person was seated or standing on the beam while no change was recorded when the person was jumping or walking on the beam.

2.1.3. Modelling of stadiums

Several works on the computer modelling of grandstands with emphasis on the dynamic behaviour have been conducted. In particular, a comparative study on the use of 2D and 3D FE models (Mandal and Ji 2004) found that a 2D model was

sufficient to examine the behaviour of a grandstand in the vertical direction. However, the presence of non-structural elements might have a significant influence on the modal properties and it is difficult to model them accurately. Discrepancies between the calculated and measured modal properties were found for a grandstand in a football stadium (Reynolds and Pavic 2002) due to additional stiffness provided by the joints between the main structural members. Another example is the City of Manchester Stadium (Reynolds et al. 2005) in which the perimeter concrete blockwork wall was found to have a significant influence on the natural frequencies of the structure.

2.2. UK codes and guidelines

Three codes and guidelines are relevant for engineers designing a stadium in the UK and they are reviewed below.

In BS 6399: Part 1 (British Standards Institution 1996), it is stated that for an empty structure with a vertical frequency less than 8.4 Hz and a horizontal frequency less than 4 Hz, a dynamic analysis is required to assess its ability to withstand the dynamic loadings in the vertical and two orthogonal horizontal directions. The vertical threshold frequency is obtained by considering up to the third harmonic of the crowd motion which has an upper frequency limit of 2.8 Hz. Guidance on individual jumping load is given in Annex A.

The 'Green Guide' (Department of National Heritage and Scottish Office 1997) adopts the same strategy of recommending a dynamic analysis for a grandstand but

with natural frequencies of less than 6 Hz vertically and 3 Hz horizontally when the structure is occupied by spectators.

In 2001, an interim guidance was published (IStructE/ODPM/DCMS Working Group 2001) due to growing concern on the dynamic performance of modern grandstands when used for pop concerts. The interim guidance recommends different natural frequency thresholds for permanent grandstands based on the degree of synchronisation of the crowd activities on the grandstands. For grandstands used solely for viewing events with no external stimulus to coordinate the crowd movement, a natural frequency threshold of 3 Hz is recommended. For grandstands used for pop concerts with the crowds coordinating their movements to the music played, a natural frequency threshold of 6 Hz is recommended. An advisory note was published subsequently (IStructE/ODPM/DCMS Working Group 2003) to address issues related to the determination of the structure's natural frequencies. It highlights the need to consider the effect of the non-structural elements. The working group is currently preparing a final guide on designing stadiums subjected to different crowd activities.

2.3. Passive crowd modelling

This section reviews the work on passive crowd modelling in the areas of civil engineering and biomechanics.

2.3.1. Civil engineering

In civil engineering, passive human occupants were known to contribute a significant amount of damping to floor systems. It was commented that human occupants provided excellent damping, with the floor damping increasing by 300 % due to the presence of four people on a steel joist-concrete slab floor (Lenzen 1966). Free vibration tests on nailed wood-joist floors with human occupants seated and lying on the floor found that the occupant's physique influenced the damping capacity provided to the floor (Polensek 1975). Heel impact and shaker impact tests conducted on a composite concrete slab and an open web steel joist floor found that the heel impact test gave higher damping than the shaker impact test due to damping provided by the person (Rainer and Pernica 1981). In the same study, it was also noted that damping increased with the modal amplitude at the location of the person.

Early efforts to model a single standing occupant using a lumped parameter model can be found in the dynamic analysis of floor response by Foschi and Gupta (1987) and Folz and Foschi (1991). The former used a SDOF system while the latter used both 2DOF and 11DOF systems. Later developments included the use of an undamped continuous model (Ji 1995) and a SDOF system (Zheng and Brownjohn 2001) to represent a standing person.

In modelling cantilever grandstands, the need is to model a group of people rather than single individuals. It is possible to represent each individual in the group using a lumped parameter model but the resultant crowd model will have too many degrees of freedom. Ellis and Ji (1997) proposed using an undamped SDOF system to represent the passive crowd on a grandstand. However, it is more desirable to include damping in the model considering the high damping capacity of the human body. Sachse et al. (2002) conducted experimental tests involving a 15000 kg beam occupied by 5 seated occupants. A SDOF system was used to model the occupants and its modal properties were obtained by curve-fitting the measured FRFs. In Sachse's tests, the total mass of the human occupants was only 5% of the mass of the structure. Hence the influence of the human occupants on the measured FRFs might be very small and it might be affected by noise in the measurements.

The ISO 5982 (International Organization of Standardisation 1981) uses 2DOF lumped parameter models to represent a seated and standing human but according to Fairley and Griffin (1984) these models were derived from studies of heavy people.

2.3.2. Biomechanics

A passive crowd on a grandstand undergoes whole-body vibration due to the motion of the structure. The interest is on the external effect of the whole-body vibration on the dynamic properties of the structure. Mathematically, the interaction between the two systems, the passive crowd and the structure, can be quantified in terms of the force transmitted across the interface. Many research studies have been undertaken in the area of biomechanics to model this behaviour of a single seated person. The purpose is to assess the comfort and health criteria for human bodies

when subjected to vehicular vibration. The common approach is to seat the test subject on a vibrating platform and measure the driving-point frequency response functions such as mechanical impedance and apparent mass. This section reviews various models which may be appropriate for modelling the passive crowd on a cantilever grandstand.

Many studies have been conducted on modelling the seated human body using lumped parameter models of varying complexity, ranging from SDOF to higher order systems. These studies include Coermann (1962), Suggs et al. (1969) and Donati and Bonthoux (1983) who developed respectively a SDOF system, two uncoupled SDOF systems and a 2DOF system. A very comprehensive study was conducted by Fairley and Griffin (1989) and Wei and Griffin (1998). The former conducted vibration tests for sixty seated subjects and the latter fitted the measured data with four models as shown in Fig. 2.2. Each model is similar to those previously developed by other researchers in terms of the number of degrees of freedom involved: Model 1a is similar to Coermann's model (1962); Model 1b is similar to Fairley and Griffin's model (1989); Model 2a is similar to Donati and Bonthoux's model (1983) and Model 2d is similar to Suggs et al.'s model (1969) but with no rigid mass. It was found that Model 2b which consisted of two SDOF systems arranged in parallel gave the best fit to the measured apparent mass data. This agreed with the test observation that there were two modes of vibration noted in the apparent mass data, at approximately 5 and 10 Hz. Linear biomechanics models with higher degrees of freedom and nonlinear models were developed by researchers such as Mertens (1978) and Boileau and Rakheja (1998) but these are too complicated for use in the modelling of cantilever grandstands.

For standing humans, a similar research approach has been adopted but considerably less research has been undertaken. In particular, a series of tests was conducted for twelve male subjects and the measured data were curve-fitted with SDOF and 2DOF systems (Matsumoto and Griffin 1998, 2003), as shown in Fig. 2.3. It was found that Models 2a and 2c gave the best fit.

2.4. Jumping load modelling

This section reviews the development of a load model defining the crowd jumping in a pop concert in a stadium. There are several important stages in this development: direct measurement of small groups, statistical analysis to simulate large groups and onsite measurement of grandstands during pop concerts. Firstly, some terminology is introduced using an idealised jumping load-time history. Then the various stages are reviewed. Several relevant issues such as crowd effect, flexibility of the structure, group jumping frequency range and impulse shape are also reviewed.

2.4.1. Terminology

An idealised jumping load-time history consists of successive impulses separated by period of zero loads when the person is in the air (see Fig. 2.4). The common practice (Bachmann and Ammann 1987, Ellis and Ji 1997) is to model each impulse using a half-sine function:

$$F(t)=\begin{cases} k_p G \sin(\pi t / t_p) & 0 \le t \le t_p \\ 0 & t_p \le t \le T_p \end{cases} \tag{2.1}$$

where G = static weight of the person

k_p = F_{max}/G = impact factor

F_{max} = peak dynamic load

t_p = contact duration

T_p = beat period

The contact ratio, α, is defined by:

$$\alpha = \frac{t_p}{T_p} \leq 1 \tag{2.2}$$

From the Law of Conservation of Momentum, the impulse of each jump equals to the weight of the person times the beat period:

$$\int_0^{t_p} k_p G \sin\left(\frac{\pi t}{t_p}\right) dt = G T_p \tag{2.3}$$

Thus the impact factor can be evaluated:

$$k_p = \frac{\pi}{2\alpha} \tag{2.4}$$

Eqn. 2.4 shows that the maximum load is inversely proportional to the contact duration.

The idealised jumping load-time history is periodic. It can also be represented using a Fourier series:

$$F(t) = G\left[1.0 + \sum_{n=1}^{\infty} r_n \sin\left(\frac{2n\pi}{T_p} t + \phi_n\right)\right] \tag{2.5}$$

where r_n is the n^{th} harmonic Fourier coefficient, also called the Dynamic Load Factor (DLF) when normalised by G, and ϕ_n is the n^{th} harmonic phase lag.

2.4.2. Direct measurement

Early studies on crowd jumping load involve direct measurements of the loads using a rigid force plate in a laboratory (Allen et al. 1985, Rainer et al. 1988, and Pernica 1990). The results were analysed in the frequency domain and presented as DLFs which were given by the amplitudes of the frequency spectra at the excitation frequency and its integer multiples. It was found that for increasing group sizes, there was a reduction in the DLFs and the amount of reduction increased for higher harmonics (Allen et al. 1985, Rainer et al. 1988). The increase in reduction for higher harmonics suggested that there was a lack of synchronisation between each individual when jumping together. For tests conducted at 1 to 4 Hz, higher DLFs were recorded for 2 to 3 Hz which showed that people were most synchronised when jumping within this frequency range (Pernica 1990). One drawback for these direct measurements is that they were conducted in laboratories using force platforms. There is a limitation to the size of the force platforms and hence the number of subjects that can be involved.

2.4.3. Monte Carlo simulation

Further developments involve a combination of direct measurement and Monte Carlo simulation, as adopted by Ebrahimpour and Sack (1989), Willford (2001), Ellis and Ji (2004), Parkhouse and Ewins (2004) and Kasperski and Agu (2005). The general approach is to collect data for a small group of people, introduce certain parameters to quantify the main characteristics and use the Monte Carlo method of sampling from some fitted probability distributions to generate the loads for a large crowd.

In order to take into account the lack of synchronisation between each individual, a phase lag, ψ_n, was introduced to the Fourier series in Eqn. 2.5 to represent the jumping load such that:

$$F(t) = G\left[1.0 + \sum_{n=1}^{\infty} r_n \sin\left(\frac{2n\pi}{T_p}t + \phi_n + \psi_n\right)\right] \tag{2.6}$$

So far, a few attempts have been made to model the phase lag. Ebrahimpour and Sack (1989) measured the loads due to individuals jumping alone and in groups of 2 and 4 at 2 Hz on a rigid platform. Taking the measured individual load as the basic model, the phase lag for each individual when jumping in a group was back calculated. An exponential distribution function was fitted to the calculated phase lag. Ji and Ellis (1993) assumed that the phase lag followed a Normal distribution and assigned arbitrary values to the standard deviation of the Normal distribution which represented different degrees of synchronisation. Wilford (2001) also used a Normal distribution but set the standard deviation to 0.14 times the beat period.

All three pieces of works (Ebrahimpour and Sack 1989, Ji and Ellis 1993 and Wilford 2001) assumed a constant phase lag for each load-time record without considering the slight time difference between each jump. Therefore, each simulated individual load was treated as perfectly periodic. In reality, each jump is slightly different in timing and shape. Ebrahimpour and Sack (1989) vaguely mentioned the use of two random error parameters following the Normal distribution, presumably to take into account the slight variation between each jump.

To take into account the slight variation between each jump, Ellis and Ji (2004) and Kasperski and Agu (2005) modelled the timing of each impulse. Ellis and Ji (2004) modelled the jumping frequency and contact ratio of each impulse using statistical models, followed by simulation of the group jumping loads. DLFs for groups of up to 8192 people were calculated. Kasperski and Agu (2005) analysed the loads of more than 70 individuals on a rigid force platform. They modelled the jumping frequency and Fourier coefficients of each impulse using statistical models, followed by simulation of the group jumping loads. Some early results were presented for groups of up to 50 people.

Parkhouse and Ewins (2004) adopted a more direct approach of adding up the individual load-time histories and obtaining the DLFs of the resultant load. They conducted an extensive experimental programme to measure the loads of 100 individuals jumping alone on a rigid force platform. Individual loads were sampled from the experimental data and summed in the time domain to give the crowd jumping loads. The DLFs were presented for groups of 5, 10 and 100 people. This approach is simple and straightforward but lacks statistical justification. It is uncertain whether the measurements provide a good sample for simulations of larger groups.

2.4.4. Crowd effect

One other aspect in modelling the crowd jumping load is the crowd effect due to synchronisation with the movements of neighbouring jumpers. This is important because most of the simulated crowd jumping loads mentioned above were based on individual jumping test results. An experimental work was conducted by

Ebrahimpour and Fitts (1996) to measure the coherency between two people jumping together at 1.5 to 3 Hz. They concluded that there was a better synchronisation when the two jumpers were facing each other than when facing opposite to each other. The best synchronisation was observed at 2 Hz.

2.4.5. Flexibility of structure

Another aspect that needs to be considered is the flexibility of the platform. Cantilever grandstands which are prone to excessive vibrations have very high flexibility whereas the studies on jumping loads mentioned so far have been conducted on rigid force platforms. So far, studies on flexible platforms include direct measurement using a purposed built flexible platform (Yao et al. 2003) and onsite measurement of the response of real structures and back calculating the crowd jumping load (Pernica 1983, Allen 1990, Karsperski and Niemann, Ellis and Littler 2004).

Yao et al. (2003) conducted individual jumping tests for subjects jumping at 1 to 3.5 Hz on a SDOF flexible platform with natural frequencies from 2 to 6 Hz. It was found that the frequency of the first spectral peak was a lot higher or lower than the metronome beat frequency when the natural frequency of the platform coincided with the metronome beat frequency, i.e. it was not possible for subjects to jump at the natural frequency of the platform.

Pernica (1983) measured the response of a stadium during a 3-hour pop concert in which the spectators were seated, clapping and foot stamping to the music performed. The stand had natural frequencies of less than 3 Hz. From the

measurements, an acceleration of up to 0.3*g* and a peak-to-peak displacement of 12 mm were recorded, due to excitation of the natural frequencies by the rhythmic actions of the spectators. From the measured acceleration levels, the crowd jumping load was back calculated and expressed as the equivalent static live load, giving a value of 3 kN/m^2. This is lower than the 4.8 kN/m^2 value required by BS 6399: Part 1 (British Standards Institution 1996), maybe due to the crowd not jumping but clapping and foot stamping.

Allen (1990) measured the floor acceleration during an aerobic class. The DLFs were back calculated from the measured acceleration based on the floor structural configuration. The group size varied from 10 to 25 people, jumping at a frequency range of 2.25 to 3.03 Hz. For jumping, setting $r_1 = 1.5$, the DLFs for the second and third harmonics were found to be: $r_2 = 0.3 \sim 0.80$ and $r_3 = 0.06 \sim 0.15$. The test subjects can be considered as well-trained in their movements and therefore, the DLF values obtained can be deemed as the worst case.

Kasperski and Niemann (2003) conducted jumping tests on a stand of a football stadium with a natural frequency of 2.45 Hz. Tests involved groups of 5 to 70 people jumping in time with loud music with a distinct rhythm. The coordination factors for various group sizes were calculated from the ratio of the measured maximum response due to a group loading to the measured maximum response due to 5 people jumping together. The results showed that for small groups, the load attenuation was small. For larger groups (more than 30 people), the attenuation increased as the group size increased. For the largest group considered which consisted of 70 people, an attenuation of about 50% was observed.

In Ellis and Littler (2004), the response of a stadium during a pop concert with the crowd bobbing to the music played was measured. The advantage of this approach is that the loads are generated by a real crowd in a real concert. However, it is often expensive to conduct such onsite measurements. In addition, the derivation of the loads is often not a straightforward task and involves a number of assumptions and simplifications. So far, no measurements have been taken on stadiums with the crowd jumping.

2.4.6. Contact ratio

BS 6399: Part 1 (British Standards Institution 1996) specifies contact ratio values varying from 0.25 to 0.67, depending on the type of jump. Yao et al. (2003) found that the contact ratio was consistently above 0.5 from all their tests and they commented that subjects jumping on a flexible platform will automatically select a contact ratio that he/she is comfortable with when jumping.

2.4.7. Group jumping frequency

The jumping frequency is determined by the beat frequency of the music played. Several studies have been conducted to determine the frequency range from field measurements or survey of songs performed in concerts. For dancing in a hall (Matthews and Montgomery 1988), it was found that the dancing frequency varied from 1.9 Hz for Waltz to 3.3 Hz for Rock 'n Roll. Field measurements at stadiums during pop concerts (Pernica 1983; Ellis and Littler 2004) and at a gymnasium during aerobic classes (Allen 1990) showed that the crowd-induced rhythmic vibrations fell within the range of 2 to 3 Hz. A survey on the beat frequency of 210

songs from the 1960s to 1990s (Ginty et al. 2001) showed that 96.2 % of the songs fell into the range from 1.0 to 2.8 Hz. Another survey of 364 songs performed in 18 rock and pop concerts (Littler 2003) showed that the songs fell into the range of 0.49 to 3.28 Hz. It was noted that the crowd might jump at every other beat for fast songs and at double the frequency of the songs for slow songs. BS 6399: Part 1 (British Standards Institution 1996) recommends a frequency range of 1.5 to 2.8 Hz for group jumping because at higher frequencies, it is difficult for a large group to maintain a coordinated rhythm.

2.5. Bobbing load modelling

It is also very common for the crowd on a cantilever grandstand to bob in a pop concert. Compared to jumping, the action of bobbing is less well-researched. Only three studies have been published so far (Yao et al. 2002, Parkhouse and Ewins 2004, Duarte and Ji 2005). Parkhouse and Ewins conducted individual bobbing tests on a rigid force plate while Yao et al. conducted similar test on a flexible platform. Duarte and Ji measured the response of a beam and used it to back calculate the bobbing loads. They found that the DLF of the first harmonic increased with the beat frequency.

2.6. Concluding remarks

2.6.1. The problem

The vibration problem on cantilever grandstands is due to the structures having low natural frequencies which are prone to excitation by the rhythmic crowd motions. In particular, the first three harmonics of the crowd-induced loadings were found to

be of significant magnitude, capable of causing concerning levels of vibration. Therefore, this thesis concentrates on structures with natural frequencies within three times the frequency range of crowd jumping, which is 1.5 to 2.8 Hz, as recommended by BS 6399: Part 1 (British Standards Institution 1996).

2.6.2. Structural modelling

A 2D model should be sufficient for the purpose of analysing the vertical mode of vibration. Various modal tests and experimental studies showed that the occupied structure had dynamic characteristics different from when it was empty. Most results showed that there was a reduction in the natural frequency and an increase in the damping when occupied by a passive crowd. Therefore, the passive crowd should be modelled as a dynamic system added to the structure.

2.6.3. Codes and guidelines

It is often uneconomical to design a stadium with its natural frequencies above the threshold frequencies recommended by various codes and guidelines. A structure with natural frequencies below the threshold value might perform perfectly well. Therefore, it is best to carry out a dynamic analysis on the structure when used for various events with different levels of crowd liveliness. For example, in a normal football game, most spectators are seated and there is minor excitation. In a lively concert or a football final match, a large proportion of the spectators can be highly active and their motions are synchronised by the music played or chanted. The worst scenario is in a pop concert in which the majority of the spectators synchronise their jumps with the music played. The challenge in the design of a

grandstand is to ascertain the highest level of crowd liveliness that the grandstand is able to withstand without causing panic to the crowd and to limit the use of the stadium to this highest permissible level.

2.6.4. Passive crowd modelling

Considering all the passive human models that have been developed so far in both civil engineering and biomechanics, the best models are those from Griffin et al. (Fairley and Griffin 1989, Wei and Griffin 1998, Matsumoto and Griffin 1998, 2003) because of the large number of subjects involved in the test series and the varieties of models tested. In addition, the subjects were subjected to a support acceleration of 1.0 m/s^2 (r.m.s.), which is within the range of acceleration measured on grandstands (Littler 1998, 1999). This thesis adopts these individual models to represent passive humans on a cantilever beam in Chapter 3 and to derive a passive crowd model in Chapter 4.

2.6.5. Jumping load modelling

A few issues relevant to modelling the crowd jumping load are discussed below.

Database from direct measurement

It is important to collect data for a large number of subjects so that the Monte Carlo simulation is statistically sound. So far, the best quality of data was gathered by Parkhouse and Ewins (2005) who have kindly provided them for use in this thesis.

Statistical analysis

In modelling the lack of synchronisation between individuals, each jump was treated as one independent event (Ellis and Ji 2004 and Kasperski and Agu 2005). Hence the jumps of all subjects were lumped together and analysed, several parameters were introduced to quantify each jump and a probability distribution function was used to curve-fit each parameter. However, it is possible that each subject has a unique jumping mechanism such that the successive jumps in each record are dependent events. This thesis treats the load-time record of each subject as one random process and assigns parameters to quantify each jumping process. The analysis is described in Chapter 5.

Impulse shape and contact ratio

There is a lack of research on the shape of the jumping impulse. Most accepted the half-sine function to represent one impulse but no verification was found. In addition, there is a discrepancy in the contact ratios given by BS 6399: Part 1 (British Standards Institution 1996) and the experimental measurements from Yao et al. (2003). Both issues are resolved in Chapter 5.

Correlation with crowd size

On the relationship between the loads generated and the crowd size, it is difficult to make a direct comparison between the various findings because the results were presented in various forms using different parameters.

Crowd effect

So far, only one work was done in investigating the effect of jumping with another person (Ebrahimpour and Fitts 1996). In this thesis, experimental tests are conducted to investigate this and the results are presented in Chapter 7.

Flexibility of structure

It was found that the jumping mechanism is affected by the flexibility of the structure and the mechanics of this is not yet fully understood. It is important to first understand the fundamental jumping mechanism on a rigid platform before considering the effect of the structural movement. This thesis focuses on the loads generated when jumping on a rigid platform.

2.6.6. Bobbing load modelling

While it is true that the most severe crowd-induced loading comes from jumping, experimental tests have shown that it is not possible to jump at the natural frequency of the structure. However, this might not be true for bobbing. As in the case of the Millennium Bridge (Dallard et al. 2001) in which the walking of the pedestrians is synchronised by the motion of the bridge, it might be possible that the motion of the cantilever grandstand is able to synchronise the bobbing of the crowd. Further research is required to investigate this. In this thesis, some initial experimental bobbing tests are conducted and reported in Chapter 7.

Chapter 3

3. Cantilever-human system

Accurate models of the passive and active crowds are crucial in carrying out a sensible dynamic analysis of a cantilever grandstand. The former is important because its presence alters the dynamic properties of the structure while the latter is needed to define the dynamic loads exerted by the crowd.

This chapter aims at carrying out an initial investigation on the critical components affecting the response of a cantilever grandstand. To achieve this, a simple model is introduced to represent a cantilever grandstand occupied by a seated crowd, called the cantilever-human system hereafter. The cantilever-human system consists of a simple continuous mass system representing one bay of a cantilever grandstand and lumped parameter models representing seated humans on the structure. These human models are taken from systems developed by Griffin et al. (Fairley and Griffin 1989, Wei and Griffin 1998, Matsumoto and Griffin 1998, 2003). In section 3.1, a description of the seated and standing human models developed by Griffin et al. is given. The rest of the chapter presents the modelling and dynamic analysis of the cantilever-human system.

3.1. Seated and standing human models

This section presents the work conducted by Griffin et al. in developing lumped parameter models to represent single seated and standing humans.

Griffin et al. conducted vibration tests on 60 seated subjects (24 men, 24 women and twelve children) and twelve standing subjects (all men). Each subject was shaken vertically on a moving platform with an acceleration level of 1.0 m/s^2 (r.m.s.) over a frequency range of 0 to 20 Hz. Each test subject adopted a comfortable, upright posture with normal muscle tension. The force across the human-structure interface and the acceleration of the platform were measured.

Work on human perception and response is usually presented in terms of acceleration, so it is natural to use the notion of 'dynamic mass' to relate acceleration and force. For a dynamic system subjected to whole body sinusoidal acceleration, $\ddot{x}_g$, with a circular frequency, ω, and giving rise to a force F, the apparent mass is given by:

$$m_{app}(i\omega) = \frac{F(i\omega)}{\ddot{x}_g(i\omega)} \tag{3.1}$$

Griffin et al. calculated a non-dimensional parameter, called the 'normalised apparent mass', by dividing the measured apparent mass by the apparent mass at 0.5 Hz. The normalised apparent masses for all sixty seated subjects and twelve standing subjects are reproduced in Figs. 3.1 and 3.2 respectively. Griffin et al. used these normalised apparent mass measurements to create an equivalent lumped parameter model for each subject. The dynamic properties of each model (mass, stiffness and damping) were obtained by curve-fitting the model to the measured apparent mass data so as to minimise the square of the error between the measured and the calculated. Various lumped parameter models were used to model the response data of each test subject (shown in Figs. 2.2 and 2.3). Griffin et al. found

that a model consisting of two separate SDOF systems gave the best fit to the measured apparent mass frequency response data. These models, reproduced in Fig. 3.3 for both the seated and standing humans, consist of two mass-spring-damper systems arranged in parallel. The difference between the seated and standing models is that the two constituent SDOF systems in the seated human models are attached to a rigid support of mass m_0, whereas the standing model has a massless support. This implies that while standing, the whole body is free to vibrate whereas while seated, there is proportion (probably representing the hips and lower spine) that is effectively rigid. The parameters (mass, stiffness and damping) defining the mass-spring-damper systems in Fig. 3.3 for each subject were published in Wei and Griffin (1998) and Matsumoto and Griffin (2003).

3.2. Cantilever-human system

The aim here is to model a section of a cantilever grandstand, with one cantilever supporting one bay of seated area occupied by passive humans. These passive humans are represented using the models in Fig. 3.3 and the published results on the model properties. The resultant model, the cantilever-human system, is analysed to find out the effect of the passive crowd on the dynamic response of the structure.

The outline of this section is as follows. First, the representation of the cantilever-human system as a feedback system is described. Next, the use of state space models to describe the system in MATLAB® Control Toolbox (MathWorks, Inc.) is given. Then a limit state design based on BS 5950: Part 1 (British Standards Institution 2000) is applied to determine the size of a cantilever subjected to loads specified in BS 6399: Part 1 (British Standards Institution 1996) for a grandstand.

Finally, the system is analysed to obtain its frequency response and the results are presented.

3.2.1. Feedback system

Consider a continuous mass cantilever discretised with *J* nodes, as shown in Fig. 3.4. Each node at coordinate x_i is occupied by either a seated human or an external load.

The response of the cantilever is obtained using modal superposition which has the advantage of using less degrees of freedom by considering only the significant modes. So, from modal superposition, $\ddot{v}(x_i,t)$, the cantilever acceleration at node x_i is given by:

$$\ddot{v}(x_i,t) = \sum_{\text{modes}} \left[\phi_n(x_i)\ddot{Y}_n(t)\right] \tag{3.2}$$

where the subscript *n* denotes the n^{th} mode of the cantilever, $\phi_n(x_i)$ is the mode shape and $\ddot{Y}_n(t)$ is the modal amplitude.

The combined human-structure system can be represented as a feedback system, shown in Fig. 3.5. The interaction force between the seated human and the cantilever is calculated from the acceleration feedback of the structure. A seated human at node x_i is subjected to a support acceleration from the cantilever $\ddot{v}(x_i,t)$. The cantilever is subjected to some external loads and the interaction forces from the seated humans.

To simplify the analysis, all seated human models are combined to form a resultant human model, as shown in Fig. 3.6. The method of implementing this will be discussed in section 3.2.2.2. The resultant human model has the support accelerations for all seated humans as the input vector and the interaction forces as the output vector. The response of the feedback system is calculated mode by mode using modal analysis. A subscript n is added to denote the n^{th} modal inputs and outputs in Fig. 3.6.

3.2.2. State space model

This section describes how each subsystem in Fig. 3.5 is represented as a state space model for analysis in MATLAB® Control Toolbox (MathWorks, Inc.).

3.2.2.1. Cantilever

The n^{th} mode SDOF equation of motion for a cantilever is:

$$\ddot{Y}_n(t) + 2\xi_n\omega_n\dot{Y}_n(t) + \omega_n^2 Y_n(t) = \frac{P_n(t)}{M_n}; \quad n = 1, 2, 3\ldots \tag{3.3}$$

where $Y_n(t)$ is the modal amplitude, $P_n(t)$ is the modal force and $M_n(t)$ is the modal mass. The input to the state space model is the modal force; the outputs are the modal amplitude and the nodal accelerations $\ddot{v}_n(x_i, t)$, as depicted in Fig. 3.7. The second order differential equation given in Eqn. 3.3 can be redefined as a set of first order differential equations in the following:

Define a set of state variables as (z_1, z_2) where

Let $z_1 = Y_n(t)$ (3.4)

and $z_2 = \dot{Y}_n(t) = \dot{z}_1$ (3.5)

$$\therefore\ \dot{z}_2 = \ddot{Y}_n(t) = -\omega_n^2 z_1 - 2\xi_n \omega_n z_2 + \frac{P_n(t)}{M_n} \tag{3.6}$$

Expressing Eqns. 3.5 and 3.6 in matrix form, the state differential equations are:

$$\begin{bmatrix} \dot{z}_1(t) \\ \dot{z}_2(t) \end{bmatrix} = \begin{bmatrix} 0 & 1 \\ -\omega_n^2 & -2\xi_n\omega_n \end{bmatrix} \begin{bmatrix} z_1(t) \\ z_2(t) \end{bmatrix} + \begin{bmatrix} 0 \\ \frac{1}{M_n} \end{bmatrix} P_n(t) \tag{3.7}$$

where the modal force $P_n(t)$ is given by the external loads $[p(x_1, t), \ldots, p(x_J, t)]$ multiplied by their corresponding mode shapes $[\phi_n(x_1), \ldots, \phi_n(x_J)]$:

$$P_n(t) = \begin{bmatrix} p(x_1,t) & p(x_2,t) & \cdots & p(x_J,t) \end{bmatrix} \begin{bmatrix} \phi_n(x_1) \\ \phi_n(x_2) \\ \vdots \\ \phi_n(x_J) \end{bmatrix} \tag{3.8}$$

The modal acceleration at node x_i is:

$$\ddot{v}_n(x_i,t) = \phi_n(x_i)\ddot{Y}_n(t) = \phi_n(x_i)\left[-\omega_n^2 z_1 - 2\xi_n\omega_n z_2 + \frac{P_n(t)}{M_n} \right] \tag{3.9}$$

From Eqns. 3.4 and 3.9, the outputs in matrix form are:

$$\begin{bmatrix} Y_n(t) \\ \ddot{v}_n(x_1,t) \\ \ddot{v}_n(x_2,t) \\ \vdots \\ \ddot{v}_n(x_J,t) \end{bmatrix} = \begin{bmatrix} 1 & 0 \\ -\omega_n^2\phi_n(x_1) & -2\xi_n\omega_n\phi_n(x_1) \\ -\omega_n^2\phi_n(x_2) & -2\xi_n\omega_n\phi_n(x_2) \\ \vdots & \vdots \\ -\omega_n^2\phi_n(x_J) & -2\xi_n\omega_n\phi_n(x_J) \end{bmatrix} \begin{bmatrix} z_1(t) \\ z_2(t) \end{bmatrix} + \begin{bmatrix} 0 \\ \frac{\phi_n(x_1)}{M_n} \\ \frac{\phi_n(x_2)}{M_n} \\ \vdots \\ \frac{\phi_n(x_J)}{M_n} \end{bmatrix} P_n(t) \tag{3.10}$$

The matrices in Eqns 3.7 and 3.10 define the state space model of the n^{th} mode response of the cantilever.

3.2.2.2. Seated human

The seated and standing human models in Fig. 3.3 are defined by the following equations of motion:

$$m_1\ddot{y}_1 + c_1\dot{y}_1 + k_1 y_1 = -m_1\ddot{x}_g \tag{3.11}$$

$$m_2\ddot{y}_2 + c_2\dot{y}_2 + k_2 y_2 = -m_2\ddot{x}_g \tag{3.12}$$

$$F(t) = m_0\ddot{x}_g + m_1\left(\ddot{y}_1 + \ddot{x}_g\right) + m_2\left(\ddot{y}_2 + \ddot{x}_g\right) = m_0\ddot{x}_g - c_1\dot{y}_1 - k_1 y_1 - c_2\dot{y}_2 - k_2 y_2 \tag{3.13}$$

where

m_0 = mass of the rigid component in the seated human model (equals to zero for standing subject)

y_1 = relative displacement of mass m_1 with respect to the support

y_2 = relative displacement of mass m_2 with respect to the support

$\ddot{x}_g$ = support acceleration

F = force transmitted across the human-structure interface

When excited by the movement of the structure with an acceleration of $\ddot{x}_g$, the human body undergoes vibration which in return exerts a force F back onto the structure. This interaction force F which exists across the human-structure interface is a function of the relative movement of the human dynamical system (y_1 and y_2) with respect to the structural system, shown in Eqn. 3.13. Therefore, for a seated human located at node x_i, the input to the state space model is the cantilever modal acceleration, $\ddot{v}_n(x_i, t)$, and the output is the interaction force, $F_{in}(t)$, as depicted in Fig. 3.8.

Similar to the cantilever system, the second order differential equations defining the equations of motion of the human system can be redefined as a set of first order differential equations using state space variables. For a human model at node i, define a set of state variables as $(z_1, z_2, z_3, z_4)_i$ where

Let $z_1 = y_1$ (3.14)

and $z_2 = \dot{y}_1 = \dot{z}_1$ (3.15)

and $z_3 = y_2$ (3.16)

and $z_4 = \dot{y}_2 = \dot{z}_3$ (3.17)

$$\therefore \dot{z}_2 = \ddot{y}_1 = -\frac{k_1}{m_1} z_1 - \frac{c_1}{m_1} z_2 - \ddot{v}_n(x_i, t) \tag{3.18}$$

$$\therefore \dot{z}_4 = \ddot{y}_2 = -\frac{k_2}{m_2} z_3 - \frac{c_2}{m_2} z_4 - \ddot{v}_n(x_i, t) \tag{3.19}$$

Expressing Eqns. 3.15 to 3.19 in matrix form, the state differential equations are:

$$\begin{bmatrix} \dot{z}_1(t) \\ \dot{z}_2(t) \\ \dot{z}_3(t) \\ \dot{z}_4(t) \end{bmatrix}_i = \begin{bmatrix} 0 & 1 & 0 & 0 \\ -k_1/m_1 & -c_1/m_1 & 0 & 0 \\ 0 & 0 & 0 & 1 \\ 0 & 0 & -k_2/m_2 & -c_2/m_2 \end{bmatrix} \begin{bmatrix} z_1(t) \\ z_2(t) \\ z_3(t) \\ z_4(t) \end{bmatrix}_i + \begin{bmatrix} 0 \\ -1 \\ 0 \\ -1 \end{bmatrix} \ddot{v}_n(x_i, t) \tag{3.20}$$

From Eqn. 3.13, expressing the interaction force in state variables:

$$F_{in}(t) = -k_1 z_1 - c_1 z_2 - k_2 z_3 - c_2 z_4 + m_o \ddot{v}_n(x_i, t) \tag{3.21}$$

Multiplying the interaction force by the mode shape to give the modal force on the cantilever:

$$F_{in}(t) = \phi_n(x_i) F_{in}(t) = \phi_n(x_i)\left[-k_1 z_1 - c_1 z_2 - k_2 z_3 - c_2 z_4 + m_o \ddot{v}_n(x_i, t)\right] \tag{3.22}$$

In matrix form, the modal force is given by:

$$F_{in}(t) = \phi_n(x_i)\begin{bmatrix} -k_1 & -c_1 & -k_2 & -c_2 \end{bmatrix} \begin{bmatrix} z_1(t) \\ z_2(t) \\ z_3(t) \\ z_4(t) \end{bmatrix}_i + m_o \phi_n(x_i) \ddot{v}_n(x_i, t) \tag{3.23}$$

The matrices in Eqns 3.20 and 3.23 define the state space model of one seated human located at node x_i.

For a cantilever occupied by multiple seated humans, each human model is represented using the state space model described above. All human models are combined to form a resultant human model. The resultant human model has an input vector consisting of all nodal accelerations and an output vector consisting of all modal forces, as shown in Fig. 3.9.

The resultant human model is obtained by appending all human models from node x_1 to node x_J. The state differential equations of the resultant human model are:

$$\begin{bmatrix} \dot{\mathbf{z}}_1 \\ \dot{\mathbf{z}}_2 \\ \vdots \\ \vdots \\ \dot{\mathbf{z}}_J \end{bmatrix} = \begin{bmatrix} \mathbf{A_1} & 0 & \cdots & \cdots & 0 \\ 0 & \mathbf{A_2} & 0 & \vdots & \vdots \\ \vdots & 0 & \ddots & 0 & \vdots \\ \vdots & \vdots & 0 & \ddots & 0 \\ 0 & \cdots & \cdots & 0 & \mathbf{A}_J \end{bmatrix} \begin{bmatrix} \mathbf{z_1} \\ \mathbf{z_2} \\ \vdots \\ \vdots \\ \mathbf{z}_J \end{bmatrix} + \begin{bmatrix} \mathbf{B} & 0 & \cdots & \cdots & 0 \\ 0 & \mathbf{B} & 0 & \vdots & \vdots \\ \vdots & 0 & \ddots & 0 & \vdots \\ \vdots & \vdots & 0 & \ddots & 0 \\ 0 & \cdots & \cdots & 0 & \mathbf{B} \end{bmatrix} \begin{bmatrix} \ddot{v}_n(x_1,t) \\ \vdots \\ \ddot{v}_n(x_J,t) \end{bmatrix} \tag{3.24}$$

The modal forces are:

$$\begin{bmatrix} F_{1n} \\ F_{2n} \\ \vdots \\ \vdots \\ F_{Jn} \end{bmatrix} = \begin{bmatrix} \mathbf{C_1} & 0 & \cdots & \cdots & 0 \\ 0 & \mathbf{C_2} & 0 & \vdots & \vdots \\ \vdots & 0 & \ddots & 0 & \vdots \\ \vdots & \vdots & 0 & \ddots & 0 \\ 0 & \cdots & \cdots & 0 & \mathbf{C}_J \end{bmatrix} \begin{bmatrix} \mathbf{z_1} \\ \mathbf{z_2} \\ \vdots \\ \vdots \\ \mathbf{z}_J \end{bmatrix} + \begin{bmatrix} \mathbf{D_1} & 0 & \cdots & \cdots & 0 \\ 0 & \mathbf{D_2} & 0 & \vdots & \vdots \\ \vdots & 0 & \ddots & 0 & \vdots \\ \vdots & \vdots & 0 & \ddots & 0 \\ 0 & \cdots & \cdots & 0 & \mathbf{D}_J \end{bmatrix} \begin{bmatrix} \ddot{v}_n(x_1,t) \\ \vdots \\ \ddot{v}_n(x_J,t) \end{bmatrix} \tag{3.25}$$

For i varying from 1 to J, $\mathbf{z}_i$ denotes the state vector for the human model at node x_i; $\mathbf{A}_i$, $\mathbf{C}_i$ and $\mathbf{D}_i$ denote the **A, C** and **D** matrices for human model at node x_i respectively. **B** is the same for all human models. Each is given by:

$$\mathbf{z}_i = \begin{bmatrix} z_1(t) \\ z_2(t) \\ z_3(t) \\ z_4(t) \end{bmatrix}_i \tag{3.26}$$

$$\mathbf{A}_i = \begin{bmatrix} 0 & 1 & 0 & 0 \\ -k_1/m_1 & -c_1/m_1 & 0 & 0 \\ 0 & 0 & 0 & 1 \\ 0 & 0 & -k_2/m_2 & -c_2/m_2 \end{bmatrix}_{\text{for human at node } i} \tag{3.27}$$

$$\mathbf{B} = \begin{bmatrix} 0 \\ -1 \\ 0 \\ -1 \end{bmatrix} \tag{3.28}$$

$$\mathbf{C}_i = \phi_n(x_i)\begin{bmatrix} -k_1 & -c_1 & -k_2 & -c_2 \end{bmatrix}_{\text{for human at node } i} \tag{3.29}$$

$$\mathbf{D}_i = \left[m_o \phi_n(x_i)\right]_{\text{for human at node } i} \tag{3.30}$$

In MATLAB® Control Toolbox (MathWorks, Inc.), each subsystem is first defined in the state space model. Then the cantilever and resultant human systems are combined using a feedback connection to form the feedback system in Fig. 3.6.

3.2.3. Limit state design

The previous section shows how to model a cantilever occupied by seated humans in MATLAB® Control Toolbox (MathWorks, Inc.). In order to provide a realistic model of the cantilever grandstand, a limit state design according to BS 5950: Part 1 (British Standards Institution 2000) is carried out to determine the size of a cantilever capable of supporting dead and imposed loads according to BS 6399: Part 1 (British Standards Institution 1996). Once the size of the cantilever is determined, the cantilever-human system is modelled in MATALB® Control Toolbox (MathWorks, Inc.) and analysed for its frequency response. Some important findings on the dynamic characteristics of such an occupied structure are discussed at the end of this section.

3.2.3.1. Cantilever member

Firstly, the tributary area of the cantilever is specified. Consider a cantilever on a grandstand with a tributary area which consists of 10 rows of seats with each row having 14 seats. Based on the guidelines given in the Guide to Safety at Sports Grounds (Dept. of National Heritage and Scottish Office 1997), the seat width is 500 mm and the seating row depth is 760 mm. Allowing 760 mm passageway at the front and back of the cantilever and 500 mm passageway on both sides, the length and span of the cantilever are:

Length, $L = 0.76 \times 12 = 9.12$ m

Span, $s = 0.5 \times 16 = 8$ m

The cantilever supports a concrete seating deck with a thickness of 170 mm. The dead load includes the self-weights of the cantilever and concrete deck. The imposed load is 5.0 kN/m^2, according to BS 6399: Part 1 (British Standards Institution 1996). By trial and error, the UB 914×419×388 section is selected, satisfying both strength and serviceability criteria according to BS 5950: Part 1 (British Standards Institution 2000). The design checks are presented in Appendix A.

The total mass of the structure is 3.38×10^4 kg; the total mass of the crowd at full capacity is 1.12×10^4 kg. The ratio of the mass of the crowd to the mass of the structure is 0.33.

3.2.3.2. Modal properties

The natural frequencies of a cantilever are given by:

$$\omega_n = (\alpha L)_n^2 \sqrt{\frac{EI}{\overline{m}}} \tag{3.31}$$

where $\overline{m}$ is the mass per unit length of the cantilever including the self-weight of the concrete deck;

$$\alpha L_1 = 1.875\,;\ \alpha L_2 = 4.694\,;\ \alpha L_3 = 7.855\,;\ \alpha L_n = \frac{\pi}{2}(2n-1) \text{ for } n = 4,5,6,...$$

The mode shapes are given by:

$$\phi_n(x) = \cos(\alpha_n x) - \cosh(\alpha_n x) - \sigma_n[\sin(\alpha_n x) - \sinh(\alpha_n x)] \tag{3.32}$$

where $\sigma_n = \dfrac{\cos(\alpha_n L) + \cosh(\alpha_n L)}{\sin(\alpha_n L) + \sinh(\alpha_n L)}$; $\quad n = 1, 2, 3\ldots$

Using the above equations, the natural frequencies of the first three modes are calculated:

$\omega_1 = 4.2$ Hz, $\omega_2 = 26.6$ Hz, $\omega_3 = 74.4$ Hz

The mode shapes are plotted in Fig. 3.10. For a simple cantilever beam, the modes are widely separated in frequency and only the first mode is within the frequency range to be considered for human-induced loading. Therefore, only the first mode will be used. The mode shape for the first mode follows a roughly parabolic shape, as shown in Fig. 3.10.

3.2.3.3. Frequency response analysis

Two analyses are conducted, one to investigate the effect of the position of the crowd and the other to look at the effect of the crowd size on the frequency response of the structure. The human models are defined using the mean value of the model parameters (m_0, m_1, m_2, c_1, c_2, k_1 and k_2) published by Wei and Griffin (1998):

m_0 = 6.7 kg, m_1,= 33.4 kg, m_2,= 10.7 kg, c_1 = 761 Ns/m, c_2 = 458 Ns/m, k_1 = 35776 N/m and k_2 = 38374 N/m.

In the first case, one row is occupied by seated spectators at one time and the modal amplitude Y_n of the cantilever at the free end due to a unit sinusoidal load applied there is obtained. Analyses are conducted for rows 1, 5 and 10 occupied by seated spectators (row 1 is the row nearest to the fixed end and row 10 is the row at the free end). The results, presented in Fig. 3.11, show that the presence of the seated crowd reduces both the modal amplitude and the resonant frequency of the structure. The reduction is greater when the occupied row is farther from the fixed end. This can be explained in terms of the bigger influence from the seated humans due to increased displacements towards the tip of the cantilever, as reflected in the mode shape of the cantilever.

In the second case, analyses are conducted with the cantilever empty; half-full and completely full with spectators. For the half-full cantilever, half of the seats in each row are occupied. The modal amplitude of the cantilever at the free end due to a unit sinusoidal load applied there is shown in Fig. 3.12. As can be seen, the modal amplitude and the resonant frequency both decrease as the crowd size increases.

3.2.3.4. Discussion

Several important key findings are found from the results presented here. Firstly, for a simple cantilever, the response is dominated by the first mode. Secondly, the presence of the seated humans contributes to lower modal amplitude and resonant frequency compared to when the structure is empty. In addition, the effect of the passive crowd is a function of the size of the crowd and the motion of the structure. Therefore, two parameters are found to be important in the analysis: the natural frequency of the empty structure and the size of the passive crowd.

At this stage, there are two options on how the research can proceed. One option is to build a more complicated model with more degrees of freedom. An attempt is made to build a system which consists of rigid planks spanning across two cantilevers. However, due to too many degrees of freedom involved, it is not possible to generalise the analysis.

The second option is to concentrate on the unknowns in the analysis, i.e. the *crowd-structure system* and the *loads exerted by the active crowd*. For the former, it seems appropriate to carry out a parametric study to investigate the human-structure interaction on structures with various natural frequencies and occupied by crowds of different sizes. However, the method of analysis used in this chapter is restrictive because it is difficult to vary the natural frequency of the cantilever while adopting an optimum member size that satisfies both strength and serviceability criteria. The dominance of the first mode suggests that a SDOF structural system is adequate.

3.3. Conclusions

Due to difficulties in generalising the analysis using a complicated model, it is decided that a SDOF system will be used to represent the cantilever grandstand. The advantage of using a simple model is such that because the dynamic characteristics of the structure are simple and well-defined, the fundamental interaction between the passive crowd and the structure can be better understood. Therefore, a SDOF structural system is adopted in subsequent chapters.

Chapter 4

4. Passive crowd-SDOF system

As mentioned in Chapter 3, the use of a simple SDOF structural system with known dynamic properties allows the fundamental interaction between the passive crowd and the structure to be investigated. This chapter looks at the modelling of such a SDOF structural system with an added dynamic system to represent the passive crowd. A few parameters are introduced to quantify the effect of the passive crowd.

This chapter presents the derivation of a crowd model (section 4.1) and the analysis of a joint crowd-SDOF system (section 4.2). The results are presented in charts with an example to illustrate how the charts can be used. Section 4.3 simplifies the joint crowd-SDOF system to two equivalent reduced-DOF systems.

4.1. Passive crowd model

The human models developed by Griffin et al. (Fairley and Griffin 1989, Wei and Griffin 1998, Matsumoto and Griffin 1998, 2003) are introduced in the literature review (section 2.3.2) and are considered to be the best models available (section 2.6.4). They are used in the cantilever-human system in Chapter 3 to represent seated humans on a cantilever. Their use is extended, in this chapter, to represent a group of people seated and standing on a structure. First, an alternative interpretation of Griffin et al.'s results is presented. Then using these results, a crowd model is derived.

4.1.1. Dynamic properties of individual human models

The values of the model parameters m_0, m_1, m_2, c_1, c_2, k_1 and k_2 were published in Table 2 in Wei and Griffin (1998) for sixty seated subjects and in Table 5 in Matsumoto and Griffin (2003) for twelve standing subjects. Using these published values, the modal properties of each of the two constituent SDOF systems are calculated for each of the sixty seated and twelve standing models. The resulting modal mass, undamped natural frequency and damping ratio are plotted in Fig. 4.1 for DOF 1 (the one with lower undamped natural frequency) and in Fig. 4.2 for DOF 2. The size of the bubble indicates the modal masses, m_1 and m_2. The mean and standard deviation for all four groups of test subjects (seated men/women/children and standing men) are presented in Table 4.1 for the undamped natural frequency and damping ratio and in Table 4.2 for the modal mass.

For all groups, the mean undamped natural frequency for DOF 1 is between 5 and 6 Hz and for DOF 2, between 9 and 16 Hz. The first resonant frequency is evident in the measured normalised apparent mass data shown in Figs. 3.1 and 3.2 while the second is less obvious. DOF 1 has significantly higher modal mass than DOF 2 but the difference is less for standing men. The damping ratios for all groups are high, within the range of 20% to 60%, indicating the ability of the human body to absorb energy when placed on a moving platform. For different postures, the standing men have a slightly higher undamped natural frequency than the seated men.

4.1.2. Crowd model

In theory, the individual models could simply be added together to produce a model of the crowd. However, this produces a model with a very high number of degrees of freedom, since there are two for each person, and hence is overly complicated. A lower order model that is a good approximation to the crowd is derived here. Using the model parameters given by Griffin et al., the apparent mass frequency response of each subject is calculated. The responses for all subjects are summed to give the total response for each group of men, women and children. The total response is then normalised by the total mass of each group to give the average normalised apparent mass of each group, presented in Fig 4.3. The apparent mass for any size of crowd can be obtained by multiplying the average normalised apparent mass data in Fig. 4.3 by the total mass of the crowd. The average normalised apparent mass calculated here is the mean response of the derived models and is therefore different from the 'average man' derived by Wei and Griffin (1998). The latter is obtained by taking the mean of each model parameters (mass, stiffness and damping).

In analysing the dynamic response of a structure occupied by a crowd, it is necessary to consider the crowd as a dynamic system added to the main structural system. The representation of a dynamic system can be in the form of differential equations of motion in the time domain or a transfer function in the frequency domain. In this case, the crowd is represented using a transfer function based on the apparent mass. The apparent mass data plotted in Fig. 4.3 are fitted from 0 to 20 Hz with rational polynomials of varying order from 1 to 6 using the damped Gauss-Newton method (Dennis and Schnabel 1983). It is found that the solution converges with polynomials of order of 4, i.e. there is no significant further

reduction in the error when increasing the order from 4 to 5. An order of 4 for the transfer function indicates that the group response can also be modelled as a 2DOF system. In other words, a crowd model consisting of numerous, different, parallel 2DOF systems, with each system representing one human, can be approximated well by using a single 2DOF system. The transfer function for this 2DOF system is given by:

$$m^*_{app}(s) = \frac{a_4 s^4 + a_3 s^3 + a_2 s^2 + a_1 s + a_0}{b_4 s^4 + b_3 s^3 + b_2 s^2 + b_1 s + b_0} \tag{4.1}$$

where

m^*_{app} = normalised apparent mass

a_n, b_n = coefficients for n = 0 to 4, values given in Table 4.3 for all four groups, each normalised with respect to b_4

s = Laplace Transform variable

From Fig. 4.3, the frequencies at the maximum normalised apparent mass are 4.42 Hz for seated men, 4.2 Hz for women, 4.53 Hz for children and 5.16 Hz for standing men. A secondary peak is observed for standing men at a frequency slightly greater than 10 Hz. In addition, the crowd of standing men has a slightly higher natural frequency than the seated groups. For all groups, the phase angles are roughly 90^o at high frequencies.

The force transmitted from the human dynamical systems to the structure is a function of the relative movement of the two (Eqn. 3.13). At low platform frequencies, the human bodies act as masses with little movement relative to the support. The relative movement between the human dynamical systems and the

support is greatest at the peak normalised apparent mass which is between 4 to 6 Hz. At high platform frequencies, the human dynamical systems behave like dampers with their masses remaining still. Knowing these behaviours of the human dynamical systems will help us to understand how these systems might affect the behaviour of structures with different natural frequencies. This will be discussed in more detail in section 4.2.

4.1.3. Error analysis

It is inevitable that there will be some errors in the derivation of the crowd model and it is important to know its order of magnitude in order to assess its significance on the results obtained from using the crowd model. The total error for the crowd model defined using the transfer function in Eqn. 4.1 equals to the sum of the errors from curve-fitting the individuals' measured apparent mass data with lumped parameter models and the error due to curve-fitting the total model response with a rational polynomial of order of 4. The error for the former procedure which was conducted by Griffin et al. was not reported. The maximum error from the latter procedure is found to be 0.7 % for the magnitude of normalised apparent mass and 0.7^{o} for the phase, for the range 0 to 20 Hz.

4.2. Dynamic analysis of crowd-structure system

This section presents a method of analysing the crowd-structure model. The displacement-frequency response of the combined system is calculated and compared to that of the empty structure. The changes in the resonant frequency and

peak response are obtained for various natural frequencies of the structure and crowd sizes.

4.2.1. Implementation of analysis

The crowd-structure model, shown in Fig. 4.4, consists of a crowd of people represented by the 2DOF model derived in section 4.1, on a structure which is itself modelled as a SDOF system with an intrinsic structural damping ratio of 2%, subjected to an external force, F_{ext}. Crowds of seated and/or standing men are considered. The relative mass of the crowd to the structure is defined by a mass ratio, γ, which has the value zero for an empty structure.

Using MATLAB® Control Toolbox (MathWorks, Inc.), the crowd-structure model is represented as a feedback system shown in Fig. 4.5. Each block represents one component: the structure is represented by a SDOF state space model and the crowd, both seated and standing, are modelled using the transfer functions derived in section 4.1 for groups of seated and standing men (Eqn. 4.1 and Table 4.3). If the structure is occupied with only a seated or a standing crowd, then the two systems are connected in a feedback loop in which the interaction force between the crowd and the structure is calculated from the acceleration feedback on the structure. If the crowd consists of both seated and standing men, there are two feedback connections to the SDOF structural system. Analyses are carried out for natural frequencies of the empty structure varying from 1 to 10 Hz and mass ratios of 0, 0.05, 0.1, 0.2, 0.3 and 0.4. The results are presented in terms of the Dynamic Magnification Factor (DMF), defined as:

$$\text{DMF} = \frac{X}{\Delta_{\text{static}}} = X \cdot k_s \tag{4.2}$$

where

X = amplitude of response due to a unit amplitude sinusoidal load, sin ($2\pi ft$)

Δ_{static} = static deflection of the empty structure due to a unit load (1 N)

k_s = stiffness of the structure

4.2.2. Frequency responses

For the design of cantilever grandstands, the frequencies where there is concern for human-induced loadings lie below 8.4 Hz (BS 6399: Part 1, British Standards Institution 1996). Fig. 4.6 shows the DMF of a seated crowd-SDOF system for four structures with natural frequencies varying from 2 to 8 Hz. Each plot shows the frequency responses for mass ratios of 0, 0.05, 0.1, 0.2 0.3 and 0.4. Several key observations can be made from the plots in Fig. 4.6. For the 2 Hz structure, the human dynamical systems are subjected to a low frequency support excitation. Therefore, each DOF is behaving like a mass with its spring acting as a rigid link between the human mass and the support. In effect, the crowd system is adding mass to the structural system which reduces both the natural frequency and the damping ratio of the occupied structure compared to the empty structure. This is evident in the reduction in natural frequency and the increase in DMF shown in Fig. 4.6. For the 4, 6 and 8 Hz structures, there are reductions in both the DMF and the natural frequency as the mass ratio increases. At these frequencies of support excitation, the human dynamical systems are undergoing large relative vibration. The effect of the crowd on the structure is to reduce its dynamic response in a way

similar to a tuned mass damper though, unlike a TMD, the crowd properties cannot be optimised for a particular structure. Very similar trends are found for a standing crowd-SDOF system and a 50:50 seated/standing-SDOF system. For example, the plots for a 6 Hz structure for both cases are presented in Fig. 4.7.

4.2.3. Reductions in natural frequency and DMF

The frequency responses for all three crowd-SDOF systems (100% seated, 100% standing and 50:50 seated/standing crowds) are evaluated for structures with natural frequencies varying from 1 to 10 Hz. In order to allow designers to estimate the structural response due to various crowd sizes, the results are summarised in Figs. 4.8 and 4.9 in terms of the *frequency reduction factor* and the *DMF reduction factor*, defined as:

Frequency reduction factor:

$$F_{\mathrm{R}} = \frac{\omega_{\mathrm{occupied}}}{\omega_{\mathrm{empty}}} \tag{4.3}$$

where

$\omega_{\mathrm{occupied}}$ = natural frequency of the occupied structure

ω_{empty} = natural frequency of the empty structure

The natural frequency is the frequency at the maximum response.

DMF reduction factor:

$$\mathrm{DMF}_{\mathrm{R}} = \frac{\mathrm{DMF}^{*}_{\mathrm{occupied}}}{\mathrm{DMF}^{*}_{\mathrm{empty}}} \tag{4.4}$$

where

$\mathrm{DMF}^{*}_{\mathrm{occupied}}$ = maximum DMF of the occupied structure

$\mathrm{DMF}^*_{\mathrm{empty}}$ = maximum DMF of the empty structure

Since the DMFs of both the occupied and the empty structures are normalised by the static deflection of the empty structure due to a unit amplitude sinusoid, the DMF reduction factor can be represented as:

$$\mathrm{DMF}_{\mathrm{R}} = \frac{X^*_{\mathrm{occupied}}}{X^*_{\mathrm{empty}}} \tag{4.5}$$

where

X^*_{occupied} = maximum displacement amplitude of the occupied structure

X^*_{empty} = maximum displacement amplitude of the empty structure

As shown in Fig. 4.8, for all three crowd-SDOF systems, the frequency reduction factor varies with the natural frequency of the empty structure and the mass ratio. The frequency reduction factor decreases as the mass ratio increases with a reduction factor of up to approximately 0.75 achieved for a mass ratio of 0.4 for all three cases. For each mass ratio, as the natural frequency of the empty structure increases, the reduction factor reduces to a minimum value. This is followed by a region where the frequency reduction factors are plotted using thin hollow lines. This is due to a complicated transition in which the frequency response curve consists of two peaks with very close maximum DMF values. Therefore, it is difficult to identify the natural frequency. At higher natural frequencies, one of the two peaks becomes more dominant and the frequency reduction factor reaches a plateau. This trend continues for structures with natural frequencies higher than 10 Hz which are not shown in Fig. 4.8. This contradicts the laboratory measurements by Ellis and Ji (1997) which showed that for a mass ratio of 0.3, there was an

increase in the resonant frequency for a 18.68 Hz reinforced concrete beam when occupied by a single standing or a seated person.

For all three crowd-SDOF systems, the DMF reduction factor, shown in Fig. 4.9, is greater than 1 for structures with natural frequencies less than 2 Hz. That is, the crowd increases the response of the empty structure by effectively adding mass and therefore reducing the damping ratio. For natural frequencies of empty structures greater than 2 Hz, there is a significant reduction in the DMF with minimum values at around 7 to 8 Hz. At higher natural frequencies, the DMF reduction factor increases gradually.

The minimum values for the standing crowd-SDOF system are located at natural frequencies slightly higher than for the seated crowd-SDOF system. This is due to the higher frequency of the maximum apparent mass of the standing crowd compared to seated crowd. For the 50:50 seated/standing-SDOF system, the transition from the minimum value to the plateau is less abrupt, spreading over a wider frequency range.

From the results presented in Figs. 4.8 and 4.9, it is clear that a passive crowd has a strong influence on the combined dynamical response by contributing added mass, damping and stiffness to the structural system. In particular, the crowd acts as an added mass to the structural system at low natural frequencies and as an added damper at high natural frequencies. There is greatest reduction in the natural frequency and the DMF for structures with natural frequencies within the range of 4

to 8 Hz. The level of reduction in the DMF increases with the mass ratio, i.e. more damping is provided as the crowd size increases.

4.2.4. Illustrative example

An example is presented here to illustrate the use of Figs. 4.8 and 4.9 for two purposes: (1) To estimate the natural frequency of an occupied structure; (2) To estimate the maximum displacement of an occupied structure when subjected to dynamic loads. The procedures are summarised in the flow chart in Fig. 4.10 and are explained below.

Consider a SDOF structural system with a natural frequency of 3 Hz, a damping ratio of 2 % and a mass of 800 kg. It is occupied by two seated individuals (possessing the dynamical properties of a crowd) each with a body mass of 80 kg, giving a mass ratio of 0.2.

Estimation of natural frequency of the occupied structure:

From Fig. 4.8, for a 3 Hz structure with $\gamma = 0.2$,

$F_R = 0.89$

From Eqn. 4.3,

$\omega_{occupied} = \omega_{empty} \times F_R$

$= 3 \times 0.89$

$= 2.7$ Hz

Estimation of maximum displacement of the occupied structure:

If one person is jumping on the occupied structure, the most severe load is when the person is jumping at a frequency coinciding with the natural frequency of the occupied structure. Considering excitation by the first harmonic of the jumping load, the force on the structure is:

$$F = \alpha_1 W \sin(2\pi \cdot 2.7\, t) \tag{4.6}$$

where

W = self-weight of the jumper

α_1 = Dynamic Load Factor of the first harmonic, typically 1.5 for jumping, according to Willford (2001)

The steady-state displacement amplitude of the empty structure, X^*_{empty}, due to F is:

$$X^*_{\text{empty}} = \frac{\alpha_1 W}{k_s}\left[\left(1-\beta^2\right)^2 + \left(2\xi\beta\right)^2\right]^{-1/2} \tag{4.7}$$

where

β = ratio of excitation frequency to natural frequency of the structure

ξ = damping ratio

Taking $\alpha_1 = 1.5$, $\beta = 1$, $\xi = 0.02$,

$W = 80 \times 9.81 = 784.8$ N (for a typical adult)

$k_s = \omega_n^2 m_s = (2\pi \cdot 3)^2 \cdot 800 = 284.2$ kN/m

Gives:

$X^*_{\text{empty}} = 0.104$ m

From Fig. 4.9, $DMF_R = 0.764$

From Eqn. 4.5, the maximum displacement of the occupied structure is

$$X^*_{\text{occupied}} = X^*_{\text{empty}} \times DMF_R$$

$$= 0.104 \times 0.764$$

$$= 0.08 \text{ m}$$

Therefore, the occupied structure which has two-thirds of the crowd seated and one-third jumping, has a calculated maximum displacement of 80 mm. This is an illustrative example that gives the worst response due to a perfectly periodic jumping load at the natural frequency of the structure. In some experimental tests, Yao et al. (2003) showed that it was not possible for a single jumper to jump at the natural frequency of the structure which had a mass ratio of 0.41. In addition, there is a slight variation between each jump which is not taken into account in the periodic loading function. Therefore, the results given in this example should be taken as a very conservative estimation.

4.2.5. Design implications

Currently, BS 6399: Part 1 (British Standards Institution 1996) adopts the threshold frequency design approach based on the natural frequency of the structure. The crowd jumping frequency is within the range of 1.5 to 2.8 Hz. In the example above, a natural frequency of 3 Hz was deliberately chosen to show that structures with natural frequencies coinciding with the second harmonic of a crowd jumping load might be excited by the first harmonic due to a reduction in the natural frequency when the passive crowd is present. Generally, structures with natural frequencies within the second or third harmonics of human-induced loads might be

prone to more severe excitation at the lower harmonics due to the presence of the passive crowd. However, the response of the structures might still be acceptable due to the additional damping provided by the passive crowd. The charts in Figs. 4.8 and 4.9 allow designers to estimate the response of a structure for various crowd activities. Structures with unacceptable vibration levels when the entire crowd is active, such as in a pop concert, might perform well if used for less lively events, such as football matches, in which only a small portion of the crowd is active.

4.3. Equivalent reduced-DOF systems

This section investigates the possibility of representing the joint crowd-structure system in section 4.2 as an equivalent reduced-DOF system. For a structure with either a seated or a standing crowd, the joint crowd-structure system is a 3DOF system while for a structure with both standing and seated crowds, the two groups of passive crowds are each modelled as an independent 2DOF system, giving a 5DOF joint crowd-structure system. In this section, the 50:50 seated/standing-SDOF system is reduced to two equivalent reduced-DOF systems - SDOF and 3DOF systems. The reduced-DOF systems have the advantage of making the analysis more straightforward because fewer DOFs are involved. In addition, the modal properties (mass, stiffness and damping) of the equivalent SDOF system will give some insight into how the passive crowd alters the dynamic response of the structure, e.g. by adding mass or damping, depending on the natural frequency of the structure. The errors between the two reduced-DOF systems and the full model are presented.

4.3.1. Equivalent SDOF system

4.3.1.1. Curve-fitting DMF-frequency response curves

Dynamic response of the full model shows that a passive crowd has a strong influence on the joint dynamical response by contributing added mass, damping and stiffness. This raises the possibility of modelling the joint system as a SDOF system with modal properties different from those of the empty structure, as first suggested by Michael Willford (Blakeborough 2005).

The equations of motion for a SDOF system subjected to a force of $F(t)$ are given by:

$$m\ddot{x}(t) + c\dot{x}(t) + kx(t) = F(t) \tag{4.8}$$

where m, c and k are the mass, damping and stiffness respectively.

Taking the Laplace Transform:

$$ms^2X(s) + csX(s) + kX(s) = F(s) \tag{4.9}$$

Rearranging to give $X(s)$:

$$X(s) = \frac{1}{ms^2 + cs + k} \times F(s) \tag{4.10}$$

Normalising Eqn. 4.10 by the static deflection due to a unit amplitude load:

$$X_0 = \frac{1}{k} \tag{4.11}$$

Hence:

$$\frac{X(s)}{X_0} = \frac{k}{ms^2 + cs + k} \times F(s) \tag{4.12}$$

The term on the left hand side of Eqn. 4.12 is the normalised displacement and is termed as DMF(s), therefore:

$$\mathrm{DMF}(s) = \frac{k}{ms^2 + cs + k} \times F(s) \tag{4.13}$$

Rearranging, the transfer function for a SDOF system is given by:

$$\frac{\mathrm{DMF}(s)}{F(s)} = \frac{k}{ms^2 + cs + k} \tag{4.14}$$

An example of the DMF-frequency response curves is shown in Fig. 4.7. The most crucial response is around the peak response. Therefore, Eqn. 4.14 is fitted over a bandwidth of $1/\sqrt{2}$ times the peak response using the damped Gauss-Newton method (Dennis and Schnabel, 1983). The modal properties of the equivalent SDOF system are obtained from the coefficients of the transfer function in Eqn. 4.14. They are expressed as mass, stiffness and damping ratios. The mass and stiffness ratios are ratios of the mass and stiffness of the equivalent SDOF system to those of the empty structure. The damping ratio is that of the equivalent SDOF system, i.e. ratio of its damping to its critical damping value.

4.3.1.2. Modal properties of equivalent SDOF system

The results, presented in Fig. 4.11 for a SDOF structure with an intrinsic damping ratio of 2%, show that the equivalent SDOF system reflects the important properties of the full model in that at low frequencies, the passive crowd is adding both mass and stiffness to the system. At frequencies greater than 5 Hz, the passive crowd is adding very significant damping to the system. The damping ratio increases with the mass ratio, with maximum damping ratio found for structures with natural frequencies between 5 and 8 Hz.

4.3.1.3. Error analysis

For assessing the accuracy of the equivalent SDOF system in representing the full model, the peak DMF relative error and resonant frequency relative error are calculated. They are defined as (see also Fig. 4.12):

Peak DMF relative error:

$$\mathrm{DMF}'_{\mathrm{RE}} = \frac{\Delta\,\mathrm{DMF}'}{\mathrm{DMF}'_{\mathrm{Full\ model}}} \times 100\% \tag{4.15}$$

where

$\mathrm{DMF}'_{\mathrm{Full\ model}}$ = Peak DMF of full model

Δ DMF' = Peak DMF of equivalent SDOF – Peak DMF of full model

Resonant frequency relative error:

$$F'_{\mathrm{RE}} \frac{\Delta F'}{F'_{\mathrm{Full\ model}}} \times 100\% \tag{4.16}$$

where

The resonant frequency refers to the frequency at the peak DMF and

$F'_{\mathrm{Full\ model}}$ = Resonant frequency of full model

$\Delta F'$ = Resonant frequency of equivalent SDOF – Resonant frequency of full model

As shown in Fig. 4.13, the equivalent SDOF system shows a very good fit for natural frequencies up to 4 Hz. This implies that the full model exhibits the behaviour of a SDOF system, with the crowd adding mass to the SDOF structure. For frequencies above 4 Hz, the relative errors increase with the mass ratio, with maximum values of 4% for the peak DMF relative error and 9% for the resonant frequency relative error, for a mass ratio of 0.4. Therefore, with an increasing

number of people on the structure, the joint system is behaving less like a SDOF system and the errors inherent in the approximation become significant.

4.3.2. Equivalent 3DOF system

For structures greater than 4 Hz, the equivalent SDOF system is not giving a very good fit, particularly for the resonant frequency. Hence in this section, an equivalent 3DOF system is attempted. For the equivalent 3DOF system, each of the seated and standing crowd is modelled as a SDOF system, added to the SDOF structural system. The method of analysis is the same as the full model, i.e. the equivalent 3DOF system is represented as a feedback system, as shown in Fig. 4.5, and analysed for its DMF-frequency response using MATLAB® Control Toolbox (MathWorks Inc.). It is important to note that this section looks at structures with both seated and standing crowds. For the cases of structures with only a seated or a standing crowd, the reduced system is a 2DOF system.

4.3.2.1. SDOF crowd model

For civil engineering structures, there are significant motions for structures less than 8.4 Hz (BS 6399: Part 1, British Standards Institution 1996). For this reason, the SDOF crowd model is obtained by curve-fitting a rational polynomial to the average normalised apparent mass at low frequencies.

The transfer function for a SDOF crowd model is given by:

$$m^*_{app}(s) = \frac{a_2 s^2 + a_1 s + a_0}{b_2 s^2 + b_1 s + b_0} \tag{4.17}$$

Eqn. 4.17 is fitted to various frequency ranges such as 0 to 5 Hz, 0 to 8 Hz and 0 to 10 Hz. By trial and error, it is found that curve-fitting from 0 to 5 Hz gives the least total absolute error for structures from 0 to 8.4 Hz.

Fig. 4.14 shows the average normalized apparent mass for seated and standing men, together with the fitted transfer functions given in Eqns. 4.1 (2DOF crowd model) and 4.17 (SDOF crowd model). While the 2DOF crowd model shows almost perfect fit, the SDOF crowd model shows deviation at high frequencies. Values of the coefficients of the transfer function in Eqn. 4.17 are presented in Table 4.4.

4.3.2.2. Dynamic analysis and error analysis

Dynamic analysis similar to the full model is performed for the equivalent 3DOF model with the crowd consisting 50% seated and 50% standing men. The peak DMF relative error and resonant frequency relative error are presented in Fig. 4.15. The relative errors increase proportionally with the mass ratio because the crowd model is obtained by multiplying the transfer function in Eqn. 4.10 by the mass of the crowd. For the peak DMF relative error, it falls within the range of ± 3%. The resonant frequency relative error is very low, less than 3%. Compared to the equivalent SDOF system, the equivalent 3DOF system gives a better fit for structures greater than 4 Hz.

4.3.2.3. Bode diagrams

Fig. 4.16 shows the DMF-frequency response curves for the full model, equivalent SDOF and 3DOF models, for 2, 4, 6 and 7 Hz structures with a mass ratio of 0.4.

The equivalent SDOF shows good fit for the 2 and 4 Hz structures. However, for the 6 and 7 Hz structures – the shape of the curve does not match that of the full model. In particular, there is a slight discrepancy in the resonant frequency but a good approximation for the maximum DMF is found. As for the equivalent 3DOF system, the shape of the curve matches and it gives good approximations for both the resonant frequency and the DMF for all structures.

4.4. Conclusions

It has been shown that a passive crowd which consists of many different 2DOF systems in parallel can be approximated as a single 2DOF system. An analysis tool is introduced to illustrate that the joint crowd-SDOF system can be represented as a feedback system. The frequency response of the combined system is quantified in terms of the natural frequency and DMF reduction factors for structures with natural frequencies from 0 to 10 Hz. For structures with low natural frequencies, a passive crowd adds significant mass to the system while for high natural frequency structures, it adds significant damping. Both effects cause a reduction in the natural frequency of the structure. At very low natural frequencies (below 2 Hz), the crowd increases the response of the structure compared to when it is empty by adding mass. For natural frequencies above 2 Hz, a significant reduction in the response of the structure is induced by the high damping contributed by the passive crowd. The results presented in Figs. 4.8 and 4.9 allow designers to estimate the changes in the natural frequency and response of an occupied structure for various crowd sizes.

Work on the reduced equivalent-DOF systems show that the joint 50:50 seated/standing crowd-SDOF system can be modelled satisfactorily as a SDOF

system for 1 to 4 Hz structures. At low natural frequencies of the empty structures, the crowd is adding mass to the structure and thus the joint system exhibits little deviation from the behaviour of a SDOF system. For structures above 4 Hz, the relative errors in DMF and resonant frequency increase with the mass ratio, indicating a deviation from the behaviour of a SDOF system as the number of people on the structure increases. Bode plots of the equivalent 3DOF system show a good match with those of the full model while a mismatch is found for the equivalent SDOF system for high natural frequency structures. Hence the equivalent 3DOF system is found to give a more accurate fit for structures above 4 Hz due to less error in the resonant frequency.

In practice, the engineer is interested in the maximum DMF. The slight discrepancy in the resonant frequency given by the equivalent SDOF should not matter. The maximum DMF relative errors for the equivalent SDOF and 3DOF systems are both within the range of ± 4%. In fact, the equivalent SDOF system gives a better fit for structures below 4 Hz. Therefore, for design purpose, the equivalent SDOF, with less DOFs, is a better option because it is more simplistic. It should be noted that theoretically, the equivalent 3DOF is a more accurate model because it gives a lower resonant frequency relative error.

Chapter 5

5. Statistical modelling of individual jumping load

There are two important aspects in the dynamic analysis of a cantilever grandstand, modelling the active and passive crowds. In Chapter 4, a joint crowd-SDOF system is developed to model a structure occupied by a passive crowd. The next task, modelling the active jumping crowd, is addressed here by deriving a load model which defines the forces due to a group of people jumping together. In the next chapter, the jumping load model is applied to the joint crowd-SDOF system.

The load model derived here is based on the experimental results from the work of Parkhouse and Ewins (2004). Parkhouse and Ewins conducted an analysis of the jumping loads using methods in the frequency domain. This thesis carries out an independent study based on an analysis in the time domain.

As mentioned in the literature review in Chapter 2, this thesis treats the load-time record of each subject as one random process and assigns parameters to quantify each jumping record. In this chapter, the jumping record of each individual is characterised by the *timing* and *shape* of the measured impulses. The strategy is to introduce a few parameters to model these two key aspects. The relevant parameters are fitted with probability distribution functions. In the next chapter, Monte Carlo simulations based on the fitted probability distribution functions are conducted to simulate group jumping loads and the responses of the joint crowd-SDOF system are evaluated.

This chapter begins with a brief description of the experimental tests conducted to measure the loads generated by individuals jumping in time to audio prompts. This is followed by analysing the load measurements in terms of the impulse timing (section 5.2) and the impulse shape (section 5.3). The relationship between these two properties of the measured impulses is considered (section 5.4) and lastly in section 5.5, all major findings are summarised.

5.1. Experimental tests

Experimental tests were conducted by Parkhouse and Ewins (2004) to measure the individual jumping loads of 100 test subjects at four distinct frequencies: 1.5, 2, 2.67 and 3.5 Hz (equivalent to 90, 120, 160 and 210 beats per minute). Each test involved a single participant jumping on a 0.8 m x 0.6 m force plate which measured the horizontal and vertical loads (see Fig. 5.1). Each participant was asked to jump in time with regular audio beeps generated by a metronome. Each test started with the participant standing still on the force plate followed by jumping for 30 to 35 s. The load and beep signals were recorded at a sampling interval of 5 ms.

5.2. Impulse timing

The modelling of the impulse timing aims to capture the lack of synchronisation between individual's timing when jumping together in a group. This is expected to lead to a less conservative load model, i.e. one not assuming perfect synchronisation between individuals. Several parameters characterising the timing of each impulse are first introduced and the criteria for selecting the test results for analysis are

stated. This is followed by a presentation of the statistics of two key parameters, namely the *mean phase delay* and *phase scatter*. The relationship between these two parameters is considered and each parameter is modelled using one or several probability distribution functions.

5.2.1. Definition of parameters

Fig. 5.2 shows a series of jumping impulses in schematic form and the variables used in the analysis. The impulses are separated by intervals of zero loads when the person is in the air. Each impulse is obtained by splitting the test record at these intervals of zero loads. The effective time of the i^{th} impulse, $t_{\text{eff},i}$, is used to define the timing of each jump. It is calculated as the time at the impulse centroid, i.e.:

$$t_{\text{eff},i} = \frac{\sum_{j=1}^{N_p} \left(F_j \cdot t_j\right)}{\sum_{j=1}^{N_p} \left(F_j\right)} \tag{5.1}$$

where F_j is the sampled load at time t_j and N_p is the number of sampled points in each jump.

The metronome generates a beep with a pulse 15 ms in duration. Since the sampling interval is 5 ms, the pulse for each beep is usually recorded in three successive samples but occasionally in two. The timing of each beep, t_{beep}, is taken from the mean value of the detected points for each pulse.

The time delay, $t_{\text{delay},i}$, is the time lag between each impulse and the corresponding beep:

$$t_{\text{delay},i} = t_{\text{eff},i} - t_{\text{beep},i} \tag{5.2}$$

The mean time delay, $\bar{t}_{\text{delay}}$, is the average time delay of each test record. The time deviation, $t_i^{'}$, is the difference between the time delay and the mean time delay. Since the mean time delay removes the DC offset, it follows that the time deviation has a mean of zero.

$$t_i' = t_{\text{delay},i} - \bar{t}_{\text{delay}} \tag{5.3}$$

It is sometimes more useful to define the time parameters in terms of the beat period, T_{beat}, giving the phase delay, $\theta_{\text{delay},i}$, mean phase delay, $\bar{\theta}_{\text{delay}}$, and phase deviation, θ_i':

$$\theta_{\text{delay},i} = \frac{t_{\text{delay},i}}{T_{\text{beat}}} \cdot 360^{\text{o}} \tag{5.4}$$

$$\bar{\theta}_{\text{delay}} = \frac{\bar{t}_{\text{delay}}}{T_{\text{beat}}} \cdot 360^{\text{o}} \tag{5.5}$$

$$\theta_i^{'} = \frac{t_i^{'}}{T_{\text{beat}}} \cdot 360^{\text{o}} \tag{5.6}$$

The standard deviation of phase deviation for each test record, referred to as the phase scatter hereafter, is given by:

$$\sigma_{\theta'} = \sqrt{\frac{\sum_{i=1}^{N_T} \theta_i^{'2}}{N_T}} \tag{5.7}$$

where N_T is the total number of impulses in each test record.

5.2.2. Synchronised tests

For each test record, the first four and last two impulses are discarded so that only the steady state jumping process is analysed. In some cases, the test subjects are not able to jump in time with the beeps, with misses or extra jumps. Only results for synchronised tests, i.e. when the subject jumps once per beep, with no misses or extras throughout the whole duration of the test, are analysed. This means that the worst loading case is being considered with all individuals able to synchronise their jumps with the beeps. Out of the 100 tests conducted for each beat frequency, the number of synchronised tests for 1.5, 2, 2.67 and 3.5 Hz are 55, 75, 67 and 41 respectively. Hence people are most synchronised when jumping at 2 and 2.67 Hz. The lower number of synchronised tests at 1.5 Hz is due to the difficulty in timing the landing and launching actions. For jumping at lower frequencies such as 1 Hz, individuals tend to land on their toes and heels whereas for higher frequencies at 2 Hz and above, individuals tend to land only on their toes. Jumping at an intermediate frequency of 1.5 Hz is a mixture of these two actions and is difficult to control. For jumping at 3.5 Hz, the small number of synchronised tests could be due to difficulty in keeping up with the fast pace. Out of the 100 test subjects, 26 are able to perform synchronised jumping at all four beat frequencies.

The impulses for all synchronised tests are presented in Figs. 5.3 to 5.6, with each plot corresponding to one test record. The vertical axis is the normalised load, F', defined as the measured load divided by the static weight of the subject. For ease of comparing the shape of the impulses, all impulses are centered about the timing of the impulse, t_{eff}, so that at $t = 0$, the time equals t_{eff}. The shape of these impulses will be discussed in section 5.3.

5.2.3. Statistics

The phase delays for all synchronised tests are presented in Fig. 5.7. Each plot shows the results for one beat frequency and within each plot, each column of data corresponds to the phase delay of one individual. The mean phase delays are plotted as triangles and the phase delays as squares. In order to impose some structure on the graphs the results are plotted in terms of increasing mean phase delay. Most of the mean phase delay values are positive, which means that the centroids of the impulses occur after the beeps. Depending on the shape of the impulse, most centroids are close to the maximum force exerted during landing. This indicates that the test subjects probably timed their jumps by coinciding their landings with the beeps.

For each test record, the impulse timing is quantified by the mean phase delay and phase scatter. The former gives an average indication of how closely a person's jumping impulse coincides with the beep and the latter quantifies the degree of variability of a person's timings.

Table 5.1 presents the mean and standard deviation of the mean time delay and mean phase delay. Generally, the mean time delay is close to 0.1 s for all four beat frequencies, indicating a common preference for timing the jumps at all beat frequencies. The standard deviation of the mean phase delay is a measure of the inter-subject variation and has the highest value for 1.5 Hz and the lowest value for 2.67 Hz. Therefore, there is least variation among individuals when jumping at 2.67 Hz and greatest variation when jumping at 1.5 Hz. The high variation at 1.5 Hz could be due to the difficulty in timing the landing and launching actions.

Jumping at 2.67 Hz involves one single action of landing and launching on toes and the pace is easy to keep up.

The phase scatter, σ_θ, is a measure of the jumper's coordination with the beeps. Its mean and standard deviation are calculated and presented in Table 5.2. The mean value shows that overall, the test subjects show best coordination when jumping at 2 and 2.67 Hz and worst coordination when jumping at 1.5 and 3.5 Hz. The standard deviation shows that similar to the mean phase delay, there is least inter-subject variation at 2.67 Hz and greatest variation at 1.5 Hz.

Fig. 5.8 shows plots of the phase scatter against the mean phase delay. Visual inspection suggests that there is no obvious correlation between the two parameters, i.e. individuals with high mean phase delay do not show significantly higher or lower phase scatter. The correlation coefficient, r, of these two parameters is calculated and shown in Table 5.2. There is a weak correlation for 2 and 3.5 Hz (r of -0.3) and no correlation for 1.5 and 2.67 Hz (r close to zero). It can be concluded that there is negligible correlation between the mean phase delay and phase scatter. Therefore, the mean phase delay and phase deviation will be treated as independent random variables in the statistical modelling process.

5.2.4. Mean phase delay

Fig. 5.9 shows histograms of the mean phase delay for all synchronised tests at each of the four beat frequencies. Superimposed on each histogram is the relative frequency curve. The most probable values for the mean phase delay are between -180° and 180°, i.e. the duration of one beat period. For all four beat

frequencies, the mean phase delay values are mostly positive with the distribution skewing to the right. Hence, a Beta distribution function is chosen for curve-fitting because of its fixed range and ability to assume widely differing shapes.

The Beta probability distribution function for a random variable y with α and β parameters is:

$$f(y)=\frac{y^{\alpha-1}(1-y)^{\beta-1}}{B(\alpha,\beta)}, \quad \alpha,\beta>0; \quad 0\le y\le 1 \tag{5.8}$$

where $B(\alpha, \beta)$ is the Beta function defined as:

$$B(\alpha,\beta)=\int_0^1 y^{\alpha-1}(1-y)^{\beta-1}dy=\frac{\Gamma(\alpha)\Gamma(\beta)}{\Gamma(\alpha+\beta)} \tag{5.9}$$

The mean phase delay range is set to be $-180^\circ \le \bar{\theta}_{\text{delay}} \le 180^\circ$ and the Beta distribution is only defined for $0 \le y \le 1$. A transformation of variable is therefore required:

$$\bar{\theta}^*_{\text{delay}}=\left(\bar{\theta}_{\text{delay}}+180^\text{o}\right)/360^\text{o} \tag{5.10}$$

where $\bar{\theta}^*_{\text{delay}}$ is called the transformed mean phase delay and $0 \le \bar{\theta}^*_{\text{delay}} \le 1$.

The α and β parameters are obtained using the method of maximum likelihood estimates. For a better fit, the outliers ($\bar{\theta}^*_{\text{delay}} \le 0.3$ or $\bar{\theta}_{\text{delay}} \le -72^\circ$) are not considered in the evaluation of the α and β values. The 0.3 cut-off value is selected based on trial and error so as to minimise error in the curve-fitting process.

A χ^2 test is performed to test the null hypothesis that the mean phase delay follows a Beta distribution. All data, including the outliers ($\bar{\theta}^*_{delay} \le 0.3$), are considered in the

χ^2 test. By using properties of the Beta distribution, the expected frequency, N_i is calculated and presented in Table 5.3, together with the observed frequency, n_i, and the X^2 value, which is defined as:

$$X^2 = \sum_{i=1}^{k} \frac{[n_i - N_i]^2}{N_i} \tag{5.11}$$

where k is the total number of class intervals. The X^2 value gives the sum of the discrepancies in each class interval normalised by the associated expected frequencies. It is a measure of the discrepancy between the observed data and the fitted theoretical probability function. Since the α and β parameters defining the Beta distribution are computed from the sample data, the number of degrees of freedom, $d = k$-3. The width of each class interval is set to be 0.4σ (σ is the standard deviation of the data) as suggested by Bendat and Piersol (1986). They also suggested that $N_i > 3$ in all class intervals so that Eqn. 5.11 gives an acceptable approximation. However, this is not possible here because the sample size is small. Instead, class intervals at both the head and the tail are merged into one interval such that the expected frequencies are greater than one (N_i>1). In addition, the first and last class intervals extend to 0 and 1 respectively. A significance level, α, of 0.05 is adopted for the hypothesis testing, i.e. 1 in 20 chance of the X^2 value exceeding the critical value of $\chi^2_{d;\,\alpha}$. Therefore, the region of acceptance is:

$$X^2 \le \chi^2_{d;\,\alpha} \tag{5.12}$$

As shown in Table 5.3, all beat frequencies except one (2 Hz) pass the χ^2 test. This is rather unfortunate because the 2 Hz beat frequency has the highest number of synchronised tests and hence has the best data among the four beat frequencies. The histogram for 2 Hz appears to be more peaky than the others and it diminishes

quite abruptly at the tail. This explains the higher X^2 value obtained. Fig. 5.10 shows the histograms superimposed with the expected relative frequency curves from the Beta distribution. Note that the first and last class intervals are much wider than the rest because a few intervals are merged to make sure (N_1, N_k) >1. The expected relative frequency for the first interval is slightly higher because it extends to 0. Considering that three out of the four beat frequencies pass the χ^2 test and for consistency of modelling, the Beta distribution is adopted to model the mean phase delay for all beat frequencies. Values of the parameters, α and β, defining the Beta distribution at each beat frequency are given in Table 5.4.

5.2.5. Phase deviation

Two methods of modelling the phase deviation of each test record are considered, first using a Normal distribution and then using an auto-regression algorithm. The former attempt is made because of the standard properties of the Normal distribution which makes it favourable in the modelling process while the latter is based on a hypothesis which will be discussed in section 5.2.5.2.

5.2.5.1. Normal distribution

The phase deviation of each test record is fitted with a Normal distribution which is defined as:

$$y_{\text{gaussian}} = \frac{1}{\sqrt{2\pi}\sigma} \exp\left[-\frac{1}{2}\left(\frac{\theta' - \mu}{\sigma} \right)^2 \right] \tag{5.13}$$

where θ' is the phase deviation, μ is the mean and σ is the standard deviation.

A χ^2 test is again conducted. The histograms for all synchronised tests at all four beat frequencies are presented in Figs. 5.11 to 5.14, superimposed with the expected relative frequency curves. The X^2 and $\chi^2_{d;\,\alpha}$ values (shown in brackets) are shown in each plot. Note that the first and last intervals extend to -∞ and +∞ respectively. For all four beat frequencies, an average of about 58% of the test records pass the χ^2 test. Hence, it can be concluded that the phase deviation does not quite follow a Normal distribution. In the next section, an attempt is made to model the phase deviation using an auto-regression algorithm.

5.2.5.2. Auto-regression process

First, let us postulate that the phase deviation of the k^{th} jump, θ_k', is a linear combination of previous *m* phase deviations added to a new random error $\Delta\theta_k'$:

$$\theta_k' = \sum_{j=1}^{m} \rho_j \, \theta_{k-j}' + \Delta\theta_k' \tag{5.14}$$

in which ρ_j is the j^{th} order auto-regression coefficient.

Consider a phase deviation sequence with *n* data points and there is *m* term regression, there are *n* - *m* equations:

$$\begin{Bmatrix} \theta_{m+1}' \\ \theta_{m+2}' \\ \vdots \\ \vdots \\ \theta_{n-1}' \\ \theta_n' \end{Bmatrix} = \begin{Bmatrix} \theta_m' & \theta_{m-1}' & \cdots & \theta_2' & \theta_1' \\ \theta_{m+1}' & \theta_m' & \cdots & \theta_3' & \theta_2' \\ \vdots & \vdots & & \vdots & \vdots \\ \vdots & \vdots & & \vdots & \vdots \\ \theta_{n-2}' & \theta_{n-3}' & \cdots & \theta_{n-m}' & \theta_{n-m-1}' \\ \theta_{n-1}' & \theta_{n-2}' & \cdots & \theta_{n-m+1}' & \theta_{n-m}' \end{Bmatrix} \begin{Bmatrix} \rho_1 \\ \rho_2 \\ \vdots \\ \rho_{m-1} \\ \rho_m \end{Bmatrix} + \begin{Bmatrix} \Delta\theta_{m+1}' \\ \Delta\theta_{m+2}' \\ \vdots \\ \vdots \\ \Delta\theta_{n-1}' \\ \Delta\theta_n' \end{Bmatrix} \tag{5.15}$$

Or in matrix form:

$$\mathbf{T} = \mathbf{A}\,\mathbf{r} + \mathbf{\Delta T} \tag{5.16}$$

If $n > m+1$ then the set is over-determined and the auto-regression coefficients in $\mathbf{r}$, obtained by minimising the sum of squared error, $\|\Delta\mathbf{T}\|_2$, are given by:

$$\mathbf{r} = \left(\mathbf{A}^T\mathbf{A}\right)^{-1}\mathbf{A}^T\mathbf{T} \tag{5.17}$$

As the order of regression increases, $\|\Delta\mathbf{T}\|_2$ reduces. The task is to select the order of regression such that the remaining errors are acceptable. Auto-regression models of increasing order from one to four (m = 1 to 4) are fitted to each of the phase deviation sequence and the standard deviation of error, $\sigma_{\Delta\theta',m}$, (square root of $\|\Delta\mathbf{T}\|_2$) is presented in Fig. 5.15. At m = 0, the standard deviation of error corresponds to the phase scatter. There is a significant reduction in the standard deviation by applying the first order regression. Table 5.5 presents the reduction in the mean of $\sigma_{\Delta\theta',m}$ relative to the mean of $\sigma_{\Delta\theta',m-1}$ as the order of regression increases. The application of the first order regression reduces the standard deviation by approximately 60% for all four beat frequencies. A further reduction of 10 to 20% is achieved from the second order regression. The errors for most subjects show distributions resembling the bell shaped curve of the Normal distribution. These observations imply that there is some structure in the phase deviation sequence which can be modelled by the auto-regression model and the subsequent error by a Normal distribution.

Considering the significant reduction in standard deviation achieved by the first order of regression and the possibility of modelling the errors using a Normal distribution, the k^{th} phase deviation is given by:

$$\theta'_k = \rho_1\,\theta'_{k-1} + \Delta\theta'_k \tag{5.18}$$

Eqn. 5.18 means that the timing of the k^{th} jump is influenced only by the timing of the $(k\text{-}1)^{th}$ jump scaled by a factor of ρ_1 plus a random error given by $\Delta\theta_k'$. In other words, the jumper adjusts the timing of the current jump according to the timing of the previous jump with a slight random error introduced to each jump. The next task is to model the ρ_1 and $\Delta\theta_k'$ of all subjects. These are presented in the following two sections.

5.2.5.3. Auto-regression coefficient

Fig. 5.16 shows histograms of the regression coefficient, ρ_1, for all subjects at each of the four beat frequencies, superimposed with the relative frequency curves. The ρ_1 values skew to the right, with most of the values between 0.8 and 1.

The regression coefficient, ρ_1, is related to the phase scatter, $\sigma_{\theta'}$, which is a measure of an individual's degree of synchronisation with the beat. Fig. 5.17 shows plots of ρ_1 against $\sigma_{\theta'}$ for each of the four beat frequencies. There is a slight parabolic trend in the data: low ρ_1 values correspond to low $\sigma_{\theta'}$ values and ρ_1 approaching 1 as the $\sigma_{\theta'}$ increases. Theoretically, a low ρ_1 value is expected for well synchronised jumps with small deviation about the mean phase delay. $\rho_1 = 0$ corresponds to a perfectly synchronised test. The plots in Fig. 5.17 show $\rho_1 > 0$ which corresponds to an increasing trend for the phase deviations, most probably due to exhaustion as the jumping duration increases. For unsynchronised tests, the ρ_1 values are found to be greater than 1. Therefore, the possible range for a synchronised test is $0 \le \rho_1 \le 1$.

Considering the skewness of the ρ_1 distributions in Fig. 5.16 and its range of

$0 \le \rho_1 \le 1$, a Beta distribution is fitted. A χ^2 test is conducted and the calculations, tabulated in Table 5.6, show that all beat frequencies pass the χ^2 test. Therefore, the Beta distribution is adopted to model the auto-regression coefficient. Values of the α and β parameters defining the Beta distribution for each beat frequency are presented in Table 5.7. Fig. 5.18 shows the histograms superimposed with the expected relative frequency curves from the Beta distribution. Note that the first and last class intervals are wider because they extend to 0 and 1 respectively.

5.2.5.4. Random error

The random error from the first order regression of each test record is fitted with a Normal distribution. The mean, $\mu_{\Delta\theta',m=1}$, and standard deviation, $\sigma_{\Delta\theta',m=1}$, defining the Normal distribution are estimated from the sample data. A χ^2 test is conducted. The histograms for all synchronised tests at all four beat frequencies are presented in Figs. 5.19 to 5.22, superimposed with the expected relative frequency curves. The corresponding X^2 and $\chi^2_{d;\,\alpha}$ values (shown in brackets) are also shown in each plot. Note that the first and last intervals extend to -∞ and +∞ respectively. For all four beat frequencies, more than 90% of the test records pass the χ^2 test. Hence, it can be concluded that the random error follows a Normal distribution. In comparison, only 58% of the phase deviation are found to pass the χ^2 test when fitted with a Normal distribution.

The mean of the random error is a function of the boundary conditions and the regression coefficient (see Appendix B for proof). Its variation between individuals is insignificant compared to the standard deviation. Therefore, it is assumed to be a

constant with a value of zero for all subjects in the simulations. Hence only the standard deviation needs to be modelled. Fig. 5.23 shows the histograms of $\sigma_{\Delta\theta',m=1}$ superimposed with the relative frequency curves for all four beat frequencies. Most values are between 0° and 20°. Considering the rather peaky and skewed distribution, a Beta distribution function is fitted. An arbitrary range of $0 \le \sigma_{\Delta\theta',m=1} \le 180^{o}$ is set for the purpose of curve-fitting. A transformation of variable is performed:

$$\sigma^{*}_{\Delta\theta',m=1} = \sigma_{\Delta\theta',m=1} / 180 \tag{5.19}$$

such that

$$0 \le \sigma^{*}_{\Delta\theta',m=1} \le 1 \tag{5.20}$$

A χ^2 test is conducted and the calculations are presented in Table 5.8. Two beat frequencies (2 and 2.67 Hz) fail the test. This is due to large discrepancies at the end intervals. The intermediate intervals, which contain most of the data points, give a good fit. Therefore, it is reasonable to use the Beta distribution to model the standard deviation of the random error. The α and β parameters defining the Beta distributions are given in Table 5.9. The histograms superimposed with the expected relative frequency curves are shown in Fig. 5.24.

5.2.5.5. Correlation

A correlation analysis is performed to investigate the linear relationship between the regression coefficient, ρ_1, and the standard deviation of random error, $\sigma_{\Delta\theta',m=1}$. Fig. 5.25 shows plots of ρ_1 against $\sigma_{\Delta\theta',m=1}$. Compared to the plots in Fig. 5.17 for the un-regressed phase deviation data, the parabolic trend has disappeared after the

application of the auto-regression algorithm. A check on the linear relationship between the two parameters finds that the correlation coefficient falls between –0.02 and 0.06 for all four beat frequencies. Therefore, it can be concluded that there is no correlation between the two parameters and they can be treated as independent random variables.

5.3. Impulse shape

As mentioned before in Chapter 2, the half-sine function is widely used to represent a single jumping impulse although no verification has been conducted. In this section, three analytical functions, including the half-cosine function which is equivalent to the half-sine function, are used to curve-fit the measured impulses. The best fit function is identified and its frequency content is compared with that of the measured impulses.

5.3.1. Load profile

The impulses for three subjects are reproduced in Fig. 5.26 for all four beat frequencies, with each column corresponding to one beat frequency and each row corresponding to one subject. The three subjects are chosen because each has a different impulse profile at 1.5 Hz which is related to the value of the maximum normalised load, called the impact factor k_p. The impact factor has values of approximately 2, 3 and 4 and above which correspond to profiles of twin peaks (first subject in Fig. 5.26), merging of twin peaks (second subject) and single peak (third subject) respectively. For the twin peaks, the first peak is the landing impulse while the second peak is the launching impulse. Among the 55 test subjects

performing synchronised jumps at 1.5 Hz, 6 are found to have the twin peaks impulse shape. The majority of the subjects have the merging of the twin peaks impulse shape. For higher frequencies of 2, 2.67 and 3.5 Hz, the impulses are mostly single peaks.

5.3.2. Curve-fitting impulse

Three analytical functions are used to curve-fit the measured impulses:

Normal distribution function:

$$y_{\text{gaussian}} = \frac{k_p}{\sqrt{2\pi}\sigma} \exp\left[-\frac{1}{2}\left(\frac{t-\mu}{\sigma} \right)^2 \right] \tag{5.21}$$

Cosine function:

$$y_{\cos} = k_p \cdot \cos\left(\frac{\pi\, t}{\tau} \right) \qquad \text{for} \quad \frac{-\tau}{2} \le t \le \frac{\tau}{2} \tag{5.22}$$

Cosine-squared function:

$$y_{\cos^2} = k_p \cdot \cos^2\left(\frac{\pi\, t}{\tau} \right) \qquad \text{for} \quad \frac{-\tau}{2} \le t \le \frac{\tau}{2} \tag{5.23}$$

The Normal distribution is used because of its standard statistical properties which would make the analysis process simpler. The cosine and cosine-squared functions are used because of their close resemblance in shape with the measured impulses. For each of these functions, one or two parameters are optimised using the method of least squared error. For the Normal distribution function, the mean, μ, and standard deviation, σ, are optimised. For the cosine and cosine-squared functions, the contact period, τ, defined as the amount of time the person is in contact with the

ground, is optimised. The constraint that the total area under the fitted curve and the measured impulse are equal is applied in the optimisation process.

For assessing the goodness of the fit, the root-mean-squared-error (RMSE) for each impulse is calculated:

$$\text{RMSE} = \sqrt{\frac{\sum (F' - F'_{\text{fitted}})^2}{N_p}} \tag{5.24}$$

where F' is the normalised measured load, F'_{fitted}, is the fitted function and N_p is the number of points fitted.

For each test record, the mean RMSE value, μ_{RMSE}, is calculated by taking the mean of the RMSE values for all the impulses in that test:

$$\mu_{\text{RMSE}} = \frac{\sum (\text{RMSE})}{N_I} \tag{5.25}$$

where N_I is the number of impulses in each test record.

For the 1.5 Hz data, impulses with twin peaks are not considered in the curve-fitting. The μ_{RMSE} values for all three functions are plotted in Fig. 5.27 with each plot corresponding to one beat frequency and within each plot, each column corresponds to one test record. The data are plotted in ascending order of the μ_{RMSE} values of the cosine-squared function. For 1.5 Hz, the cosine function gives the best fit. The cosine-squared function gives the best fit for 2 and 3.5 Hz. The higher μ_{RMSE} values given by the cosine and Normal distribution functions at these frequencies are due to poorer fit of the contact period. For 2.67 Hz, both the cosine-squared and Normal distribution functions are equally good. The error for 1.5 Hz is slightly higher than

those of the higher frequencies which have μ_{RMSE} values less than 0.2. Fig. 5.28 shows a sample of the measured impulses superimposed with the fitted cosine-squared functions for a range of RMSE values. The cosine-squared function fits very well except for 1.5 Hz with high RMSE values due to local irregularities in the measured impulses. For modelling, it is better to adopt one analytical function to define the impulse profile. To achieve this, the mean of all μ_{RMSE} values for all three functions are calculated and presented in Table 5.10. The last column gives the sum of the mean μ_{RMSE} values for all four beat frequencies. The cosine-squared function gives the lowest total error and hence is adopted to model the impulse profile.

5.3.3. Frequency content

This section compared the frequency content of the measured and fitted cosine-squared impulses. First, the average impulse of each test record is obtained by taking the mean of the time-shifted impulses shown in Figs. 5.3 to 5.6.

Any periodic signal, $x_p(t)$, can be represented as a Fourier Series,

$$x_p(t) = a_0 + \sum_{n=1}^{\infty} [r_n \sin(2n\pi f t + \phi_n)] \tag{5.26}$$

The Fourier coefficients, r_n, for a periodic signal generated from the average impulse are obtained by taking the Fast Fourier Transform at a sampling frequency of 200 Hz. Test records with twin peaks impulse shape at 1.5 Hz are not considered. The Fourier coefficients for the first three harmonics are presented in Fig. 5.29. Each plot corresponds to one beat frequency. The mean values of the Fourier coefficients are given in Table 5.11. For all beat frequencies, the average impulse is

dominated by the first harmonic with decreasing Fourier coefficients for higher harmonics.

Similarly, the Fourier coefficients of the cosine-squared function fitted to each average impulse are calculated. The Fourier coefficient relative error, given by the difference between the Fourier coefficients of the cosine-squared function and the average impulse, divided by the Fourier coefficient of the average impulse, is shown in Fig. 5.30 for the first two harmonics. Most of the relative errors are within the range of ±10%, indicating good compatibility in the frequency content between the measured and the fitted cosine-squared impulses. The Fourier coefficients for the higher harmonics are not considered because they are of very small magnitude.

5.4. Relationship between impulse size and timing

In section 5.2, the impulse timing is modelled using the auto-regression algorithm. In section 5.3, the cosine-squared function is used to model the impulse shape. For simulating a jumping load-time history, it is necessary to know the relationship between the impulse timing and size. This section looks at the relationship between these two aspects.

Firstly, a relationship between the impulse size and timing is established. Then, the contact ratios of each test record, which define the impulse sizes, are modelled using the Normal distribution function. Lastly, the correlation between the contact ratio and the impulse timing is investigated.

5.4.1. Impulse size and timing

First, define the magnitude of the k^{th} impulse, I_k, as the area under each impulse:

$$I_k = \int_0^{\tau} F' dt \tag{5.27}$$

where F' is the normalised load and τ is the contact period.

Assume that the jumping impulses are infinitesimally short. Consider what governs the magnitude of the k^{th} impulse, I_k, which we shall say occurs at time t_k. Immediately prior to the impulse the jumper (of mass m) will be descending with a velocity, $v_k^{\downarrow}$, and afterwards will be ascending with a velocity $v_k^{\uparrow}$. The magnitude of the impulse is therefore given by:

$$I_k = m(v_k^{\downarrow} + v_k^{\uparrow}) \tag{5.28}$$

The time the jumper spends in the air before the next impulse is:

$$t_{k+1} - t_k = \frac{2v_k^{\uparrow}}{g} \tag{5.29}$$

and because the jumper loses no energy whilst in the air:

$$v_{k+1}^{\downarrow} = v_k^{\uparrow} \tag{5.30}$$

Each impulse is therefore made up of two components - a launching impulse which projects the jumper into the air from rest and a landing impulse, which is necessary to bring the mean velocity of the jumper to zero and is the same magnitude as the previous launching impulse. We can combine these last three equations to give:

$$I_k = \frac{mg}{2}(t_{k+1} - t_{k-1}) \tag{5.31}$$

The timing of each impulse is given by t_{eff} and the measured impulse is normalised by the static weight of the subject, hence giving:

$$i_k = \frac{1}{2}(t_{\text{eff},k+1} - t_{\text{eff},k-1}) \tag{5.32}$$

Eqn. 5.32 is verified with the experimental measurements, shown in Fig. 5.31 as plots of the measured i_k against the theoretical i_k, with both parameters normalised by the beat period. The measured i_k is obtained from Eqn. 5.27 and the theoretical i_k from Eqn. 5.32. Ideally, the data should show a linear relationship with a slope of 1. Instead, the data show a linear relationship but with a slope of slightly greater than 1. A line of best fit is fitted to the data in Fig. 5.31 and the coefficients are presented in Table 5.12. There are some measured i_k values which are much lower than the theoretical values because the jumper landed partially outside the force plate. Hence when curve-fitting the data, measurements with i_k values less than 0.75 times the beat period are not considered in the linear regression. Also shown in Table 5.12 is the maximum absolute i_k error, given by the maximum absolute difference between the theoretical and measured i_k values within the range of 0.9375 to 1.0625 in which most data fall into. The maximum error is small, i.e. 0.02 times the beat period for 1.5 Hz. One possible cause of error is the assumption that the impulse is instantaneous. In reality, the jumping impulse is distributed over the contact period with the landing and launching actions occurring one after the other. Due to the small magnitude of error involved, no attempt is made to find out the cause of the error.

5.4.2. Contact ratio and impulse timing

Using the cosine-squared function in Eqn. 5.23, the impulse size can be expressed

as a function of the contact ratio and impact factor:

$$i_k = \int_{-\tau/2}^{\tau/2} k_p \cdot \cos^2\left(\frac{\pi t}{\tau}\right) dt = \frac{k_p \tau}{2} \tag{5.33}$$

Relating the impulse size to the impulse timing:

$$\frac{k_p \tau}{2} = \frac{1}{2}(t_{\text{eff}\,(k+1)} - t_{\text{eff}\,(k-1)}) \tag{5.34}$$

One of the two parameters defining the cosine-squared function (k_p and τ) needs to be modelled in order to simulate the jumping impulses. The following section presents modelling of the contact ratio.

5.4.2.1. Contact ratio modelling

All measured impulses are approximated using the cosine-squared function, giving the contact ratios. The contact ratios of each test record are fitted with a Normal distribution function. The mean, μ_α, and standard deviation, σ_α, defining the Normal distribution function are estimated from the sample data. A χ^2 test is conducted. The histograms for all contact ratios at all four beat frequencies are presented in Figs. 5.32 to 5.35, superimposed with the expected relative frequency curves. Also shown in each plot are the corresponding X^2 and $\chi^2_{d;\,\alpha}$ values (shown in brackets). Note that the first and the last intervals extend to -∞ and +∞ respectively. For all four beat frequencies, more than 90% of the test records pass the χ^2 test. Hence, it can be concluded that the variation of the contact ratio is adequately described by a Normal distribution.

The mean and standard deviation of the random error, μ_α and σ_α, need to be modelled. Figs. 5.36 and 5.37 show the histograms of μ_α and σ_α respectively for all

four beat frequencies superimposed with the relative frequency curves. As shown in Fig. 5.36, the mean contact ratios are higher than 0.4 for all four beat frequencies. This agrees with the findings from Yao et al. (2003) which found that the contact ratios were above 0.5. The range of 0.25 to 0.67 given in BS 6399: Part 1 (British Standards Institution 1996) seems to be too low. The distribution becomes narrower as the beat frequency increases, indicating there is less inter-subject variation as the jumping pace increases. Considering the rather peaky and skewed distributions, Beta distribution functions are fitted over the range of $0 \le \mu_\alpha \le 1$ and $0 \le \sigma_\alpha \le 1$.

A χ^2 test is conducted and the calculations are presented in Tables 5.13 and 5.14. All pass the χ^2 test except one (μ_α for 3.5 Hz), which fails the χ^2 test due to the unusually large count for the middle interval. Hence it can be concluded that both parameters are adequately described by the Normal distribution function. The histograms superimposed with the expected relative frequency curves are shown in Figs. 5.38 and 5.39. The α and β parameters defining the Beta distributions are given in Tables 5.15 and 5.16.

A correlation analysis is conducted to investigate the relationship between the mean and standard deviation of the contact ratio. Fig. 5.40 shows plots of the standard deviation versus the mean for all four beat frequencies. The correlation coefficient is calculated and shown as the k values in the figure. The first three beat frequencies show moderate correlation with k values of around 0.6 while the last beat frequency shows no correlation with $k = 0.1$. There are two options available: either treating both parameters as dependent or independent variables. Both options

are equally appropriate considering the k values very close to 0.5 for the first three beat frequencies. Hence, it is decided that both parameters will be treated as independent random variables.

5.4.2.2. Correlation between contact ratio and impulse timing

Knowing that the impulse size and impulse timing are related according to Eqn. 5.34, this section looks at the correlation between the contact ratio and impulse timing.

Figs. 5.41 to 5.44 show plots of the contact ratio against the impulse size for all four beat frequencies. Also shown in each plot is the value of the correlation coefficient, k, and the plots are arranged in order of increasing k values. The k values fall between 0 and 1. A low k value, say $k < 0.3$, means that there is no correlation between the two variables and both can be modelled as independent random variables. A high k value, say $k > 0.7$, means that there is a strong linear relationship between the two variables and it should be modelled using a regression line. Overall, the k values are found to be lower for higher beat frequencies, indicating there is a higher degree of randomness and hence less correlation between the contact ratio and impulse size as the subject jumps faster. At lower beat frequencies, the jumpers vary their impulse sizes by controlling their contact durations with the ground.

There are two ways of modelling the contact ratio, depending on the degree of dependency between the two parameters, a regression line for high k values and a Normal distribution function for low k values. An error analysis is conducted by

calculating the response of a SDOF structure due to three load cases: (1) the actual measured load; (2) a load-time history generated using the measured impulse timing and the impulse shape defined by the contact ratio modelled using a regression line; (3) a load-time history generated using the measured impulse timing and the impulse shape defined by the contact ratio sampled from a Normal distribution presented in section 5.4.2.1. The difference between load cases (2) and (3) is that the former is treating the contact ratio as linearly dependent on the impulse size while the latter treats the contact ratio as an independent variable following a Normal distribution.

The relative errors of load cases (2) and (3) compared to load case (1) are calculated. The error analysis is conducted for all test records with $k > 0.7$. No analysis is conducted for the 3.5 Hz beat frequency because only one test record has $k > 0.7$. It is expected that the error due to load case (3) is the upper bound because the loads generated in (2) are closer to the actual measured loads compared to (3). Analyses are conducted for SDOF structures with natural frequencies within ±10% of the first three harmonics of the beat frequency.

From the calculated responses, two parameters are obtained: maximum displacement and the root-mean-square (RMS) acceleration, both normalised by the stiffness of the structure. An example of the results, plotted as the normalised maximum displacement versus the natural frequency of the structure, is presented in Fig. 5.45 for beat frequency of 1.5 Hz with each plot corresponding to one load case.

The errors of load cases (2) and (3) relative to (1) are calculated and their means for

structures within ±10% of each harmonic are presented. Figs. 5.46 to 5.48 present the mean relative error for the normalised maximum displacement at beat frequencies of 1.5, 2 and 2.67 Hz. Similar plots for the normalised RMS acceleration are presented in Figs. 5.49 to 5.51. In each figure, there are three plots, giving the mean relative error for structures at each harmonic. All results show that the simulated loads give higher responses than the measured loads.

The overall mean, tabulated in Tables 5.17 and 5.18, reveals that the first and second harmonics show results as expected, i.e. the relative error due to load case (3-Normal) is higher than that due to load case (2-Regression) although the difference is not large. However, for the third harmonic, the error due to load case (2) is significantly higher than (3). This is probably due to the linear regression not taking into account the high frequency local variation in the contact ratio which can be significant on high frequency structures. Hence, it is decided to use the Normal distribution to model the contact ratio. From the analysis, it is found that the maximum relative error from the simulated loads is approximately 25% for the maximum displacement and 50% for the RMS acceleration, as shown in Tables 5.17 and 5.18.

5.5. Conclusions

The work presented in this chapter is based on the premise that the jumping record of each individual should be analysed separately. Each jumping record is modelled as successive cosine-squared impulses and the timing of each impulse is given by the time at the impulse centroid. The impulse timings of each record are modelled using an auto-regression algorithm based on the hypothesis that the timing of the

previous jump influences the timing of the next jump due to the jumper wanting to synchronise his timings with the audio beeps. Using the assumption that the human body is a rigid mass, the size of each impulse, derived from the Law of Conservation of Momentum, is a function of the impulse timing.

From the auto-regression model, the phase delay of the k^{th} jump is given by:

$$\theta_{\text{delay},k} = \overline{\theta}_{\text{delay}} + \rho_1 \, \theta'_{k-1} + \Delta\theta'_k \tag{5.35}$$

All parameters in Eqn. 5.35 are fitted with probability distribution functions, as summarised in the flowchart in Fig 5.52. The impulse shape, modelled using a cosine-squared function, is defined by the contact ratio, its modelling is summarised in the flowchart in Fig. 5.53. The various correlation analyses show that each variable can be treated as an independent variable in the simulation process. Monte Carlo simulations, based on the fitted probability distribution functions, are presented in the next chapter.

Chapter 6

6. Joint crowd-SDOF system subjected to crowd jumping loads

This chapter puts together the tools developed in the previous chapters. The aim is to calculate the response of the joint crowd-SDOF system developed in Chapter 4 when subjected to crowd jumping loads. This chapter consists of two main parts. The first part is about simulating individual jumping loads based on the statistical models developed in Chapter 5 (section 6.1). The second part analyses the joint crowd-SDOF system subjected to these simulated jumping loads (section 6.2). The structural responses due to crowd jumping loads of various crowd sizes are obtained and presented in charts. An example is presented to illustrate the use of these charts. Various factors affecting the structural response due to crowd jumping loads are discussed. Lastly, the limitations to the results presented here are stated.

6.1. Jumping load simulation

The procedures for simulating individual load-time histories are illustrated in the flow chart in Fig. 6.1. For each load-time history, two sets of parameters need to be generated: one set describing the impulse timing and the other the impulse shape. The impulse timing is defined by the effective timing, t_{eff}, which can be calculated from three parameters: mean phase delay, $\overline{\theta}_{\text{delay}}$, auto-regression coefficient, ρ_1, and random error $\Delta\theta'$. For the impulse shape, each impulse is modelled by a cosine-squared function defined by the contact ratio, α. All these parameters are fitted with either Beta or Normal distributions, as presented in Chapter 5. A Monte Carlo method, i.e. sampling of random variables from probability distribution

functions, is used to simulate individual jumping loads. The whole process, described in the flowchart in Fig. 6.1, is implemented in MATLAB® Statistics Toolbox (MathWorks, Inc.).

First, one needs to decide the number of load-time histories to be simulated, denoted as N. Simulations are conducted for beat frequencies of 2, 2.67 and 3.5 Hz. No simulation is conducted for the 1.5 Hz beat frequency because most of the measured impulses have either twin peaks or merging of the twin peaks impulse shapes which cannot be modelled accurately using the cosine-squared function (see sections 5.3.1 and 5.3.2). Considering the duration of one pop song to be between two and three minutes, each load-time history is simulated for duration of two minutes and at a sampling rate of 0.005 s. Five random variables: mean phase delay, $\overline{\theta}_{\text{delay}}$, auto-regression coefficient, ρ_1, standard deviation of contact ratio, $\sigma_{\Delta\theta'}$, mean of contact ratio, μ_α, and standard deviation of random error, σ_α, are sampled from their corresponding probability distribution functions. For each variable, N values are sampled. The number of impulses in each record, M, equals $120/T_{\text{beat}}$, where T_{beat} is the beat period. For each load-time history, M values of $\Delta\theta_k'$ and α_k are sampled (the subscript k refers to the k^{th} impulse). Using these sampled data, four parameters are calculated: effective timing, $t_{\text{eff},k}$, impulse size, i_k, contact period, τ_k, and impact factor, $k_{p,k}$. Each impulse is modelled by the cosine-squared function defined by the τ_k and $k_{p,k}$ values. In the time domain, each impulse is defined by its centroid at $t_{\text{eff},k}$.

In simulating a load-time history, a series of instantaneous pulses are first generated

at times $t_{\text{eff},k}$. Each instantaneous pulse is discretised into two pulses 0.005 s apart with their magnitudes determined by linear weighting from $t_{\text{eff},k}$. The simulated load is obtained by convolving the cosine-squared impulses with their corresponding discretised pulses.

To minimise the error due to discretisation of the pulses, each convolved impulse is scaled such that the impulse size, given by the load-time integral in Eqn, 6.1, equals i_k. The scaling is important to make sure that the total momentum in each impulse is conserved.

$$i_k = \int_0^\tau F' dt \tag{6.1}$$

As an example, Fig. 6.2 shows six simulated load-time histories at beat frequency 2 Hz in the interval from 1 to 4 seconds. As shown in the figure, there is quite a distinctive variation in the impulse timing and impact factor between the six load-time histories. The impact factor varies from 2.5 to 4 and the impulse timing (t_{eff}), which is located at the maximum load, can vary by up to 0.15 s within one beat period. The implications of all these variations on the structural response will be investigated in the next section.

6.2. Joint crowd-SDOF system subjected to crowd jumping loads

6.2.1. Structural response to crowd jumping loads

With N simulated load-time histories now available, it is possible to analyse the response of the joint crowd-SDOF system subjected to these simulated loads, first by calculating the response due to each individual load-time history and then

randomly sampling the responses (i.e. Monte Carlo method) and summing them to get the response due to loading by a crowd. The steps are outlined in the flow chart in Fig. 6.3. The block diagrams on the left show the steps in the analysis while those on the right give the outputs of each step.

The joint crowd-SDOF system being analysed here is the same as the one specified in Chapter 4 and shown in Fig. 4.4. It consists of a crowd of standing people represented by the 2DOF model derived in section 4.1, on a SDOF structure with an intrinsic structural damping ratio, ζ, of 2% and a natural frequency of ω_n when empty. The relative mass of the standing crowd to the structure is defined by the mass ratio, γ. Analyses are conducted for various ω_n and γ values.

A total of $N = 1024$ load-time histories are simulated at beat frequencies of 2, 2.67 and 3.5 Hz. For each set of ω_n and γ values, the response of the joint crowd-SDOF system subjected to each load-time history is calculated, giving 1024 sets of acceleration and displacement records.

Out of the 1024 acceleration and displacement records, n records are sampled without replacement and summed to give the resultant structural response due to a group of n jumping loads. Two parameters are used to characterise the structural response: the maximum displacement and the root-mean-squared (RMS) acceleration. The former, given by the maximum absolute value of displacement, is important in assessing the maximum stress in the structure. The latter, defined in Eqn. 6.2, is used for assessing human comfort criteria.

$$\ddot{x}_{\text{rms}} = \sqrt{\frac{\sum_{i=1}^{L} \ddot{x}_i}{L}} \tag{6.2}$$

where L is the total number of sampled point in the acceleration record.

Analyses are conducted for group sizes of n = 2, 4, 8, 16, 32 and 64. For each group size, a total of 200 samplings are made. The running mean, standard deviation and 95-percentile value for the maximum displacement and RMS acceleration are calculated for increasing numbers of samples, with the aim of obtaining the steady average response of the structure.

6.2.2. Example

An example will serve to illustrate the procedure outlined in the flow chart in Fig. 6.3. Analyses are conducted for the following parameters:

Beat frequency = 2 Hz

Natural frequency of structure, ω_n = 2, 4 and 6 Hz

Damping ratio, ζ = 2%

Mass ratio, γ = 0

Number of load-time histories simulated, N = 1024

Group size, n = 2, 4, 8, 16, 32 and 64

Duration of load-time history = 120 s

Sampling rate = 0.005 s

The natural frequencies of the structures are chosen such that each structure is excited by one harmonic of the jumping load. Six out of the 1024 simulated

individual loads are presented previously in Fig. 6.2. The corresponding displacement and acceleration responses are presented in Figs. 6.4 and 6.5 respectively. The displacement is normalised by the static deflection due to a unit load. In the analysis, the mass of the structure is set to 1 kg. The acceleration is normalised by the gravitational acceleration, g = 9.81 m/s^2.

As shown in Figs. 6.4 and 6.5, for the 2 Hz structure, the responses are highly periodic but for the 4 Hz and 6 Hz structures, a greater variation in the periodicity and the magnitude is observed. This indicates that the lack of synchronisation between individuals jumping together affects higher frequencies more. In addition, the third harmonic of loading is less well synchronised compared to lower harmonics.

As expected, the acceleration shown in Fig. 6.5 is identical in shape to the displacement in Fig 6.4 but differs in magnitude and sign. Considering resonance due to excitation by only one harmonic, the acceleration of each structure is approximately $1/k_s \times \omega_n^2$ times the normalised displacement, where k_s is the stiffness of the structure and ω_n is the natural frequency of the structure. Since the mass of the structure is set to 1 kg,

$$k_s = \omega_n^2 \tag{6.3}$$

$$\therefore \ddot{X} = -X / g \tag{6.4}$$

where X is the normalised displacement, $\ddot{X}$ is the acceleration in g (=9.81 m/s^2).

As mentioned before, for each record, the maximum displacement and the RMS acceleration are obtained. Since the jumping load is normalised by the static weight

of the jumper, the maximum displacement, when normalised by the static deflection due to a unit load, is the Dynamic Magnification Factor (DMF).

The distributions of the DMF and RMS acceleration are presented in Figs. 6.6 and 6.7 respectively. As shown in both figures, the distributions seem to shift from a Normal distribution to a skewed (perhaps Rayleigh) distribution as the natural frequency of the structure increases. As we know, each structure is excited by one harmonic of the jumping load. Therefore, each distribution depicts the distribution of one harmonic of the jumping load. The first harmonic of the jumping load follows a Normal distribution while the third harmonic follows a skewed distribution. The second harmonic is in between the two.

Out of the 1024 responses, random samplings are conducted to generate the structural response for group sizes of n = 2, 4, 8, 16, 32 and 64. Altogether, 200 samplings are made for each group size and the running mean, standard deviation and 95-percentile values are calculated. As an example, the running mean, standard deviation and 95-percentile value for the DMF and RMS acceleration are presented in Figs. 6.8 and 6.9 respectively, for the 2 Hz structure. The results are presented as the average response per person (dividing the response by the group size). The 95-percentile value is calculated after every 20 samplings. As seen in these figures, there are some fluctuations in the parameters during the early samplings but they settle to steady state after about 50 samplings. Generally, the steady state is reached at lesser number of samplings for larger crowd sizes. The last value for the running mean, standard deviation and 95-percentile is taken as the representative value.

Recognising that the jumping loads include some random variations, the idea of characteristic response is used. The 95-percentile value is used to represent the characteristic response of the structure (that is, the response that will be exceeded in one case in 20). This is the same as the limit state design philosophy adopted in the British Standards structural design codes. Suppose the structural response follows a Normal distribution, the 95-percentile rule implies that the characteristic response is related to the mean and standard deviation of the response:

$$\mathrm{DMF}_{\mathrm{char}} = \mathrm{DMF}_{\mathrm{mean}} - 1.645 \times \mathrm{DMF}_{\sigma} \tag{6.5}$$

$$\ddot{X}^{\mathrm{rms}}_{\mathrm{char}} = \ddot{X}^{\mathrm{rms}}_{\mathrm{mean}} - 1.645 \times \ddot{X}^{\mathrm{rms}}_{\sigma} \tag{6.6}$$

Using Eqns. 6.5 and 6.6, the 95-percentile values are calculated and compared to those obtained from the sampled values. Both are plotted against the group size in Fig. 6.10 for the DMF and in Fig. 6.11 for the RMS acceleration. As shown, a good match is found between the two. Hence, it can be concluded that the responses follow a Normal distribution. In addition, the characteristic responses are found to vary non-linearly with group sizes up to 16 people and they exhibit an asymptotic behaviour for group sizes larger than 16.

6.2.3. Overall results

The final stage of work involves extending the analyses in section 6.2.2 to structures with natural frequencies varying from 1 to 13 Hz. In addition, structures occupied by a standing crowd with $\gamma = 0.15$ are analysed. The parameters are summarised below:

Beat frequency = 2, 2.67 and 3.5 Hz

Natural frequency of structure, ω_n = 1 to 13 Hz

Structural damping ratio, ζ = 2%

Mass ratio, γ = 0 and 0.15

Number of load-time histories simulated, N = 1024

Group size, n = 2, 4, 8, 16, 32 and 64

Duration of load-time history = 120 s

Sampling rate = 0.005 s

A sample size of 1024 is chosen after an error analysis is conducted. The error analysis looks at the relative error between samples of 256, 512 and 1024 load-time histories. The 512 and 1024 samples are found to give very similar results with minimal discrepancy.

Characteristic response

The example presented in section 6.2.2 shows that the DMF and RMS acceleration follow a Normal distribution. The idea of characteristic response is used by taking the 95-percentile value. From a design perspective, this means that the probability of a structure having a response greater than the characteristic value is one in 20.

Only the characteristic response for the DMF and RMS acceleration are presented in this chapter. The mean, standard deviation and the characteristic responses calculated using Eqns. 6.5 and 6.6 are presented in Appendix C.

Variation of characteristic response with natural frequency of structure

Results for variation of the characteristic DMF with the natural frequency of the

empty structure are presented for beat frequency of 2 Hz, $\gamma = 0$ (Fig. 6.12) and $\gamma = 0.15$ (Fig. 6.13); beat frequency of 2.67 Hz, $\gamma = 0$ (Fig. 6.14) and $\gamma = 0.15$ (Fig. 6.15); beat frequency of 3.5 Hz, $\gamma = 0$ (Fig. 6.16) and $\gamma = 0.15$ (Fig. 6.17). Results for the characteristic RMS acceleration are presented in the same sequence in Figs. 6.18 to 6.23.

From these figures, the general observation is that there are three resonant peaks due to excitation by the first three harmonics of loading. There is a significant reduction as the group size increases and this will be discussed further in the next paragraph. Overall, for $\gamma = 0$, the characteristic DMF falls within the range of 30 to 45 for all three beat frequencies while the characteristic RMS acceleration falls within the range of 2g to 3g, due to excitation by the first harmonic. Jumping loads at 2 Hz produce the highest DMF, follow by jumping loads at 2.67 Hz and 3.5 Hz. Comparing results between $\gamma = 0$ and 0.15, the presence of the passive crowd adds significant damping to the structure. The damping effect of the passive crowd is most significant on structures with natural frequencies from 4 to 8 Hz. Hence the greatest reduction in structural response is found on the second and third harmonic resonant peaks. In addition, for $\gamma = 0.15$, the resonant peaks are located at natural frequencies slightly higher than the harmonic frequencies. This is due to the occupied structures having natural frequencies slightly lower than the empty structures.

Variation of characteristic response with group size

To summarise, results for the variation of the maximum response at each resonant peak with the group size are presented in Figs. 6.24 ($\gamma = 0$) and 6.25 ($\gamma = 0.15$) for

the DMF; and in Figs. 6.26 ($\gamma = 0$) and 6.27 ($\gamma = 0.15$) for the RMS acceleration. Similar to the trends shown earlier in Figs. 6.10 and 6.11, a non-linearity is found for groups of up to 16 people and an asymptotic behaviour for groups with more than 16 people.

For experimental tests conducted to measure the jumping loads of a large crowd on a cantilever grandstand, the results in Figs. 6.24 to 6.27 imply that tests with less than 16 jumpers are likely to overestimate the jumping loads. On the other hand, the asymptotic trend observed for groups with more than 16 people suggests that when modelling large crowds, a group size of 16 or 32 is sufficient.

Estimating response of a cantilever grandstand

For design purposes, the charts in Figs. 6.12 to 6.17 allow one to estimate the characteristic DMF for one mode of the cantilever grandstand. Similarly, the charts in Figs. 6.18 to 6.23 allow one to estimate the characteristic RMS acceleration for one mode of the cantilever grandstand. These charts are derived from analyses on SDOF structures having a damping ratio of 2% and are for group sizes up to 64 people. For groups with more than 64 people, the values for group size of 64 people can be used since the trend seems to reach an asymptotic behaviour as noted in Figs. 6.24 to 6.27. The guidelines on how to use these charts are summarised in the flow chart in Fig. 6.28 and illustrated using an example below.

Example

Consider one bay of seating decks supported by a cantilever having a span of 9 m between steel frames and a length of 14 m. The bay has 15 rows and each row has

approximately 14 seats (estimated from a seat width of 500 mm). Therefore, the total number of seats per bay is 210. For a typical mass of 80 kg for one person, the total weight of the crowd is 165 kN. Assuming that the mass of the crowd is 0.3 times the mass of the structure, therefore, the mass of the structure, m_s is 56000 kg. Assume that the structure's fundamental mode is 4 Hz and its modal mass equals the actual mass, its modal stiffness, k_s is given by:

$$k_s = \omega_n^{\,2} \cdot m_s = (4 \cdot 2 \cdot \pi)^2 \cdot 56000 = 35.4\,\text{MN/m} \tag{6.7}$$

Obtaining the DMF_{char} values from Figs. 6.12 and 6.17 (for n = 64), the maximum deflection of the structure is given by:

$$X_{\max} = \text{DMF}_{\text{char}} / k_s \times W_{\text{active}} \tag{6.8}$$

where W_{active} is the weight of the jumping crowd in Newton.

Obtaining the $\ddot{X}_{\text{char}}^{\text{rms}}$ values from Figs. 6.18 and 6.23 (for n = 64) and since in the analysis, the mass of the structure is set to 1 kg, the RMS acceleration of the structure is given by:

$$\ddot{X}_{\text{rms}} = \ddot{X}_{\text{char}} / m_s \times W_{\text{active}} \tag{6.9}$$

where m_s is the mass of the structure and W_{active} is the weight of the jumping crowd in Newton.

The results are tabulated in Tables 6.1 and 6.2 for γ = 0 (all the spectators jumping) and γ = 0.15 (50% jumping and 50% standing) respectively. From Tables 6.1 and 6.2, a maximum displacement of 69.5 mm and a maximum RMS acceleration of 2.21*g* are obtained when the whole crowd jumps at 2 Hz. These large responses are due to resonance excited by the second harmonic of the jumping loads. The

responses are significantly reduced when half of the crowds are standing. In fact, a reduction of up to 89% is found for the RMS acceleration at 2 Hz beat frequency when half of the crowd are standing. The reduction in structural response is due to both the halving of the jumping loads and the damping contributed by the standing crowd. For the 3.5 Hz beat frequency, it is interesting to note that the RMS accelerations for both $\gamma = 0$ and $\gamma = 0.15$ are the same. This is due to the resonant peak located at frequencies slightly higher than 3.5 Hz due to the presence of the passive crowd. The higher response for a 4 Hz structure with $\gamma = 0.15$ compared to $\gamma = 0$ compensates for the halving of the jumping loads.

6.2.4. Discussion

One of the limitations with using the charts in Figs. 6.12 to 6.23 is that only three beat frequencies are considered. A structure with natural frequency of say, 5 Hz, is prone to resonance due to a jumping load at 2.5 Hz. Due to only three beat frequencies being considered, no attempt is made to investigate the variation of the structural response with the beat frequency. However, the general observation from the results is that the structural response tends to reduce with increasing beat frequency.

There is also the issue on the upper limit for the crowd jumping frequency. Assume it is 3.5 Hz, therefore, structures with natural frequencies less than 3.5 Hz are prone to resonance by the first harmonic of the crowd jumping load. Structures with natural frequencies between 3.5 and 7 Hz are prone to resonance by the second harmonic and similarly, structures with natural frequencies between 7 and 10.5 Hz are prone to resonance by the third harmonic. However, if the highest crowd

jumping frequency is 2.8 Hz, then structures with natural frequencies greater than 5.6 Hz undergo resonance due to excitation by the third harmonic and not the second harmonic. Most research seems to agree on an upper limit of 2.8 Hz. The upper limit also varies with the type of event, e.g. pop concert by a pop rock band is more lively than a normal premier league football match; as well as the age group of the audience.

In addition, it is important to bear in mind that the statistical models of the jumping loads are derived from tests of individuals jumping alone. The effect from jumping together with others is not considered. This issue is dealt with briefly in the next chapter.

The possibility of jumping at a frequency which coincides with the natural frequency of the structure is still uncertain. Yao et al.'s tests (2003) showed that this was not possible but their tests involved very few test subjects. Testing more subjects might give a more convincing finding.

In addition, only results for synchronised tests are analysed. Hence the worst case scenario is considered here, without taking into account individuals who are jumping out of synchronisation with the beat.

The charts in Figs. 6.24 to 6.27 are useful for predicting the maximum response due to excitation by the first three harmonics. Due to several limitations mentioned above, it is left to the discretion of the engineers to decide how these results are to be used in their analysis of a cantilever grandstand.

6.3. Conclusions

This chapter puts together all the tools that have been developed throughout this thesis in order to analyse the response of a SDOF system either empty or occupied by a passive crowd. The Monte Carlo method of random sampling is adopted to simulate a sample which consists of 1024 jumping load-time histories. Random samplings are then conducted to calculate the structural responses due to crowd jumping loads of various group sizes. The results, presented in charts in Figs. 6.12 to 6.27, allow engineers to estimate the response of a SDOF system subjected to crowd jumping loads. These results should be used with discretion, taking into consideration the possible crowd jumping frequency and the harmonic of excitation. In addition, it is important to be aware that the visual effect due to jumping in a group and the flexibility of the structure are not considered in the derivation of the crowd jumping model.

Chapter 7

7. Experimental jumping and bobbing tests

Two areas are covered in this chapter. Firstly, an initial investigation on bobbing loads is carried out by conducting individual bobbing tests in the laboratory. As mentioned in Chapter 2, bobbing is an interesting mechanism which has the potential of being synchronised by the movement of the structure and hence, producing high level of structural response. Secondly, the effect of jumping together with another person is investigated. The results will give an indication on the reliability of the statistical load models developed in Chapter 5 which is based on measurements of individual jumping tests.

This chapter reports on the experimental tests conducted in the Structural Dynamics Laboratory at the University of Oxford. It is divided into two sections. The first part reports on jumping and bobbing tests conducted to investigate the effect of the beat frequency on the forces that can be generated by one individual on a rigid platform. The second part reports on jumping tests involving two people facing each other, aiming to investigate the degree of synchronisation between two people. For each part, a description of the experimental tests is first given, followed by a description on how the data are handled. Lastly, an analysis of the load measurements in terms of the degree of synchronisation, impulse timing and impulse shape is presented.

7.1. Individual jumping and bobbing tests

7.1.1. Experimental tests

A total of 10 male participants took part in the test series. The means and standard deviations of the age and body weight of the subjects are presented in Table 7.1.

Tests are conducted at six beat frequencies: from 1 to 3.5 Hz at an increment of 0.5 Hz. Each test involves a single participant jumping on a 0.4 m x 0.4 m load cell which measures the vertical loads (see Fig. 7.1). The load cell comprises three load-sensing elements sandwiched between 20 mm thick aluminium alloy top and bottom plates. The overall depth is 85 mm. The top plate has dimensions 400 mm × 400 mm, it is sufficiently rigid with a fundamental frequency of around 150 Hz, allowing the load to be transferred to the elements without excessive vibration or deformation within the load cell. A calibration test is conducted by successive loadings of dead weights up to a maximum load of 200 kg and unloadings at the centre and the four corners of the rectangular top plate. The calibration factor is taken from the mean of all five locations. The five measurements have a mean of 2145.08 kg/volt and a standard deviation of 4.4 kg/volt.

During each test, the load cell is placed on a very stiff floor, enclosed by a wooden platform so that the subject would not fall if landing outside the top plate. Each test starts with the subject standing still on the load cell followed by jumping for 40 s in time to regular beeps. The beeps are generated from a digital pulse signal converted to an analogue signal and transmitted to an audio transformer. The digital periodic

pulses are defined in terms of the pulse period and width. The pulse period is given by the inverse of the beat frequency while the pulse width is varied for each beat frequency such that the sharpest beep is heard. Both the beep and load signals are recorded at a sampling interval of 1 ms.

7.1.2. Data handling

The jumping test records are handled in the same way as the load measurements from Parkhouse and Ewins (2004), presented in Chapter 5. Each test record is separated into individual impulses by splitting at intervals of zero loads. For bobbing, each test record is separated into individual impulses at instants when the body momentum equals zero. The procedure is based on Newton's Second Law of Motion which states that the integral of the force acting on the body is given by the change in its momentum,

$$\int_{t_1}^{t_2} F \, \mathrm{d}t = m(v_2 - v_1) \tag{7.1}$$

where F is the force acting on a rigid body of mass m and v is the velocity of the body.

At the start of each test, the subject stands still on the load cell. Therefore, the initial velocity v_1 equals zero. When bobbing, the velocity changes and at the end of each bob, the velocity returns to zero, i.e. v_2 equals zero. The impulse is given by the area under the effective dynamic load F_d, which is defined as the measured force minus the self-weight of the subject:

$$F_d = F_{\text{measured}} - mg \tag{7.2}$$

Therefore,

$$\int_{t_1}^{t_2} F_{measured}\ \mathrm{d}t = mg\left(t_2 - t_1\right) \tag{7.3}$$

Each bobbing impulse is therefore split at the intersection of the measured force-time and static weight-time integrals. The first attempt to separate the bobbing impulse fails because this 'zero momentum' method, although theoretically sound, is highly sensitive to noise in the measurements. A high pass filter with a cut-off frequency of 0.1 Hz is applied to the measured load to eliminate noise in the measurements before calculating the measured force-time integral. As an example, Fig. 7.2 shows the integral of the filtered measured load over time for subject 9 bobbing at 1 Hz. Due to the high pass filter, the DC offset in the load signal is removed. Instants of zero momentum are thus given by the intersections of the force-time integral and the horizontal axis (marked by circles in the figure). Even after filtering, there is ambiguity in the results because there are a few instants of zero momentum in one single bob and it is sometimes difficult to define which marks the end of a bobbing impulse.

7.1.3. Degree of synchronisation

For each test record, the first four and last two impulses are discarded so that only the steady state jumping and bobbing processes are analysed. Only results for synchronised tests, i.e. when the subject jumps or bobs once for every beep, are considered in the analysis. Table 7.2 gives a summary on the number of deficit or extra jumps recorded for all 10 subjects. A value of zero refers to a synchronised

test while a positive value gives the number of extra jumps and a negative value the number of deficit jumps. The bobbing results are presented in Table 7.3.

As shown in Table 7.2, there is a good synchronisation for jumping at all beat frequencies except for 3.5 Hz where only four individuals are able to perform synchronised jumping. This is probably due to difficulty in keeping up with the fast pace. Several subjects express difficulty in jumping at 1.5 Hz due to difficulty in controlling the landing and launching timings. At 1 Hz, the subject lands on the heel and pauses for a while before launching on the toe. At higher beat frequencies (2 Hz and above), the subject lands and launches the next jump on the toe without landing on the heel. Jumping at 1.5 Hz is a mixture of these two jumping actions.

Overall, three subjects (subjects 3, 5 and 10) show large numbers of jump discrepancies and are considered as having difficulty in synchronising their jumps with the audio prompts. Seven subjects show a small number of jump discrepancies and are considered able to synchronise their jumps with the audio prompts.

For bobbing, the subjects show significantly better synchronisation at all six beat frequencies compared to jumping, indicating it is easier to control one's timing when bobbing compared to jumping. Only two (subjects 3 and 5) have difficulty in synchronising their bobbing while eight subjects show good synchronisation at almost all six beat frequencies.

7.1.4. Impulse timing

The phase delays for all synchronised jumping test records are presented in Fig. 7.3, with each plot corresponding to one beat frequency. The results agree with those from Parkhouse and Ewins (2004), with most phase delays within the range of 0 to 200°. The mean and standard deviation of the mean phase delay and phase scatter are compared with those calculated in Chapter 5 from measurements of Parkhouse and Ewins (2004) in Tables 7.4 and 7.5 respectively. A reasonable agreement is found for both parameters.

7.1.5. Impulse shape

Figures 7.4 and 7.5 show the jumping and bobbing impulses of all subjects who are able to perform synchronised tests at all six beat frequencies respectively. Each row corresponds to one beat frequency and each column corresponds to one subject. All impulses are plotted on a time scale shifted by t_{eff} such that at $t = 0$, the time equals the timing of the impulse t_{eff}. For the jumping impulses, the vertical axis is the normalised load, F' (the measured load divided by the weight of the subject). For the bobbing impulses, it is plotted as the normalised effective dynamic load, F_d' (the effective dynamic load divided by the weight of the subject).

As shown in Figure 7.4, the jumping impulses exhibit three general profiles: twin peaks, merging of twin peaks and single peak, as the beat frequency increases. The twin peaks impulse shape exhibited at 1 and 1.5 Hz shows a clear separation of the landing and launching impulses by a ‘stationary interval’ when the subject stands still on the load cell. As the beat frequency increases, this ‘stationary interval’ reduces to the merging of the twin peaks and a single peak. The impulse shape of

each test subject is fairly consistent, especially at high beat frequencies (2 Hz and above). In addition, there is less inter-subject variation in the impulse shape as the beat frequency increases.

For bobbing, there are generally two bobbing patterns. Two out of ten subjects (subjects 7 and 10) flex their knees while the rest of the eight subjects rise to their toes and land on their heels when asked to bob. The impulses presented in Figure 7.5 show significant inter-subject variation at each beat frequency, indicating that the bobbing action is highly variable between individuals. For subjects 7 and 10 who flex their knees when bobbing, no point of zero momentum is found at the trough of the impulse whereas for all other subjects, a point of zero momentum at the trough is used to split each bobbing impulse.

The average impulse of each load-time record is obtained by taking the mean of the time-shifted impulses. The Fourier coefficients, r_n for a periodic jumping or bobbing load generated from the average impulse are obtained by taking the Fast Fourier Transform at a sampling frequency of 1 kHz. The Fourier coefficients for the first five harmonics are presented in Figures 7.6 and 7.7 for jumping and bobbing respectively. Each plot corresponds to one beat frequency and within each plot, each line corresponds to the Fourier coefficients of the average impulse of one test subject. The mean and standard deviation of the Fourier coefficients are given in Tables 7.6 and 7.7 for jumping and bobbing respectively. The standard deviation gives an indication of the inter-subject variation in the impulse profile.

The Fourier coefficients are related to the impulse shape. In particular, jumping impulses at 1 and 1.5 Hz with a twin peaks impulse shape are dominated by the second harmonic. For higher beat frequencies, the jumping impulse is dominated by the first harmonic with decreasing Fourier coefficients for higher harmonics. The standard deviations for 1, 1.5 and 2 Hz are significantly higher than other beat frequencies, indicating that there is a significant inter-subject variation in the impulse shape at these beat frequencies.

For bobbing, the average bobbing impulse is truncated at both ends so that its length is equal to one period of the beat frequency. For all beat frequencies, the Fourier coefficients are significantly lower than for jumping. At low beat frequencies (1, 1.5 and 2 Hz), there is no distinct dominance by one harmonic, the Fourier coefficients spread over a few harmonics. For higher beat frequencies of 3 and 3.5 Hz, there is a clear dominance at the first harmonic with decreasing Fourier coefficients for higher harmonics. This indicates a resemblance to the jumping impulse when bobbing at high beat frequencies. In contrast to jumping, the standard deviation of bobbing shows higher values for 2.5, 3 and 3 Hz, indicating greater inter-subject variation in the impulse profile for higher beat frequencies.

The average impulse for bobbing is less reliable because there are greater inconsistencies in the shape of the impulse. The time-shifted bobbing impulses do not line up as well as the jumping impulses. Taking the mean values will average out the variations and therefore contributes to a loss of information on the shape of the impulse.

Unlike the jumping impulse which has a distinct half-sinusoid curve, the bobbing impulse is highly variable, the effective timing expressed in Eqn. 5.1 is not appropriate in defining the timing of each bob. Another approach is attempted to model the bobbing load by deconvolving the measured load-time signal with the average signal in order to retrieve the timing of each bob. Unfortunately, the deconvolution process is highly sensitive to error and no meaningful result is obtained.

7.1.6. Conclusions

The experimental tests show that for the beat frequency range of 1 to 3.5 Hz, seven out of ten subjects are able to synchronise their jumping and bobbing with the audio prompts. It is found that synchronised bobbing is easier to perform than jumping as the subject has more control of the timing. Compared to jumping, the bobbing action is found to have a higher inherent variability between individuals.

7.2. Two people jumping tests

The work presented in Chapters 5 and 6 is from measurements of individuals jumping alone. Two parameters are introduced to quantify each individual's impulse timing: *mean phase delay* and *phase scatter*. Both parameters measure one's degree of synchronisation with respect to the auditory signal, without the influence of another person jumping together, i.e. the visual effect. In a pop concert, an individual's jumping would be affected by both the music played and the people jumping around. Therefore, experimental tests are conducted to investigate the coherency between people due to both auditory and visual effects. The results are

compared with those from individual jumping tests. The findings give an indication of any improvement necessary for the crowd jumping loads presented in Chapters 5 and 6.

7.2.1. Experimental tests

Each test involves two people standing on two separate load cells, facing each other and about 2 m apart. The ten subjects involved in the individual jumping tests in the previous section are ranked according to their abilities to synchronise their jumps with the audio beeps. The best five subjects (subjects 4,6-9) are selected to participate in the tests conducted at 6 beat frequencies, from 1 to 3.5 Hz, at an increment of 0.5 Hz. Each subject is paired with three other subjects except one paired with four subjects, giving a total of 8 pairs.

7.2.2. Results and discussion

For each pair, the results for both subjects when jumping alone and together are compared. For each case, two parameters are introduced, $\Delta\overline{\theta}$ and $\Delta\sigma_{\theta'}$. $\Delta\overline{\theta}$ is defined as the absolute difference in mean phase delay between the two subjects while $\Delta\sigma_{\theta'}$ is the absolute difference in phase scatter. Both are plotted in Figs. 7.8 and 7.9 respectively. In each figure, each plot corresponds to one pair of subjects, giving their $\Delta\overline{\theta}$ and $\Delta\sigma_{\theta'}$ when jumping separately and together, at six beat frequencies. Most results show that both parameters are less when jumping together than when separately. This implies that the visual effect provided by another jumper improves the coherency between the two jumpers. The average reduction for each pair over the six beat frequencies are presented in Table 7.8 for $\Delta\overline{\theta}$ and

$\Delta\sigma_{\theta'}$. Overall, $\Delta\bar{\theta}$ falls between 35% and 74% while $\Delta\sigma_{\theta'}$ falls between 52% and 86%. Therefore, both parameters should have lower standard deviations than those calculated in Chapter 5 due to a better synchronisation provided by the visual effect. Hence the crowd jumping load generated in Chapter 6 might be lower than they ought to be. Due to the small number of tests conducted, it is not possible to provide a statistically sound quantification of the crowd coherency.

Chapter 8

8. Conclusions and recommendations

8.1. Conclusions

Vibration problems have been reported on several cantilever grandstands both in the UK and overseas. These cantilever grandstands, which have large spans, are prone to excessive vibrations due to rhythmic crowd motions. Various codes and guidelines have stated the need to carry out a dynamic analysis on these structures. It is the responsibility of the design engineers to assess the performance of such structures when being used for lively events such as pop concerts. However, current practice is incapable of doing so due to a lack of knowledge on human-structure interaction on cantilever grandstands. This thesis is directed towards modelling and analysing the response of a cantilever grandstand. It involves studying the active and passive crowds occupying the structure and the resultant structural response. The work in this thesis consists of three main areas:

- Modelling of a passive crowd
- Modelling of the crowd jumping load
- Analysing a combined crowd-structure system with a jumping crowd.

A brief experimental study on bobbing load is also conducted. In this chapter, the main findings are summarised, conclusions drawn and some possible directions for future research are presented.

8.1.1. Initial study

Analysis of the cantilever-human system shows that, for a simple cantilever system, the response is dominated by the first mode. The seated humans are found to lower the modal amplitude and resonant frequency compared to when the structure is empty. Two parameters are important in the analysis: the natural frequency of the empty structure and the relative mass of the passive crowd. All these suggest that a SDOF structural system is adequate for further work. Hence subsequent work uses a SDOF system to represent the structure. By using such a simple structural model with well-defined dynamic characteristics, the fundamental interaction between the passive crowd and the structure can be better understood.

8.1.2. Modelling of passive crowd

A 2DOF system is developed to represent a passive crowd. By curve-fitting the apparent mass of sixty seated and twelve standing individuals, it is found that a rational polynomial of the order of 4 is sufficient for the crowd model. This means that a crowd model which consists of numerous independent 2DOF systems can be approximated well by using a single 2DOF system. This reduces the computational time and effort significantly because fewer DOFs are involved.

A parametric study shows that for low natural frequency structures (say 2 Hz), the crowd adds mass to the structural system, which reduces both the natural frequency and the damping ratio of the occupied structure compared to the empty structure. At higher natural frequencies (> 4 Hz), the crowd reduces the structural response by

adding significant damping in a way similar to a tuned mass damper though, unlike a TMD, the crowd properties cannot be optimised for a particular structure.

The results for three joint systems (100% seated, 100% standing and 50:50 seated/standing crowds) are presented in charts in terms of the *frequency reduction factor* and the *DMF reduction factor*. There is greatest reduction in the natural frequency and the DMF for structures with natural frequencies within the range of 4 to 8 Hz, due to the very significant damping provided by the passive crowd. The amount of reduction in the DMF increases with the mass ratio, i.e. more damping is provided as the crowd size increases. Using these charts, designers are able to estimate the changes in resonant frequency and peak response. In order to estimate the structural response, a load model is required and this is dealt with in Chapters 5 and 6.

It is recognised that the transfer function representation for the crowd model might not be the common practice among engineers. It was suggested by Michael Willford (Blakeborough 2005) that the combined system be reduced to a SDOF system. In this thesis, work is conducted to represent the 5DOF joint 50:50 seated/standing crowd-structure system as SDOF and 3DOF systems. It is shown that the joint crowd-structure system can be modelled as a SDOF system for 1 to 4 Hz structures. For structures above 4 Hz, the joint system is best represented as a 3DOF system. For design purpose where the interest is on the maximum response, the equivalent SDOF is more appropriate because it is more simplistic compared to the 3DOF system and also, there is not much difference in the maximum DMF values estimated from both systems. The modal properties of the equivalent SDOF

system confirm the findings that the passive crowd behaves as an added mass for low natural frequency structures and as an added damper for structures 4 Hz and above.

8.1.3. Modelling of crowd jumping load

A statistical approach is developed to model the jumping loads. Several parameters, each described by a probability distribution function, are used to model the randomness in the impulse timing and shape.

From the experimental measurements of Parkhouse and Ewins (2004), out of the four beat frequencies (1.5, 2, 2.67 and 3.5 Hz), jumping at 2 Hz shows the highest number of synchronised tests, i.e. 75 tests. Overall, 26 test subjects are able to perform synchronised jumping at all four beat frequencies. Ten additional individual jumping tests conducted by the author show that four subjects show good synchronisation at six beat frequencies, from 1 to 3.5 Hz, at an increment of 0.5 Hz. Three subjects are found to have difficulty in synchronising their jumps with the audio beeps at almost all six beat frequencies. In addition, most subjects express difficulty in jumping at 1.5 Hz due to awkwardness in controlling the landing and launching actions.

In the statistical analysis conducted on the measurements of Parkhouse and Ewins (2004), the mean phase delay and phase deviation are introduced to quantify the impulse timing. A mean value of approximately 0.1 s is observed for the mean phase delay at all four beat frequencies. The standard deviations of both parameters show that there is least inter-subject variation when jumping at beat frequencies of 2

and 2.67 Hz, i.e. the most severe crowd loading can be expected at these beat frequencies.

It is found that the phase deviation does not follow a Normal distribution. Further analysis shows that there is some structure in the phase deviation sequence. It is found that the jumper adjusts the timing of the current jump based on the timing of the previous jump with a random error added to each jump. This phenomenon is modelled by a first order auto-regression algorithm and the residual error characterised by a Normal distribution. All impulse timing parameters are modelled using either a Normal or a Beta distribution, as summarised in Fig. 5.52. The majority of the parameters pass the chi-squared tests with a significance level of 0.05. Correlation analyses show that all variables can be treated as independent random variables.

Three impulse shapes are observed from the experimental measurements: twin peaks, merging of twin peaks and single peak. The first two shapes are dominant for jumping at 1.5 Hz while the single peak impulse shape is observed for jumping at 2, 2.67 and 3.5 Hz. For the twin peaks, the first peak is the landing impulse while the second peak is the launching impulse. As the beat frequency increases, both the landing and launching impulses merge, giving the single peak impulse shape. For the single peak impulse shape, it is found that a cosine-squared function gives the best fit among the three analytical functions tested (the other two are the Normal distribution function and the cosine function). In addition, experimental tests conducted by the author show that the Fourier coefficients for beat frequencies of 1 and 1.5 Hz are dominated by the second harmonic due to the twin peaks impulse

shape.

It is found that the contact ratios of each test record can be adequately described by a Normal distribution. Both the mean and standard deviation of the contact ratio are modelled using Beta distributions, as summarised in the flow chart in Fig. 5.53. In particular, the mean contact ratio is found to be higher than 0.4, in contrast to the lower values suggested by the BS 6399: Part 1 (British Standards Institution 1996). A moderate correlation is found between the mean and standard deviation of contact ratio, however, it is decided that be treated as independent variables.

8.1.4. Analysis of joint crowd-SDOF system with jumping crowd

Dynamic analyses are conducted for the joint crowd-SDOF system with a mass ratio of 0 (empty structure) and 0.15 (with standing crowd).

A closer look at the results for the 2 Hz beat frequency shows that the lack of synchronisation between individuals is more dominant at higher structural frequencies. The distributions of the DMF and RMS acceleration shift from a Normal distribution to a skewed (perhaps Rayleigh) distribution as the natural frequency of the structure increases.

For all three beat frequencies, the characteristic DMF (Figs. 6.12 to 6.17) and RMS acceleration (Figs. 6.18 to 6.23) show three resonant peaks due to excitation by the first three harmonics of the jumping loads. Comparing the results for the empty and occupied structures, a significant reduction in the structural response is observed due to damping contributed by the passive crowd. In addition, the resonant peaks

are located at frequencies slightly higher than those for the empty structure. The discrepancy is greatest for structures with natural frequencies between 4 and 8 Hz when empty, i.e. structures excited by the second and third harmonics of the crowd jumping loads. Both the reduction in structural response and the shift in resonant frequency are due to damping provided by the passive crowd.

The peak characteristic DMF and RMS acceleration at each harmonic are plotted against the group size in Figs. 6.24 to 6.27. A non-linear trend is observed for group sizes of up to 16 people. For groups with more than 16 people, an asymptotic behaviour is observed. This implies that for a real cantilever grandstand with a large crowd, the steady state structural response observed along the asymptotic trend should provide a good estimation. Engineers could use these steady state values as estimation to the response of a cantilever grandstand subjected to crowd jumping loads.

8.1.5. Experimental jumping and bobbing tests

Two bobbing patterns are observed: Two out of the ten subjects flex their knees while the rest of the eight subjects rise to their toes and land on their heels. A significantly better synchronisation is found for bobbing compared to jumping. Eight out of the ten subjects are able to perform synchronised tests at almost all six frequencies compared to only four for jumping. The Fourier coefficients for bobbing are lower compared to those for jumping. In terms of the impulse shape, the bobbing action is found to have a higher inherent variability between individuals compared to jumping.

Tests on two people jumping together show that the visual effect provided by another jumper improves the coherency between the two jumpers. The results show that there is quite a significant improvement in the timings of both jumpers.

8.2. Limitations and further research

This thesis has contributed to the current understanding on the dynamic performance of grandstands by presenting a very straightforward method of analysing a SDOF system occupied by active and passive crowds. A 2DOF crowd model is developed and applied successfully to a SDOF system through the use of a feedback system. A comprehensive statistical analysis on the jumping loads is also conducted to take into account the lack of synchronisation between individuals. The results presented in this thesis allow engineers to estimate the structural response for various crowd sizes and structures with various natural frequencies. Realistically, designers should use the results presented here with caution, considering the various limitations which will be discussed below. In addition, suggestions on further research are made where appropriate.

In terms of the crowd jumping loads, the worst case scenario is being considered because only results for the synchronised tests are used. The calculated structural response does not take into account spectators who are not jumping in time with the beat, i.e. the whole active crowd is treated to be jumping in time with the beat, whereas tests suggest that a significant proportion of people are unable to do so.

On the other hand, an initial experimental study on the effect of jumping together with another person shows that the visual effect provided by another jumper

improves the coherency between the two jumpers. This implies that the crowd jumping loads generated in Chapter 6 might be lower than they ought to be because they are based on test data from independent jumpers. Further work is needed to quantify the crowd coherency. One possible way of achieving this is to measure the loads of a group of people jumping together. The results presented in Chapter 6 show that a group of 16 is sufficient since an asymptotic trend is observed for larger groups.

Experimental tests are conducted on rigid force plates. Therefore, the flexibility of the structure is not taken into account in the derivation of the jumping load model. Since cantilever grandstands, especially those with vibration problems, are highly flexible, it is very important to take into account the flexibility of the structure. Further work is needed to investigate how the jumping loads vary with the flexibility of the structure.

Work on bobbing is a whole new area of research that is worth pursuing considering the better synchronisation observed and its potential to be synchronised by the movement of the structure, as seen in the Millennium footbridge phenomenon (Dallard et al. 2001). For bobbing, the person is in contact with the ground all the time. The challenge is to model both the damping capacity of the human body and the external force exerted by the person onto the structure.

REFERENCES

Allen, D. E. (1990). "Floor vibrations from aerobics." *Canadian Journal of Civil Engineering*, 17(5), 771-779.

Allen, D. E., Rainer, J. H., and Pernica, G. (1985). "Vibration criteria for assembly occupancies." *Canadian Journal of Civil Engineering*, 12(3), 617-623.

Almeida, P. A. O., and Rodrigues, J. F. S. (1998). "Investigation of the vibrations induced by people in soccer stadiums." *1998 SEM Spring Conference and Exhibition*, Houston, Texas, 271-274.

Bachmann, H., and Ammann, W. (1987). *Vibration problems in structures induced by man and machines, Structural Engineering Document No. 3e*. International Assoc. of Bridge and Structural Engineering, AIPC-IVBH, Zurich.

Batista, R. C., and Magluta, C. (1993). "Spectator-induced vibration of Maracana Stadium." *EURODYN '93,* Trondheim, Norway, 985-992.

Bendat, J. S., and Piersol, A. G. (1986). *Random data*, 2nd Ed., John Wiley & Sons. New York.

Blakeborough, A. (2005). *Personal communication*.

Boileau, P. E., and Rakheja, S. (1998). "Whole-body vertical biodynamic response characteristics of the seated vehicle driver measurement and model development." *International Journal of Industrial Ergonomics*, 22, 449-472.

British Standards Institution (BSI). (2000). *BS 5950-1:2000 Structural use of steelwork in building. Code of practice for design. Rolled and welded sections*. London, UK.

British Standards Institution (BSI). (1996). *BS 6399: Part 1: Code of practice for dead and imposed loads*. London, UK.

Coermann, R. R. (1962). "The mechanical impedance of the human body in sitting and standing position at low frequencies." *Human Factors*, 4, 227-253.

Dallard, P., Fitzpatrick, T., Flint, A., Low, A., and Smith, R. R. (2001). "The Millennium Bridge, London: problems and solutions." *The Structural Engineer*, 79(8), 15-17.

Dennis, J. E., Jr., and Schnabel, R. B. (1983). *Numerical Methods for Unconstrained Optimization and Nonlinear Equations*. Englewood Cliffs, NJ: Prentice-Hall.

Department of National Heritage and Scottish Office. (1997). *Guide to Safety at Sports Grounds.* 4th Ed., Stationary Office, London.

Donati, P. M., and Bonthoux, C. (1983). "Biodynamic response of the human body in the sitting position when subjected to vertical vibration." *Journal of Sound and Vibration*, 90(3), 423-442.

Duarte, E., and Ji, T. (2005). "Bouncing loads induced by an individual." *6th European Conference on Structural Dynamics – EURODYN 2005*, Paris, France. C. Soize & G.I. Schueller Eds, Millpress, Rotterdam.

Ebrahimpour, A., and Sack, R. L. (1989). "Modelling dynamic occupant loads." *Journal of Structural Engineering*, 115(6), 1476-1496.

Ebrahimpour, A., and Fitts, L. L. (1996). "Measuring coherency of human-induced rhythmic loads using load-plates." *Journal of Structural Engineering*, 122(7), 829-831.

Ellis, B. R., and Ji, T. (1997). "Human-structure interaction in vertical vibrations." *Proceedings of Institution of Civil Engineers*, *Structures and Buildings,* 122(1), 1-9.

Ellis, B. R., and Ji, T. (2004). "Loads generated by jumping crowds: numerical modelling." *The Structural Engineer*, 82(17), 35-40.

Ellis, B. R. and Littler, J. D. (2004). "Response of cantilever grandstands to crowd loads." *Proceedings of the Institution of Civil Engineers, Structures and Buildings*, 157(SB5), 297-307.

Fairley, T. E., and Griffin, M. J. (1989). "The apparent mass of the seated human body: vertical vibration." *Journal of Biomechanics*, 22(2), 81-94.

Foschi, R. O., and Gupta, A. (1987). "Reliability of floors under impact vibration." *Canadian Journal of Civil Engineering*, 14(5), 683-689.

Folz, B., and Foschi, R. O. (1991). "Coupled vibrational response of floor systems with occupants." *Journal of Engineering Mechanics*, 117(4), 872-892.

GERB Vibration Control Systems. "Tuned mass dampers. Spectator stands – Morumbi Soccer Stadium, Sao Paulo, Brazil." <http://www.gerb.com/en/bibliothek/projektbeispiele/show_projektbeispiel.php?rubrik=tilger&projekt=morumbi_stadion> (Sept. 26, 2005).

Ginty, D., Derwent, J. M., and Ji, T. (2001). "The frequency ranges of dance-type loads." *The Structural Engineer*, 79(6), 27-31.

Harrison, R. E., and Wright, J. R. (2004). "Combined active and passive human loading on a flexible platform." *23rd International Modal Analysis Conference (IMAC XXIII),* Orlando, Florida, USA.

International Organization of Standardisation. (1981). *Vibration and shock – Mechanical driving point impedance of the human body, ISO 5982: 1981*, Geneva, Switzerland.

IStructE/ODPM/DCMS working group. (2001). *Dynamic performance requirements for permanent grandstands subject to crowd actions. Interim guidance on assessment and design*. London, UK.

IStructE/ODPM/DCMS working group. (2003). "Advisory note on calculation of natural frequencies of grandstand seating decks." *The Structural Engineer*, 81(22), 20-21.

Ji, T. (1995). "A continuous model for the vertical vibration of the human body in a standing position." *Proc. of the UK informal Group Meeting on Human Response to Vibration,* Silsoe.

Ji, T., and Ellis, B. R. (1993). "Evaluation of dynamic crowd effects for dance loads." *IABSE symposium, Structural Serviceability of Buildings*, Goteburg.

Karsperski, M., and Agu, E. (2005). "Prediction of crowd-induced vibrations via simulation." *23rd International Modal Analysis Conference (IMAC XXIII)*, Orlando, Florida, USA.

Karperski, M. and Niemann, H. J. (!993). "Man induced vibrations of a stand structure." *1st European Conference on Dynamics EURODYN,* Trondheim, Norway, 977-983.

Lenzen, K. H. (1996). "Vibration of steel joist-concrete slab floors." *American Institute of Steel Construction (AISC) Engineering Journal*, 3(July), 133-136.

Littler, J. D. (1998). "Full-scale testing of large cantilever grandstands to determine their dynamic response." *Stadia, arenas and grandstands*, Thompson, P.D., Tollocako, J.J.A., Clarke, J.N. eds. E and FN Spon, London, 123-134.

Littler, J. D. (1999). "The dynamic response of a three tier cantilever grandstand." *3rd European Conference on Structural Dynamics – EURODYN '99*, 623-628.

Littler, J. D. (2003). "Frequencies of synchronised human loading from jumping and stamping." *The Structural Engineer*, 18(22), 27-35.

Mandal, P., and Ji, T. (2004). "Modelling dynamic behaviour of a cantilever grandstand." *Structures and Buildings, The Proceedings of the Institution of Civil Engineers*, 157(3), 173-184.

MathWorks Inc. *MATLAB® Signal Processing Toolbox.*

MathWorks Inc. *MATLAB® Control Toolbox*.

Matsumoto, Y., and Griffin, M. J. (1998). "Dynamic response of the standing human body exposed to vertical vibration: influence of posture and vibration magnitude." *Journal of Sound and Vibration*, 212(1), 85-107.

Matsumoto, Y., and Griffin, M. J. (2003). "Mathematical models for the apparent masses of standing subjects exposed to vertical whole-body vibration." *Journal of Sound and Vibration*, 2003, 260(3), 431-451.

Matthews, C. M., and Montgomery, C. J. (1988). "A dance floor with unsatisfactory dynamic response." *Proceedings, Symposium/Workshop on Serviceability of Buildings (Movements, Deformations, Vibrations)*, Ottawa, Canada.

Mertens, H. (1978). "Nonlinear behaviour of sitting humans under increasing gravity." *Aviation, Space and Environmental Medicine*, 49, 287-298.

National Building Code of Canada. (1990). Commentary A, Canada.

Otlet, M. (from WS Atkins) (2004). *Personal communication*.

Parker, D. (2001). "A sporting chance." *New Civil Engineer*, 8 February 2001.

Parkhouse, J. G., and Ewins, D. J. (2004). "Vertical dynamic loading produced by people moving to a beat." *Proc. ISMA 2004*, Leuven, Belgium, 821-835.

Pernica, G. (1983). "Dynamic live loads at a rock concert." *Canadian Journal of Civil Engineering*, 10(2), 185-191.

Pernica, G. (1990). "Dynamic load factors for pedestrian movements and rhythmic exercises." *Canadian Acoustics*, 1990, 18(2), 3-18.

Polensek, A. (1975). "Damping capacity of nailed wood-joist floor." *Wood Science*, 8(2), 141-151.

Rainer, J. H., and Pernica, G. (1981). "Damping of a floor sample." *The Second Speciality Conference on Dynamic Response of Structures: Experimentation, Observation, Prediction and Control,* Atlanta, Georgia, USA, G. Hart ed., 859-873.

Rainer, J. H., Pernica, G., and Allen, D. E. (1988). "Dynamic loading and response of footbridges." *Canadian Journal of Civil Engineering*, 15(1), 66-71.

Reid, W. M., Dickie, J. F., and Wright, J. R. (1997). "Stadium structures: are they excited." *Institution of Structural Engineers*, 75(22), 383-388.

Reynolds, P., and Pavic, A. (2002) "Modal Testing of a Sports Stadium." *20th International Modal Analysis Conference (IMAC XX)*, Los Angeles, USA.

Reynolds, P., Pavic, A., and Ibrahim, Z. (2004). "Changes of modal properties of a stadium structure occupied by a crowd." *22nd International Modal Analysis Conference (IMAC XXII)*, Dearborn, Detroit, USA.

Reynolds, P., Pavic, A., and Willford, M. (2005) "Prediction and Measurement of Stadia Dynamic Properties." *23rd International Modal Analysis Conference (IMAC XXIII)*, Orlando, Florida, USA.

Rogers, D. (2000). "Two more 'wobbly' stands." *Construction News*, 17 August 2000.

Rogers, D., and Thompson, R. (2000). "Liverpool stand gets a red card." *Construction News*, 10 August 2000.

Sachse, R., Pavic, A. and Reynolds, P., (2002). "The influence of a group of humans on modal properties of a structure." *5th European Conference on Dynamics EURODYN,* Munich, 1241-1246.

Staalduinen, V. P. and Courage, W. (1994). "Dynamic loading of Feyenoord stadium during pop concerts." *Symposium: Places of assembly and long-span building structures, Birmingham, UK, 7-9 September 1994, Report 71, International Association for Bridge and Structural Engineering (IABSE)*, 283-288.

Suggs, C. W., Abrams, C. F., and Stikeleather, L. F. (1969). "Application of a damped spring-mass human vibration simulator in vibration testing of vehicle seats." *Ergonomics*, 12(1), 79-90.

Tuan, C. Y., and Saul, W. E. (1985). "Loads due to spectator movements." *Journal of Structural Engineering*, 111(2), 418-434.

Staalduinen, V. P., and Courage, W. (1994). "Dynamic loading of Feyenoord stadium during pop concerts." *Symposium: Places of Assembly and Long-Span Building Structures,* Birmingham, UK, Report 71, 283-288, IABSE, Zürich, Switzerland.

Wei, L., and Griffin, M. J. (1998). "Mathematical models for the apparent mass of the seated human body exposed to vertical vibration." *Journal of Sound and Vibration*, 212(5), 855-874.

Willford, M. (2001). "An investigation into crowd-induced vertical dynamic loads using available measurements." *The Structural Engineer*, 79(12), 21-25.

Yao, S., Wright, J. R., Pavic, A., and Reynolds, P. (2003). "Forces generated when bouncing or jumping on a flexible structure." *Proceedings of ISMA,* Leuven, Belgium.

Zheng, X. H., and Brownjohn, J. M. W. (2001). "Modelling and simulation of human-floor system, under vertical vibration." *Smart Structures and Materials 2001: Smart Structures and Integrated* Systems, *Proceedings of SPIE*, L. P. Davis ed., Vol. 4327.

APPENDIX A

Try UB 914×419×388

Dead and imposed loads
The loads expressed as uniform loads per unit length of the cantilever are:

Dead load, ω_D = 36.4 kN/m
Imposed load, ω_I = 40.0 kN/m
Applying a load factor of 1.4 for dead load and 1.6 for imposed load, giving:
Factored design load, ω = 115.0 kN/m

Limit state strength and serviceability design
Assuming that the cantilever is restrained against torsion and lateral displacement by the concrete seating deck, the resultant maximum shear force and bending moment acting on the cantilever:

Maximum shear force acting:
$F_v = \omega L =$ 1049 kN

Maximum bending moment acting:
$M = \frac{\omega L^2}{2} = 4784$ kNm

The following checks show that the selected member satisfies the strength and serviceability limit state criteria according to BS 5950: Part 1 (British Standards Institution 2000).

Compact section
Clause 3.5.2
For rolled sections, limit is 9.5ϵ with $\epsilon = \left(\frac{275}{P_y}\right)^{1/2} = 1$

$b/T = B/2/T = 5.7 < 9.5\epsilon$
∴ Section is compact

Shear buckling
Clause 4.2.3
$d/t = 37.4 < 63\epsilon$
∴ No need to check for shear buckling

Bending resistance
Clause 4.2.5
$M_c = P_y S = 275 \times 720 \times 10^{-3} = 4868$ kNm (> 4784 kNm applied) OK!

Shear resistance
Clause 4.2.3
$A_v = tD = 21.4 \times 921 = 19709$ mm^2
$P_v = 0.6 P_y A_v = 0.6*275 \times 19709 \times 10^{-3} = 3252$ kN (> 1049 kN applied) OK!

Deflection

Clause 2.5.1

$$\text{Maximum deflection} = \frac{\omega_l L^4}{8EI_{xx}} = \frac{45\times10^3\times9.12^4}{8\times205\times10^9\times720000\times10^{-8}}\times10^3 = 26.4\,\text{mm}$$

$$\text{Deflection limit} = \frac{L}{180} = \frac{9.12\times10^3}{180}\,50.7\text{ mm}\,(>26.4\text{ mm}) \quad \text{OK!}$$

APPENDIX B

For regression of order of one and a phase deviation sequence with n data points,

$$\begin{Bmatrix} \theta'_2 \\ \theta'_3 \\ \vdots \\ \vdots \\ \theta'_{n-1} \\ \theta'_n \end{Bmatrix} = \rho_1 \begin{Bmatrix} \theta'_1 \\ \theta'_2 \\ \vdots \\ \vdots \\ \theta'_{n-2} \\ \theta'_{n-1} \end{Bmatrix} + \begin{Bmatrix} \Delta\theta'_2 \\ \Delta\theta'_3 \\ \vdots \\ \vdots \\ \Delta\theta'_{n-1} \\ \Delta\theta'_n \end{Bmatrix} \tag{B1}$$

$$\sum_{i=2}^{n} \theta'_i = \rho_1 \sum_{i=1}^{n-1} \theta'_i + \sum_{i=2}^{n} \Delta\theta'_i \tag{B2}$$

Rearranging,

$$\sum_{i=2}^{n} \Delta\theta'_i = \sum_{i=2}^{n} \theta'_i - \rho_1 \sum_{i=1}^{n-1} \theta'_i \tag{B3}$$

Knowing that the mean of the n-point phase deviation sequence equals zero, i.e.

$$\sum_{i=1}^{n} \theta'_i = 0 \tag{B4}$$

Therefore,

$$\sum_{i=2}^{n} \theta'_i = -\theta'_1 \tag{B5}$$

$$\rho_1 \sum_{i=1}^{n-1} \theta'_i = -\rho_1 \theta'_n \tag{B6}$$

Substitute Eqns. B4 and B5 into Eqn. B6,

$$\sum_{i=2}^{n} \Delta\theta'_i = -\theta'_1 + \rho_1 \theta'_n \tag{B7}$$

Divide by (n-1) to get the mean,

$$\frac{1}{(n-1)} \sum_{i=2}^{n} \Delta\theta'_i = -\left(\frac{1}{n-1}\right)\theta'_1 + \rho_1 \theta'_n \tag{B8}$$

Eqn. B8 shows that the mean of the random error is a function of the boundary conditions, θ_1' and θ_n'; and the regression coefficient, ρ_1.

TABLES

	Undamped natural frequency (Hz)				Damping ratio (%)			
	f_1		f_2		ζ_1		ζ_2	
	Mean	SD	Mean	SD	Mean	SD	Mean	SD
Seated men	5.1	0.58	9.3	2.01	31.1	10.11	43.7	43.41
Seated women	5.3	1.06	9.2	2.85	38.5	14.90	31.7	11.63
Seated children	5.2	5.16	15.9	24.20	37.5	39.23	31.2	36.35
Standing men	5.8	0.54	12.6	2.34	33.1	7.21	45.9	17.21

Table 4.1: Mean and standard deviation of undamped natural frequency and damping ratio.

	Subject body mass (kg)		Modal mass (kg)					
	m_{body}		m_0		m_1		m_2	
	Mean	SD	Mean	SD	Mean	SD	Mean	SD
Seated men	58.2	14.00	7.6	3.01	37.4	10.36	13.7	7.01
Seated women	50.8	6.70	7.3	1.75	32.0	6.02	11.1	5.45
Seated children	35.9	8.08	3.9	1.84	28.1	4.40	4.58	5.61
Standing men	73.9	7.57	-	-	43.1	16.90	28.5	19.07

Table 4.2: Mean and standard deviation of modal mass.

	a_4	a_3	a_2	a_1	a_0
Seated men	0.1406	32.23	3502	145.8×10^3	4.120×10^6
Seated women	0.1512	35.52	3866	152.8×10^3	3.892×10^6
Seated children	0.1115	33.50	3738	233.0×10^3	6.866×10^6
Standing men	0.0050	42.69	4940	255.3×10^3	8.739×10^6

	b_4	b_3	b_2	b_1	b_0
Seated men	1	81.03	6509	144.9×10^3	4.127×10^6
Seated women	1	91.04	6808	154.3×10^3	3.919×10^6
Seated children	1	87.99	9098	235.0×10^3	6.854×10^6
Standing men	1	96.20	9517	258.7×10^3	8.715×10^6

Table 4.3: Coefficients for transfer function defining the 2DOF crowd model (Eqn. 4.1).

	a_2	a_1	a_0	b_2	b_1	b_0
Seated men	0.2805	21.20	994.9	1	20.55	994.4
Seated women	0.2846	22.85	927.1	1	22.41	933.9
Seated children	0.1400	26.88	1096.0	1	27.15	1094.0
Standing men	0.2135	29.50	1454.0	1	29.39	1454.0

Table 4.4: Coefficients for transfer function defining the SDOF crowd model (Eqn. 4.17).

Beat	Mean time delay (s)		Mean phase delay (^{o})	
frequency (Hz)	Mean	Standard Dev.	Mean	Standard Dev.
1.5	0.077	0.09	41.60	46.7
2	0.077	0.05	55.49	37.1
2.67	0.097	0.03	93.33	30.5
3.5	0.088	0.03	111.00	36.1

Table 5.1: Mean and standard deviation of mean time delay and mean phase delay.

Beat frequency (Hz)	Mean of $\sigma_{\theta'}$ (^{o})	Standard Dev. of $\sigma_{\theta'}$ (^{o})	Correlation coefficient, r
1.5	31.76	16.3	-0.004
2	24.61	11.7	-0.270
2.67	24.49	8.7	-0.032
3.5	31.91	11.1	-0.329

Table 5.2: Mean and standard deviation of $\sigma_{\theta'}$ and correlation coefficient of $\sigma_{\theta'}$ and mean phase delay.

(a) Beat frequency = 1.5 Hz

Class interval	Number observed, n_i	Number expected, N_i	$\frac{(n_i - N_i)^2}{N_i}$
0 – 0.45	4	2.17	1.55
0.45 – 0.50	3	3.34	0.04
0.50 – 0.55	7	6.04	0.15
0.55 – 0.60	3	8.91	3.92
0.60 - 0.65	15	10.68	1.75
0.65 – 0.71	10	10.28	0.01
0.71 – 0.76	9	7.68	0.23
0.76 – 0.81	3	4.17	0.33
0.81 - 1	1	1.73	0.31
			$X^2 = 8.26$

$\chi^2_{d=6;\,\alpha=0.05} = 12.59 \quad \therefore X^2 < \chi^2_{d;\alpha}$

(b) Beat frequency = 2 Hz

Class interval	Number observed, n_i	Number expected, N_i	$\frac{(n_i - N_i)^2}{N_i}$
0 – 0.50	6	1.63	11.70
0.50 – 0.54	3	3.12	0.004
0.54 – 0.58	3	6.55	1.93
0.58 – 0.62	8	11.02	0.83
0.62 – 0.67	10	14.74	1.52
0.67 - 0.71	17	15.43	0.16
0.71 – 0.75	22	12.25	7.77
0.75 – 1	6	10.27	1.77
			$X^2 = 25.68$

$\chi^2_{d=5;\,\alpha=0.05} = 11.07 \quad \therefore X^2 > \chi^2_{d;\alpha}$

(c) Beat frequency = 2.67 Hz

Class interval	Number observed, n_i	Number expected, N_i	$\frac{(n_i - N_i)^2}{N_i}$
0 – 0.58	2	2.62	0.15
0.58 – 0.61	1	2.15	0.61
0.61 – 0.65	2	3.37	0.55
0.65 – 0.68	6	4.90	0.25
0.68 – 0.72	8	6.62	0.29
0.72 - 0.75	7	8.25	0.19
0.75 – 0.78	17	9.39	0.17
0.78 – 0.82	12	9.60	0.60
0.82 – 0.85	3	8.58	3.63
0.85 - 0.88	4	6.40	0.90
0.88 – 0.92	3	3.64	0.11
0.92 - 1	2	1.48	0.19
			$X^2 = 13.63$

$\chi^2_{d=9;\,\alpha=0.05} = 16.92 \quad \therefore X^2 < \chi^2_{d;\alpha}$

(d) Beat frequency = 3.5 Hz

Class interval	Number observed, n_i	Number expected, N_i	$\frac{(n_i - N_i)^2}{N_i}$
0 – 0.62	1	1.64	0.26
0.62 – 0.66	2	1.42	0.24
0.66 – 0.70	4	2.28	1.30
0.70 – 0.74	1	3.42	1.71
0.74 – 0.78	5	4.74	0.01
0.78 – 0.82	5	6.03	0.18
0.82 - 0.86	8	6.89	0.18
0.86 – 0.90	8	6.77	0.22
0.90 – 0.94	4	5.21	0.28
0.94 - 1	3	2.59	0.06
			$X^2 = 4.44$

$\chi^2_{d=7;\,\alpha=0.05} = 14.07 \quad \therefore X^2 < \chi^2_{d;\alpha}$

Table 5.3: Calculations for χ^2 goodness-of-fit test for fitting a Beta distribution to the transformed mean phase delay, $\overline{\theta}^*_{\text{delay}}$:
(a) 1.5 Hz. (b) 2 Hz. (c) 2.67 Hz. (d) 3.5 Hz.

Beat frequency (Hz)	α	β
1.5	13.67	7.97
2	24.34	12.30
2.67	15.16	4.77
3.5	12.63	3.00

Table 5.4: Values of the α and β parameters defining the Beta distribution of the transformed mean phase delay, $\overline{\theta}^{*}_{\text{delay}}$.

Order of regression, m	Relative reduction in mean of $\sigma_{\Delta T,\, m}$ (%)			
	1.5 Hz	2 Hz	2.67 Hz	3.5 Hz
1	58.3	65.4	59.1	62.1
2	18.1	12.7	11.90	8.9
3	2.7	2.0	2.3	1.3
4	3.8	1.4	1.0	0.8

Table 5.5: Relative reduction in the mean of standard deviation of random order, $\sigma_{\Delta T,\, m}$, for increasing regression order (m = 1 to 4).

(a) Beat frequency = 1.5 Hz

Class interval	Number observed, n_i	Number expected, N_i	$\frac{(n_i - N_i)^2}{N_i}$
0 – 0.72	1	2.02	0.51
0.72 – 0.75	1	1.35	0.09
0.75 – 0.77	3	2.05	0.44
0.77 – 0.80	2	3.01	0.34
0.80 – 0.82	4	4.22	0.01
0.82 - 0.85	10	5.62	3.42
0.85 – 0.87	5	7.04	0.59
0.87 – 0.90	8	8.15	0.003
0.90 - 0.92	11	8.45	0.77
0.92 – 0.95	5	7.38	0.77
0.95 – 0.97	2	4.62	1.48
0.97 - 1	3	1.10	3.28
			$X^2 = 11.70$

$\chi^2_{d=9;\,\alpha=0.05} = 16.92 \quad \therefore X^2 < \chi^2_{d;\alpha}$

(b) Beat frequency = 2 Hz

Class interval	Number observed, n_i	Number expected, N_i	$\frac{(n_i - N_i)^2}{N_i}$
0 – 0.71	2	1.26	0.43
0.71 – 0.74	2	1.13	0.68
0.74 – 0.77	1	1.95	0.46
0.77 – 0.80	2	3.22	0.46
0.80 – 0.83	5	5.07	0.0009
0.83 - 0.85	7	7.53	0.04
0.85 – 0.88	7	10.44	1.13
0.88 – 0.91	15	13.19	0.25
0.91 – 0.94	18	14.49	0.85
0.94 – 0.97	13	12.19	0.05
0.97 - 1	3	4.53	0.52
			$X^2 = 4.87$

$\chi^2_{d=8;\,\alpha=0.05} = 15.51 \quad \therefore X^2 < \chi^2_{d;\alpha}$

(c) Beat frequency = 2.67 Hz

Class interval	Number observed, n_i	Number expected, N_i	$\frac{(n_i - N_i)^2}{N_i}$
0 – 0.75	4	1.97	2.10
0.75 – 0.77	0	1.73	1.73
0.77 – 0.80	2	2.92	0.29
0.80 - 0.82	3	4.63	0.58
0.82 – 0.85	6	6.86	0.11
0.85 – 0.87	11	9.34	0.30
0.87 – 0.90	15	11.41	1.13
0.90 - 0.92	10	12.01	0.34
0.92 – 0.95	12	9.98	0.41
0.95 – 0.97	3	5.30	1.00
0.97 - 1	1	0.85	0.03
			$X^2 = 8.00$

$\chi^2_{d=8;\,\alpha=0.05} = 15.51 \quad \therefore X^2 < \chi^2_{d;\alpha}$

(d) Beat frequency = 3.5 Hz

Class interval	Number observed, n_i	Number expected, N_i	$\frac{(n_i - N_i)^2}{N_i}$
0 – 0.74	1	1.57	0.20
0.74 – 0.77	1	1.04	0.001
0.77 – 0.80	5	1.60	7.22
0.80 – 0.83	2	2.39	0.06
0.83 – 0.86	1	3.44	1.73
0.86 – 0.88	4	4.75	0.12
0.88 - 0.91	5	6.21	0.24
0.91 – 0.94	11	7.49	1.65
0.94 – 0.97	7	7.76	0.07
0.97 - 1	4	4.75	0.12
			$X^2 = 11.42$

$\chi^2_{d=7;\,\alpha=0.05} = 14.07 \quad \therefore X^2 < \chi^2_{d;\alpha}$

Table 5.6: Calculations for χ^2 goodness-of-fit test for fitting a Beta distribution to the auto-regression coefficient, ρ_1: (a) 1.5 Hz. (b) 2 Hz. (c) 2.67 Hz. (d) 3.5 Hz.

Beat frequency (Hz)	α	β
1.5	18.94	2.86
2	18.98	2.40
2.67	25.74	3.55
3.5	15.08	1.76

Table 5.7: Values of the α and β parameters defining the Beta distribution of the auto-regression coefficient, ρ_1.

(a) Beat frequency = 1.5 Hz

Class interval	Number observed, n_i	Number expected, N_i	$\frac{(n_i - N_i)^2}{N_i}$
0 – 0. 041	5	6.12	0.21
0.041 – 0.052	11	7.88	1.23
0.051 – 0.063	8	9.64	0.28
0.063 – 0.075	10	9.33	0.05
0.075 - 0.086	11	7.61	1.51
0.086 – 0.097	4	5.46	0.39
0.097 – 0.108	0	3.54	3.54
0.108 – 0.119	3	2.10	0.39
0.119 – 0.131	0	1.16	1.16
0.131 - 1	2	1.15	0.63
			$X^2 = 9.38$

$\chi^2_{d=7;\,\alpha=0.05} = 14.07 \qquad \therefore X^2 < \chi^2_{d;\alpha}$

(b) Beat frequency = 2 Hz

Class interval	Number observed, n_i	Number expected, N_i	$\frac{(n_i - N_i)^2}{N_i}$
0 – 0.033	3	3.82	0.18
0.033 – 0.037	2	5.70	2.40
0.037 – 0.040	15	9.05	3.91
0.040 – 0.044	11	11.39	0.01
0.044 – 0.048	12	11.77	0.005
0.048 – 0.052	14	10.27	1.35
0.052 – 0.055	3	7.75	2.91
0.055 – 0.059	4	5.15	0.26
0.059 – 0.063	1	3.05	1.38
0.063 - 1	6	3.05	2.85
			$X^2 = 15.26$

$\chi^2_{d=7;\,\alpha=0.05} = 14.07 \qquad \therefore X^2 > \chi^2_{d;\alpha}$

(c) Beat frequency = 2.67 Hz

Class interval	Number observed, n_i	Number expected, N_i	$\frac{(n_i - N_i)^2}{N_i}$
0 – 0.035	1	4.09	2.34
0.035 – 0.041	6	6.46	0.03
0.041 – 0.048	13	9.65	1.16
0.048 – 0.054	20	11.09	7.15
0.054 – 0.060	6	10.39	1.85
0.060 – 0.066	6	8.25	0.61
0.066 – 0.073	3	5.72	1.29
0.073 – 0.079	1	3.53	1.81
0.079 – 0.085	3	1.97	0.54
0.085 - 1	4	1.85	2.49
			$X^2 = 19.29$

$\chi^2_{d=7;\,\alpha=0.05} = 14.07 \qquad \therefore X^2 > \chi^2_{d;\alpha}$

(d) Beat frequency = 3.5 Hz

Class interval	Number observed, n_i	Number expected, N_i	$\frac{(n_i - N_i)^2}{N_i}$
0 – 0.046	2	1.51	0.16
0.046 – 0.051	2	2.36	0.05
0.051 – 0.056	3	3.97	0.24
0.056 – 0.061	7	5.33	0.52
0.061 – 0.066	7	5.91	0.20
0.066 – 0.071	3	5.57	1.19
0.071 – 0.077	3	4.55	0.53
0.077 – 0.082	4	3.27	0.16
0.082 – 0.087	4	2.10	1.71
0.087 - 1	2	2.43	0.08
			$X^2 = 4.83$

$\chi^2_{d=7;\,\alpha=0.05} = 14.07 \qquad \therefore X^2 < \chi^2_{d;\alpha}$

Table 5.8: Calculations for χ^2 goodness-of-fit test for fitting a Beta distribution to the transformed standard deviation of random error, $\sigma^*_{\Delta\theta',m=1}$: (a) 1.5 Hz. (b) 2 Hz. (c) 2.67 Hz. (d) 3.5 Hz.

Beat frequency (Hz)	α	β
1.5	6.86	91.00
2	25.68	528.07
2.67	13.86	237.30
3.5	26.08	365.23

Table 5.9: Values of the α and β parameters defining the Beta distribution of the transformed standard deviation of random error, $\sigma^*_{\Delta\theta',m=1}$.

	1.5 Hz	2 Hz	2.67 Hz	3.5 Hz	Total
Gaussian	0.2551	0.1261	0.0878	0.0984	0.5673
cos(t)	0.1670	0.1298	0.1435	0.1108	0.5511
$\cos^2(t)$	0.1976	0.0894	0.0808	0.0649	0.4327

Table 5.10: Mean of all μ_{RMSE} for curve-fitting measured impulses with Gaussian distribution, cosine and cosine-squared functions.

Beat frequency	Mean		
(Hz)	1st	2nd	3rd
1.5	1.429	0.495	0.199
2	1.573	0.735	0.192
2.67	1.550	0.702	0.169
3.5	1.462	0.513	0.057

Table 5.11: Mean of Fourier coefficients for the first three harmonics at four beat frequencies.

Beat frequency	Line of best fit: $y = mx + c$		Maximum absolute error
(Hz)	m	c	(times period of beat)
1.5	1.2791	-0.2830	0.021
2	1.1934	-0.1953	0.014
2.67	1.1970	-0.1994	0.015
3.5	1.1808	-0.1831	0.014

Table 5.12: Coefficients for the line of best fit and the maximum absolute error evaluated for i_k from 0.9375 to 1.0625.

(a) Beat frequency = 1.5 Hz

Class interval	Number observed, n_i	Number expected, N_i	$\frac{(n_i - N_i)^2}{N_i}$
0 – 0. 481	2	1.97	0.0006
0.481 – 0.526	2	2.01	0.0001
0.526 – 0.570	4	3.22	0.19
0.570 – 0.614	3	4.57	0.54
0.614 – 0.659	6	5.74	0.01
0.659 – 0.703	4	6.35	0.87
0.703 – 0.747	10	6.08	2.53
0.747 – 0.792	4	4.91	0.17
0.792 – 0.836	3	3.18	0.01
0.836 – 1	2	1.98	0.0001
			$X^2 = 4.31$

$\chi^2_{d=7;\,\alpha=0.05} = 14.07 \quad \therefore X^2 < \chi^2_{d;\alpha}$

(b) Beat frequency = 2 Hz

Class interval	Number observed, n_i	Number expected, N_i	$\frac{(n_i - N_i)^2}{N_i}$
0 – 0. 448	3	4.22	0.35
0.448 – 0.484	7	4.24	1.79
0.484 – 0.520	9	6.52	0.94
0.520 – 0.556	6	8.72	0.85
0.556 – 0.591	8	10.16	0.46
0.591 – 0.627	9	10.29	0.16
0.627 – 0.663	11	8.97	0.46
0.663 – 0.698	8	6.66	0.27
0.698 – 0.734	2	4.11	1.09
0.734 – 0.770	3	2.05	0.44
0.770 – 0.1	1	1.05	0.002
			$X^2 = 6.81$

$\chi^2_{d=8;\,\alpha=0.05} = 15.51 \quad \therefore X^2 < \chi^2_{d;\alpha}$

(c) Beat frequency = 2.67 Hz

Class interval	Number observed, n_i	Number expected, N_i	$\frac{(n_i - N_i)^2}{N_i}$
0 – 0. 502	4	4.91	0.17
0.502 – 0.530	3	4.40	0.45
0.530 – 0.558	11	6.42	3.26
0.558 – 0.586	8	8.16	0.003
0.586 – 0.614	11	9.00	0.45
0.614 – 0.642	5	8.57	1.49
0.642 – 0.670	7	6.99	0.000004
0.670 – 0.698	4	4.83	0.14
0.698 – 0.726	1	2.78	1.14
0.726 - 1	4	1.93	2.21
			$X^2 = 9.31$

$\chi^2_{d=7;\,\alpha=0.05} = 14.07 \quad \therefore X^2 < \chi^2_{d;\alpha}$

(d) Beat frequency = 3.5 Hz

Class interval	Number observed, n_i	Number expected, N_i	$\frac{(n_i - N_i)^2}{N_i}$
0 – 0. 596	1	1.42	0.12
0.596 – 0.616	1	1.59	0.22
0.616 – 0.636	1	2.70	1.07
0.636 – 0.655	5	3.98	0.26
0.655 – 0.675	12	5.09	9.36
0.675 – 0.695	1	5.61	3.79
0.695 – 0.715	3	5.28	0.99
0.715 – 0.735	4	4.19	0.009
0.735 – 0.755	4	2.76	0.56
0.755 – 1	3	2.37	0.17
			$X^2 = 16.55$

$\chi^2_{d=7;\,\alpha=0.05} = 14.07 \quad \therefore X^2 > \chi^2_{d;\alpha}$

Table 5.13: Calculations for χ^2 goodness-of-fit test for fitting a Beta distribution to the mean contact ratio, μ_α: (a) 1.5 Hz. (b) 2 Hz. (c) 2.67 Hz. (d) 3.5 Hz.

(a) Beat frequency = 1.5 Hz

Class interval	Number observed, n_i	Number expected, N_i	$\frac{(n_i - N_i)^2}{N_i}$
0 – 0. 042	3	2.24	0.26
0.042 – 0.051	2	3.41	0.58
0.051 – 0.060	5	5.09	0.002
0.060 – 0.069	4	6.05	0.69
0.069 – 0.079	6	6.06	0.0005
0.079 – 0.088	9	5.30	2.58
0.088 – 0.097	1	4.16	2.40
0.097 – 0.106	5	2.98	1.37
0.106 – 0.115	4	1.98	2.07
0.115 - 1	1	2.75	1.11
			$X^2 = 11.07$

$\chi^2_{d=7;\,\alpha=0.05} = 14.07 \quad \therefore X^2 < \chi^2_{d;\alpha}$

(b) Beat frequency = 2 Hz

Class interval	Number observed, n_i	Number expected, N_i	$\frac{(n_i - N_i)^2}{N_i}$
0 – 0. 022	5	4.56	0.042
0.022 – 0.027	8	7.19	0.092
0.027 – 0.032	9	10.34	0.174
0.032 – 0.036	13	11.52	0.191
0.036– 0.041	12	10.60	0.185
0.041 - 0.046	6	8.41	0.691
0.046– 0.051	6	5.93	0.0009
0.051 – 0.056	4	3.79	0.012
0.056 – 0.061	0	2.23	2.233
0.061 – 0.066	1	1.23	0.042
0.066 – 0.1	3	1.20	2.681
			$X^2 = 6.34$

$\chi^2_{d=8;\,\alpha=0.05} = 15.51 \quad \therefore X^2 < \chi^2_{d;\alpha}$

(c) Beat frequency = 2.67 Hz

Class interval	Number observed, n_i	Number expected, N_i	$\frac{(n_i - N_i)^2}{N_i}$
0 – 0. 020	8	7.21	0.088
0.020 – 0.024	9	7.87	0.163
0.024– 0.028	10	9.69	0.010
0.028– 0.031	9	9.65	0.044
0.031 – 0.035	8	8.16	0.003
0.035– 0.039	4	6.06	0.702
0.039 – 0.043	2	4.05	1.035
0.043 – 0.046	4	2.47	0.977
0.046 – 1	4	2.84	0.477
			$X^2 = 3.47$

$\chi^2_{d=6;\,\alpha=0.05} = 12.59 \quad \therefore X^2 < \chi^2_{d;\alpha}$

(d) Beat frequency = 3.5 Hz

Class interval	Number observed, n_i	Number expected, N_i	$\frac{(n_i - N_i)^2}{N_i}$
0 – 0. 018	3	2.50	0.101
0.018 – 0.020	3	3.20	0.013
0.020 – 0.022	3	4.68	0.606
0.022 – 0.024	6	5.53	0.040
0.024 – 0.027	6	5.48	0.050
0.027 – 0.029	6	4.67	0.378
0.029 – 0.031	2	3.51	0.650
0.031 – 0.033	3	2.36	0.171
0.033 – 0.035	2	1.45	0.211
0.035 – 1	1	1.61	0.231
			$X^2 = 2.45$

$\chi^2_{d=7;\,\alpha=0.05} = 14.07 \quad \therefore X^2 < \chi^2_{d;\alpha}$

Table 5.14: Calculations for χ^2 goodness-of-fit test for fitting a Beta distribution to the standard deviation of contact ratio, σ_α: (a) 1.5 Hz. (b) 2 Hz. (c) 2.67 Hz. (d) 3.5 Hz.

Beat frequency (Hz)	α	β
1.5	12.15	5.99
2	17.40	12.19
2.67	28.58	18.99
3.5	61.56	28.50

Table 5.15: Values of the α and β parameters defining the Beta distribution of the mean contact ratio, μ_α.

Beat frequency (Hz)	α	β
1.5	9.10	109.67
2	9.98	256.01
2.67	10.79	347.52
3.5	20.43	788.00

Table 5.16: Values of the α and β parameters defining the Beta distribution of the standard deviation of contact ratio, σ_α.

Beat frequency = 1.5 Hz		
Harmonic	Regression	Normal distribution
1st	8.2	9.3
2nd	14.3	25.3
3rd	36.8	25.8
Beat frequency = 2 Hz		
Harmonic	Regression	Normal distribution
1st	7.4	8.2
2nd	8.3	12.5
3rd	19.5	12.7
Beat frequency = 2.67 Hz		
Harmonic	Regression	Normal distribution
1st	5.6	6.2
2nd	6.7	9.7
3rd	16.3	9.5
Beat frequency = 3.5 Hz		
Harmonic	Regression	Normal distribution
1st	3.6	4.1
2nd	4.9	6.3
3rd	16.5	6.8

Table 5.17: Overall mean relative error for normalised maximum displacement due to loads generated from modelling contact ratio using regression and Normal distribution.

Beat frequency = 1.5 Hz		
Harmonic	Regression	Normal distribution
1st	9.5	9.4
2nd	15.5	20.4
3rd	61.0	49.3

Beat frequency = 2 Hz		
Harmonic	Regression	Normal distribution
1st	5.9	6.1
2nd	8.0	8.3
3rd	32.2	23.9

Beat frequency = 2.67 Hz		
Harmonic	Regression	Normal distribution
1st	4.1	4.3
2nd	5.7	6.9
3rd	29.0	20.3

Beat frequency = 3.5 Hz		
Harmonic	Regression	Normal distribution
1st	4.4	4.5
2nd	6.6	7.0
3rd	29.3	21.4

Table 5.18: Overall mean relative error for normalised RMS acceleration due to loads generated from modelling contact ratio using regression and Normal distribution.

	Beat Frequency (Hz)		
γ	2	2.67	3.5
0	69.5	21.1	32.5
0.15	14.1	10.9	23.3

Table 6.1: Maximum displacement in mm for a 4 Hz structure when all spectators are jumping ($\gamma = 0$) and when 50% are jumping ($\gamma = 0.15$).

	Beat Frequency (Hz)		
γ	2	2.67	3.5
0	2.21	0.27	0.50
0.15	0.25	0.13	0.49

Table 6.2: RMS acceleration (g) for a 4 Hz structure when all spectators are jumping ($\gamma = 0$) and when 50% are jumping ($\gamma = 0.15$).

	Mean	Std. Dev.
Age (years)	29	3.7
Weight (kg)	71.07	11.5

Table 7.1: Age and body weight of test subjects.

Test Subject	Jumping beat frequency (Hz)					
	1	1.5	2	2.5	3	3.5
1	0	+1	0	0	0	+2
2	0	+11	+1	+3	0	-1
3	+1	-4	+1	-9	-14	-30
4	0	0	0	0	0	0
5	0	-3	+1	-3	-4	-7
6	0	0	0	0	0	-8
7	0	0	0	0	0	0
8	0	0	0	0	0	0
9	0	0	0	0	0	0
10	0	0	0	-13	-7	-13
Number of synchronised test	9	6	7	6	7	4

Table 7.2: Number of extra or deficit jumps.

Test Subject	Bobbing beat frequency (Hz)					
	1	1.5	2	2.5	3	3.5
1	0	1	0	0	0	4
2	0	0	0	1	0	3
3	0	0	-3	0	4	-2
4	0	0	0	0	0	0
5	0	-6	-2	-11	-14	-9
6	0	0	0	0	0	0
7	0	0	0	0	0	0
8	0	0	0	0	0	0
9	0	0	0	0	0	0
10	0	0	0	0	0	0
Number of synchronised test	10	8	8	8	8	6

Table 7.3: Number of extra or deficit bobs.

Beat	Mean phase delay (^{o})	
frequency (Hz)	Mean	Standard Dev.
1	77	106
1.5	115 (42)	43 (47)
2	67 (55)	34 (37)
2.5	65 (93)	52 (31)
3	84	31
3.5	89 (111)	38 (36)

Table 7.4: Mean and standard deviation of mean phase delay for individual jumping tests compared with results from Parkhouse and Ewins's experimental data (2004) (given in brackets).

Beat	Phase scatter (^{o})	
frequency (Hz)	Mean	Standard Dev.
1	28	13
1.5	26 (32)	19 (16)
2	28 (25)	12 (12)
2.5	29 (24)	9 (9)
3	30	10
3.5	29 (32)	5 (11)

Table 7.5: Mean and standard deviation of phase scatter for individual jumping tests compared with results from Parkhouse and Ewins's experimental data (2004) (given in brackets).

Beat frequency (Hz)	Mean			Std. Dev.		
	1st	2nd	3rd	1st	2nd	3rd
1	0.286	0.965	0.279	0.12	0.20	0.23
1.5	0.506	0.744	0.200	0.39	0.39	0.08
2	1.343	0.451	0.132	0.26	0.18	0.07
2.5	1.480	0.532	0.105	0.06	0.08	0.05
3	1.521	0.598	0.133	0.10	0.16	0.07
3.5	1.434	0.460	0.035	0.04	0.06	0.02

Table 7.6: Mean and standard deviation of Fourier coefficients for average jumping impulse.

Beat frequency (Hz)	Mean			Std. Dev.		
	1st	2nd	3rd	1st	2nd	3rd
1	0.077	0.209	0.142	0.05	0.17	0.10
1.5	0.149	0.223	0.138	0.09	0.10	0.09
2	0.356	0.311	0.106	0.29	0.17	0.08
2.5	0.479	0.270	0.107	0.27	0.13	0.07
3	0.587	0.236	0.097	0.27	0.09	0.05
3.5	0.663	0.242	0.089	0.21	0.07	0.04

Table 7.7: Mean and standard deviation of Fourier coefficients for average bobbing impulse.

Pair number	Amount of reduction (%)	
	$\Delta\bar{\theta}$	$\Delta\sigma_{\theta'}$
1	73	56
2	53	68
3	39	65
4	74	64
5	35	76
6	53	52
7	37	86
8	68	71

Table 7.8: Average reduction in $\Delta\bar{\theta}$ and $\Delta\sigma_{\theta'}$ when jumping together and separately.

FIGURES

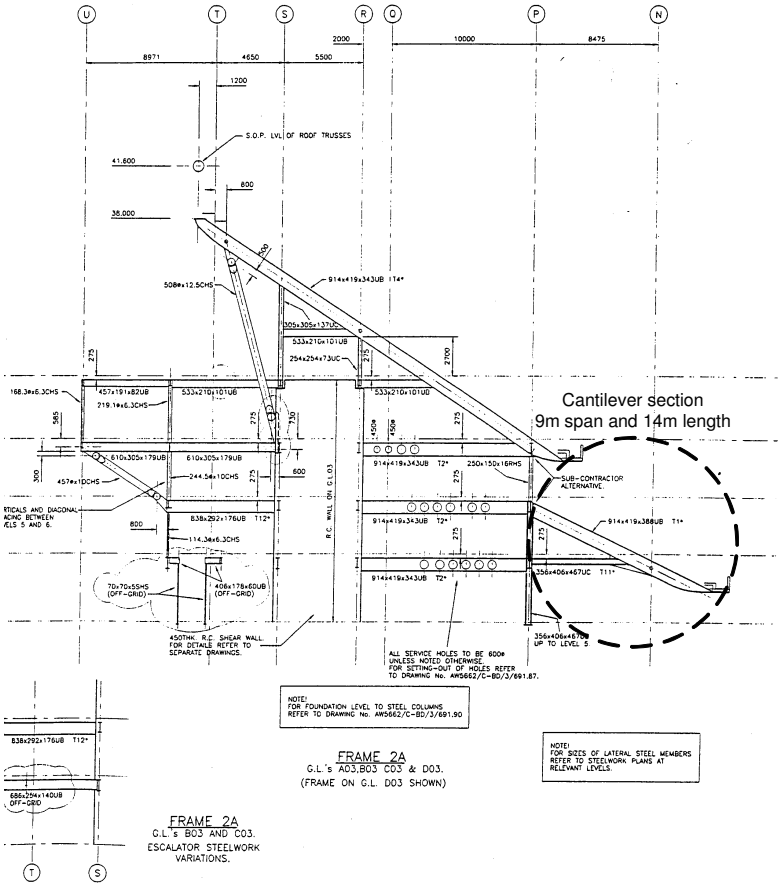

Figure 2.1: Cross-section of the Millennium Stadium in Cardiff, courtesy of W S Atkins. Shown in the circle is the cantilever grandstand.

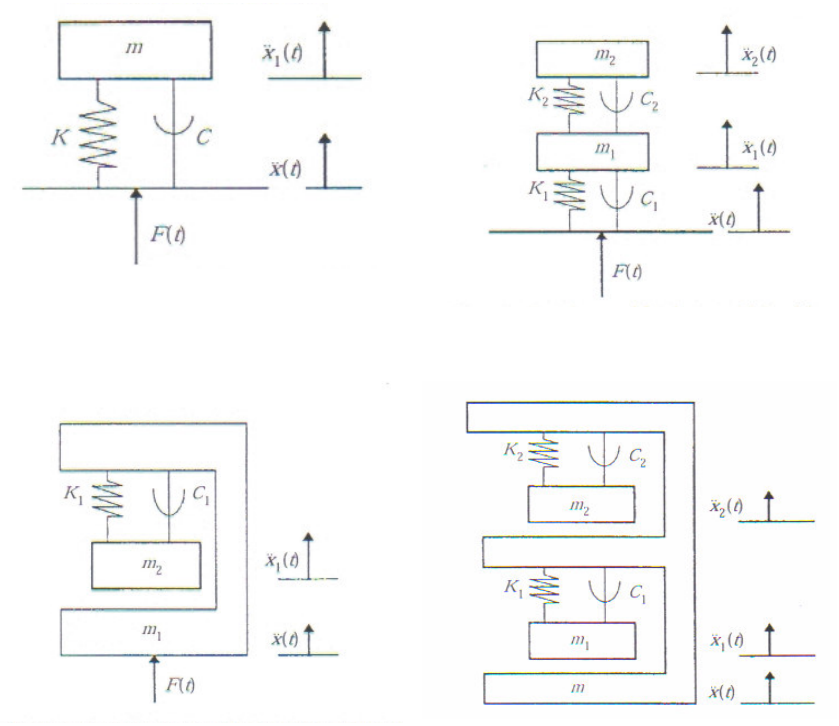

Figure 2.2: Mass-spring-damper systems developed by Wei and Griffin (1998) for seated humans: Model 1a (top left), Model 1b (top right), Model 2a (bottom left) and Model 2b (bottom right).

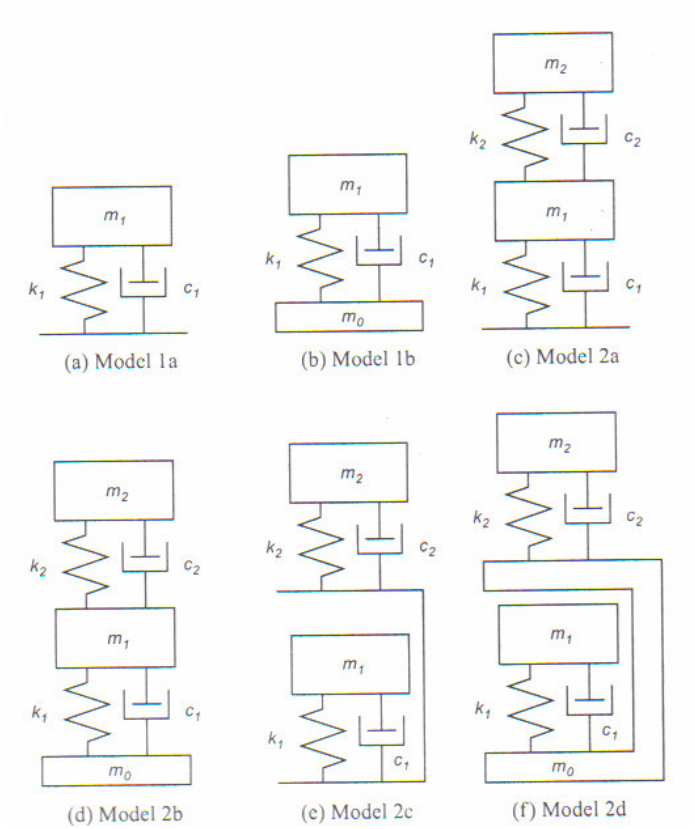

Figure 2.3: Mass-spring-damper systems developed by Matsumoto and Griffin (2003) for standing humans.

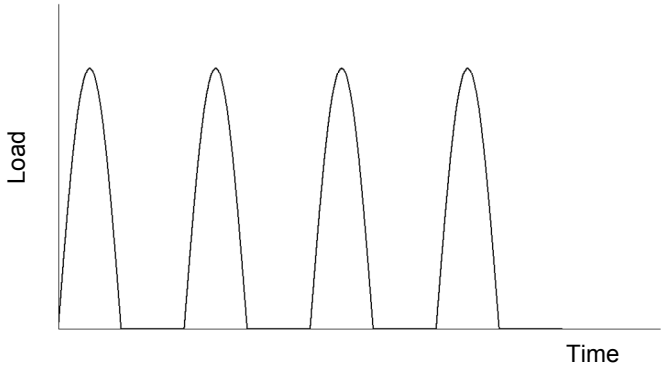

Figure 2.4: Idealised load-time history.

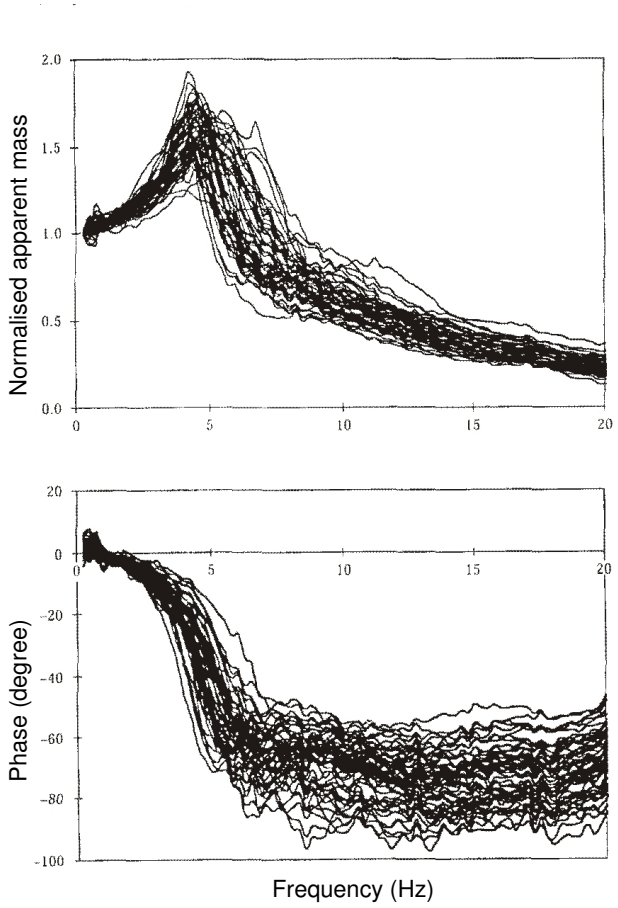

Figure 3.1: Normalised apparent mass and phase for 60 seated subjects, from Wei and Griffin (1998).

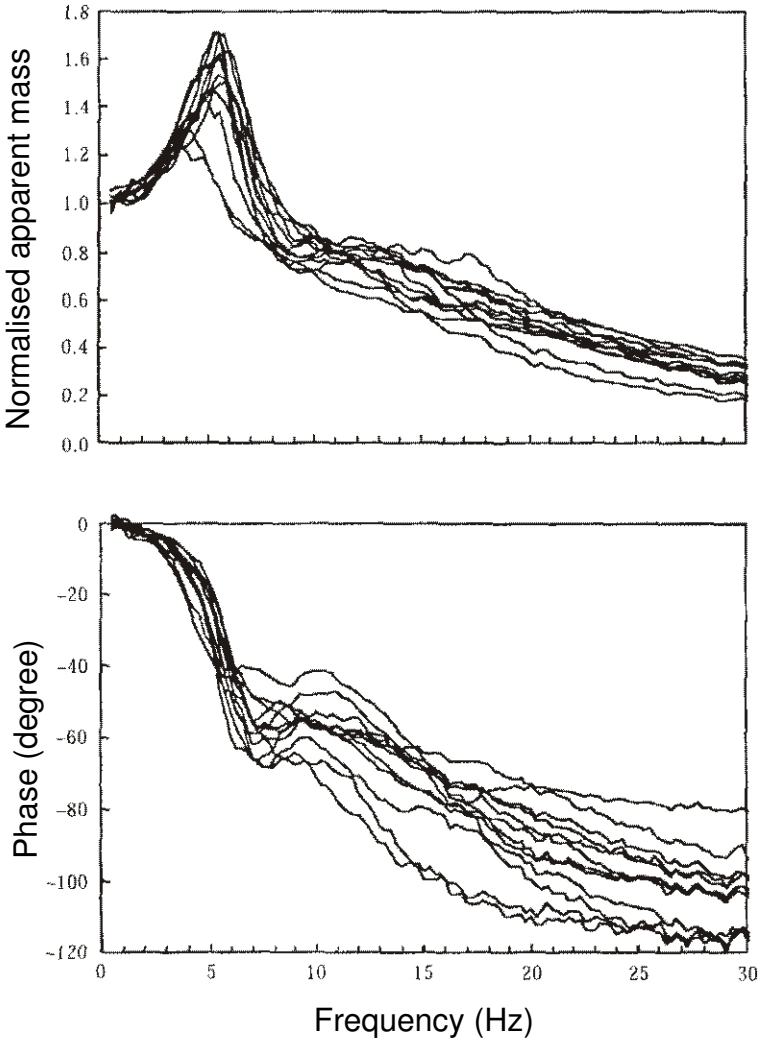

Figure 3.2: Normalised apparent mass and phase for 12 standing subjects, from Matsumoto and Griffin (2003).

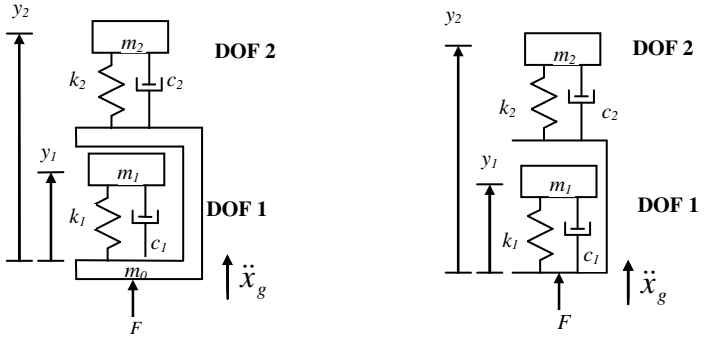

Figure 3.3: Lumped parameter model for a seated human (left) and a standing human (right), reproduced from Wei and Griffin (1998) and Matsumoto and Griffin (2003).

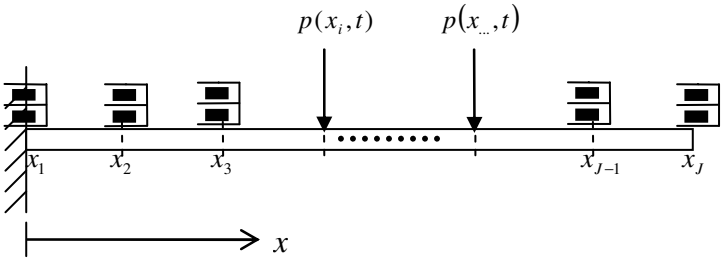

Figure 3.4: Discretised cantilever with seated human models and subjected to external loads.

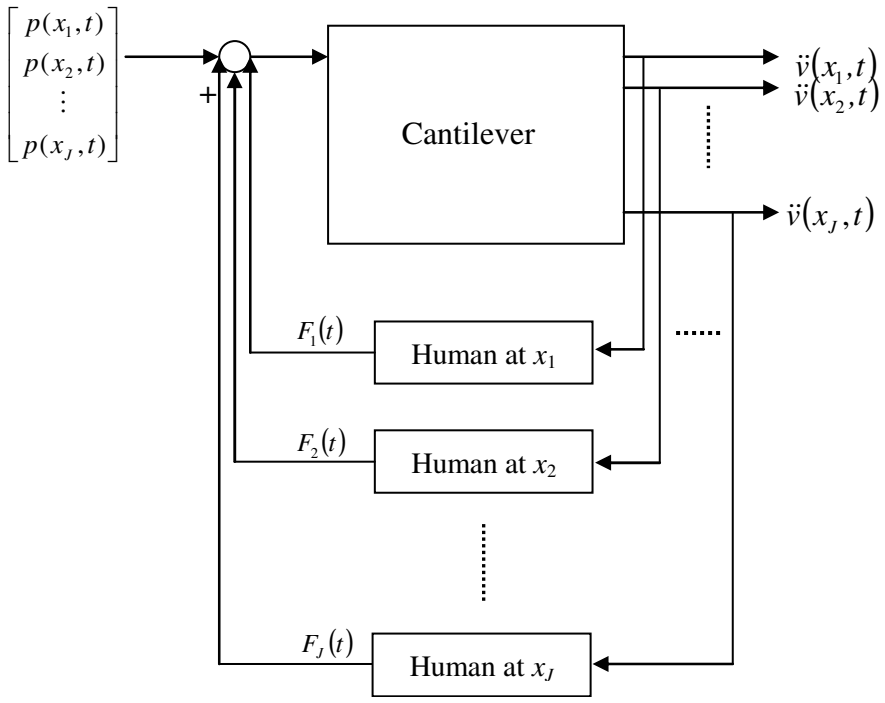

Figure 3.5: Feedback system representation for the cantilever-human system.

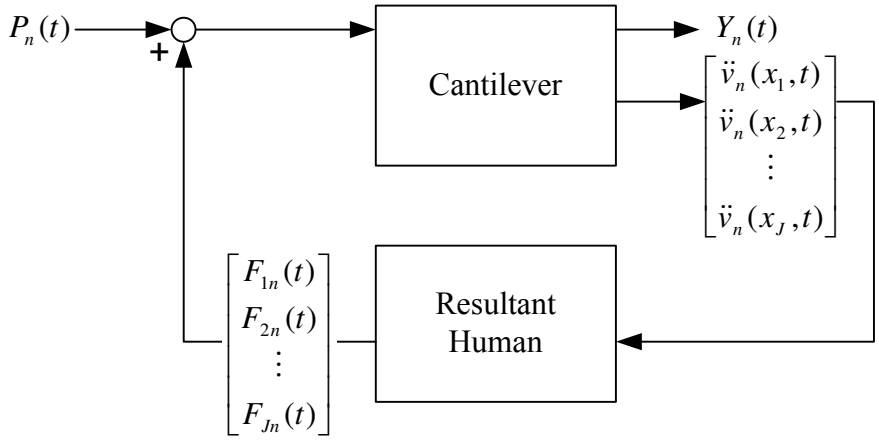

Figure 3.6: Simplified feedback system representation for the cantilever-human system.

Figure 3.7: Block diagram for the cantilever.

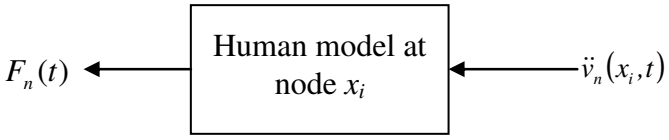

Figure 3.8: Block diagram for one seated human.

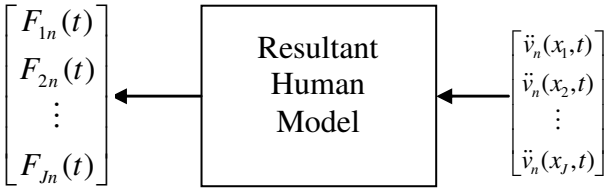

Figure 3.9: Block diagram for the resultant human model.

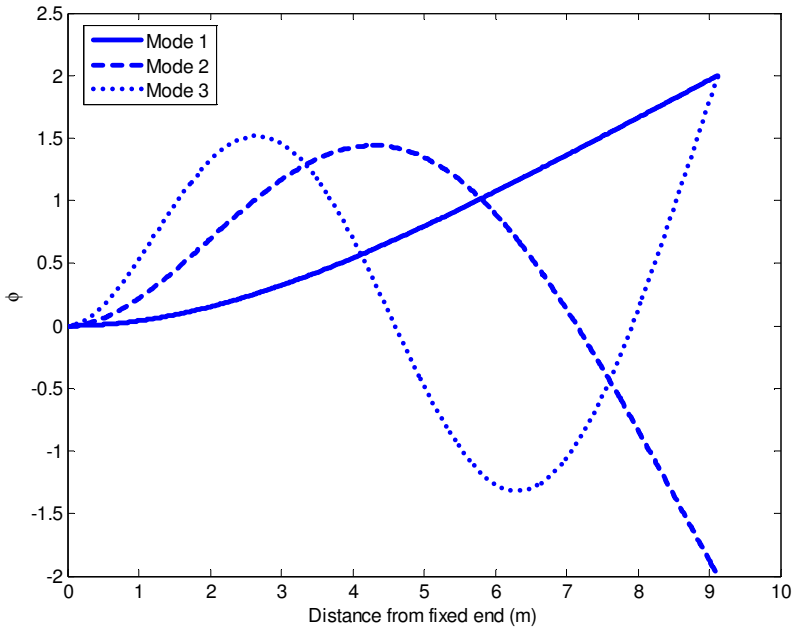

Figure 3.10: Mode shapes for the 4.2 Hz cantilever.

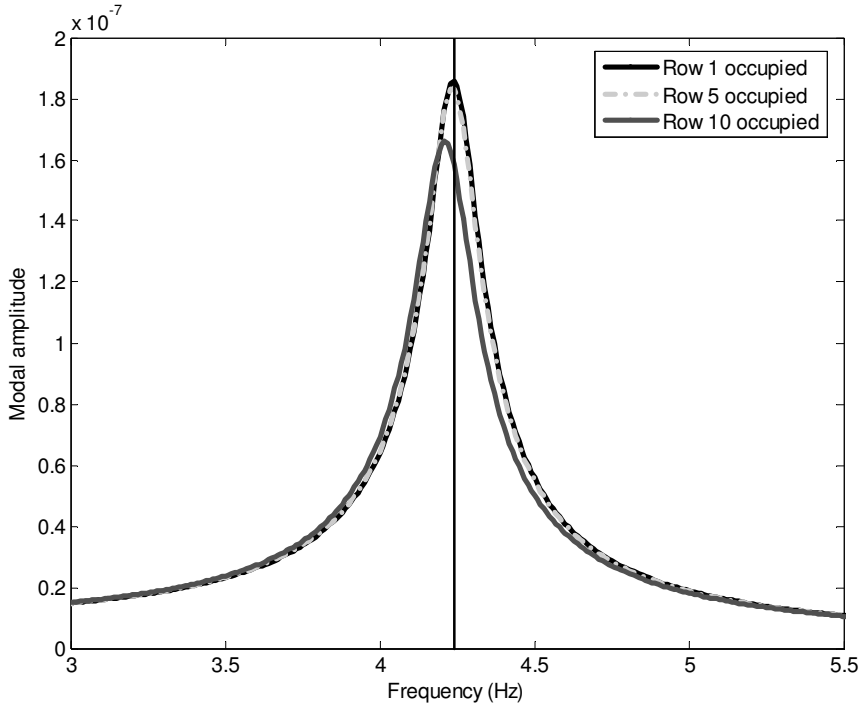

Figure 3.11: Modal amplitude frequency response of the 4.2 Hz cantilever with one row occupied by seated humans. (The vertical line marks the natural frequency of the empty structure).

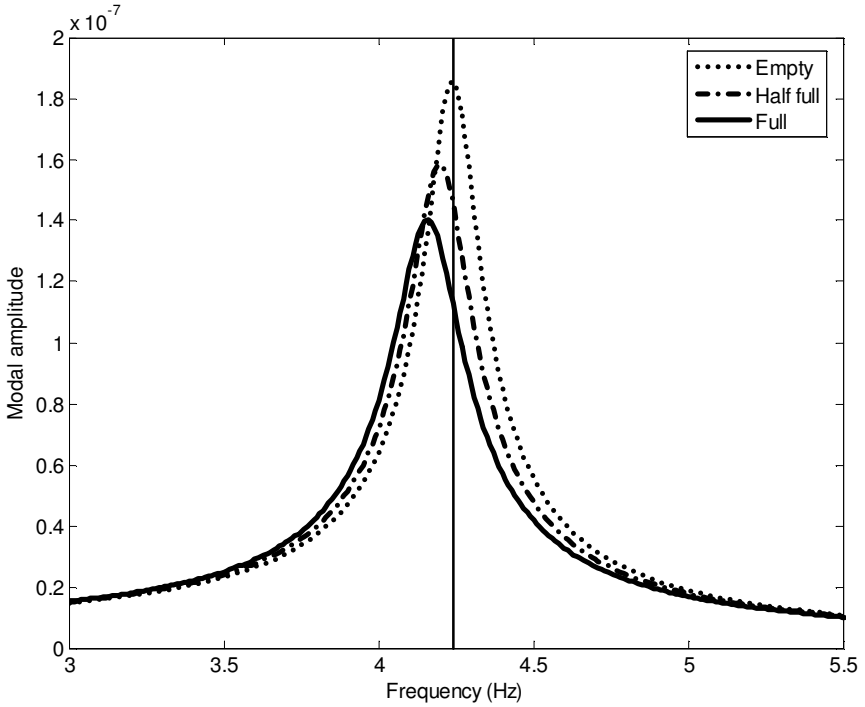

Figure 3.12: Modal amplitude frequency response of the 4.2 Hz cantilever when empty, half-full and full. (The vertical line marks the natural frequency of the empty structure).

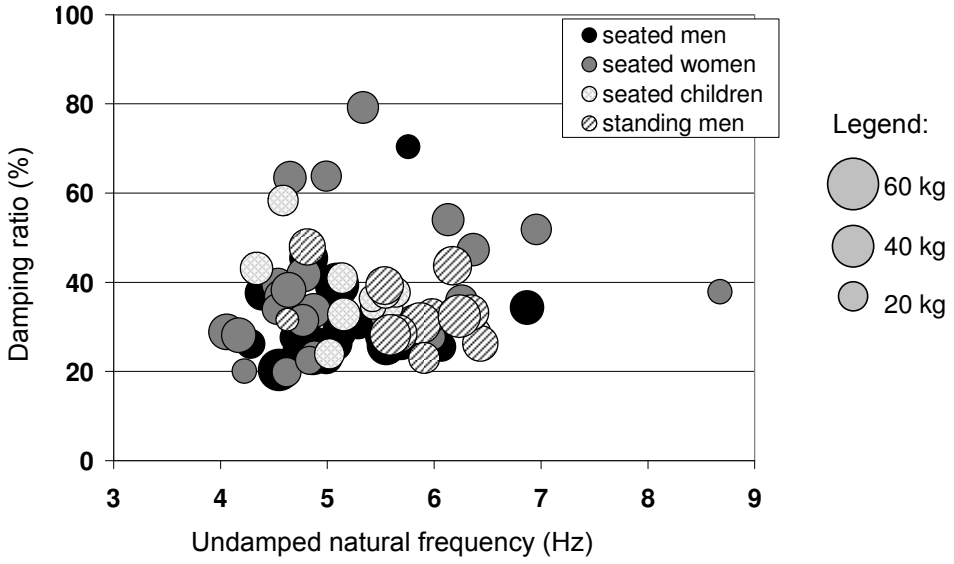

Figure 4.1: Plot of damping ratio, undamped natural frequency and mass ratio for DOF 1.

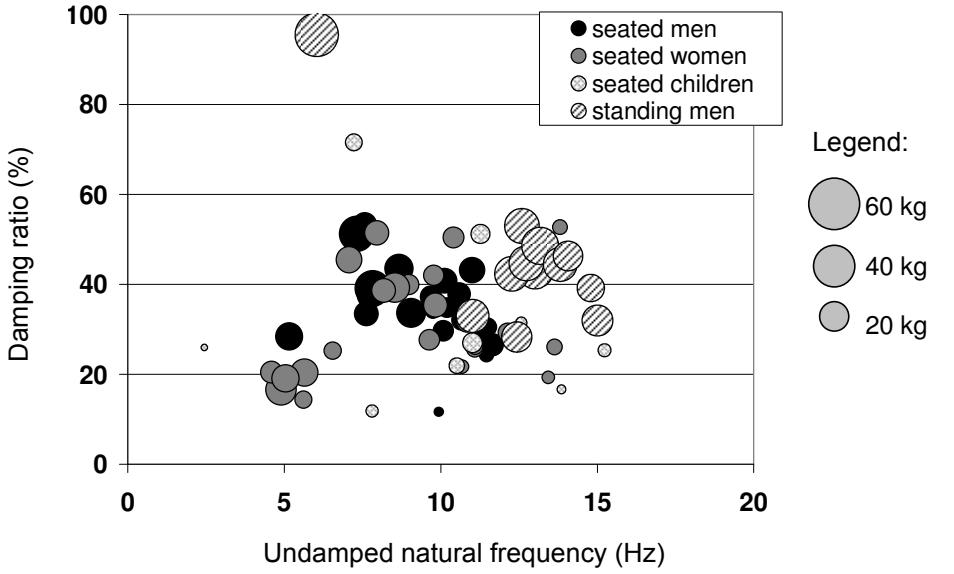

Figure 4.2: Plot of damping ratio, undamped natural frequency and mass ratio for DOF 2.

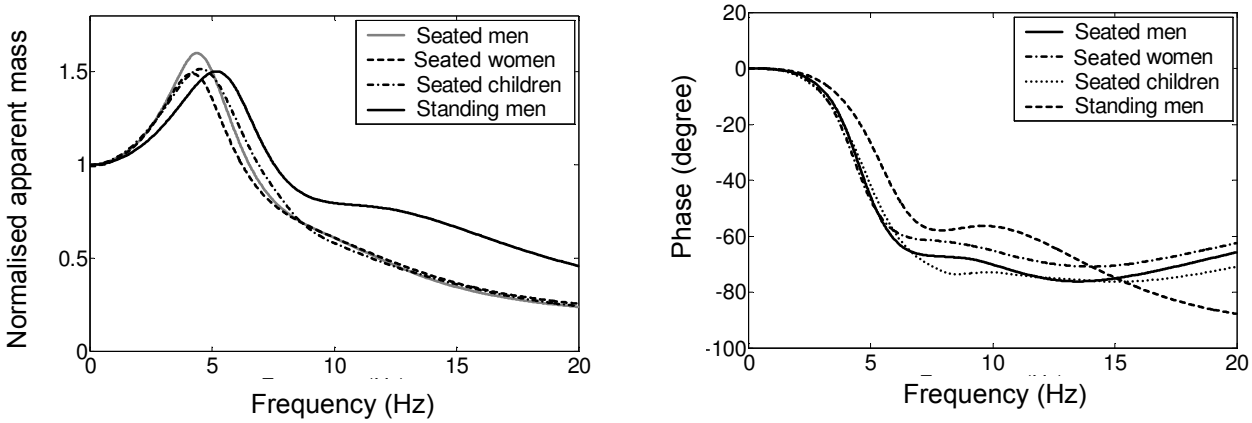

Figure 4.3: Average normalised apparent mass (top) and phase (bottom) for each group.

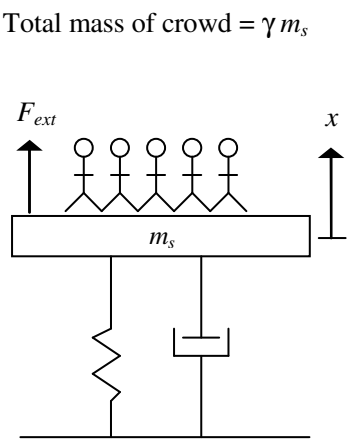

Figure 4.4: Crowd-structure model.

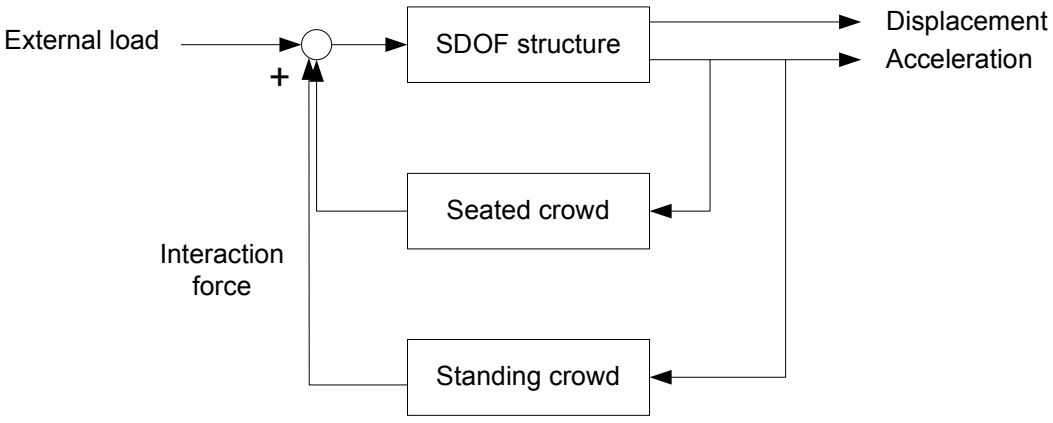

Figure 4.5: Block diagram representation for the crowd-structure model.

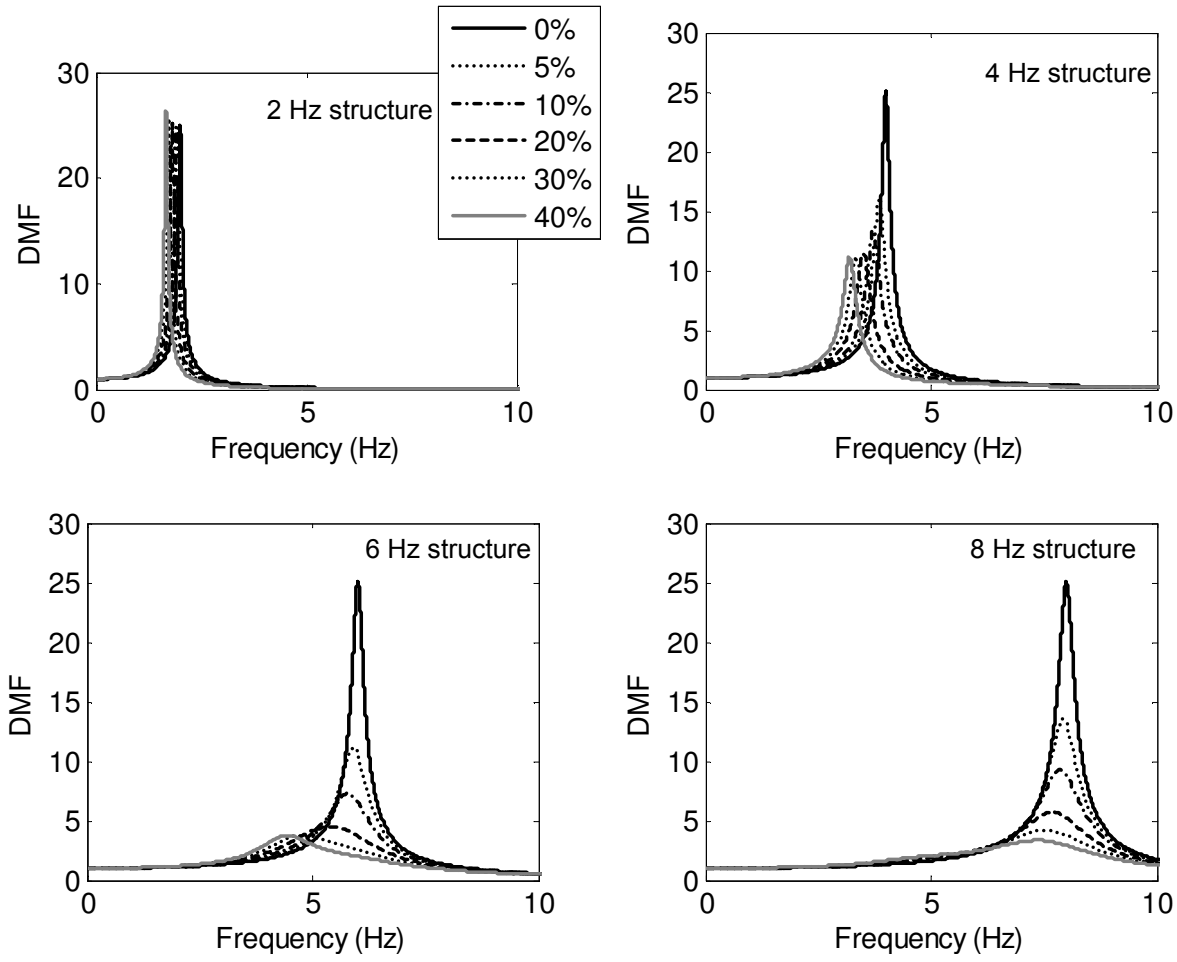

Figure 4.6: DMF for structures with 100% seated crowd and natural frequencies of 2, 4, 6 and 8 Hz.

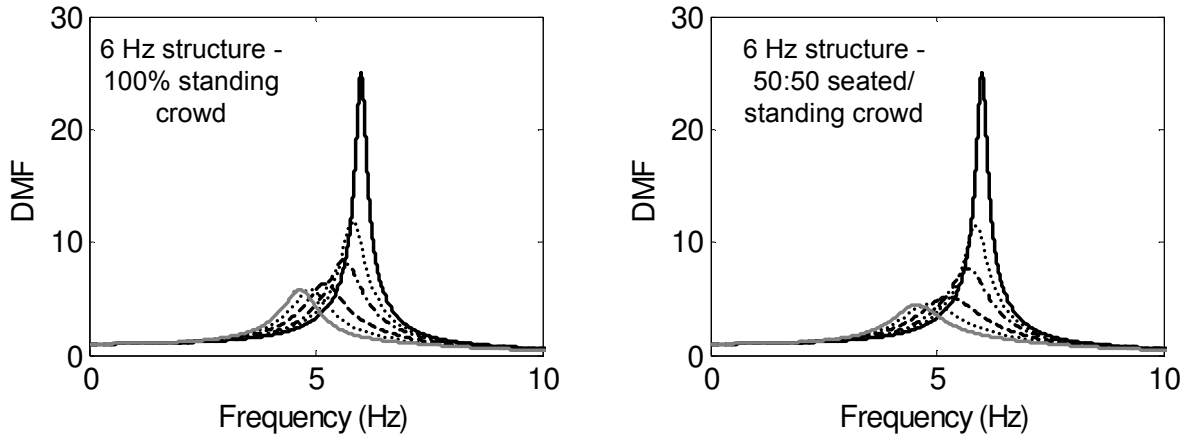

Figure 4.7: DMF for 6 Hz structure with 100% standing crowd (left) and 50:50 seated/standing crowd (right).

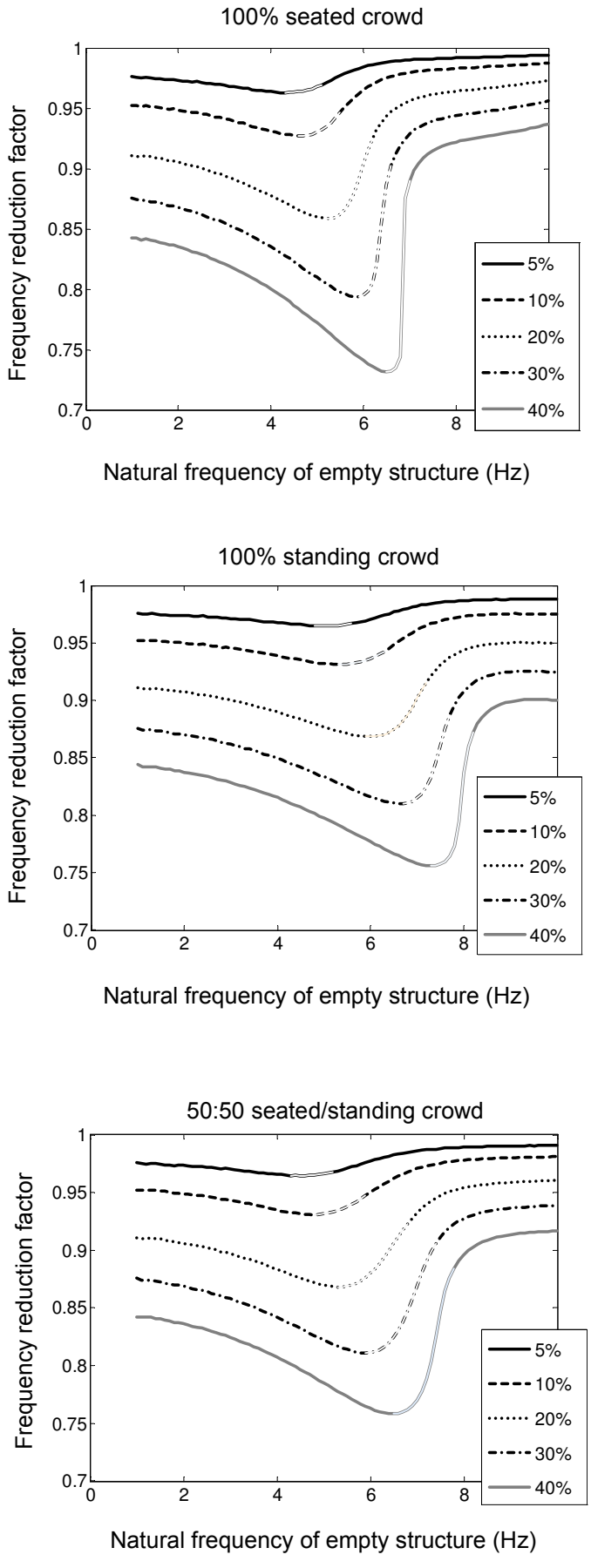

Figure 4.8: Frequency reduction factor for 100% seated crowd (top), 100% standing crowd (middle) and 50:50 seated/standing crowds (bottom).

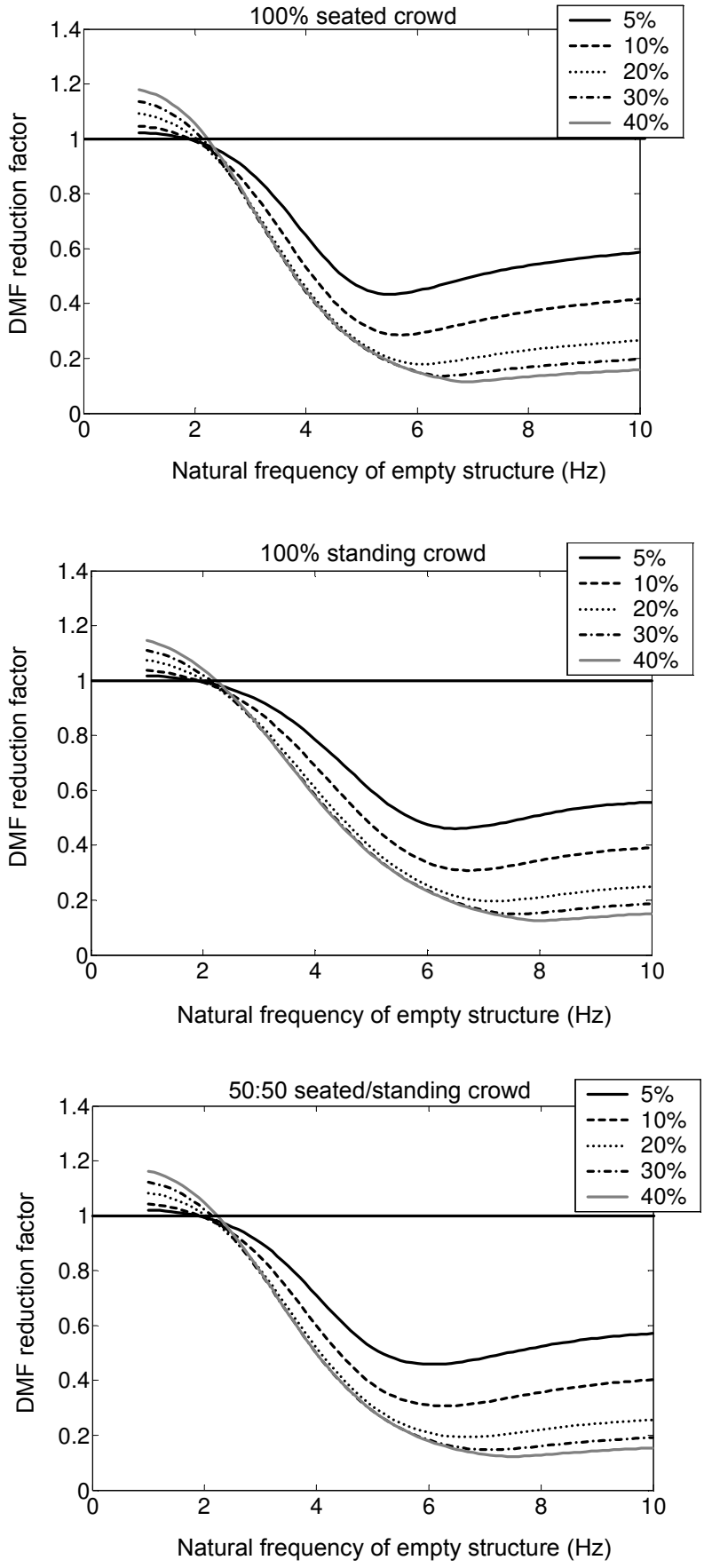

Figure 4.9: DMF reduction factor for 100% seated crowd (top), 100% standing crowd (middle) and 50:50 seated/standing crowds (bottom).

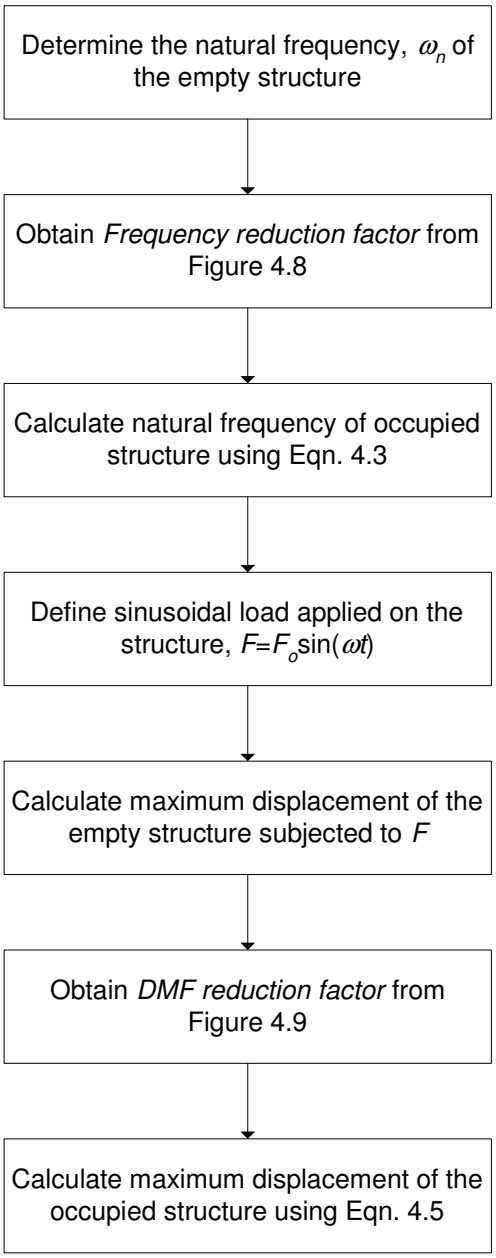

Figure 4.10: Flow chart for estimating the natural frequency and maximum displacement of an occupied structure using plots in Figures 4.8 and 4.9.

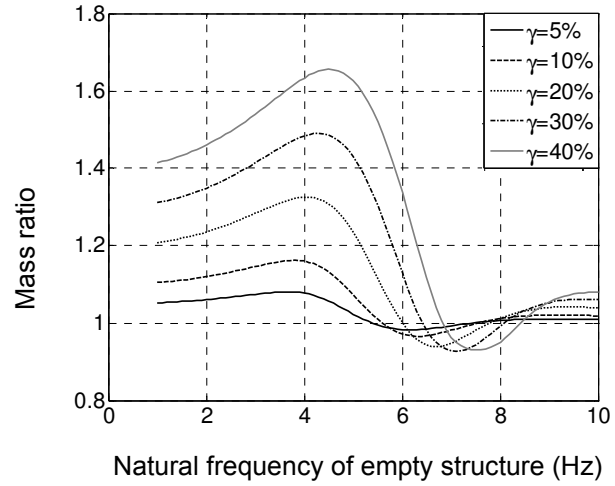

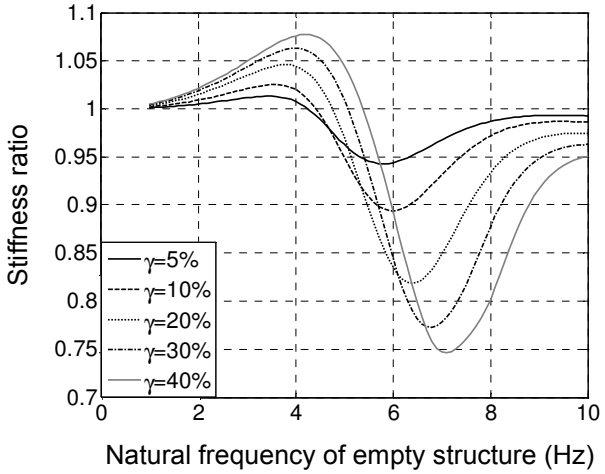

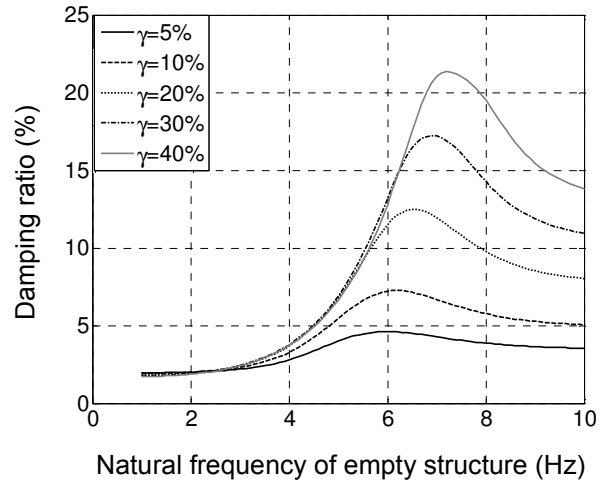

Figure 4.11: Mass, stiffness and damping ratios for equivalent SDOF system of a 50:50 seated/standing joint crowd-SDOF system, for a structure having 2% damping ratio when empty.

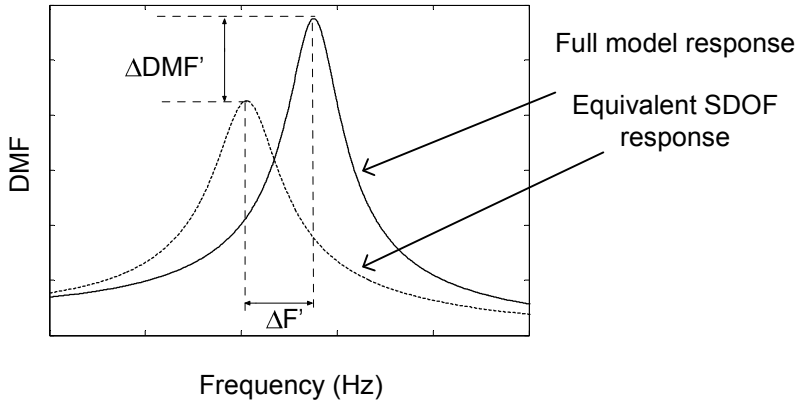

Figure 4.12: Illustrations on peak DMF and resonant frequency relative errors.

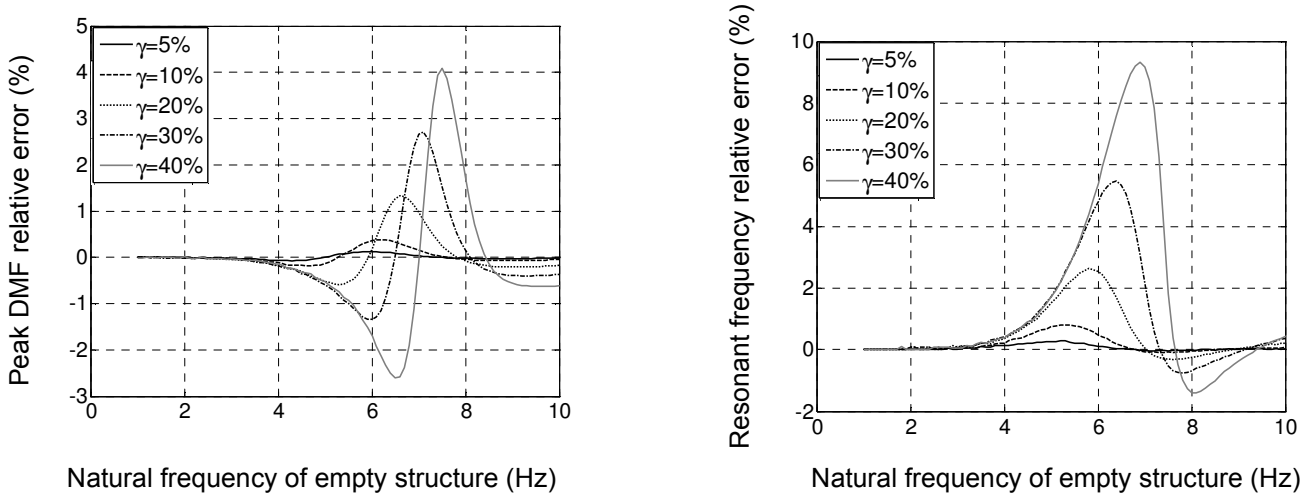

Figure 4.13: Peak DMF relative error (left) and resonant frequency relative error (right) for equivalent SDOF system.

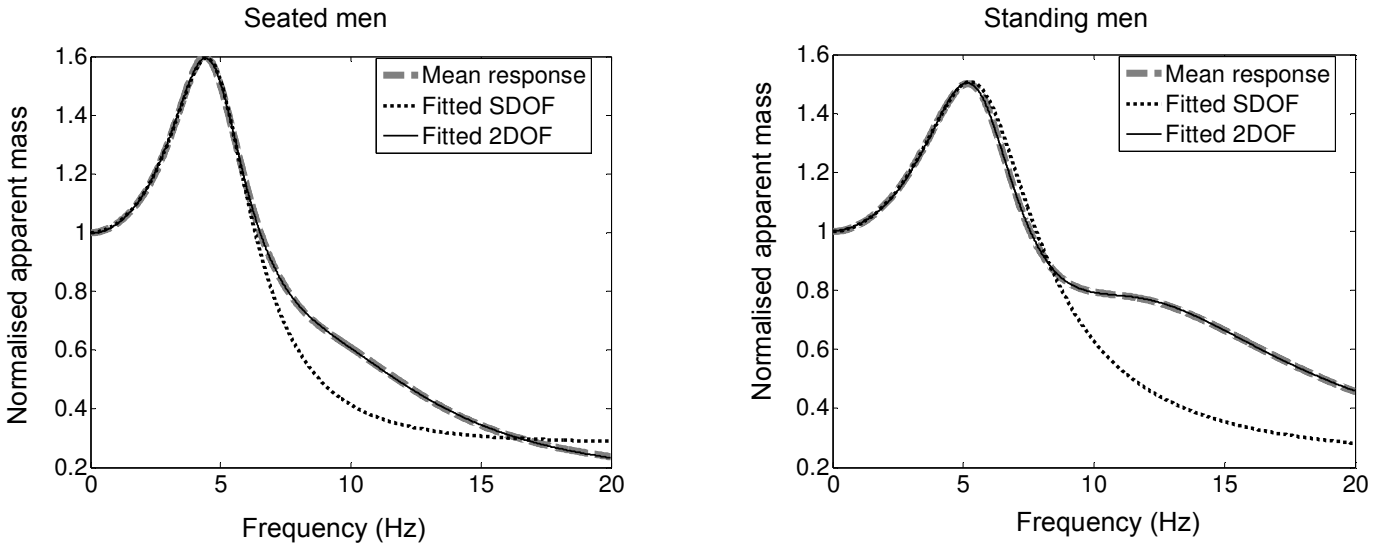

Figure 4.14: Average normalised apparent mass of seated (left) and standing (right) men plotted with fitted SDOF and 2DOF models.

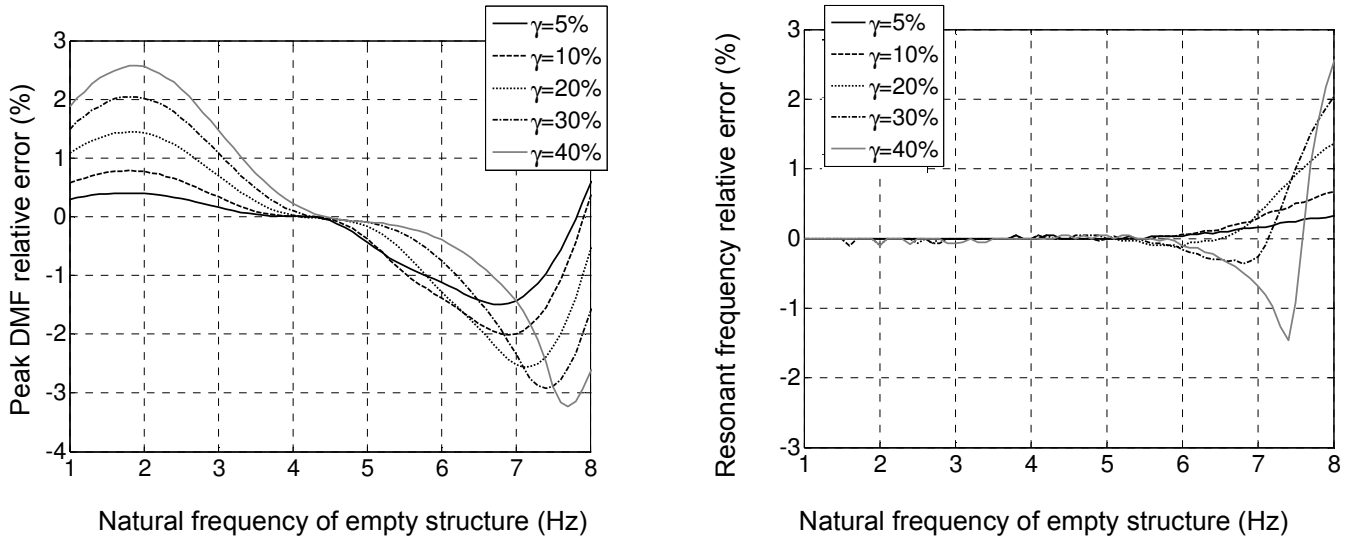

Figure 4.15: Peak DMF relative error (left) and resonant frequency relative error (right) for equivalent 3DOF system.

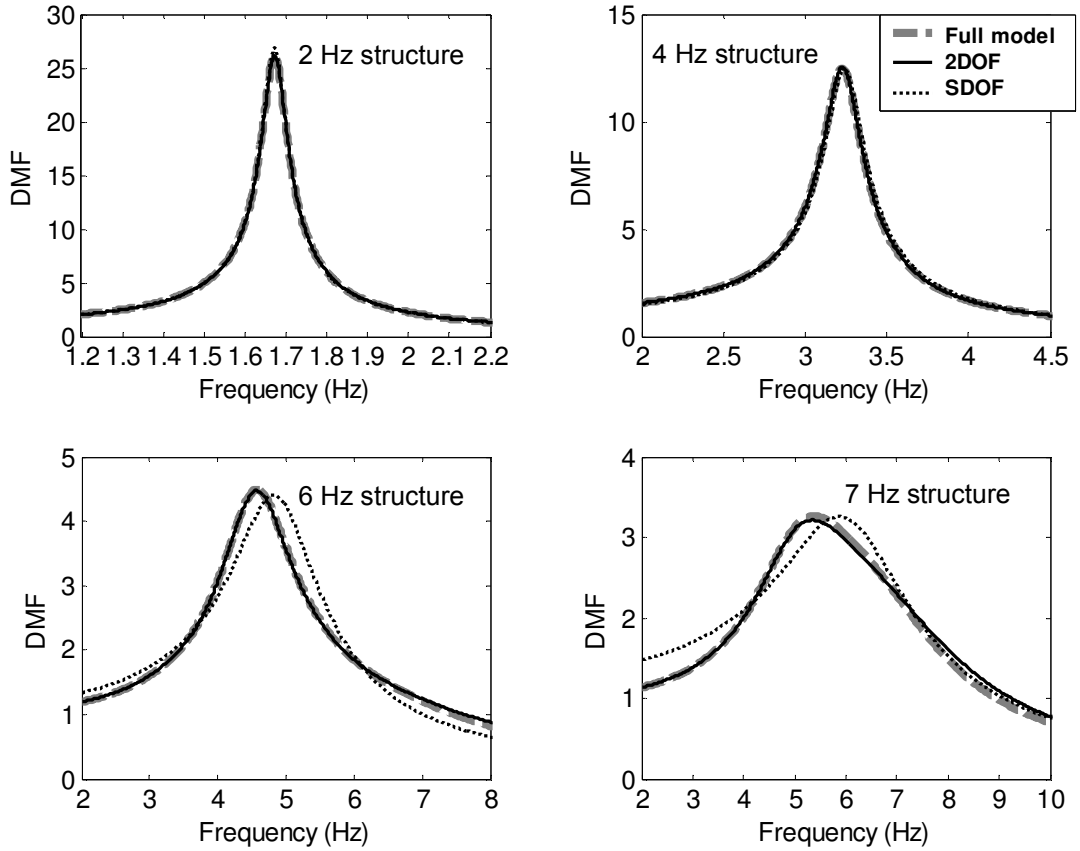

Figure 4.16: DMF-frequency response curves for 2, 4, 6 adnd 7 Hz structures with mass ratio of 0.4. Each plot showing the responses of full model, equivalent SDOF and 3DOF models.

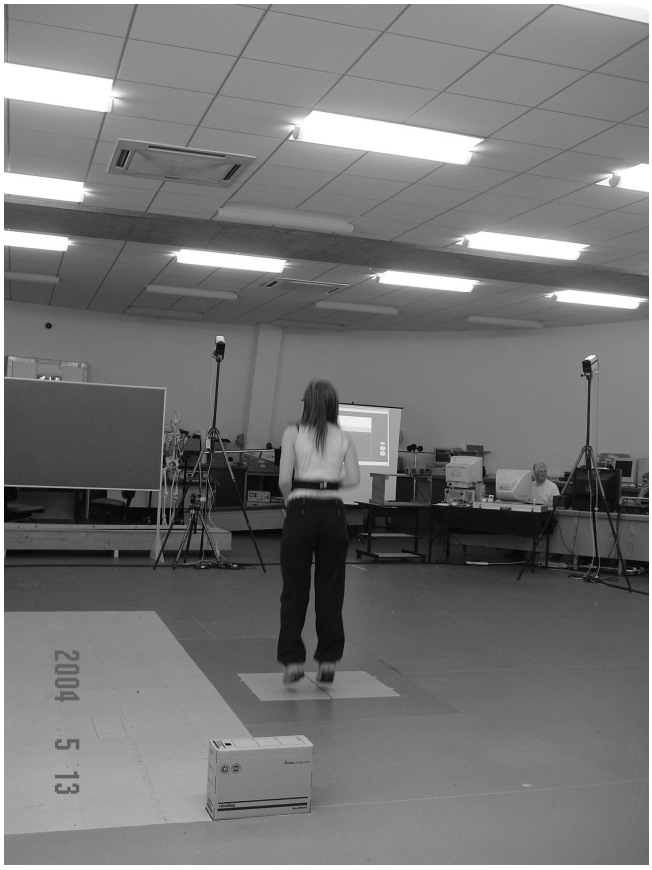

Figure 5.1: Photo showing one test subject jumping on a force plate.

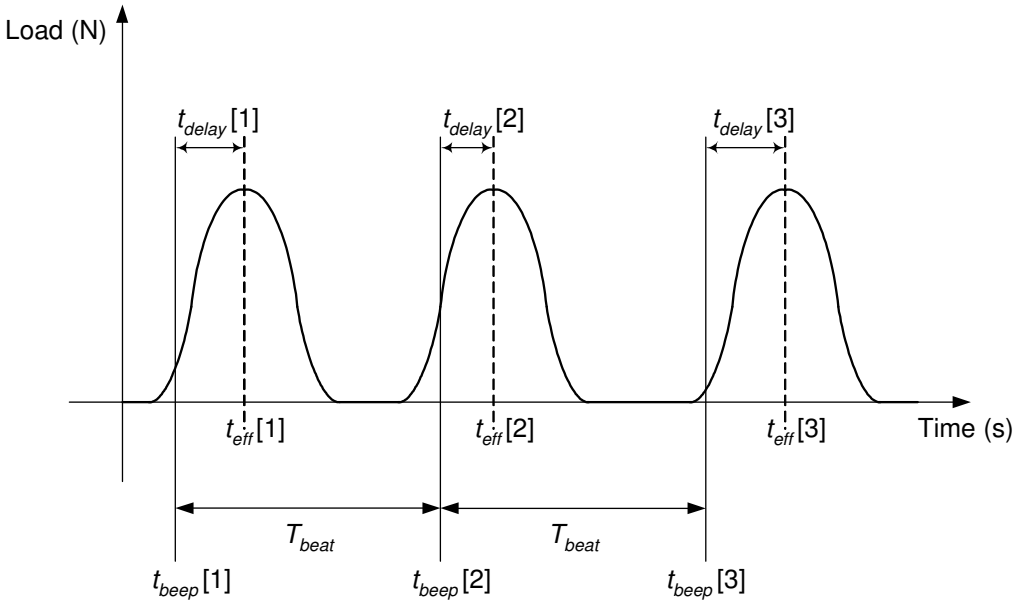

Figure 5.2: Schematic description of parameters.

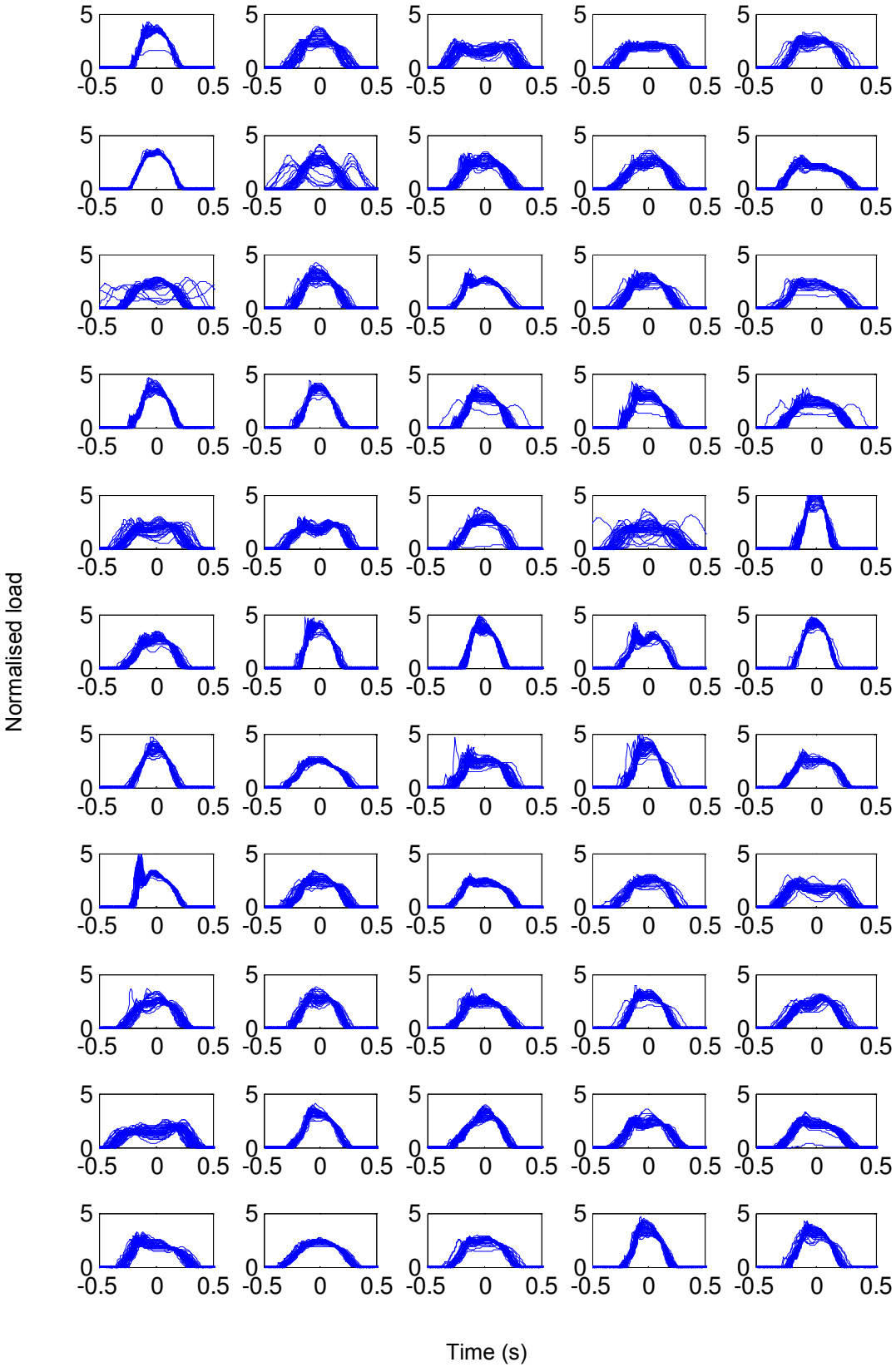

Figure 5.3: Jumping impulses for all synchronised tests at 1.5Hz.

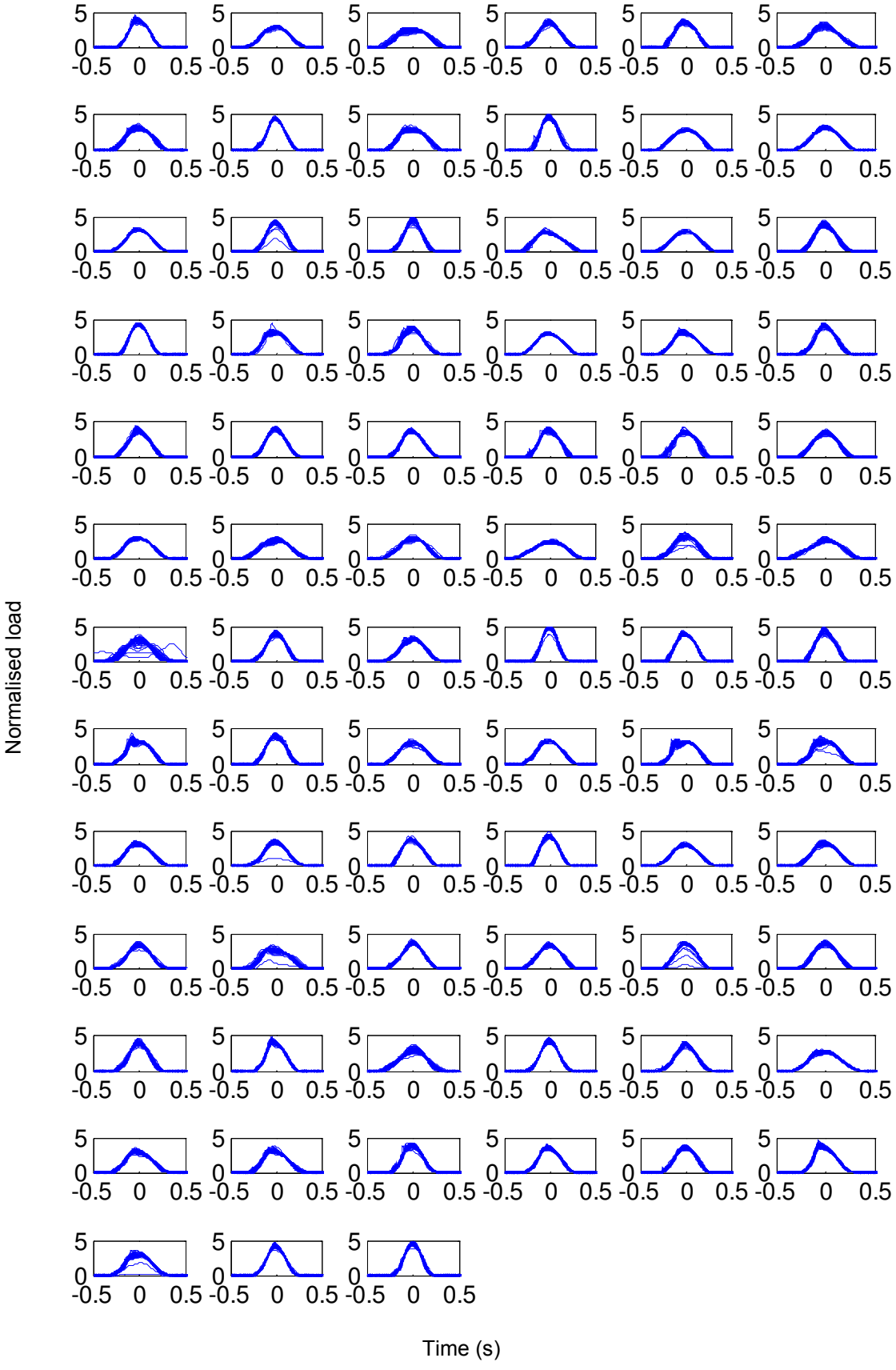

Figure 5.4: Jumping impulses for all synchronised tests at 2Hz.

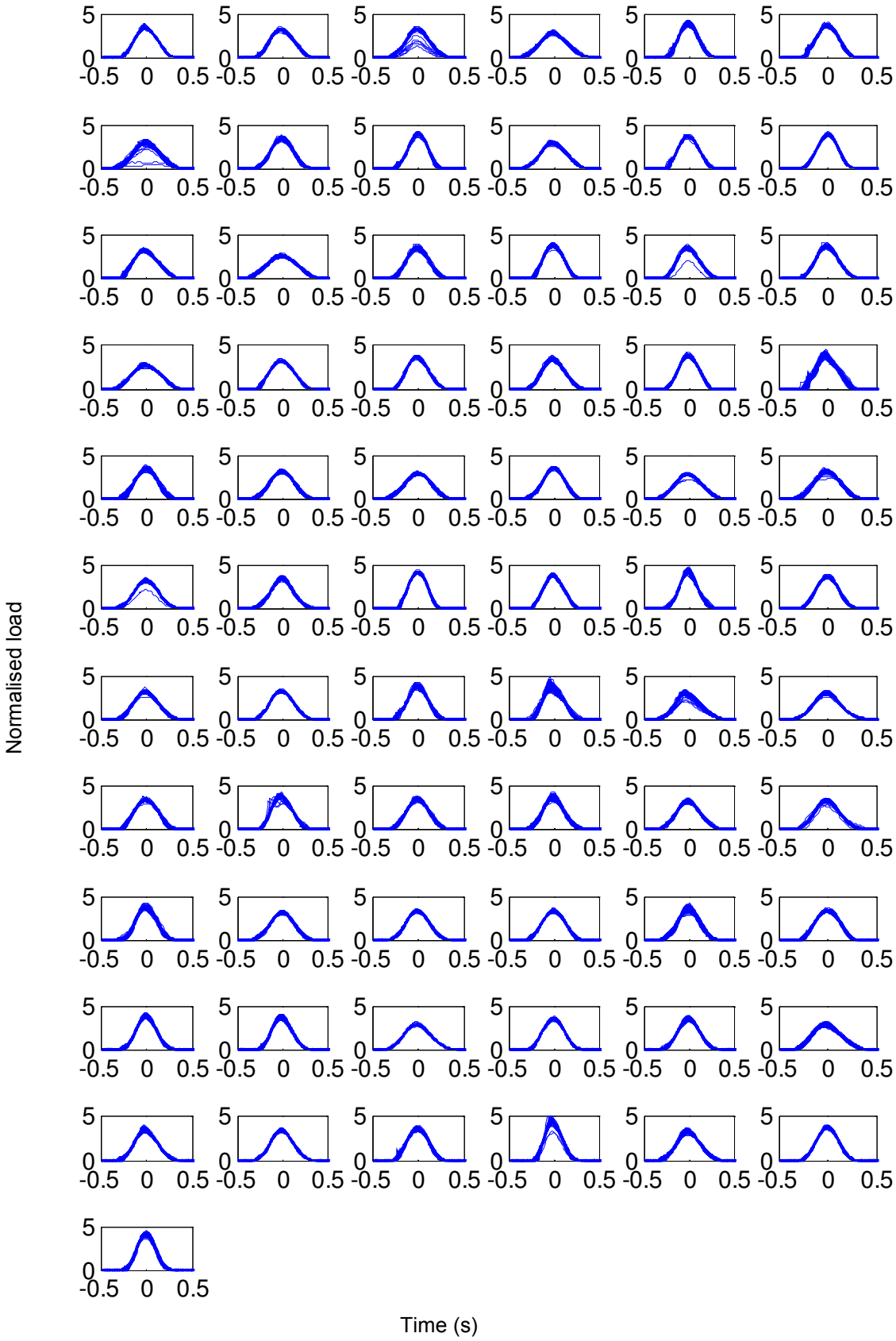

Figure 5.5: Jumping impulses for all synchronised tests at 2.67Hz.

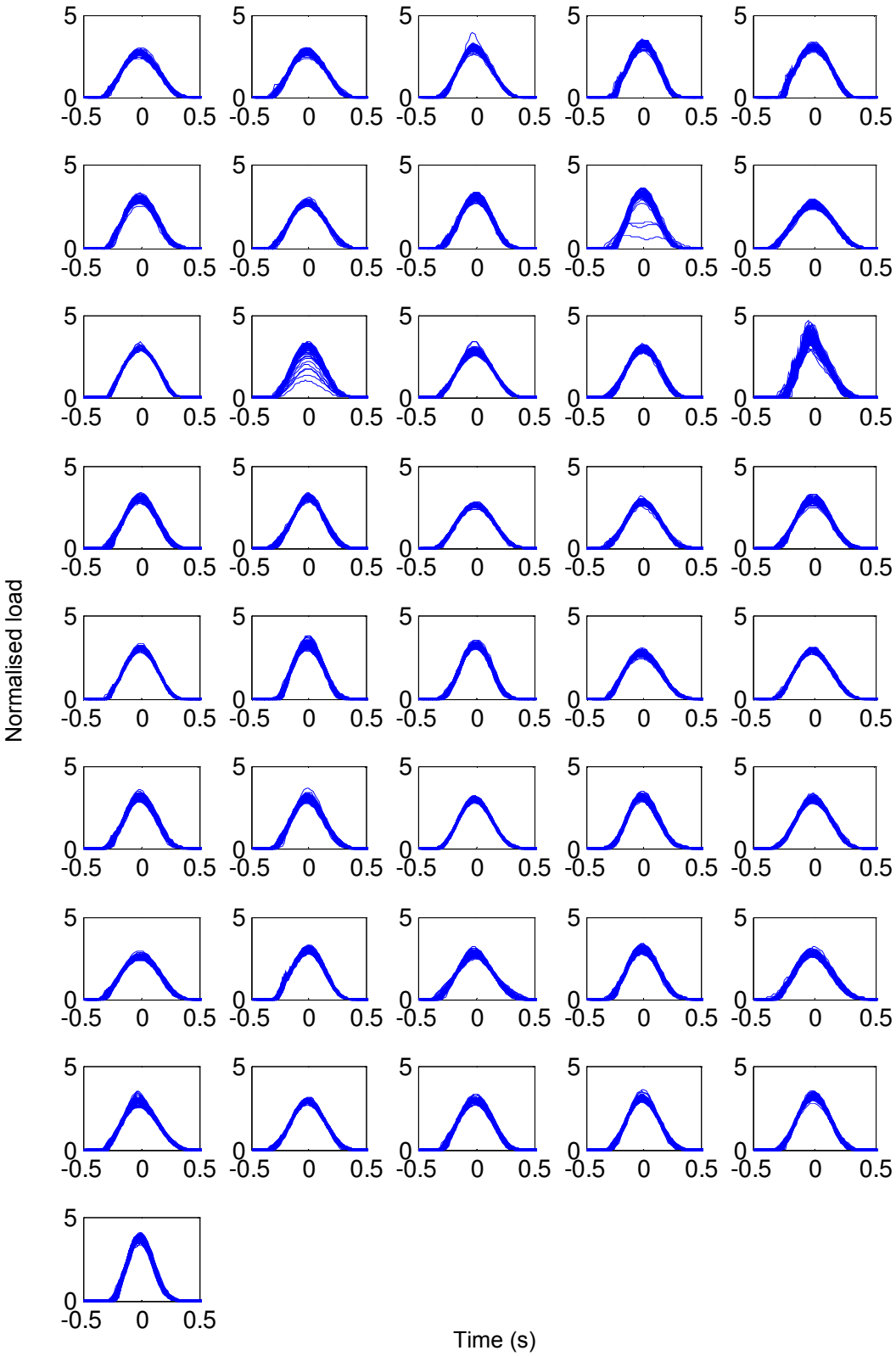

Figure 5.6: Jumping impulses for all synchronised tests at 3.5Hz.

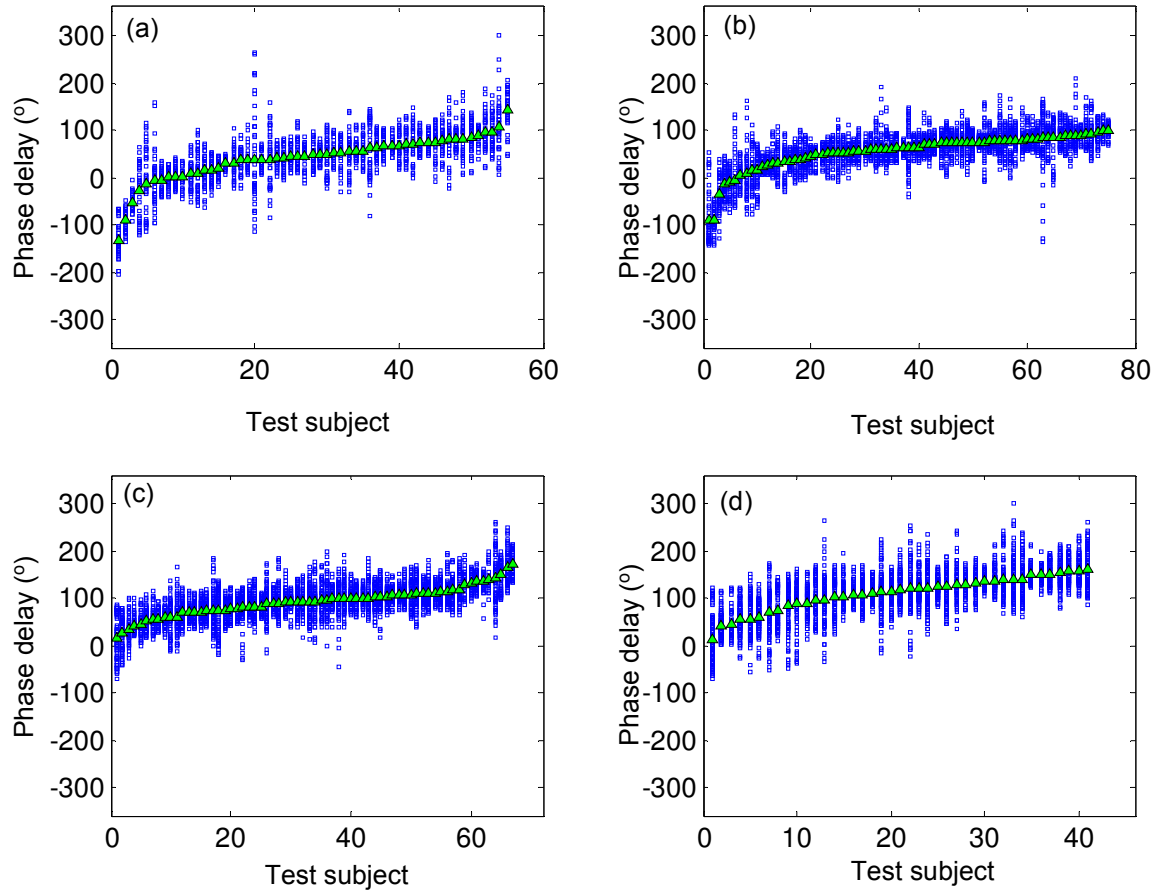

Figure 5.7: Phase delays for all synchronised tests: (a) 1.5 Hz. (b) 2 Hz. (c) 2.67 Hz. (d) 3.5 Hz.

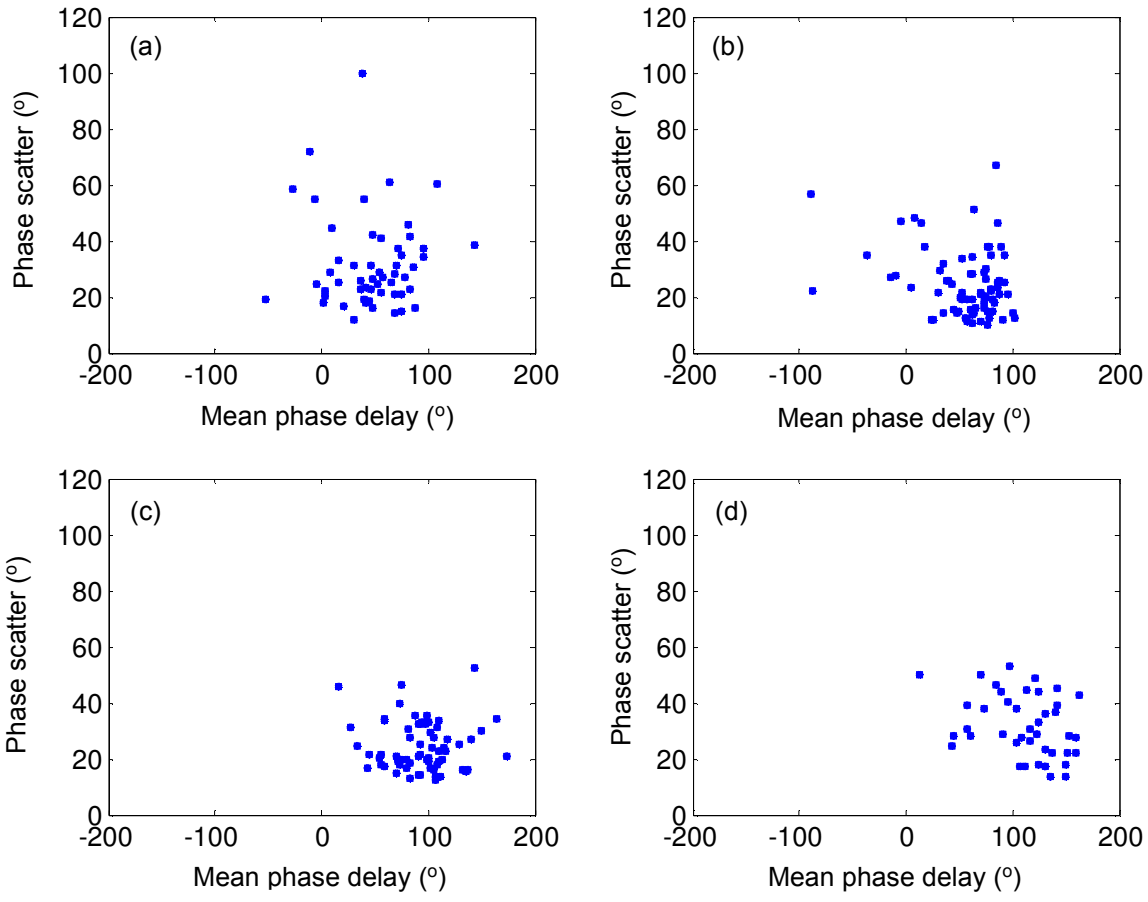

Figure 5.8: Relationship between phase scatter and mean phase delay: (a) 1.5 Hz. (b) 2 Hz. (c) 2.67 Hz. (d) 3.5 Hz.

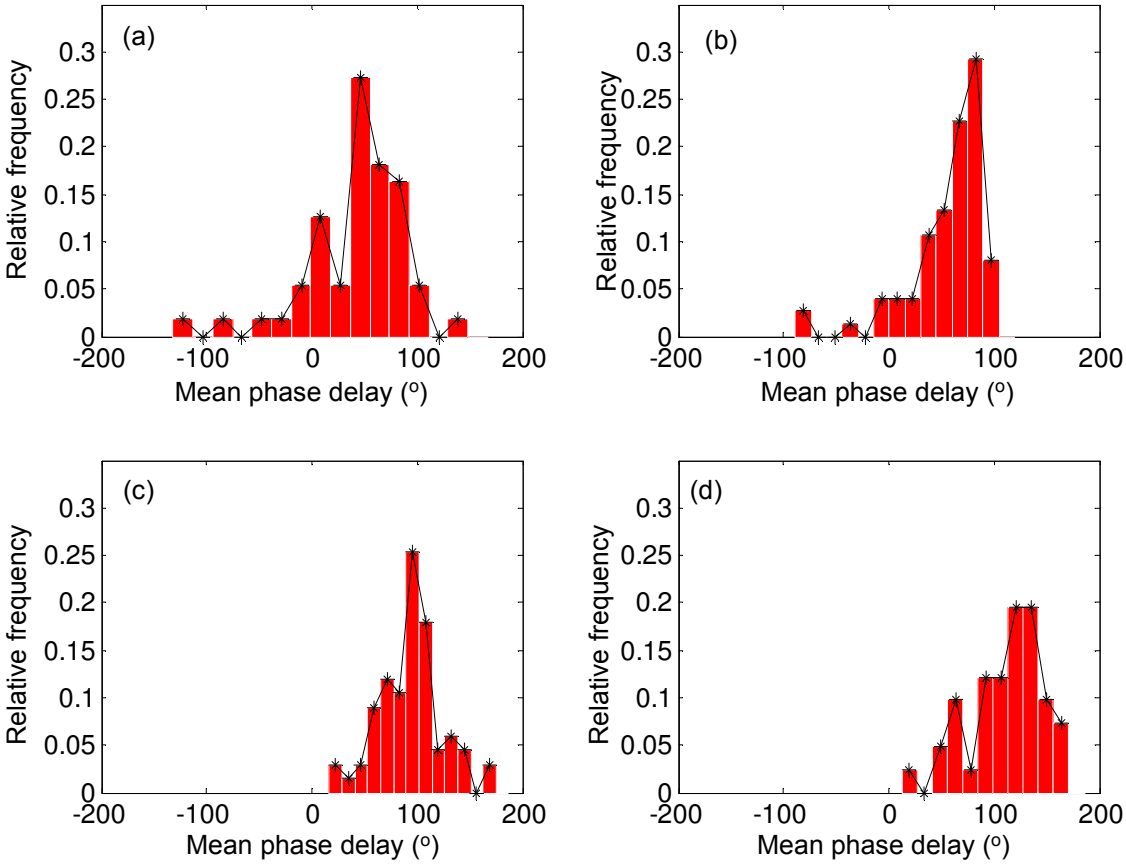

Figure 5.9: Histograms for mean phase delay: (a) 1.5 Hz. (b) 2 Hz. (c) 2.67 Hz. (d) 3.5 Hz.

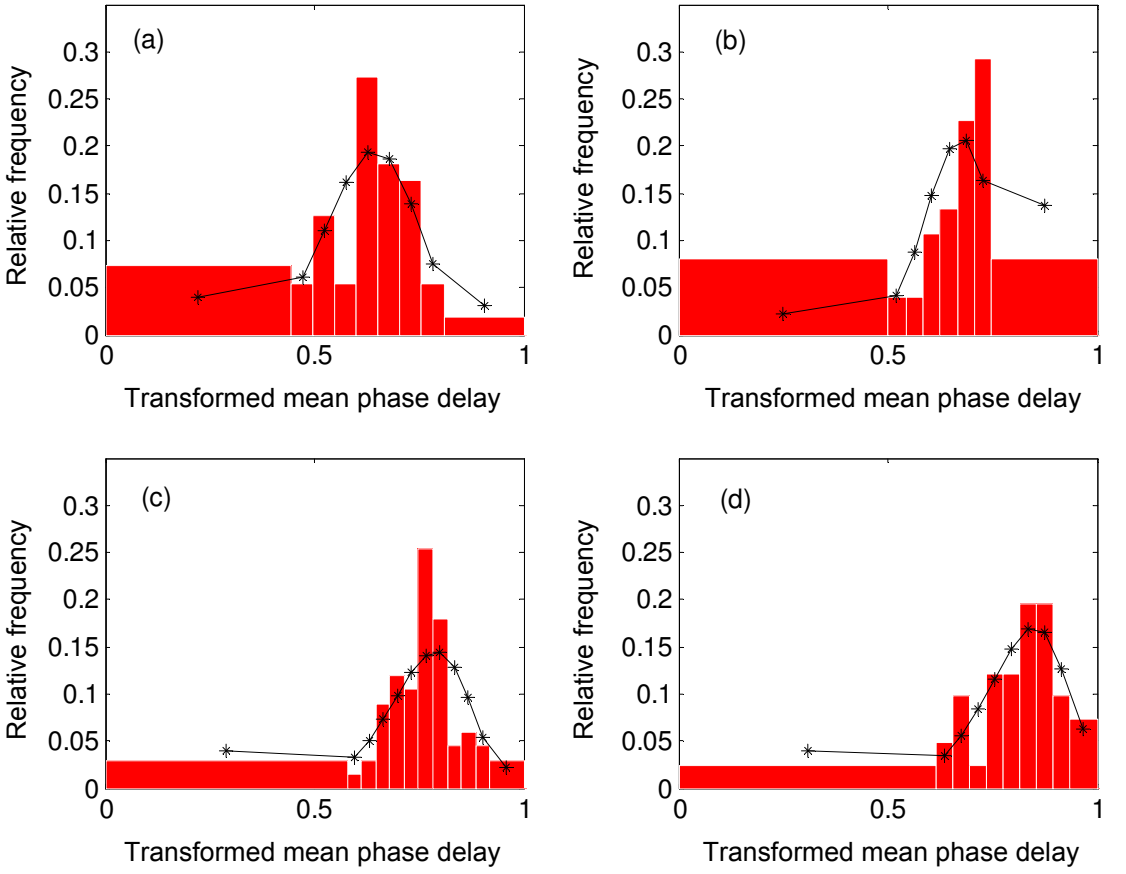

Figure 5.10: Histograms for the transformed mean phase delay superimposed with expected relative frequency from Beta distribution: (a) 1.5 Hz. (b) 2 Hz. (c) 2.67 Hz. (d) 3.5 Hz.

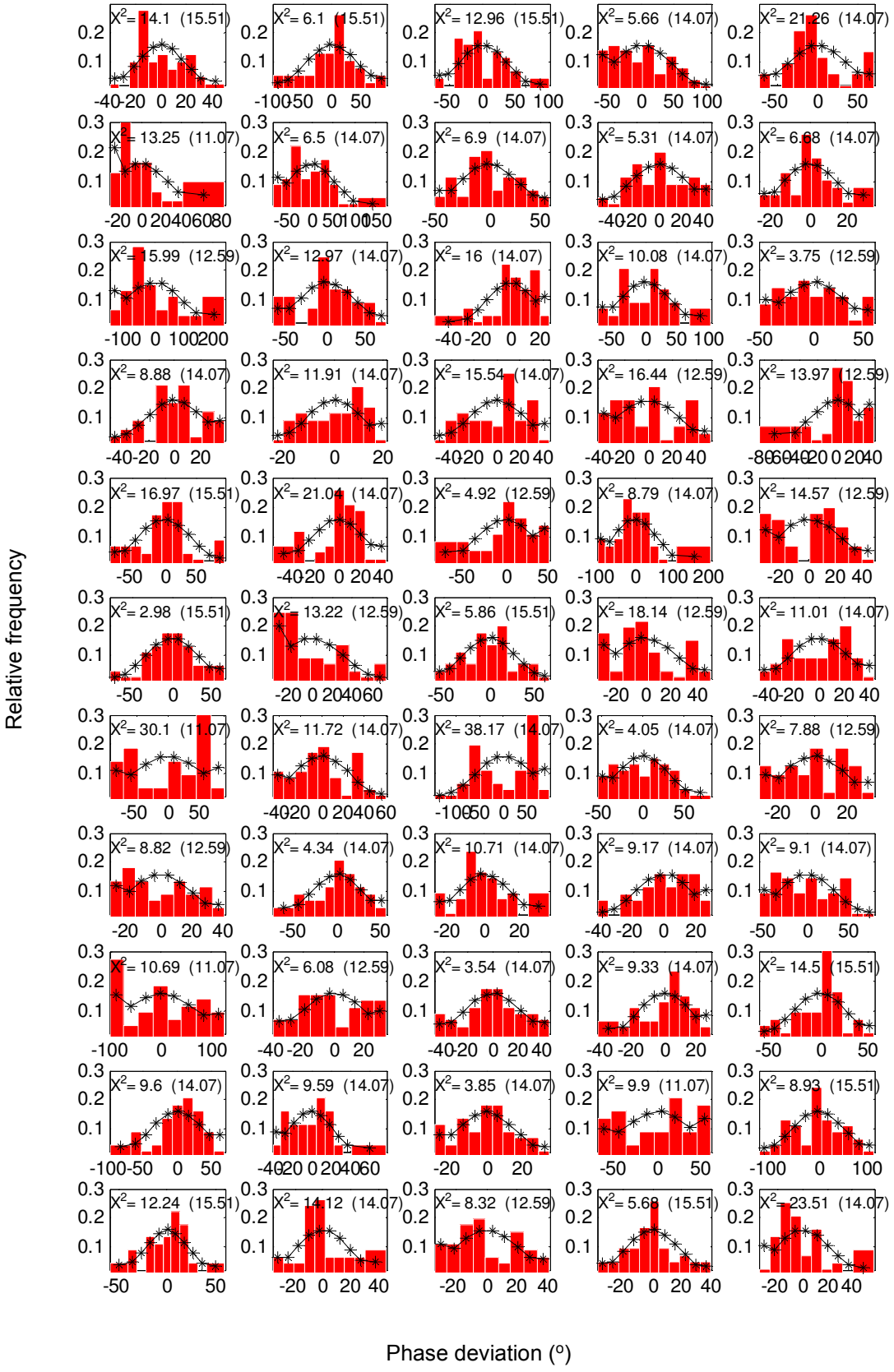

Figure 5.11: Phase deviation of all synchronised tests at 1.5 Hz superimposed with expected relative frequency from Normal distribution.

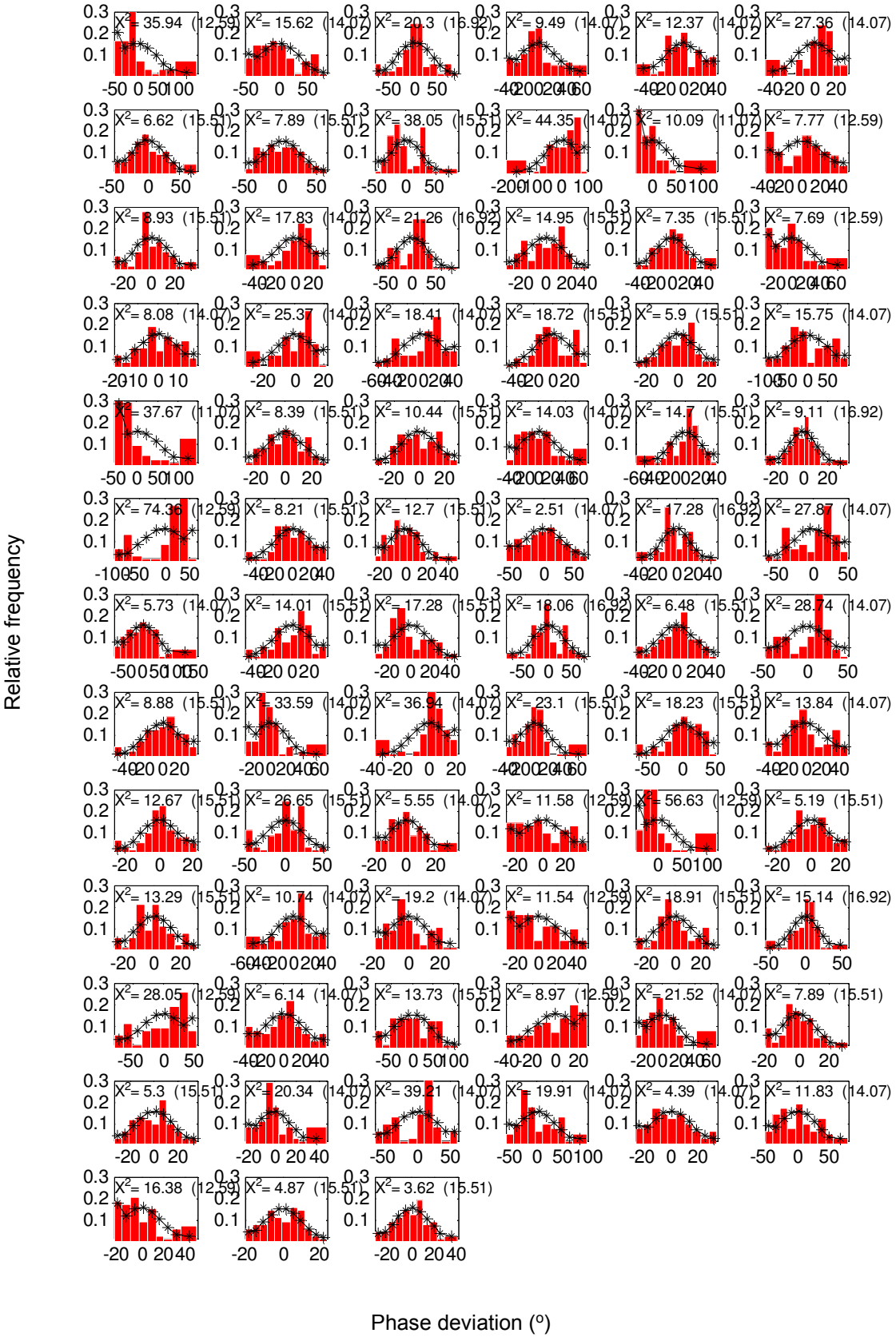

Figure 5.12: Phase deviation of all synchronised tests at 2 Hz superimposed with expected relative frequency from Normal distribution.

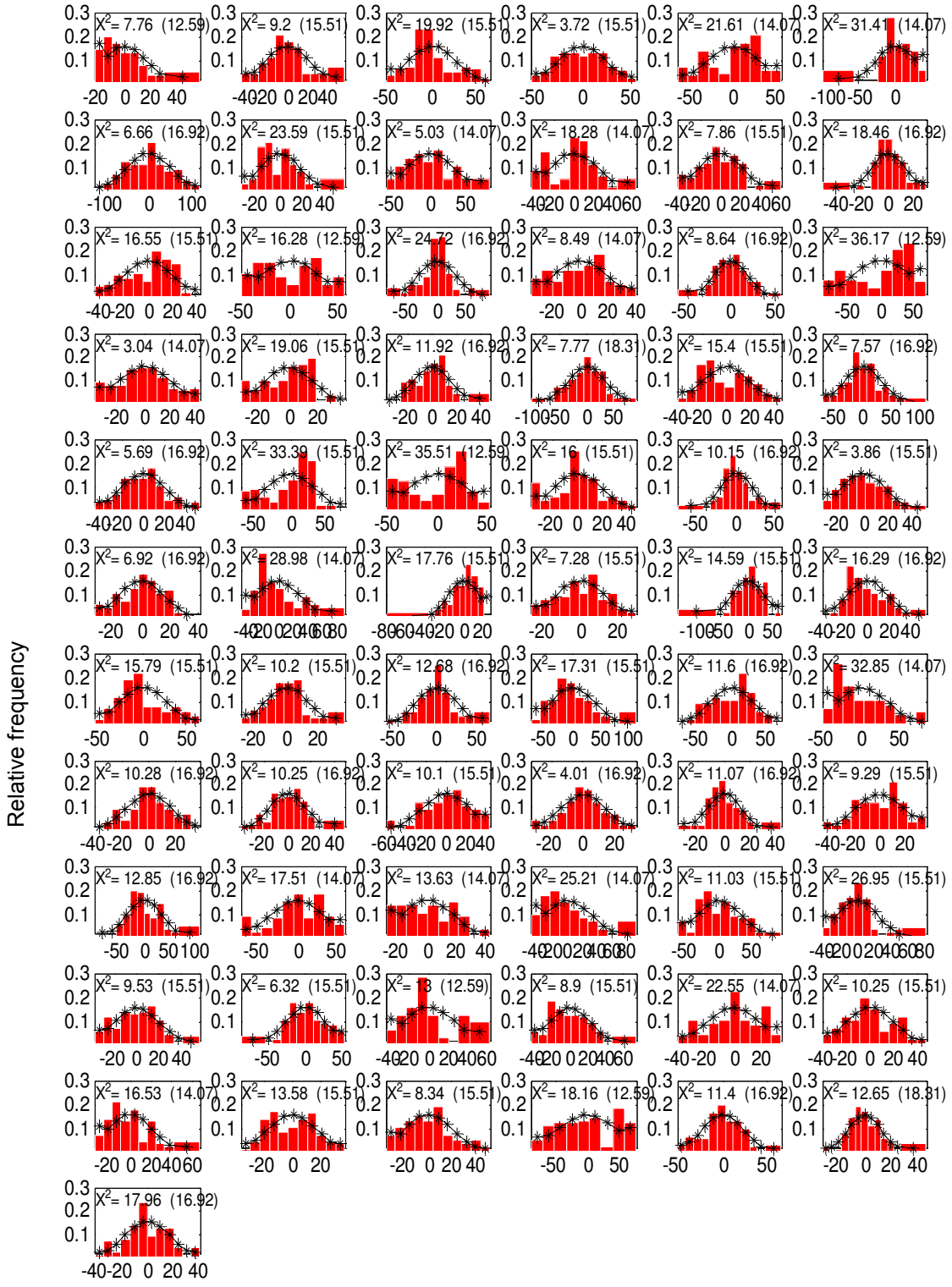

Figure 5.13: Phase deviation of all synchronised tests at 2.67 Hz superimposed with expected relative frequency from Normal distribution.

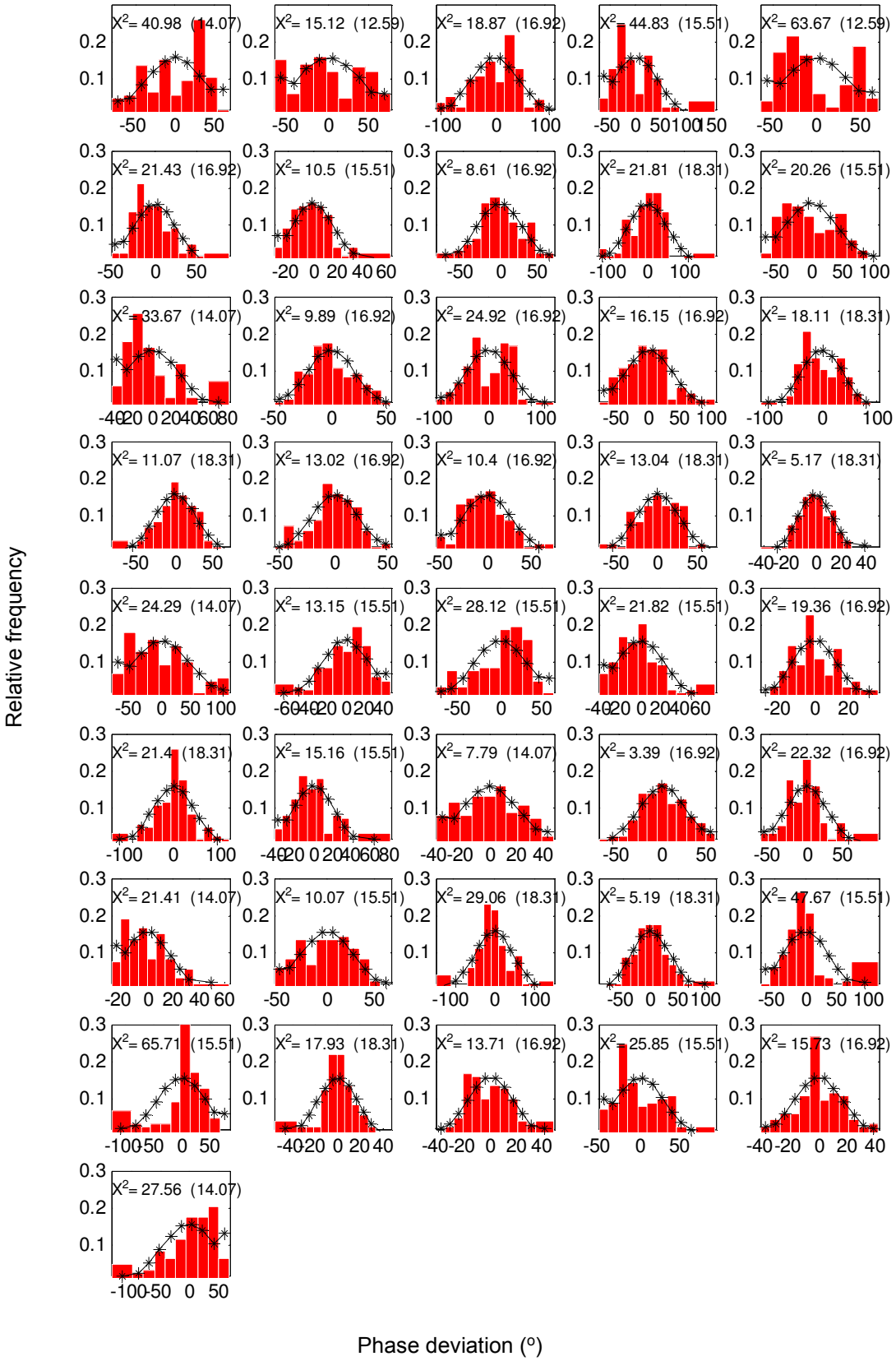

Figure 5.14: Phase deviation of all synchronised tests at 3.5 Hz superimposed with expected relative frequency from Normal distribution.

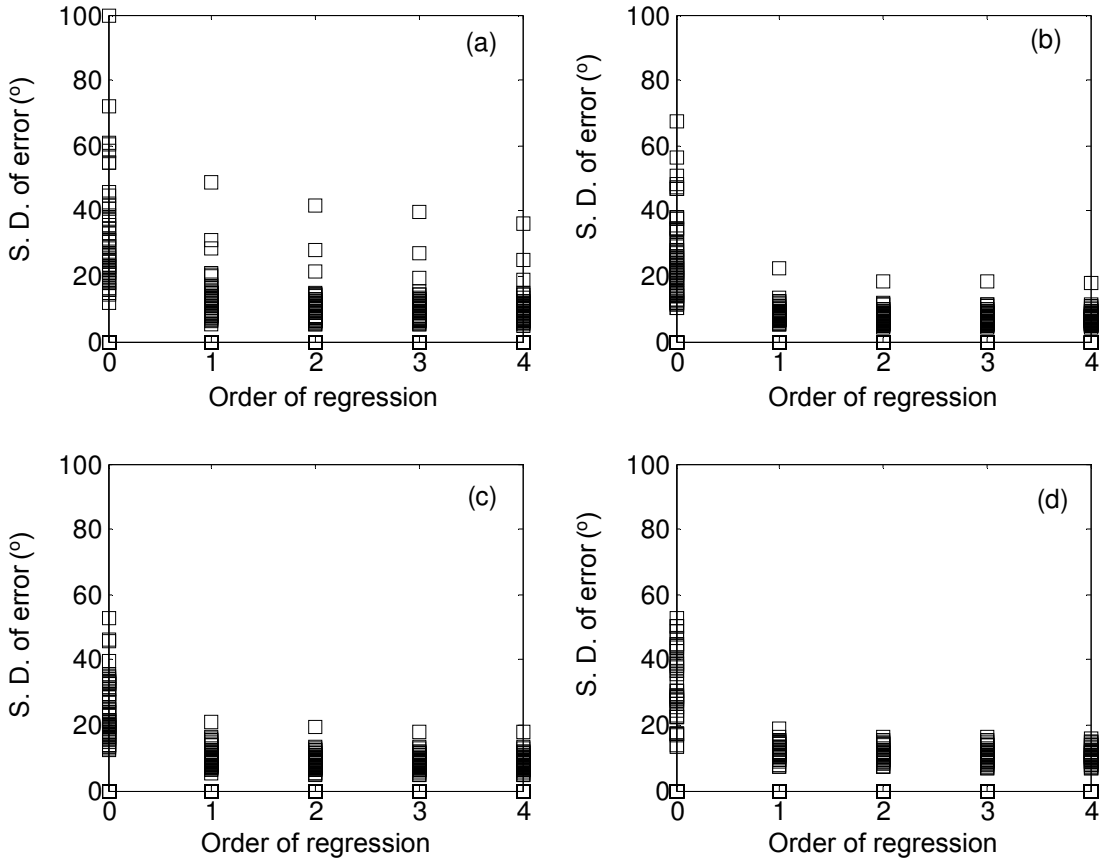

Figure 5.15: Standard deviation of random error for increasing order of regression: (a) 1.5 Hz. (b) 2 Hz. (c) 2.67 Hz. (d) 3.5 Hz.

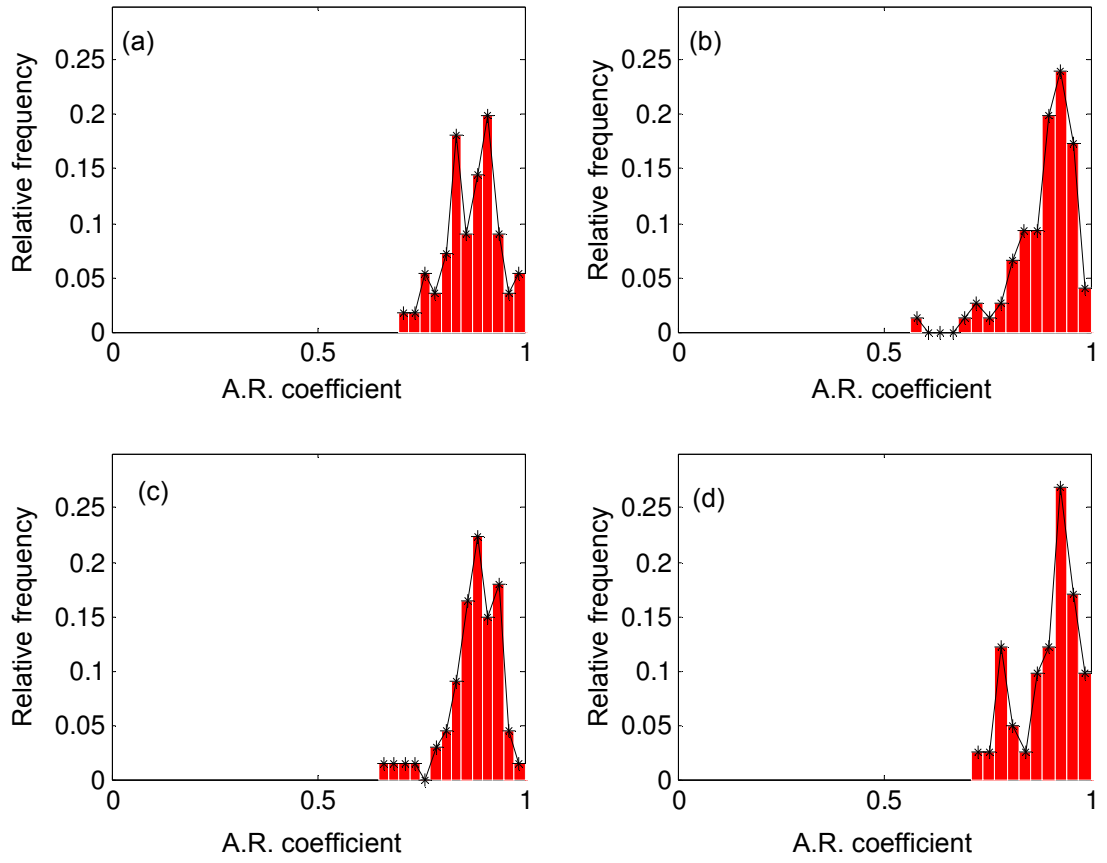

Figure 5.16: Histograms for auto-regression coefficient: (a) 1.5 Hz. (b) 2 Hz. (c) 2.67 Hz. (d) 3.5 Hz.

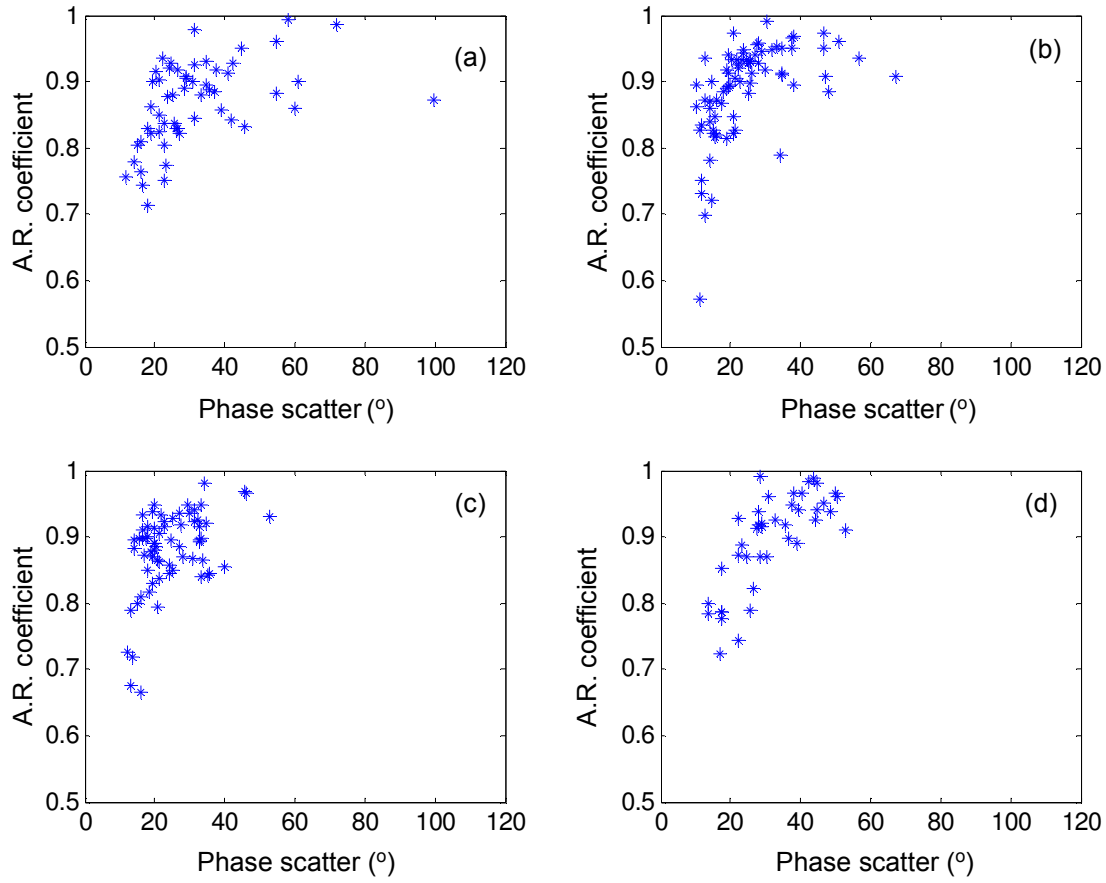

Figure 5.17: Variation of auto-regression coefficient with phase scatter: (a) 1.5 Hz. (b) 2 Hz. (c) 2.67 Hz. (d) 3.5 Hz.

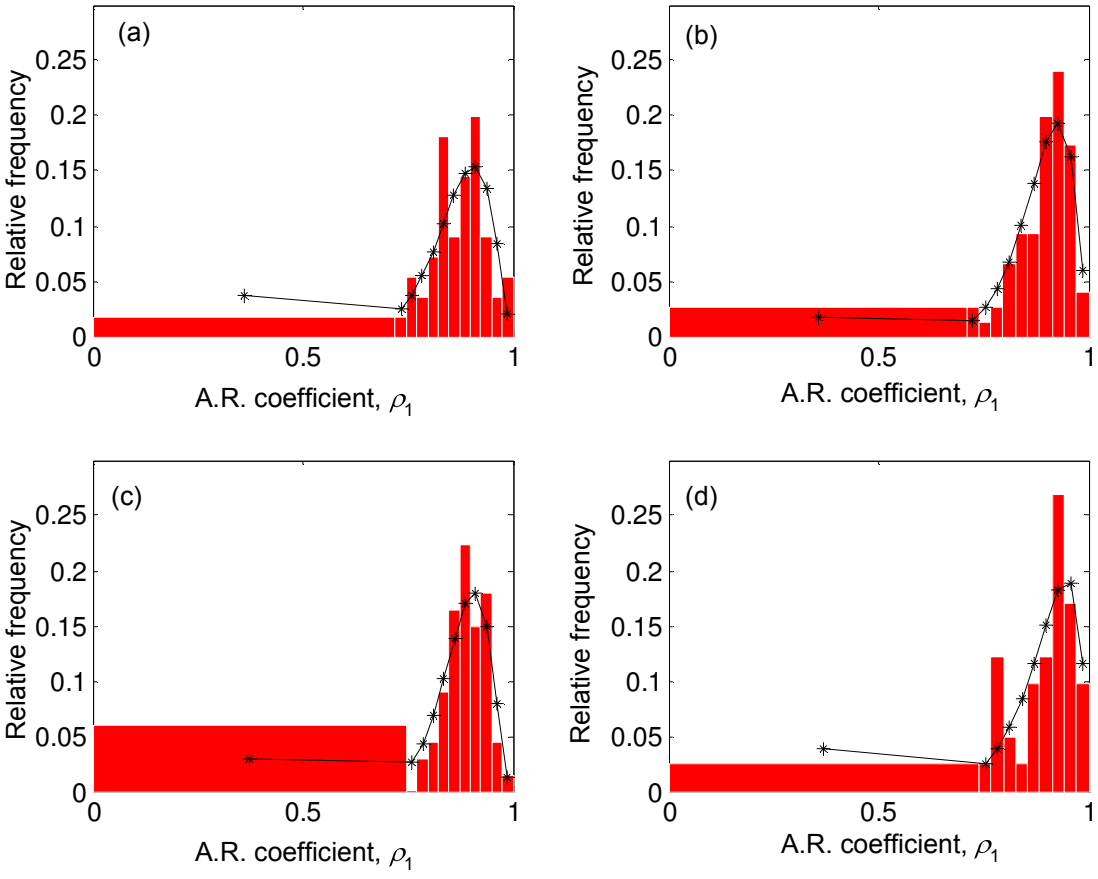

Figure 5.18: Histograms for auto-regression coefficient superimposed with expected relative frequency from Beta distribution: (a) 1.5 Hz. (b) 2 Hz. (c) 2.67 Hz. (d) 3.5 Hz.

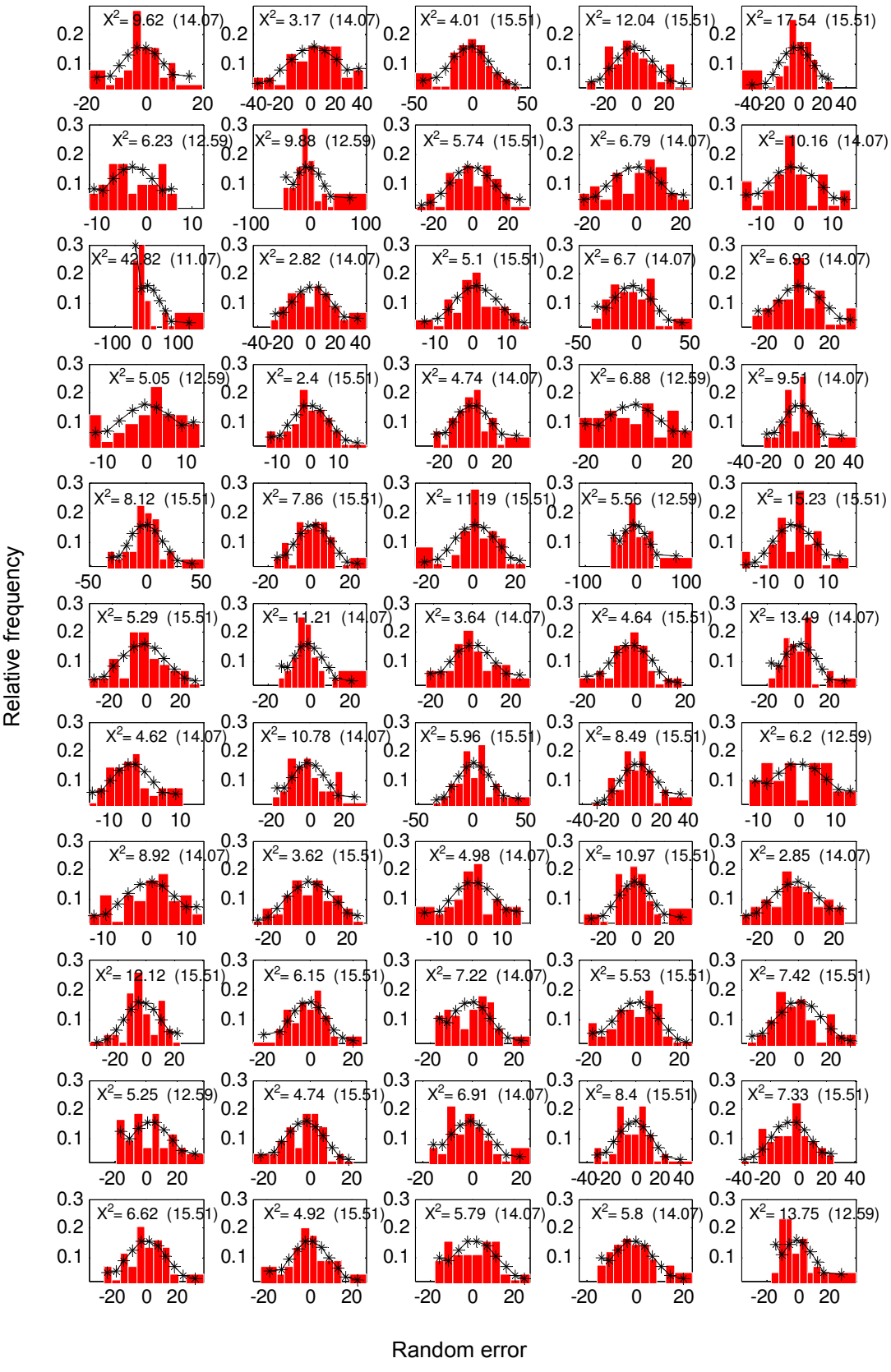

Figure 5.19: Random error of all synchronised tests at 1.5 Hz superimposed with expected relative frequency from Normal distribution.

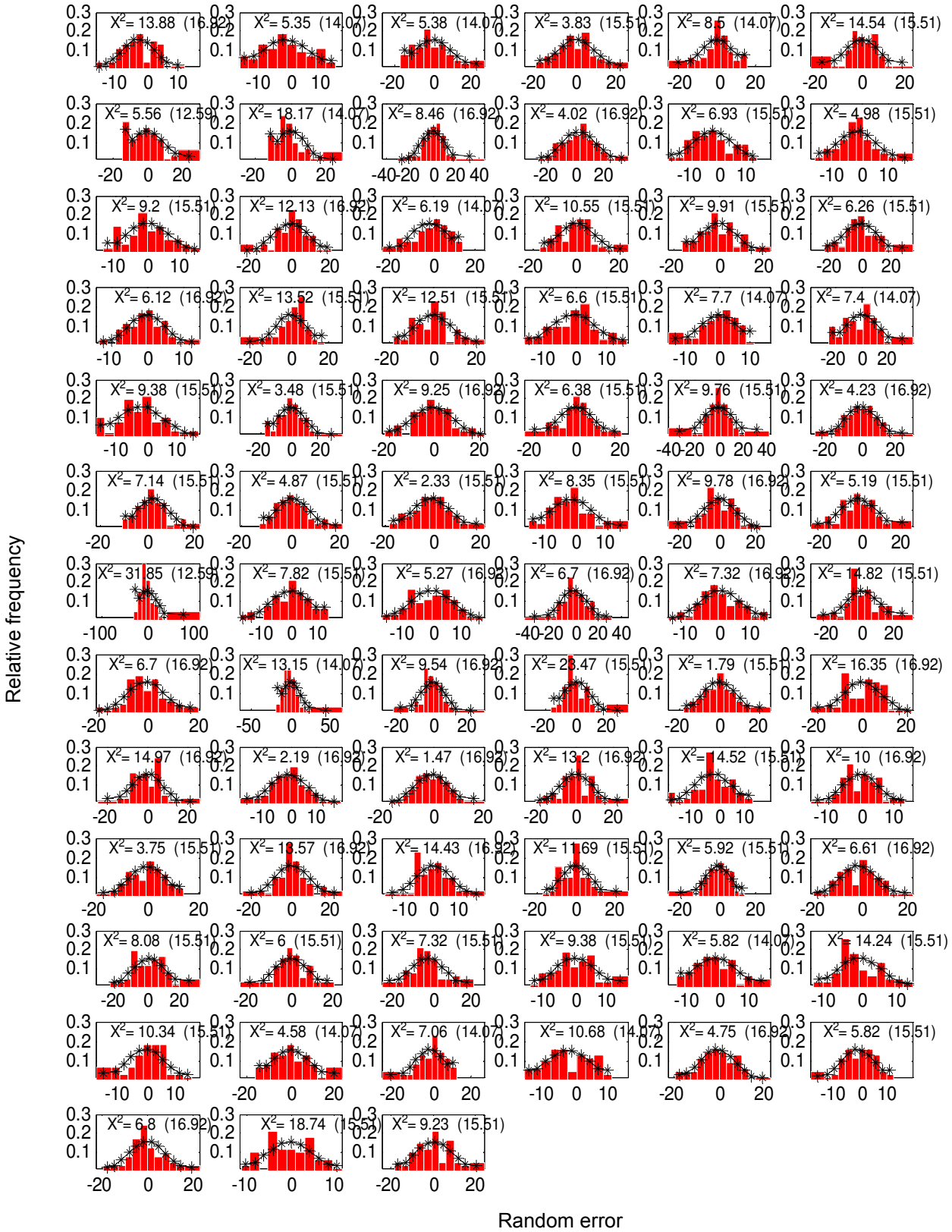

Figure 5.20: Random error of all synchronised tests at 2 Hz superimposed with expected relative frequency from Normal distribution.

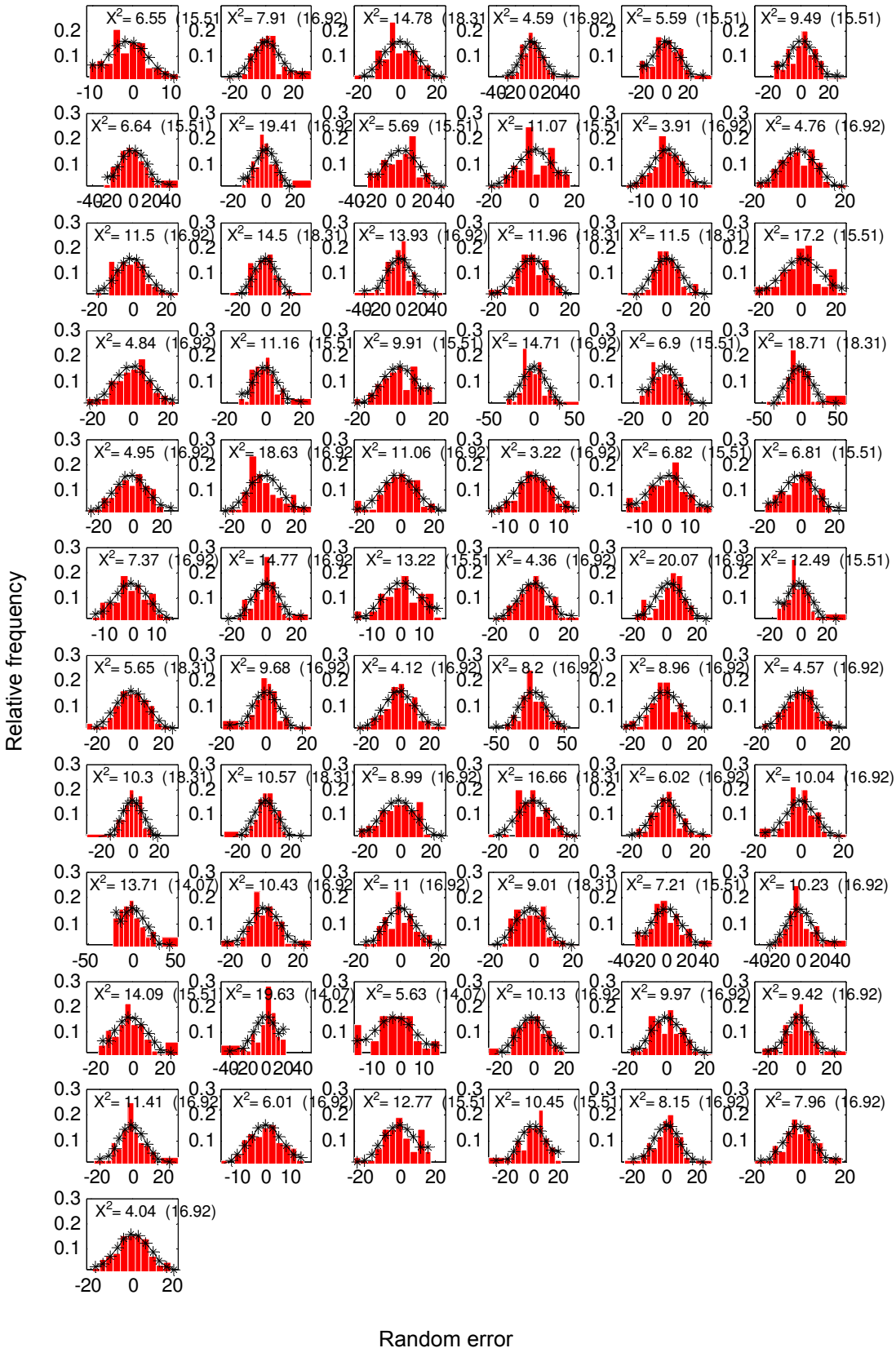

Figure 5.21: Random error of all synchronised tests at 2.67 Hz superimposed with expected relative frequency from Normal distribution.

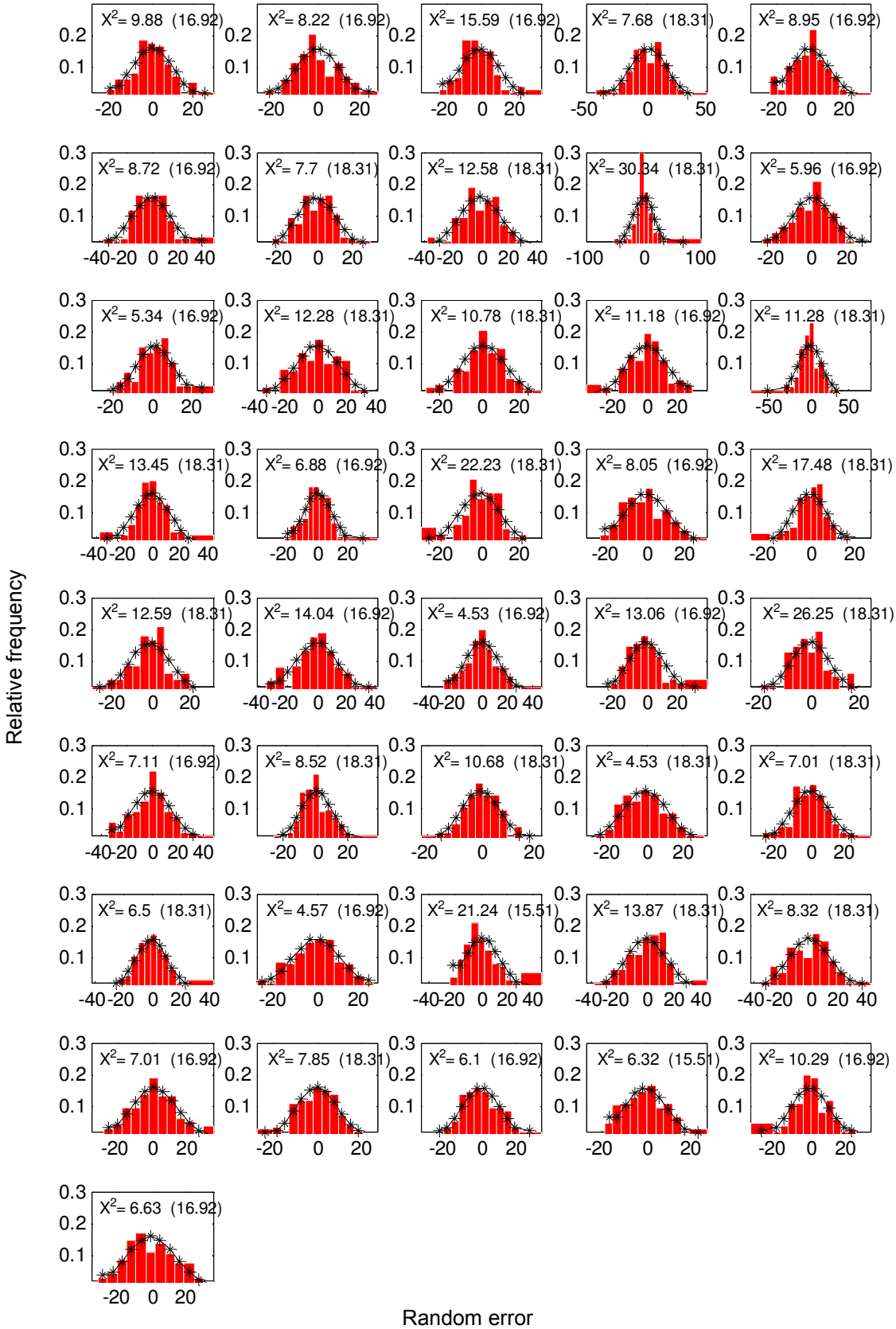

Figure 5.22: Random error of all synchronised tests at 3.5 Hz superimposed with expected relative frequency Normal distribution.

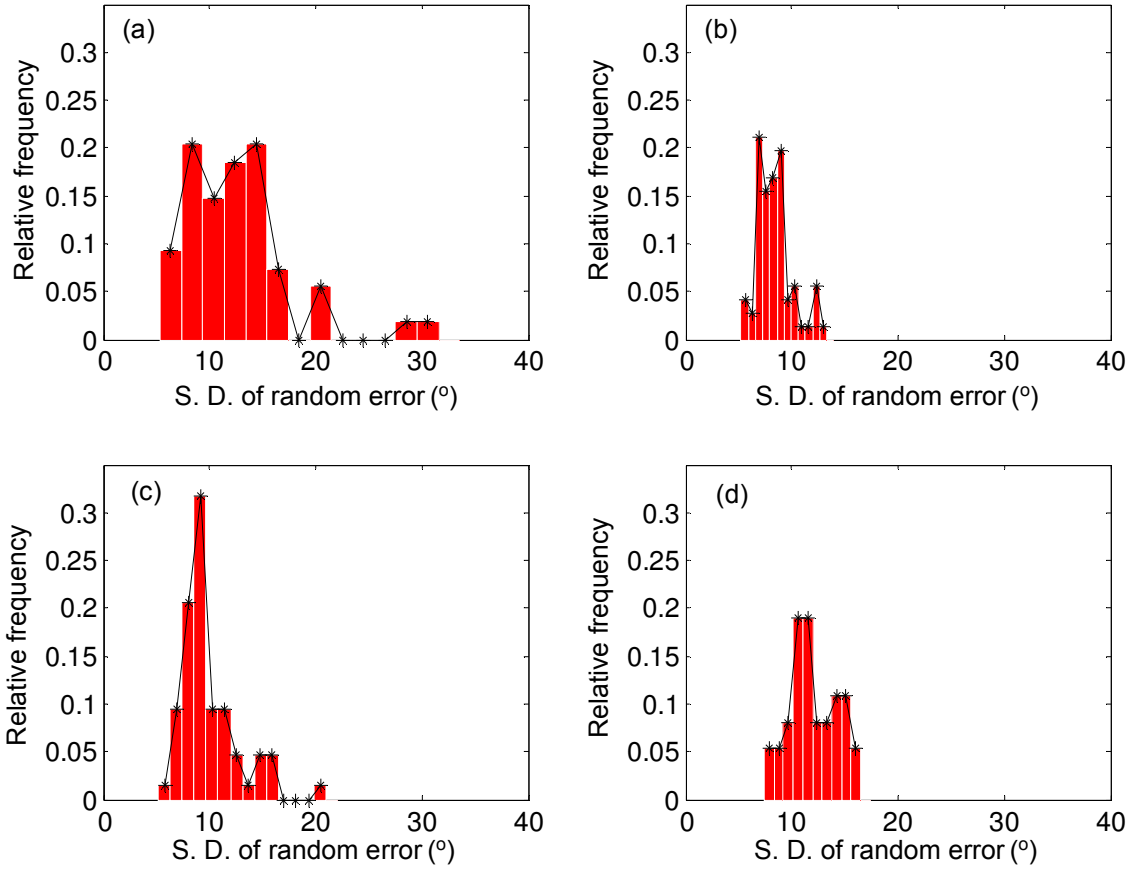

Figure 5.23: Histograms for the standard deviation of random error: (a) 1.5 Hz. (b) 2 Hz. (c) 2.67 Hz. (d) 3.5 Hz.

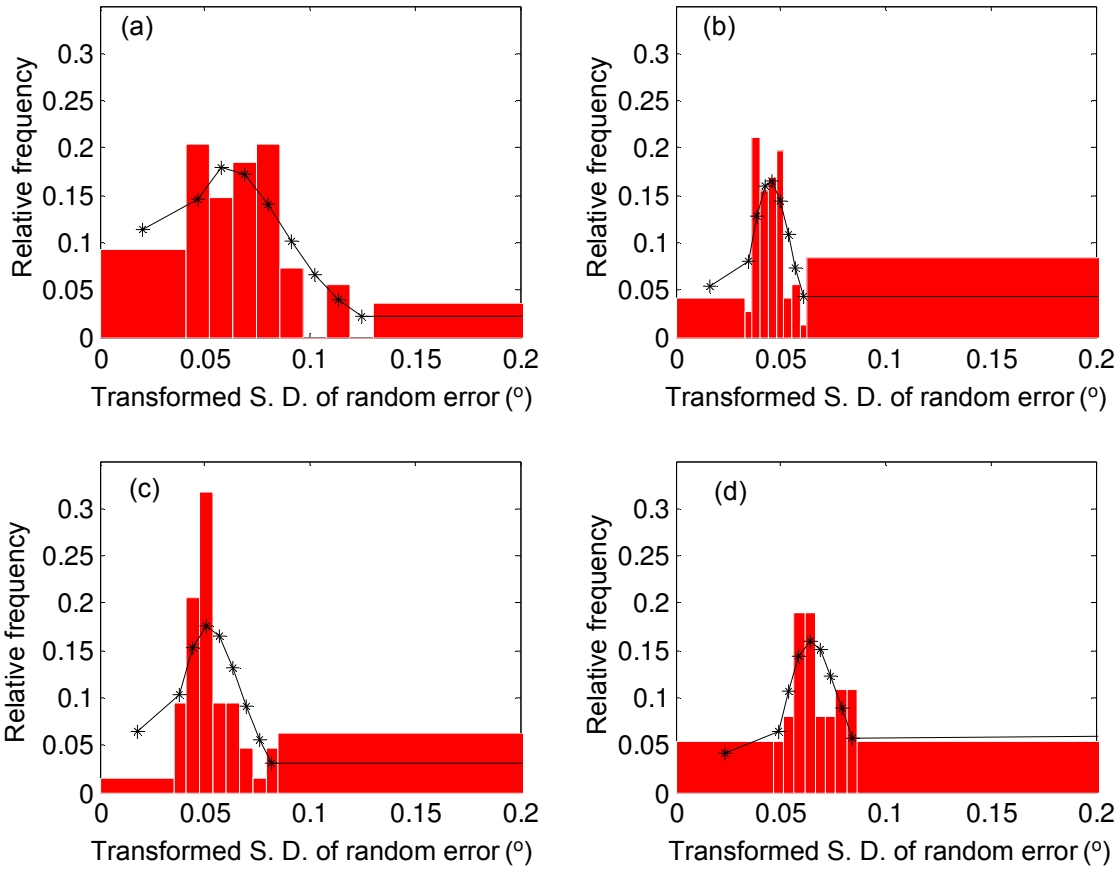

Figure 5.24: Histograms for the standard deviation of random error superimposed with expected relative frequency from Beta distribution: (a) 1.5 Hz. (b) 2 Hz. (c) 2.67 Hz. (d) 3.5 Hz.

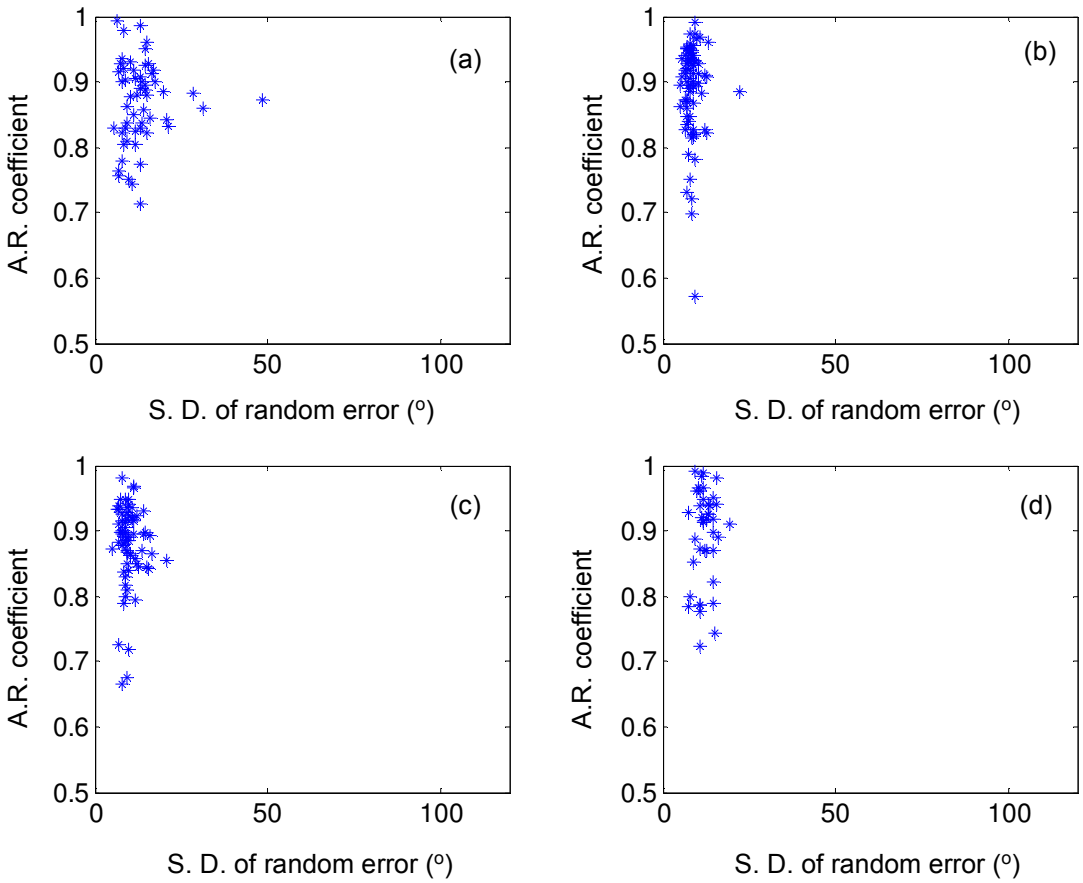

Figure 5.25: Variation of auto-regression coefficient with standard deviation of random error: (a) 1.5 Hz. (b) 2 Hz. (c) 2.67 Hz. (d) 3.5 Hz.

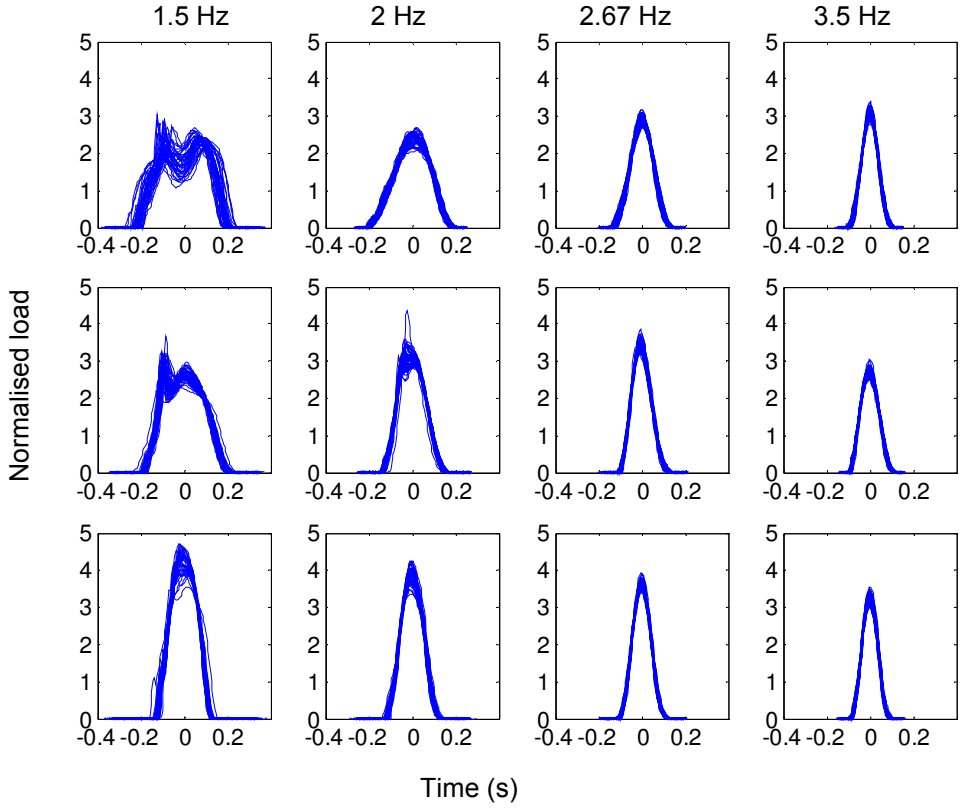

Figure 5.26: Jumping impulses for three subjects at four beat frequencies.

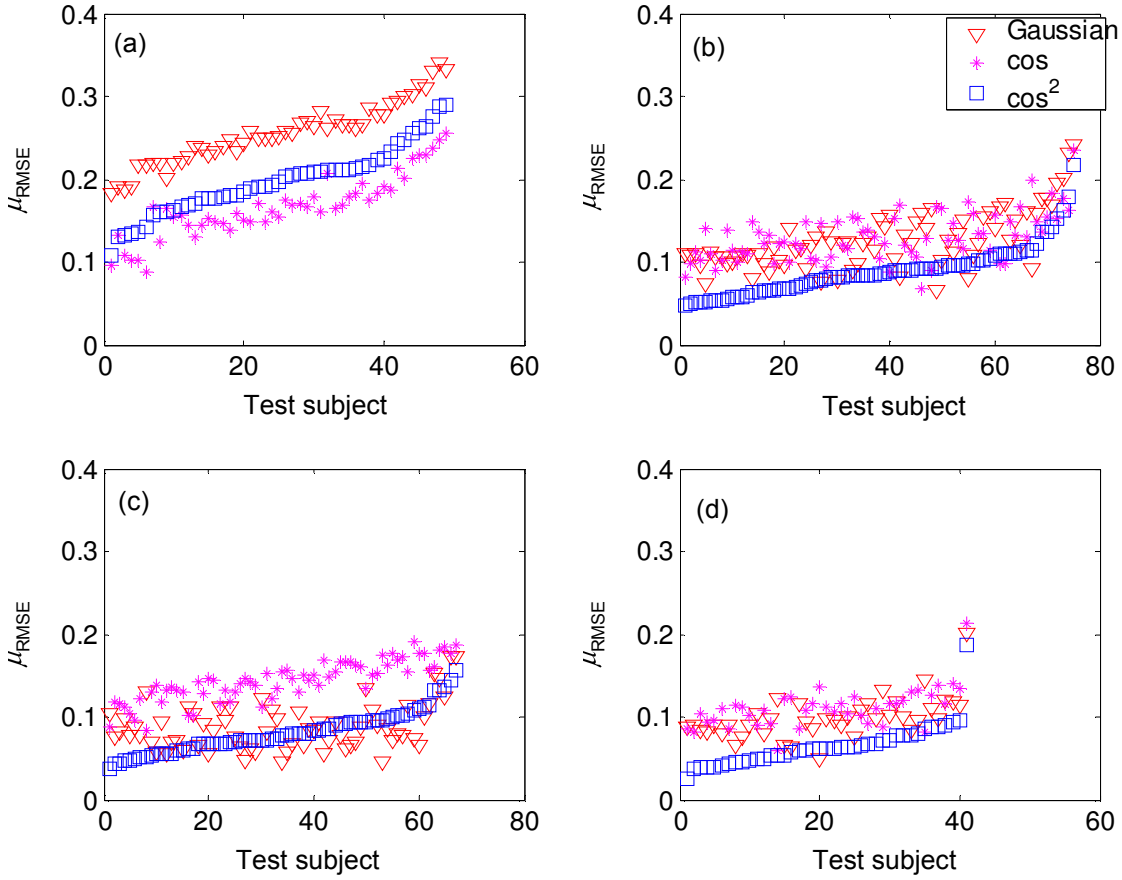

Figure 5.27: Mean RMSE for curve-fitting impulse with Normal distribution, cosine and cosine-squared functions: (a) 1.5 Hz. (b) 2 Hz. (c) 2.67 Hz. (d) 3.5 Hz.

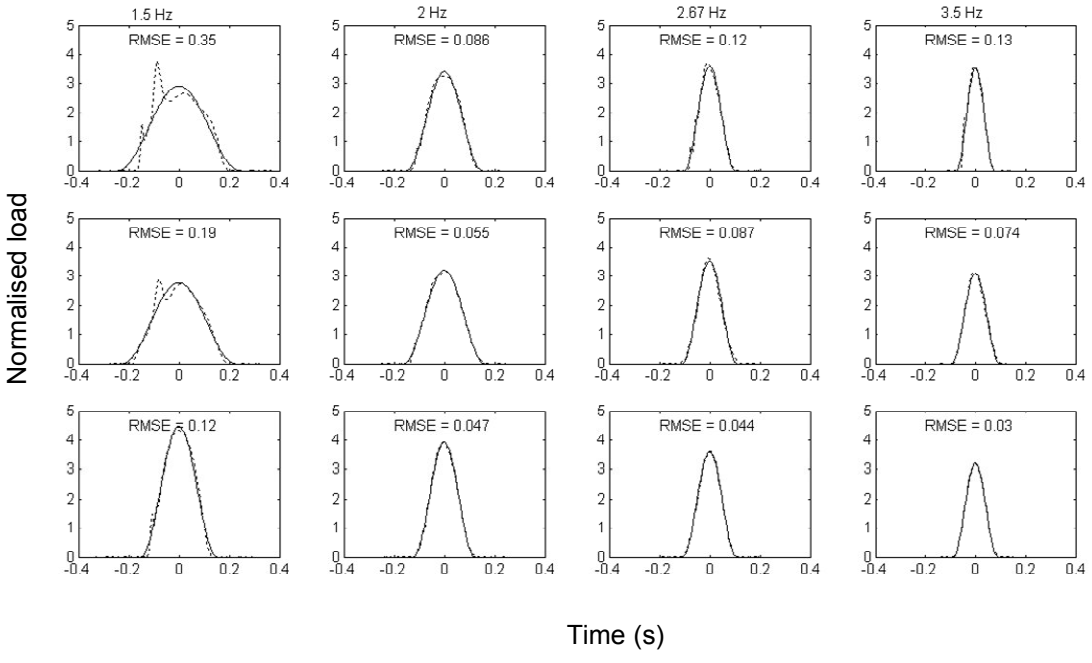

Figure 5.28: Examples of measured impulse (dotted line) and fitted cosine-squared function (full line) for three subjects with the corresponding RMSE values.

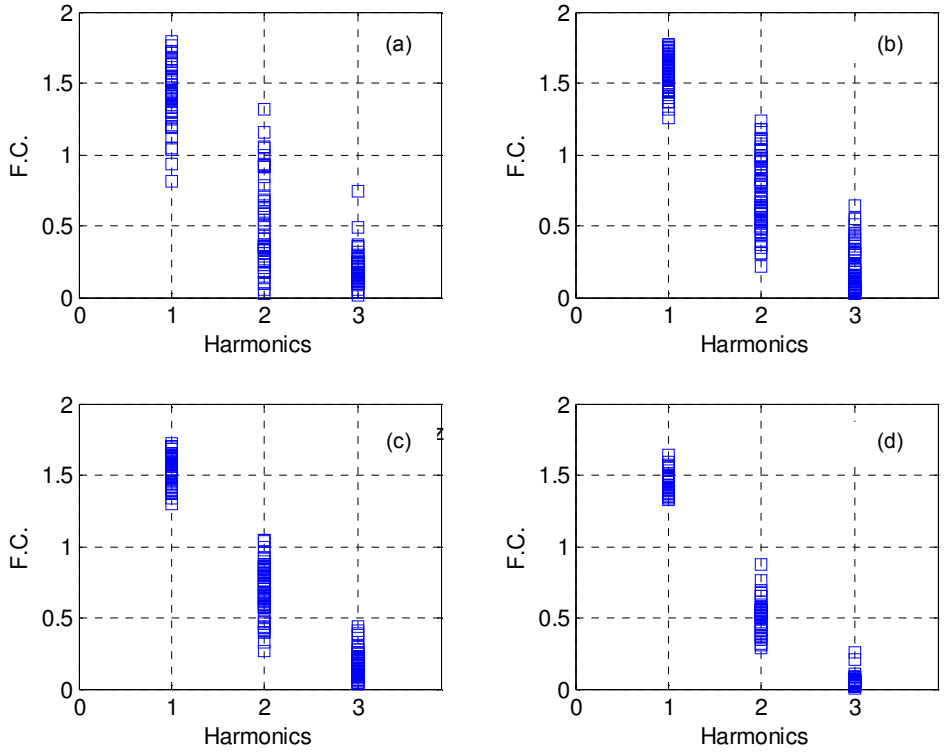

Figure 5.29: Fourier coefficients of average impulse: (a) 1.5 Hz. (b) 2 Hz. (c) 2.67 Hz. (d) 3.5 Hz.

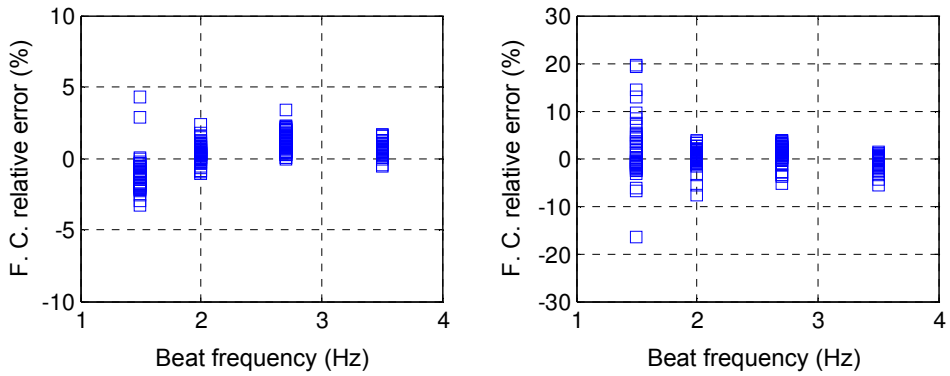

Figure 5.30: Fourier coefficient relative error for first (left) and second (right) harmonics.

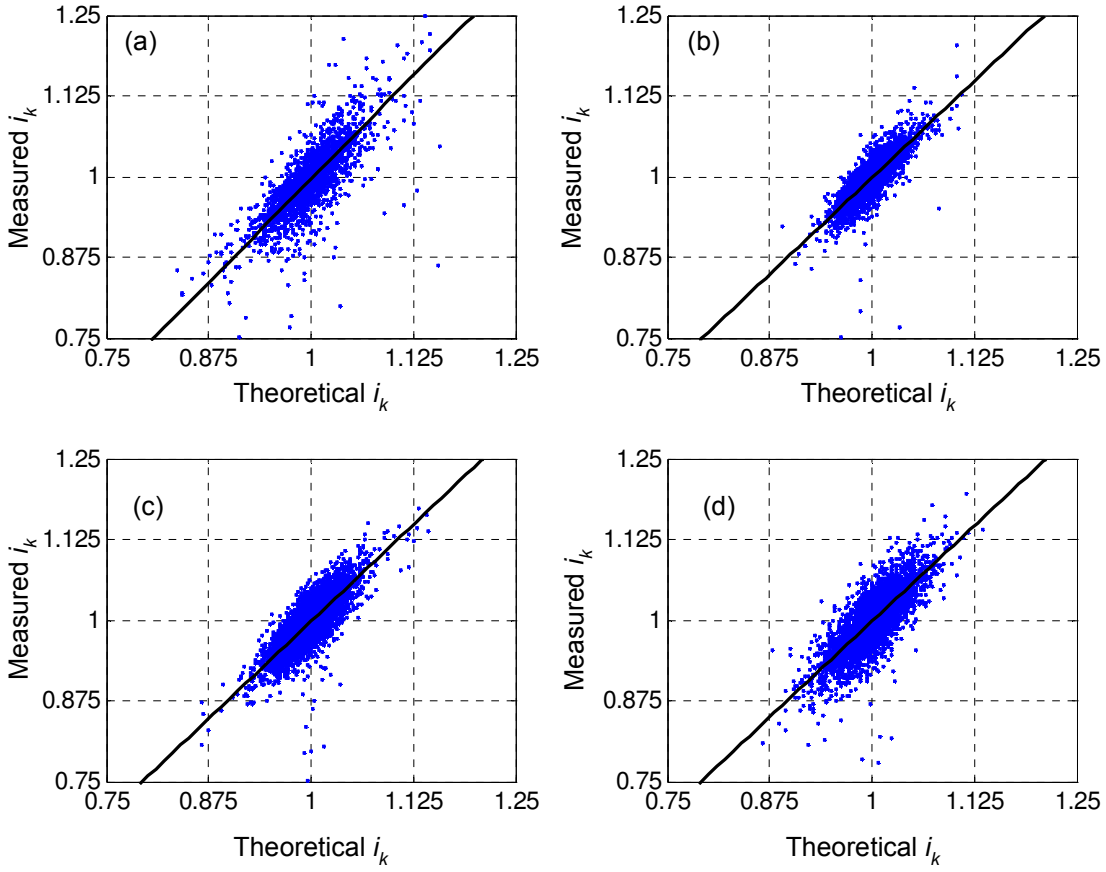

Figure 5.31: Comparison of measured and theoretical impulse magnitudes: (a) 1.5 Hz. (b) 2 Hz. (c) 2.67 Hz. (d) 3.5 Hz.

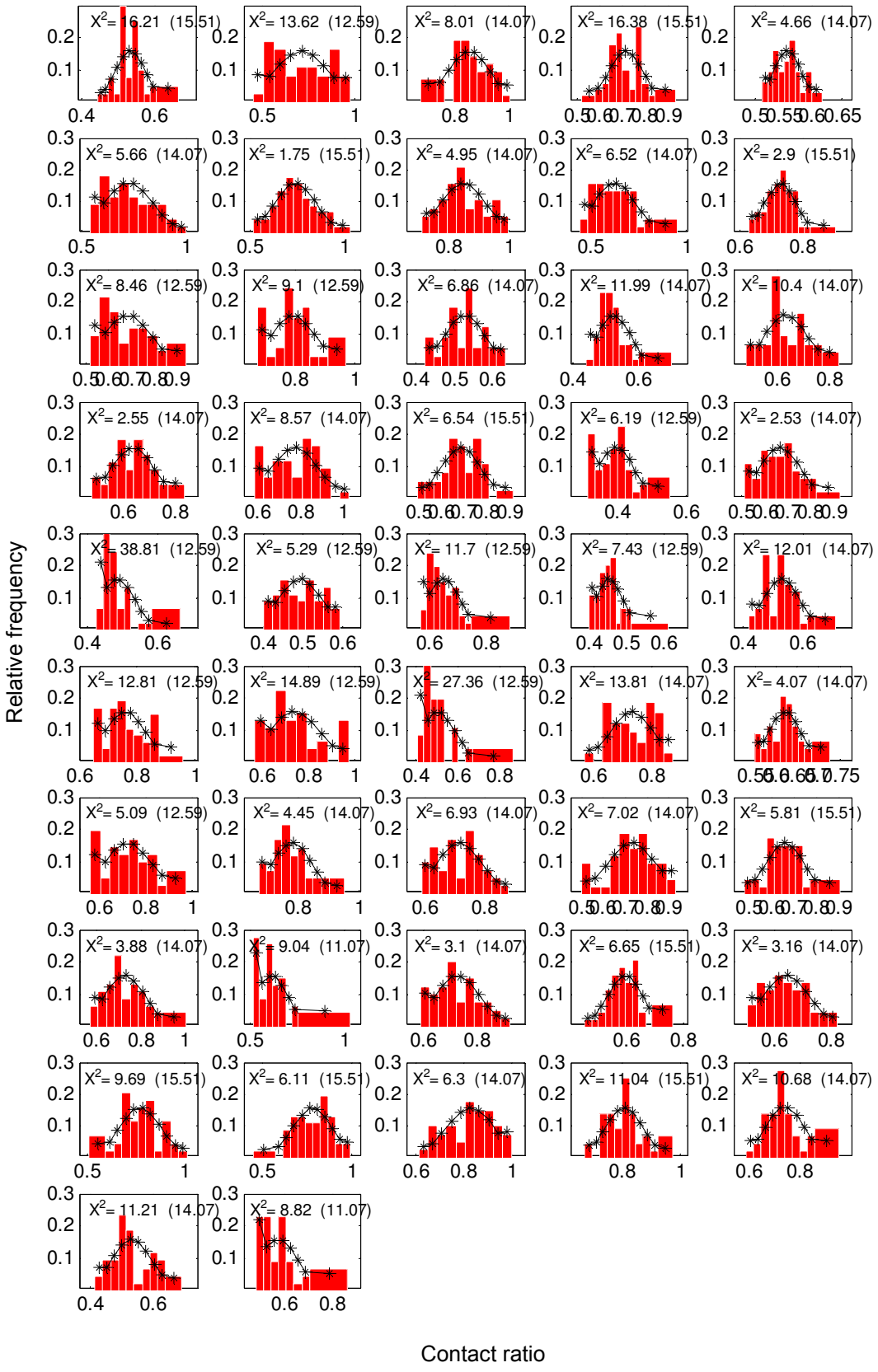

Figure 5.32: Contact ratio of synchronised tests at 1.5 Hz superimposed with the expected relative frequency from the Normal distribution.

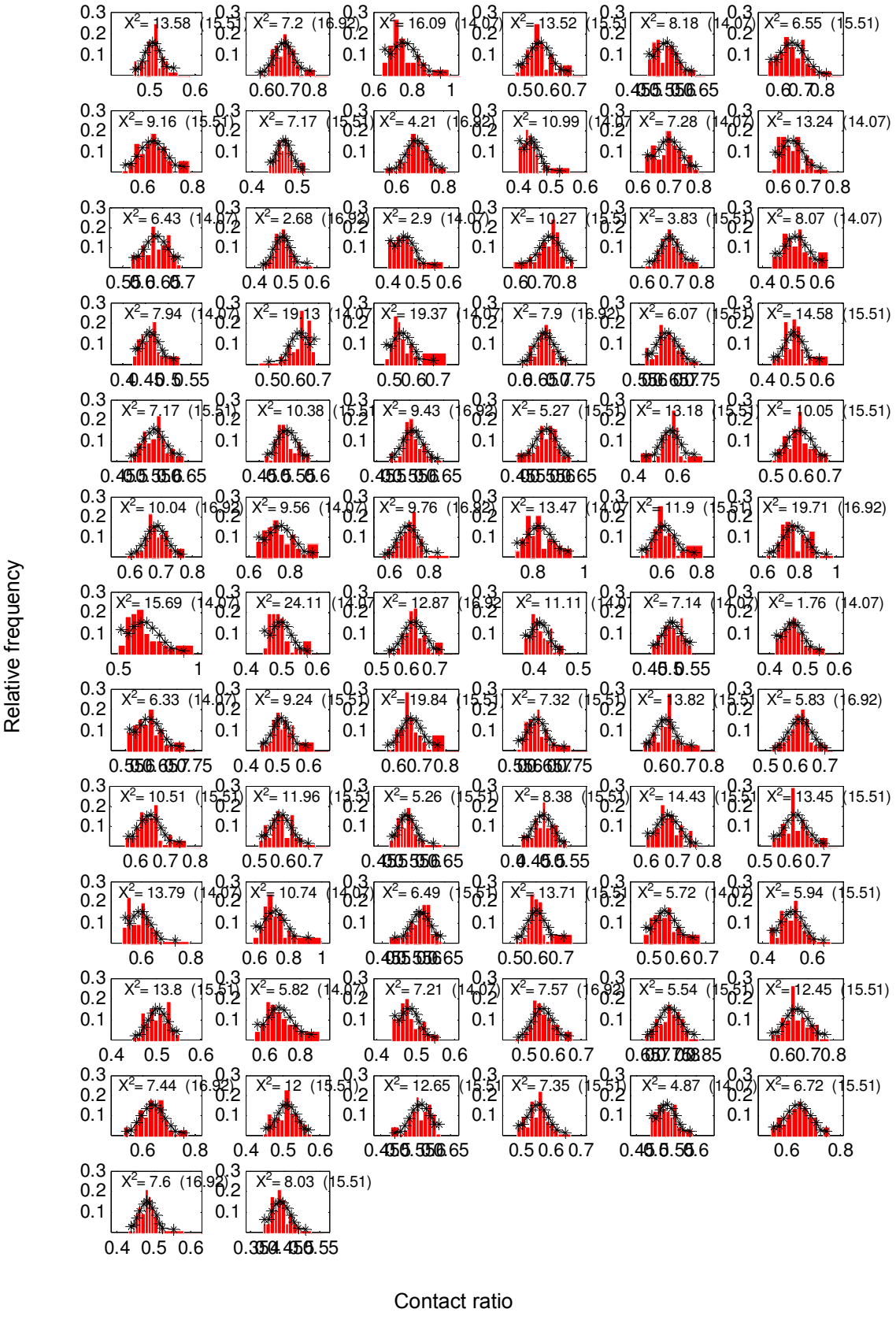

Figure 5.33: Contact ratio of synchronised tests at 2 Hz superimposed with the expected relative frequency from the Normal distribution.

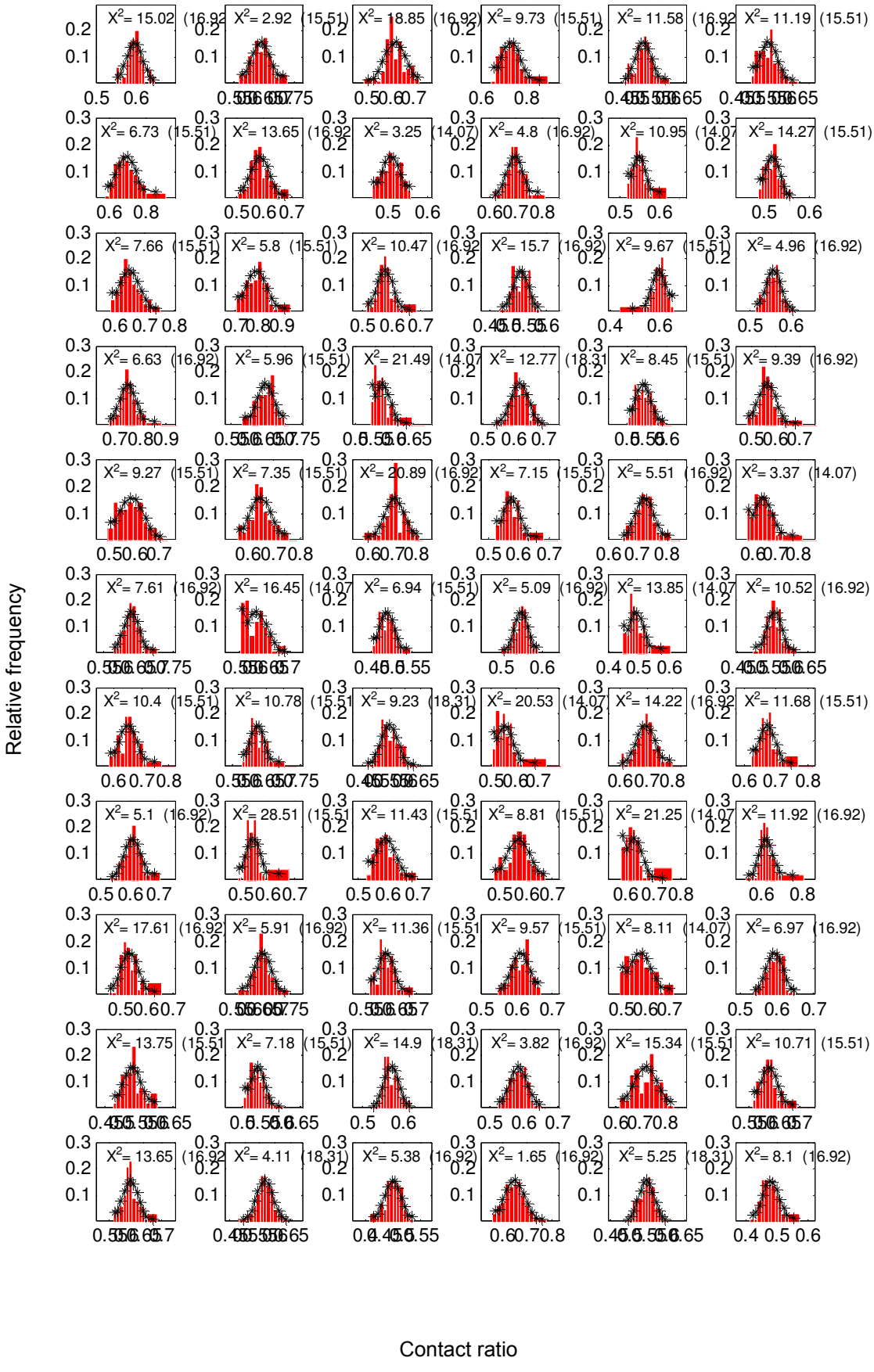

Figure 5.34: Contact ratio of synchronised tests at 2.67 Hz superimposed with the expected relative frequency from the Normal distribution.

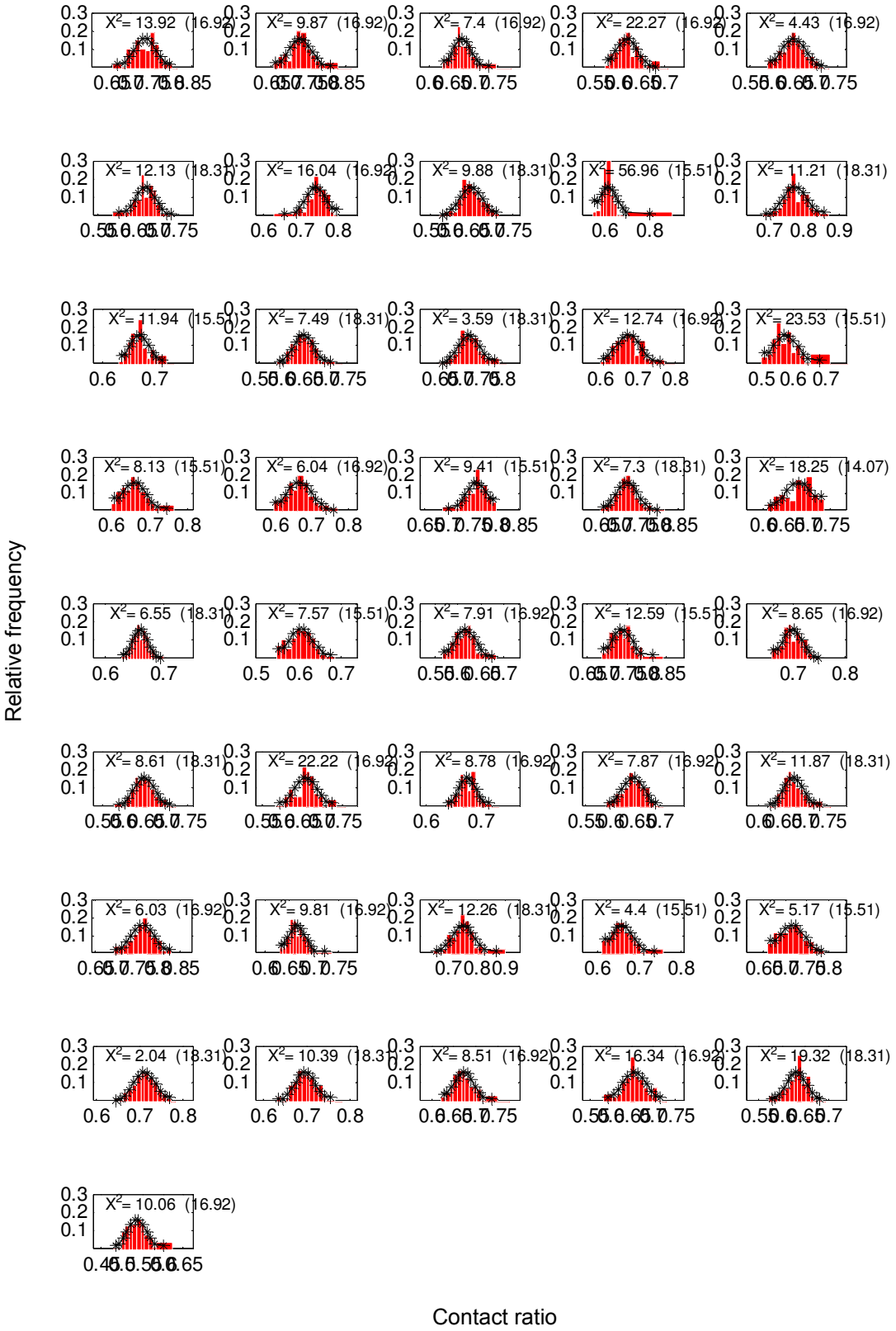

Figure 5.35: Contact ratio of synchronised tests at 3.5 Hz superimposed with the expected relative frequency from the Normal distribution.

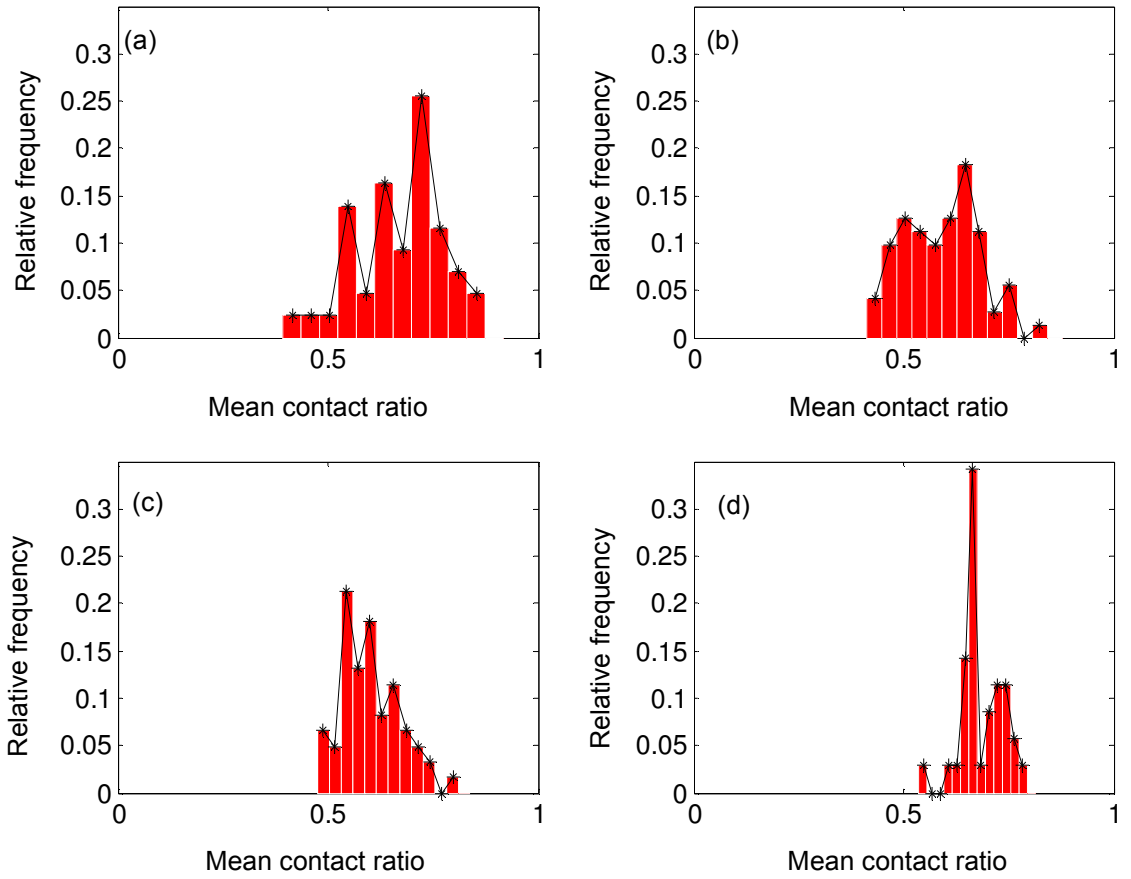

Figure 5.36: Histograms for mean contact ratio: (a) 1.5 Hz. (b) 2 Hz. (c) 2.67 Hz. (d) 3.5 Hz.

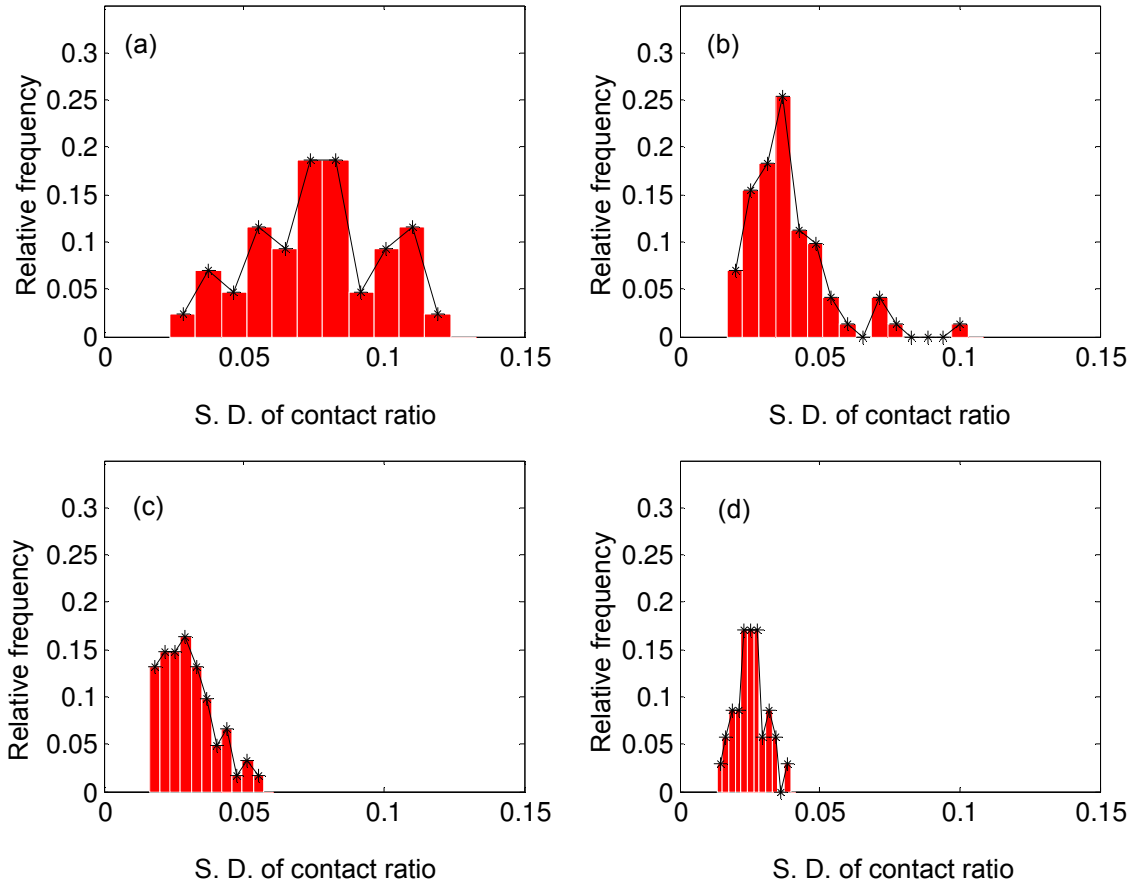

Figure 5.37: Histograms for the standard deviation of contact ratio: (a) 1.5 Hz. (b) 2 Hz. (c) 2.67 Hz. (d) 3.5 Hz.

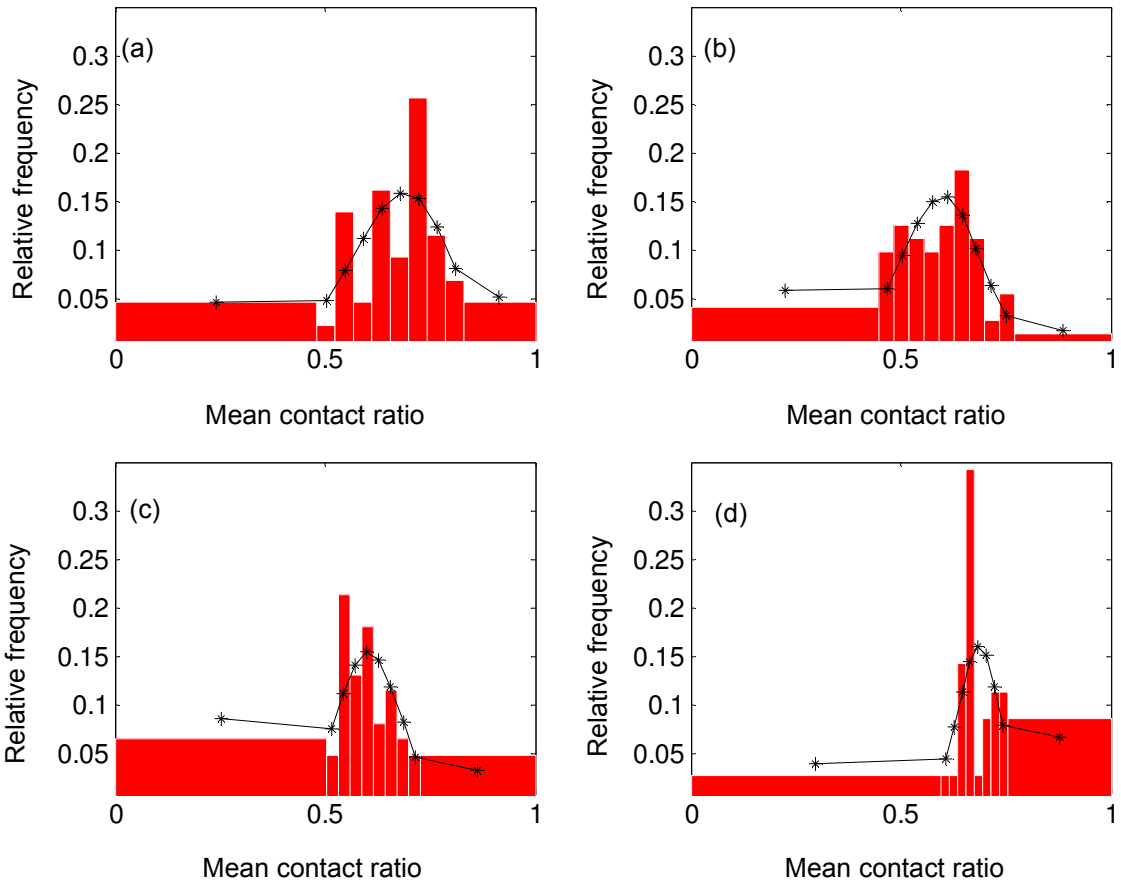

Figure 5.38: Histograms for mean contact ratio superimposed with expected relative frequency from Beta distribution: (a) 1.5 Hz. (b) 2 Hz. (c) 2.67 Hz. (d) 3.5 Hz.

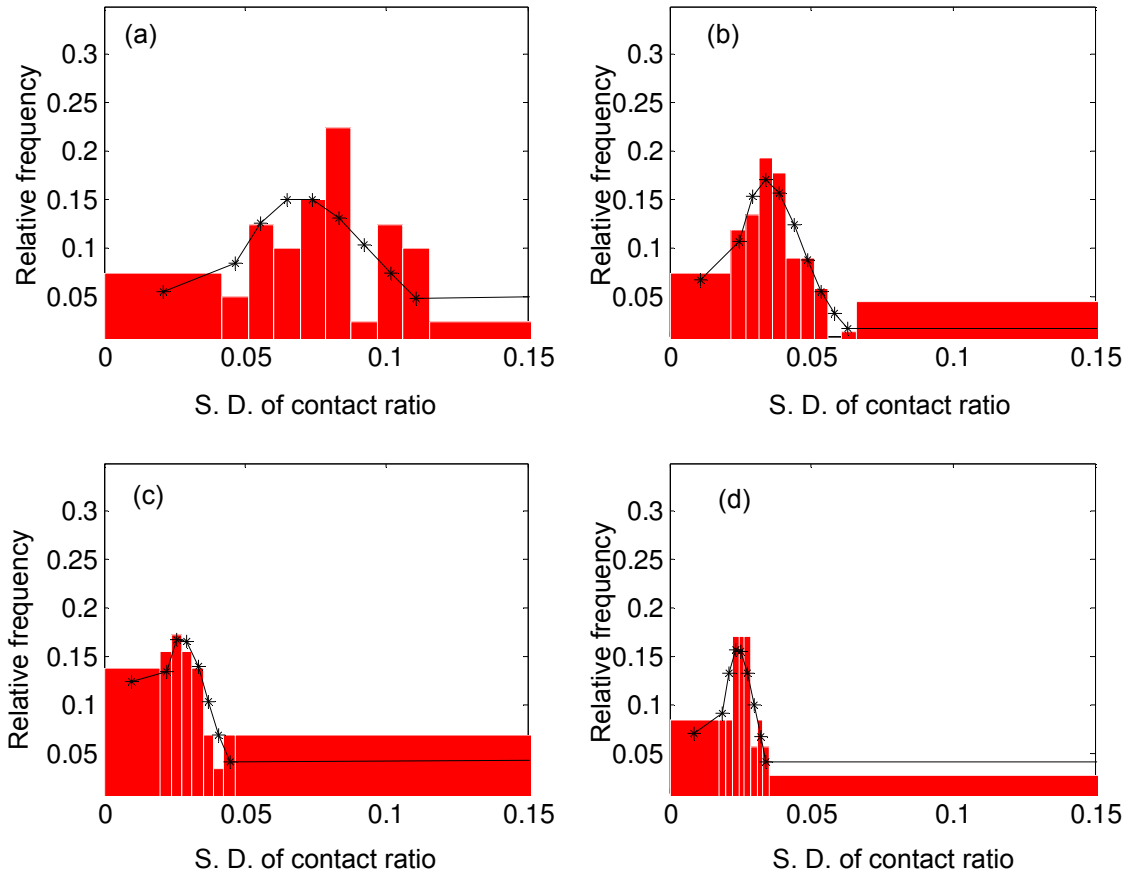

Figure 5.39: Histograms for the standard deviation of contact ratio superimposed with expected relative frequency from Beta distribution: (a) 1.5 Hz. (b) 2 Hz. (c) 2.67 Hz. (d) 3.5 Hz.

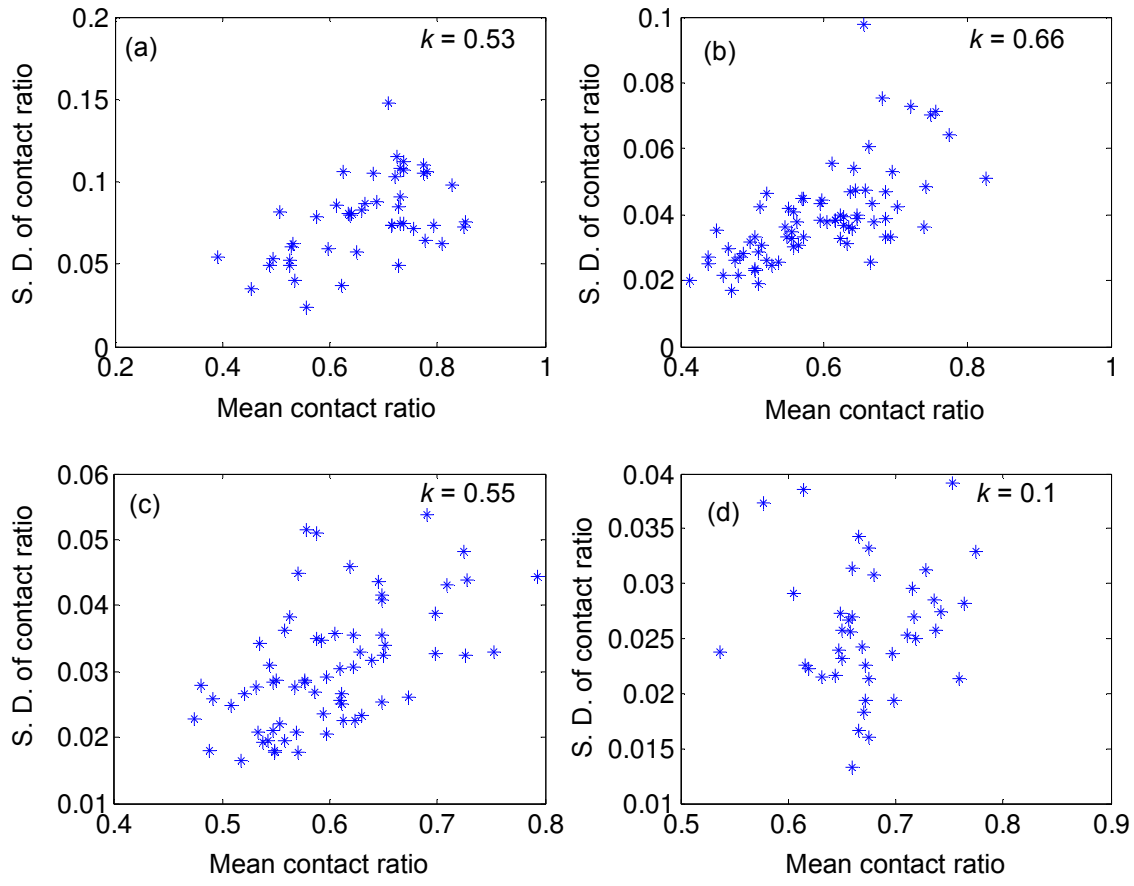

Figure 5.40: Relationship between mean and standard deviation of contact ratio: (a) 1.5 Hz. (b) 2 Hz. (c) 2.67 Hz. (d) 3.5 Hz.

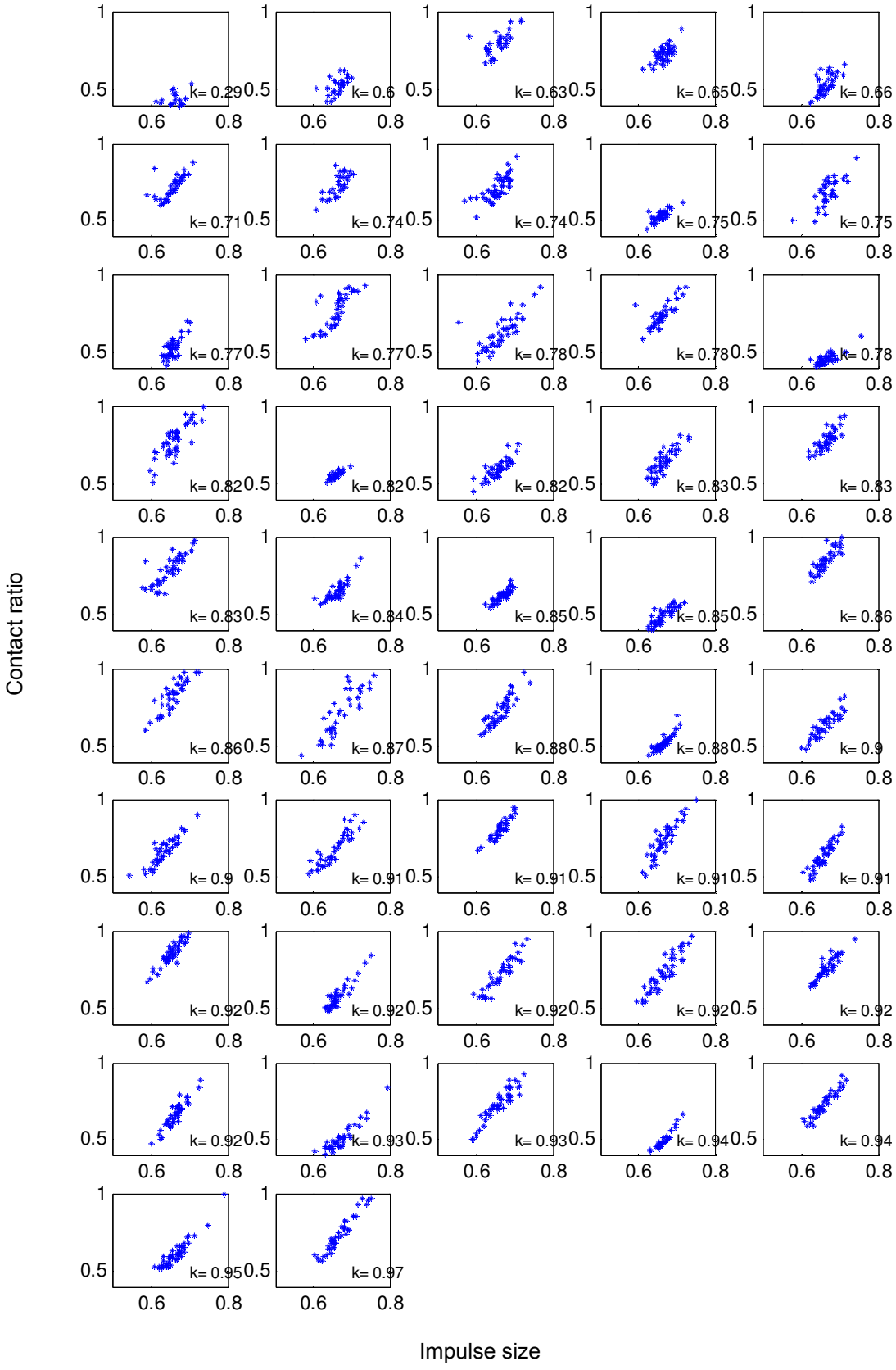

Figure 5.41: Variation of contact ratio with impulse size for synchronised tests at 1.5 Hz.

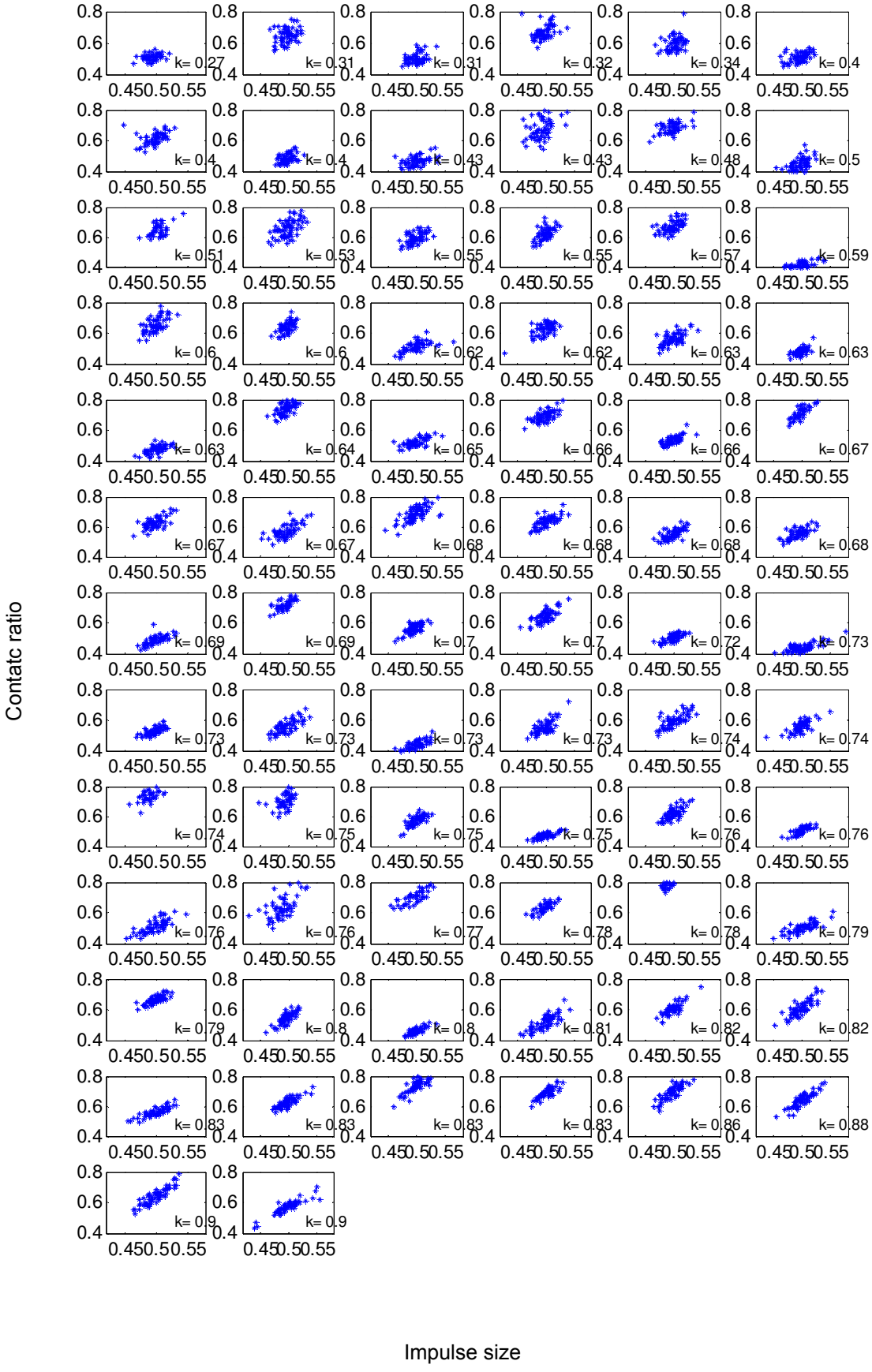

Figure 5.42: Variation of contact ratio with impulse size for synchronised tests at 2 Hz.

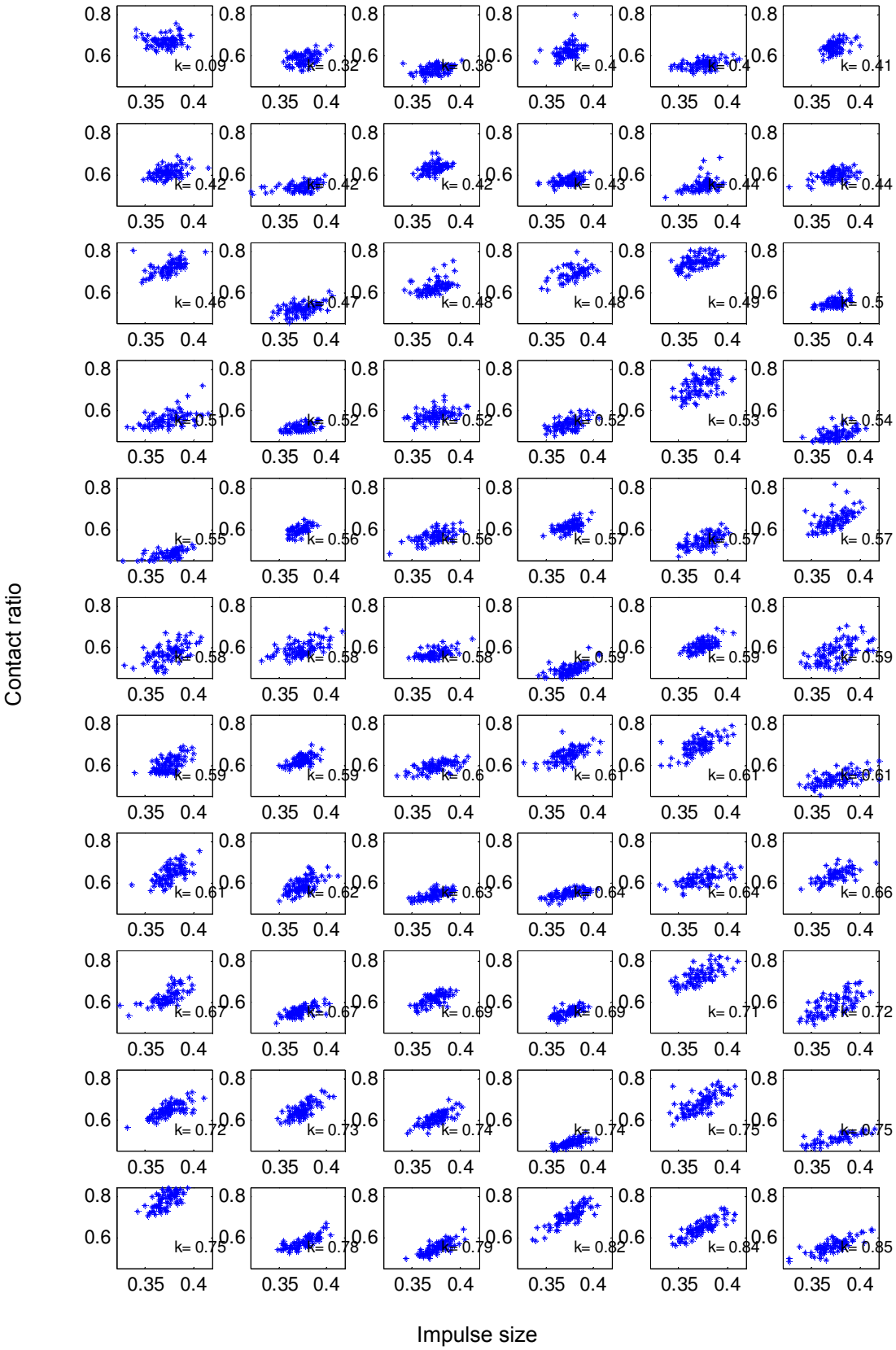

Figure 5.43: Variation of contact ratio with impulse size for synchronised tests at 2.67 Hz.

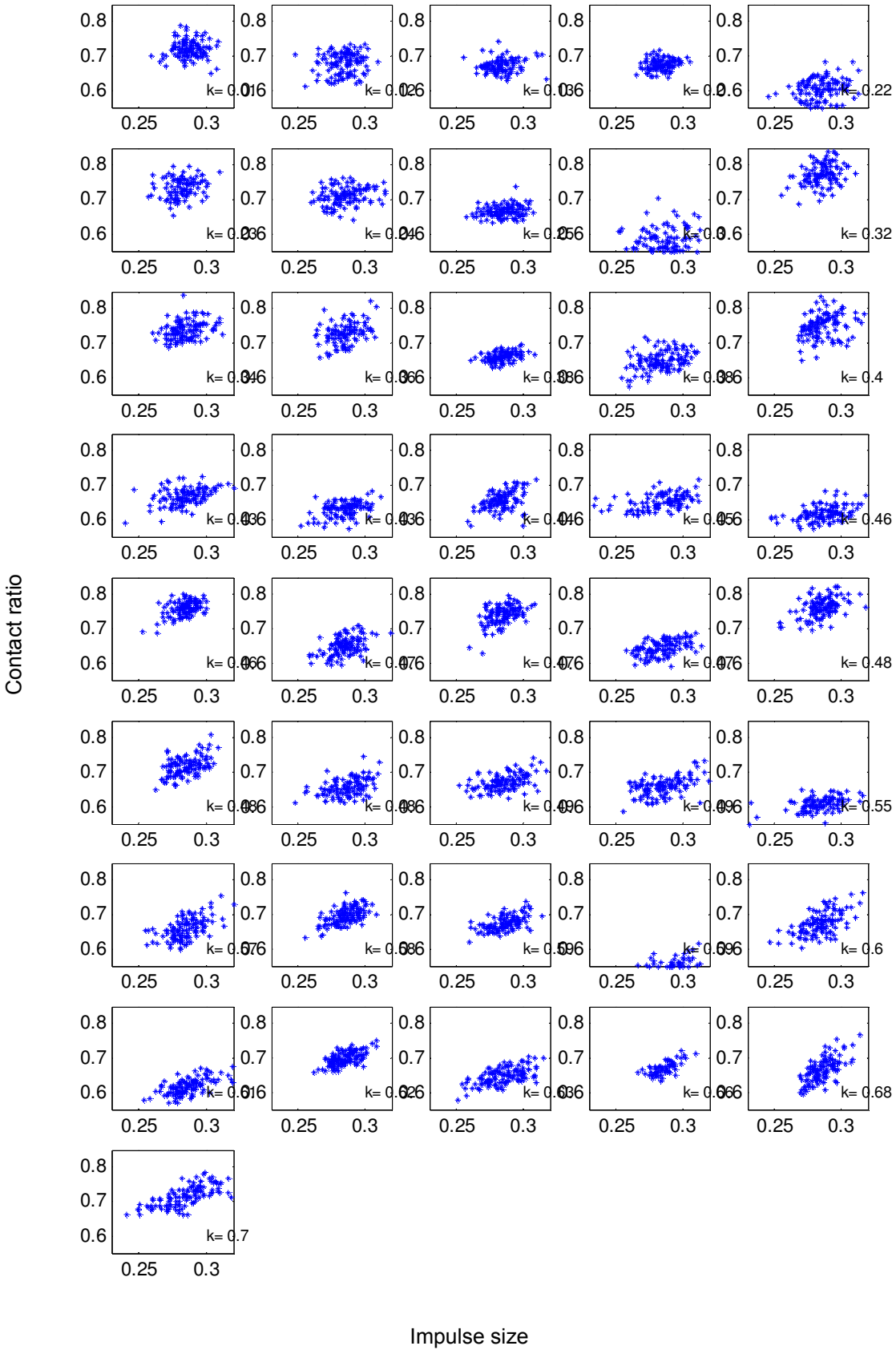

Figure 5.44: Variation of contact ratio with impulse size for synchronised tests at 3.5 Hz.

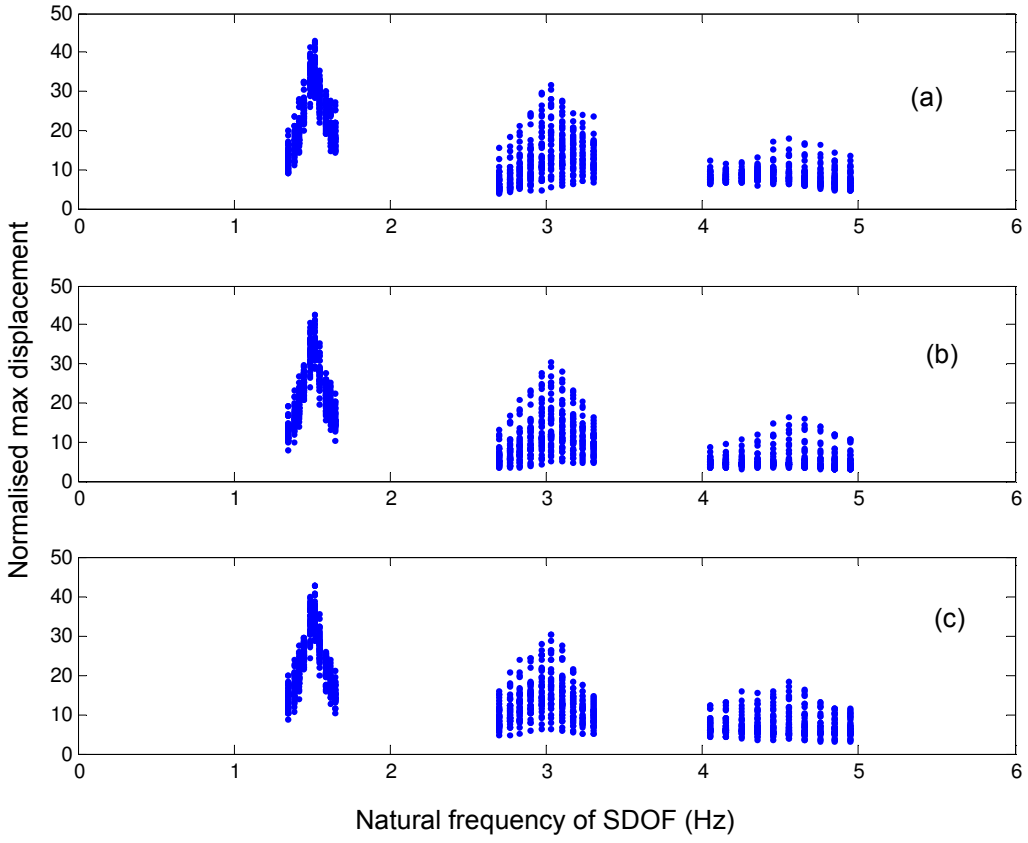

Figure 5.45: Normalised maximum displacement due to three load cases at 1.5 Hz beat frequency: (a) measured load. (b) simulated load with contact ratio varying linearly with impulse size. (c) simulated load with contact ratio modelled using Normal distribution.

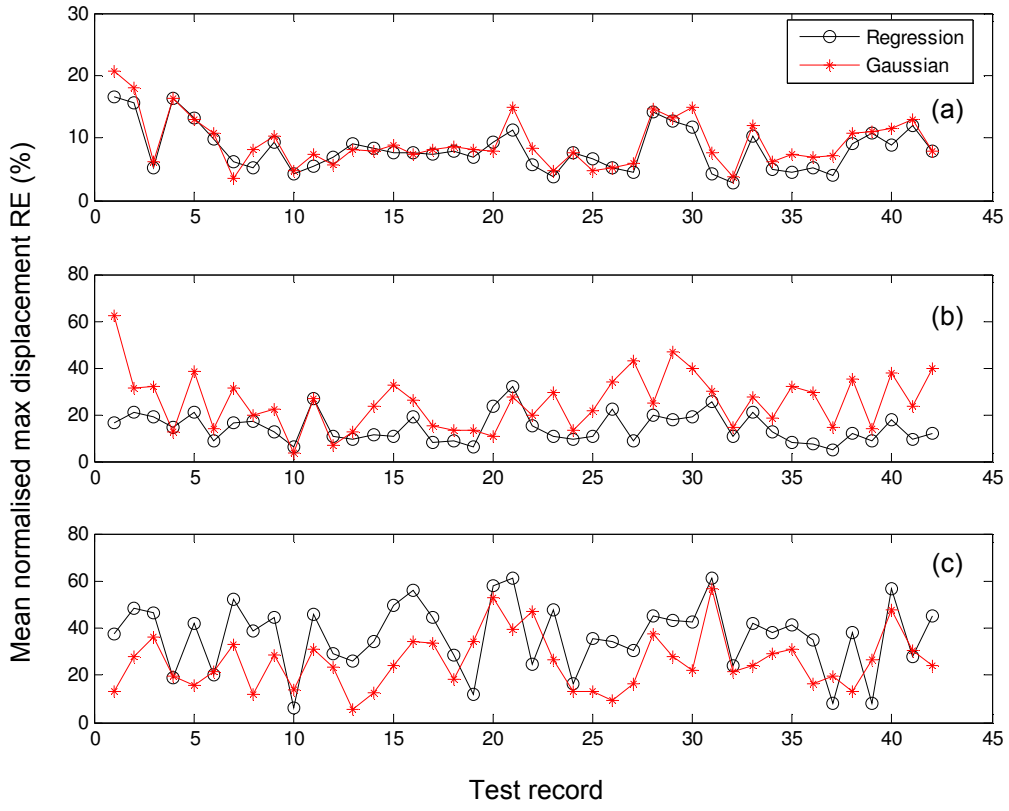

Figure 5.46: Comparing relative error of normalised maximum displacement due to contact ratio modelled as dependent on impulse size (Regression) and using Normal distribution (Gaussian) for 1.5 Hz beat frequency: (a) 1st harmonic. (b) 2nd harmonic (c) 3rd harmonic.

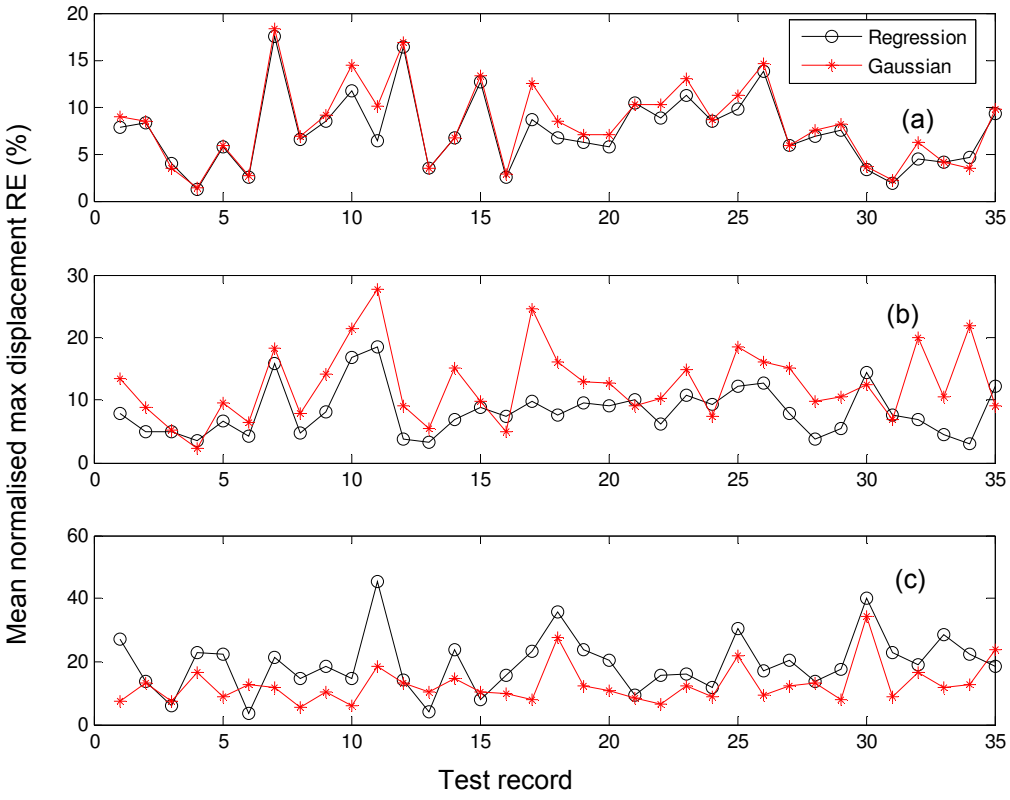

Figure 5.47: Comparing relative error of normalised maximum displacement due to contact ratio modelled as dependent on impulse size (Regression) and using Normal distribution (Gaussian) for 2 Hz beat frequency: (a) 1st harmonic. (b) 2nd harmonic (c) 3rd harmonic.

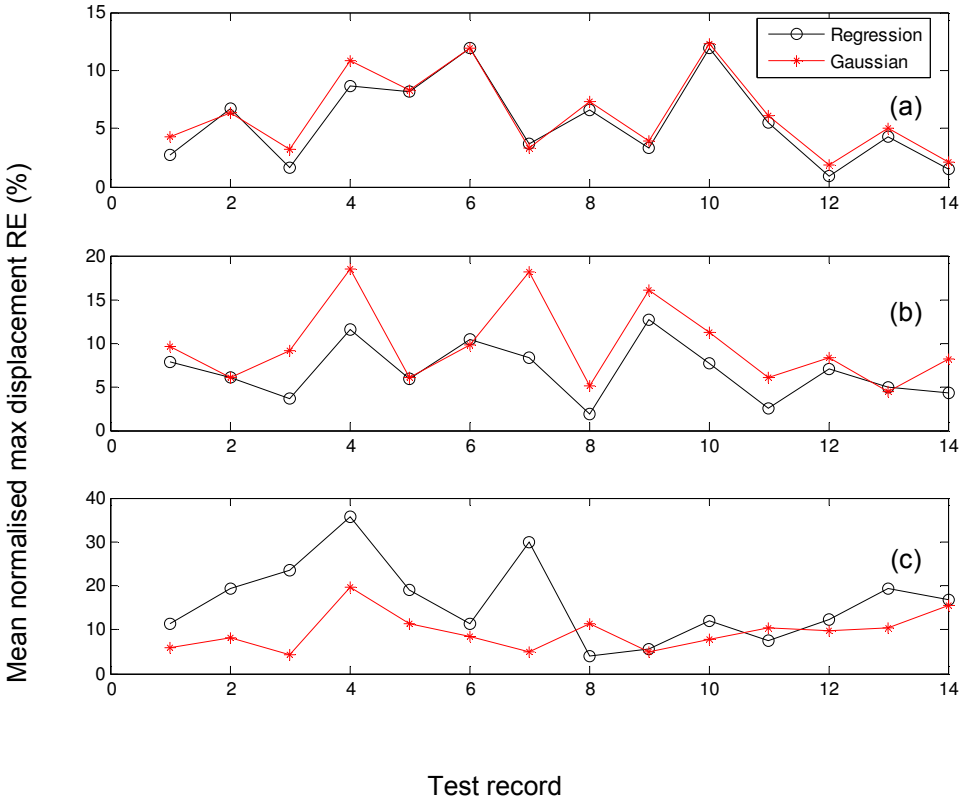

Figure 5.48: Comparing relative error of normalised maximum displacement due to contact ratio modelled as dependent on impulse size (Regression) and using Normal distribution (Gaussian) for 2.67 Hz beat frequency: (a) 1st harmonic. (b) 2nd harmonic (c) 3rd harmonic.

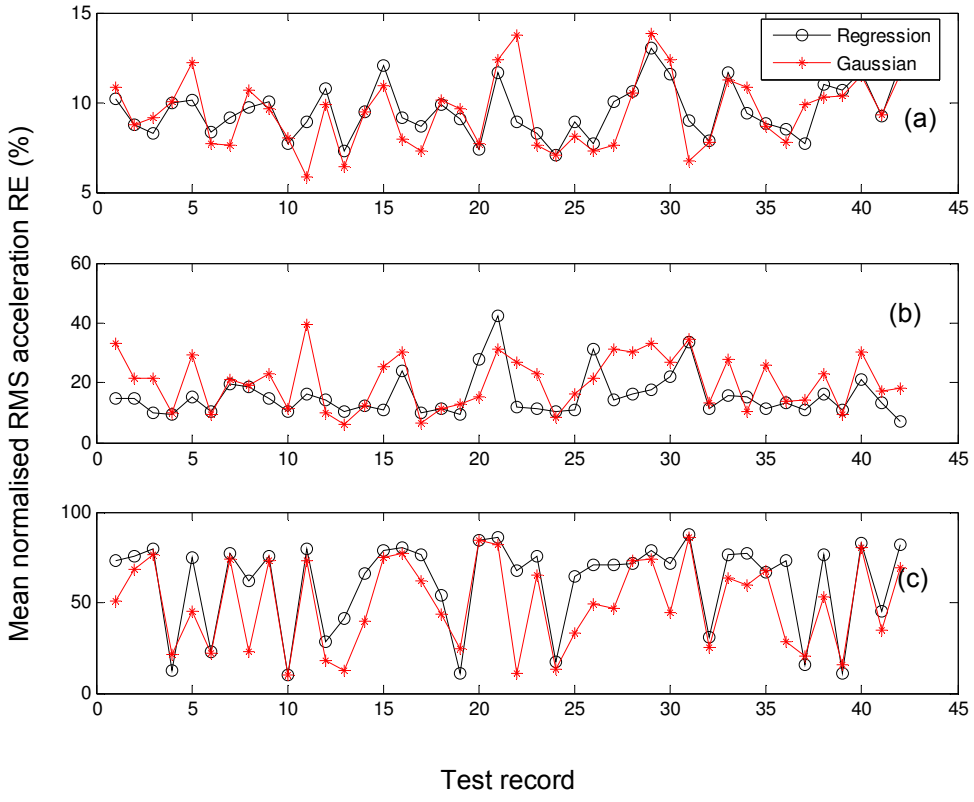

Figure 5.49: Comparing relative error of normalised RMS acceleration due to contact ratio modelled as dependent on impulse size (Regression) and using Normal distribution (Gaussian) for 1.5 Hz beat frequency: (a) 1st harmonic. (b) 2nd harmonic (c) 3rd harmonic.

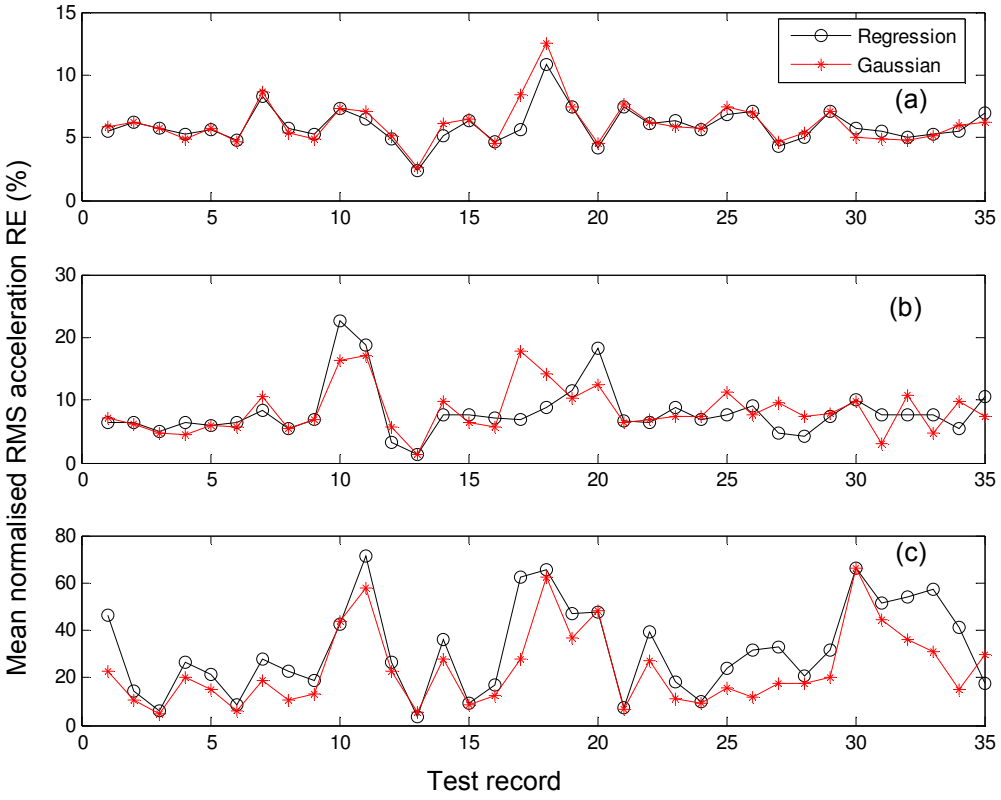

Figure 5.50: Comparing relative error of normalised RMS acceleration due to contact ratio modelled as dependent on impulse size (Regression) and using Normal distribution (Gaussian) for 2 Hz beat frequency: (a) 1st harmonic. (b) 2nd harmonic (c) 3rd harmonic.

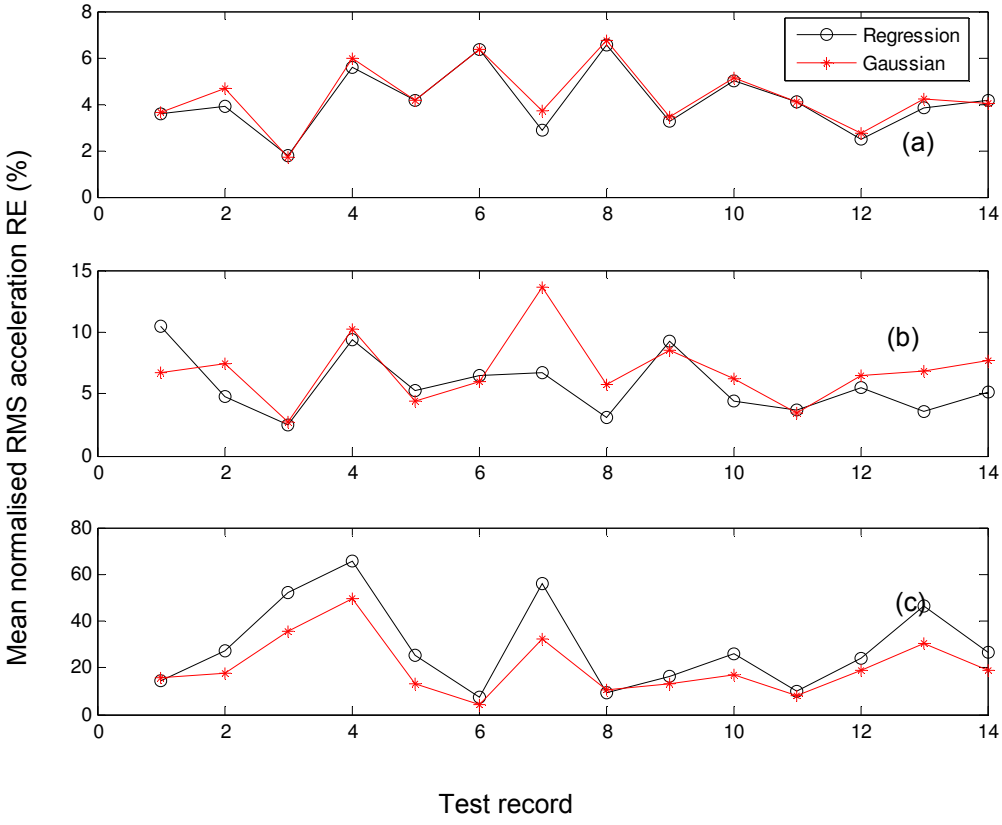

Figure 5.51: Comparing relative error of normalised RMS acceleration due to contact ratio modelled as dependent on impulse size (Regression) and using Normal distribution (Gaussian) for beat frequency 2.67 Hz: (a) 1st harmonic. (b) 2nd harmonic (c) 3rd harmonic.

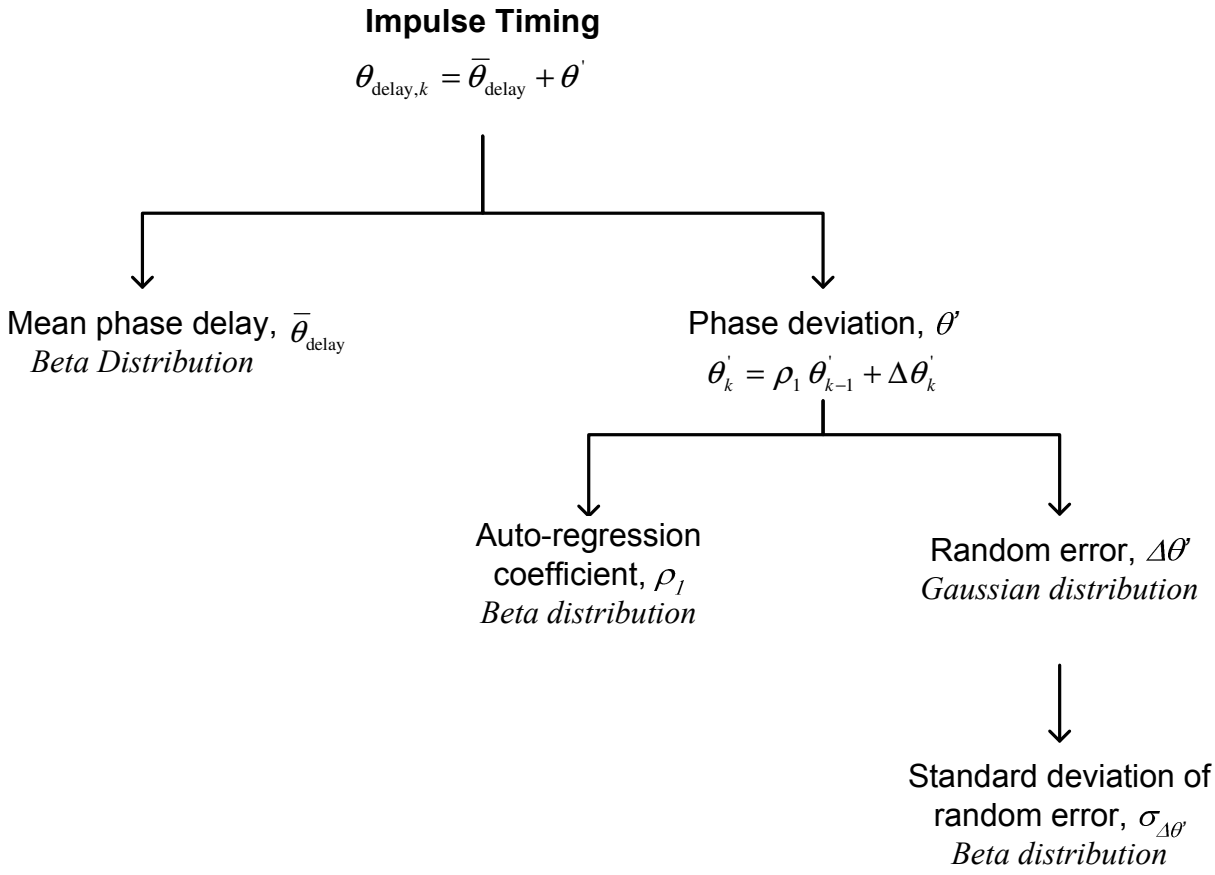

Figure 5.52: Summary of modelling of impulse timing.

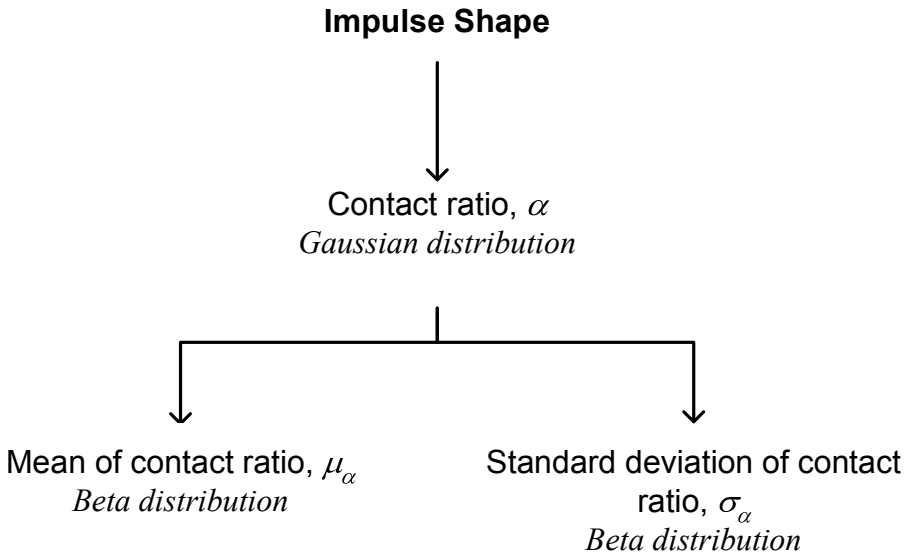

Figure 5.53: Summary of modelling of impulse shape.

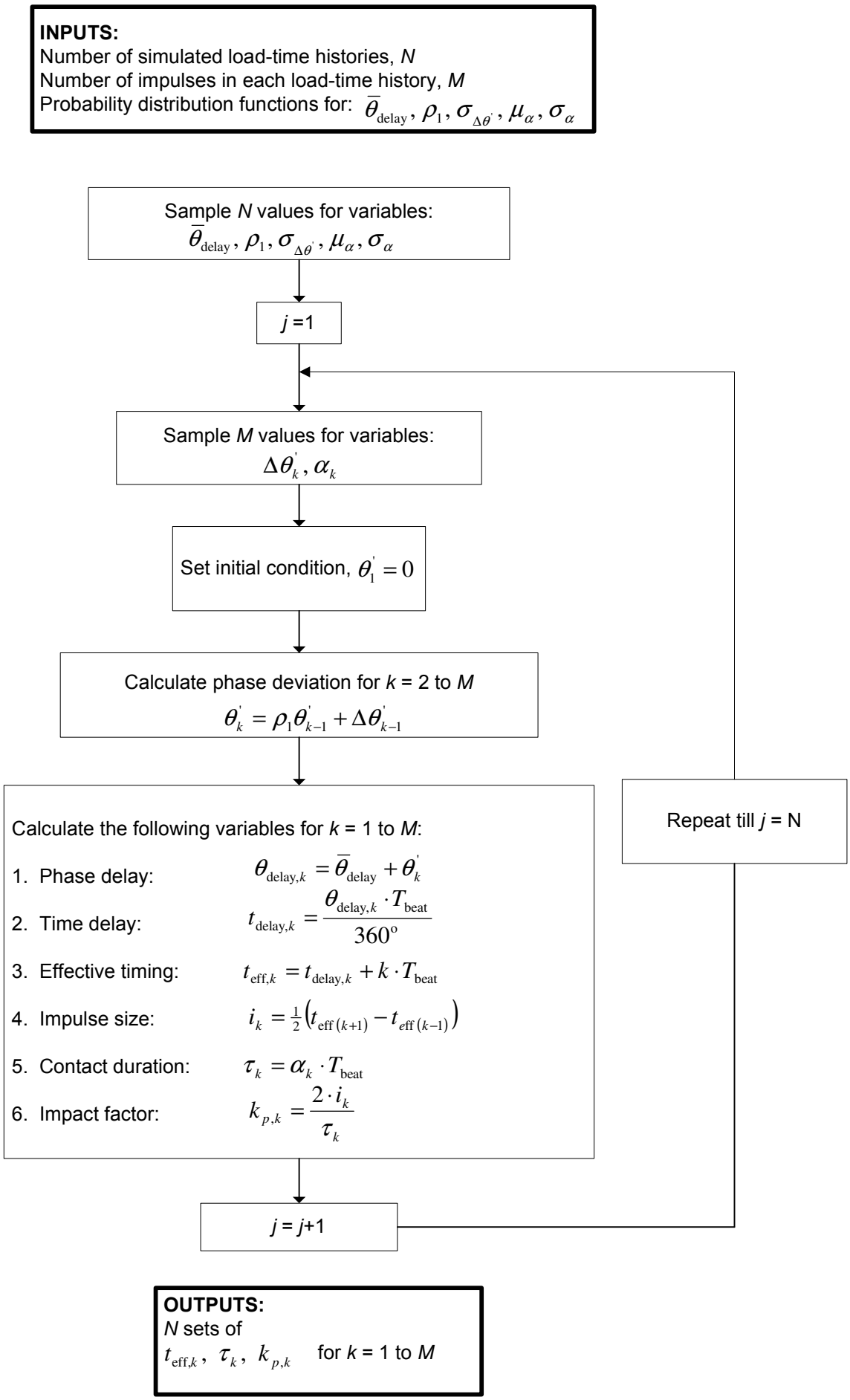

Figure 6.1: Flow chart for simulating jumping loads.

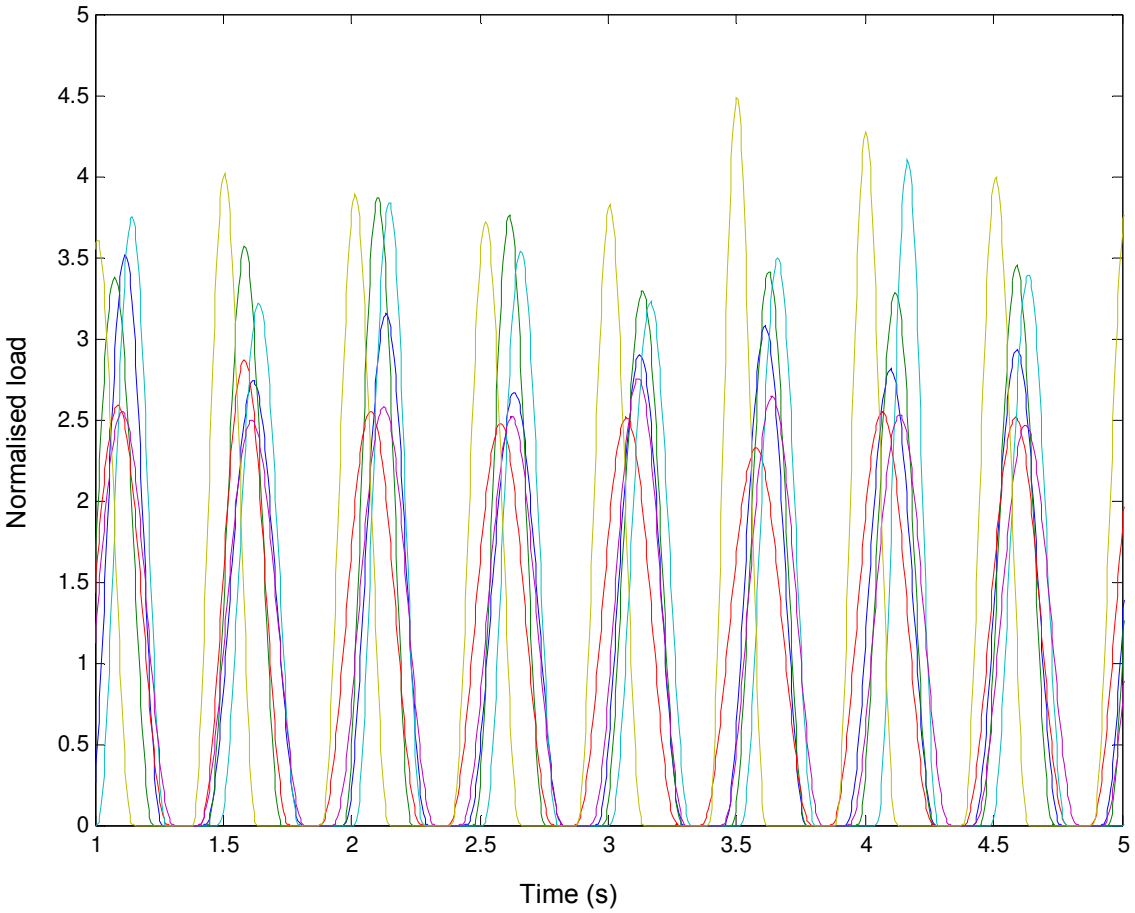

Figure 6.2: Some examples of the simulated jumping loads.

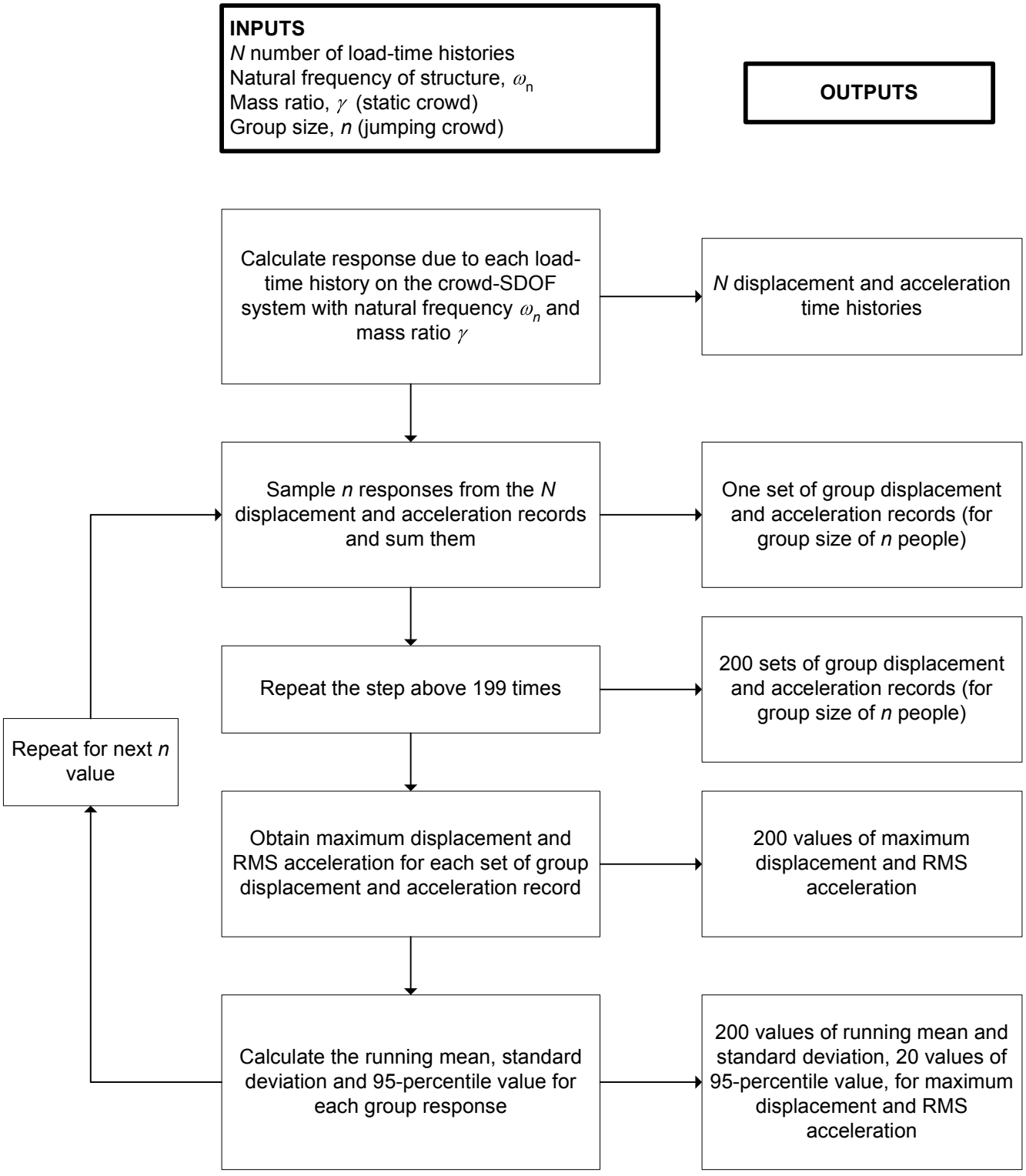

Figure 6.3: Flow chart for calculating the crowd-SDOF system response due to various jumping crowd sizes.

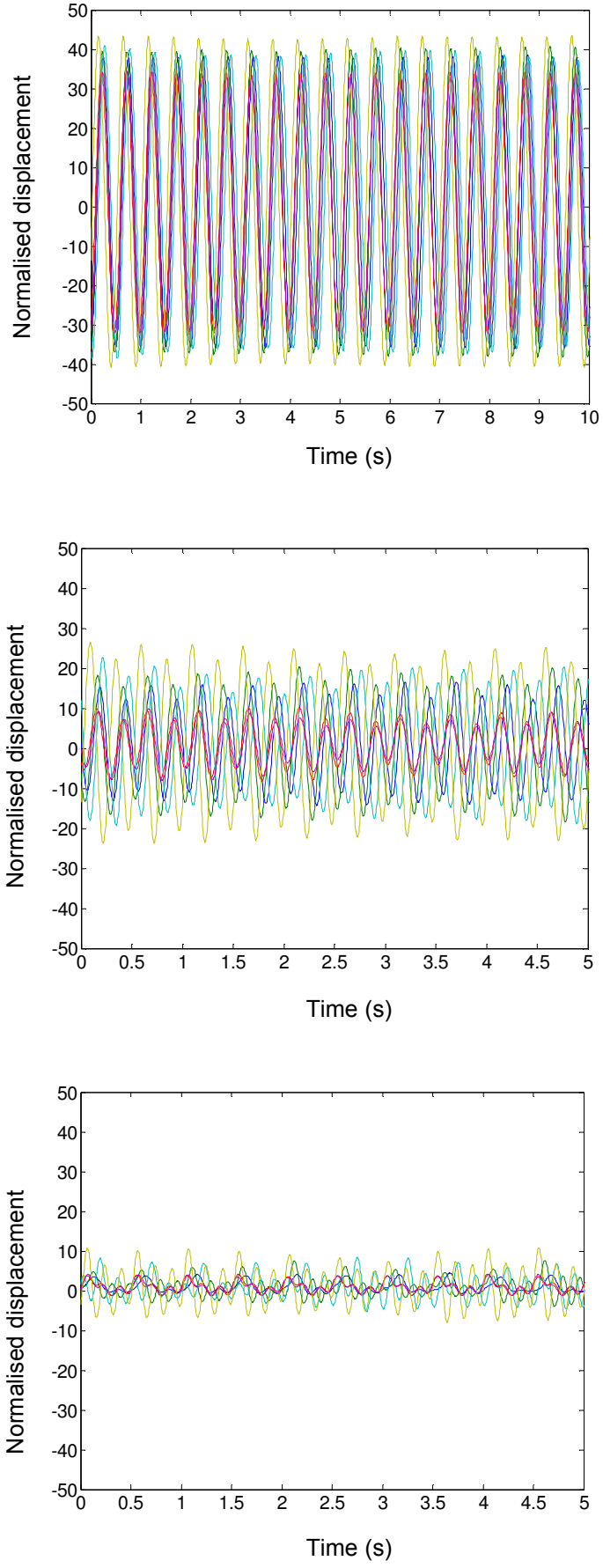

Figure 6.4: Normalised displacement due to simulated loads shown in Figure 6.2 on 2Hz (top), 4Hz (middle) and 6Hz (bottom) structures, with mass 1 kg. The normalised displacement is given by the displacement divided by the static deflection due to a unit load (1N).

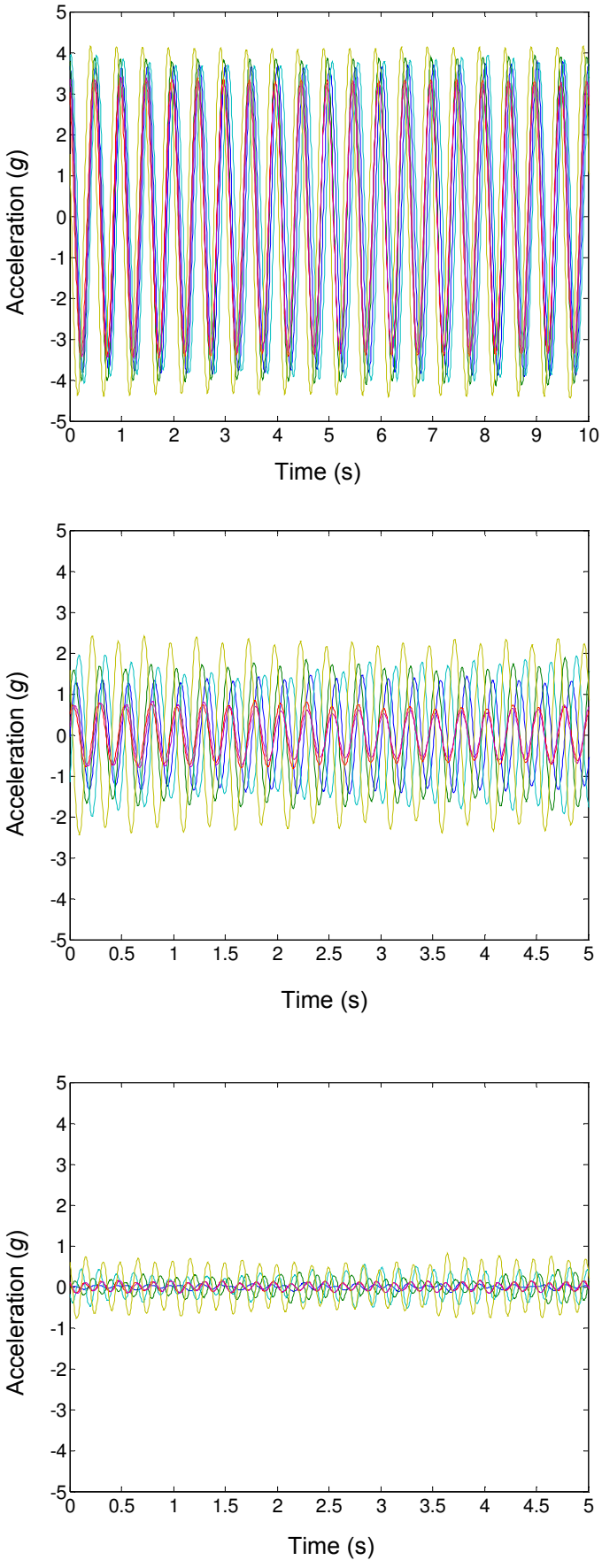

Figure 6.5: Acceleration due to simulated loads shown in Figure 6.2 on 2Hz (top), 4Hz (middle) and 6Hz (bottom) structures, with mass 1 kg.

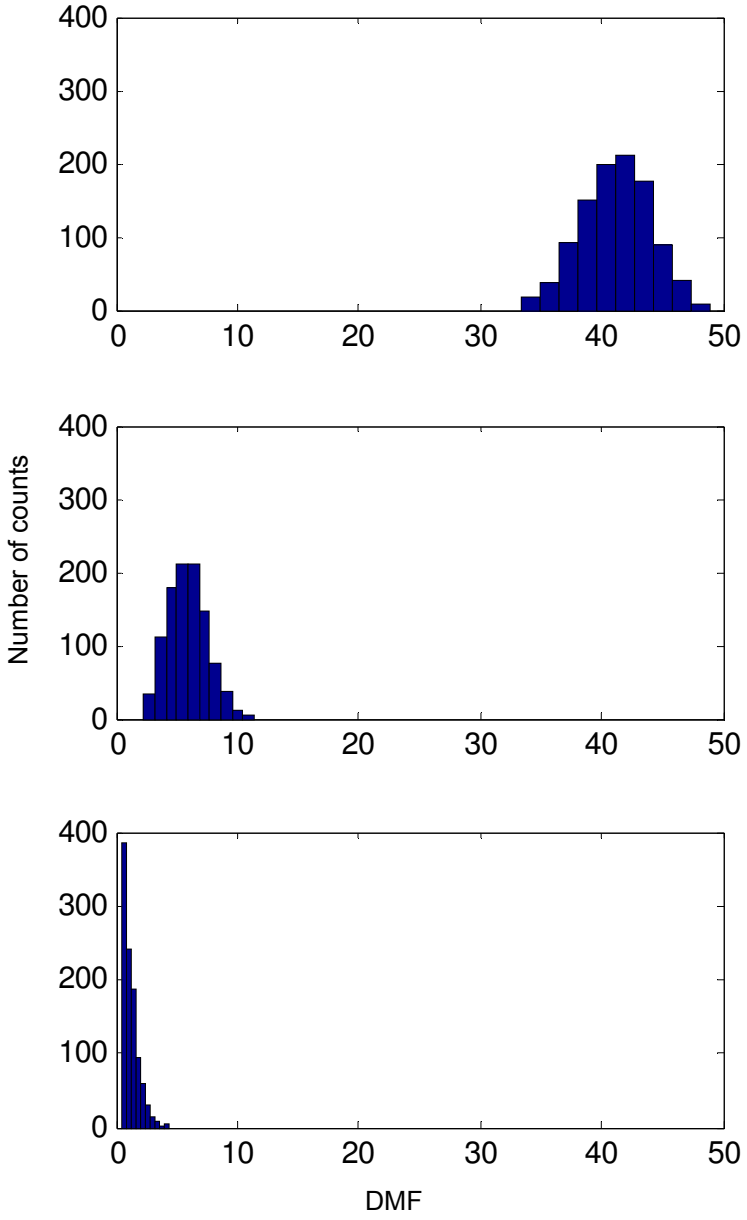

Figure 6.6: Distribution of DMF for 1024 simulated loads at beat frequency of 2Hz on 2Hz (top), 4Hz (middle) and 6Hz (bottom) structures.

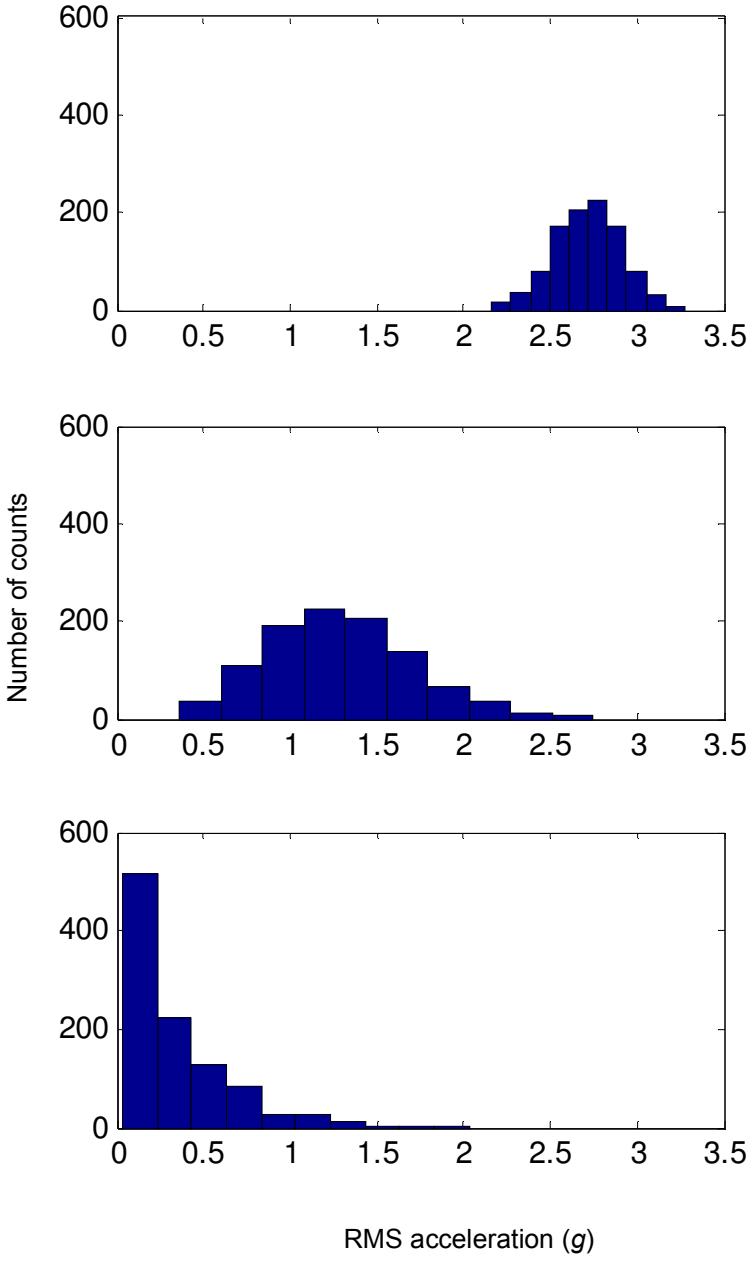

Figure 6.7: Distribution of RMS acceleration for 1024 simulated loads at beat frequency of 2Hz on 2Hz (top), 4Hz (middle) and 6Hz (bottom) structures.

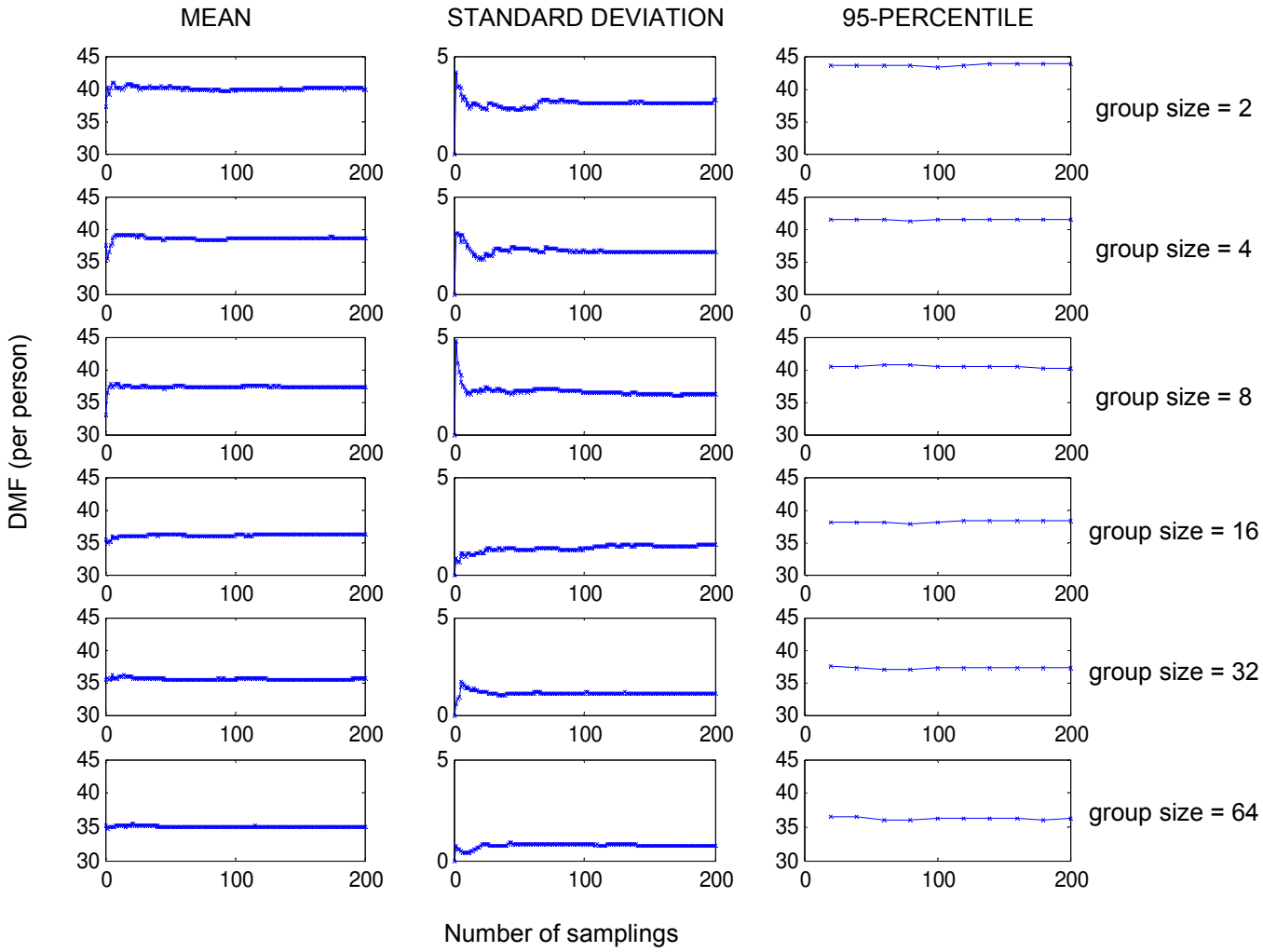

Figure 6.8: Running mean (left cloumn), standard deviation (middle column) and 95-percentile value (right column) for DMF (per person) of jumping loads at 2Hz on a 2Hz structure, group sizes of 2, 4, 8, 16, 32 and 64.

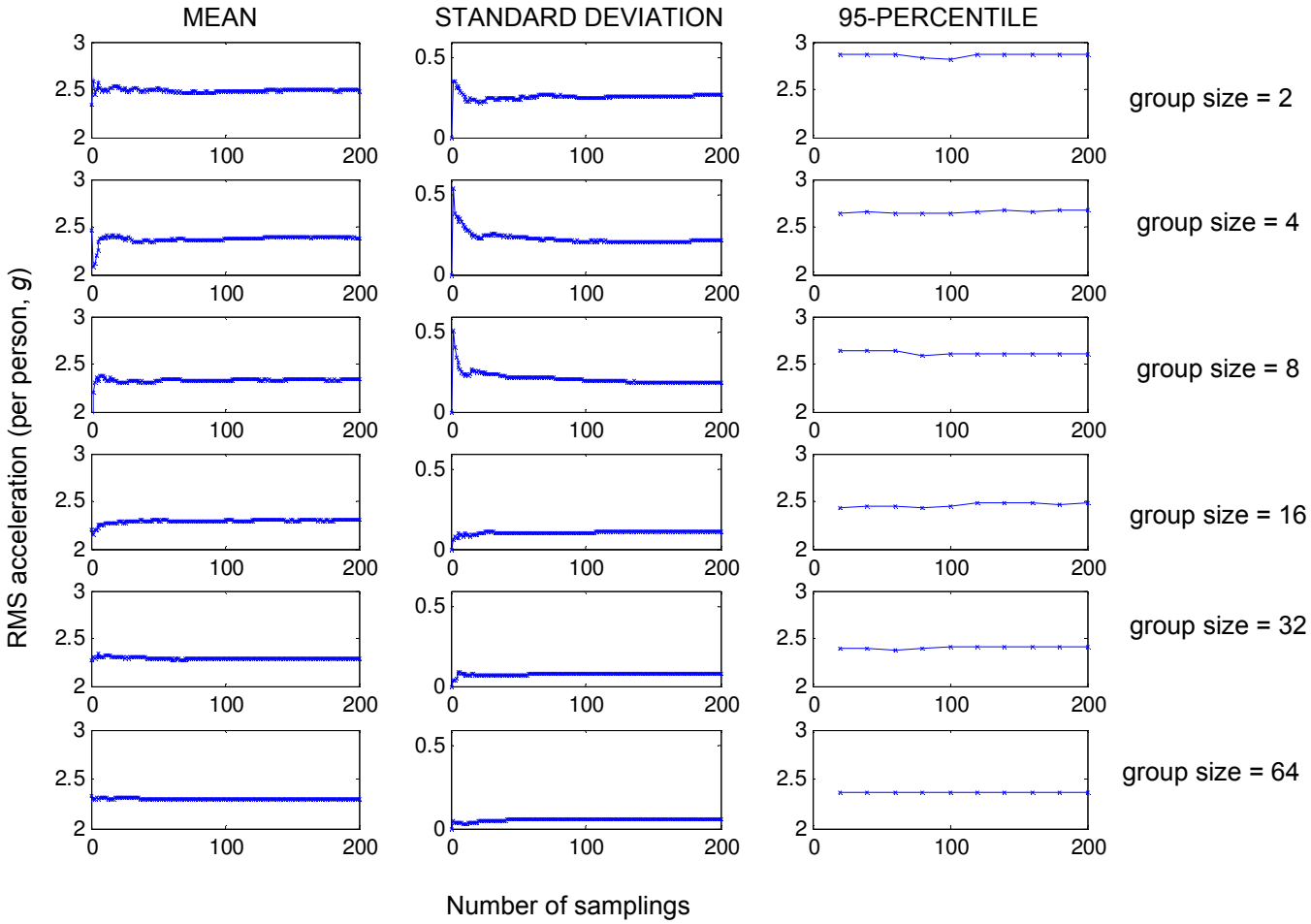

Figure 6.9: Running mean (left cloumn), standard deviation (middle column) and 95-percentile value (right column) for RMS acceleration of jumping loads at 2Hz on a 2Hz structure, group sizes of 2, 4, 8, 16, 32 and 64.

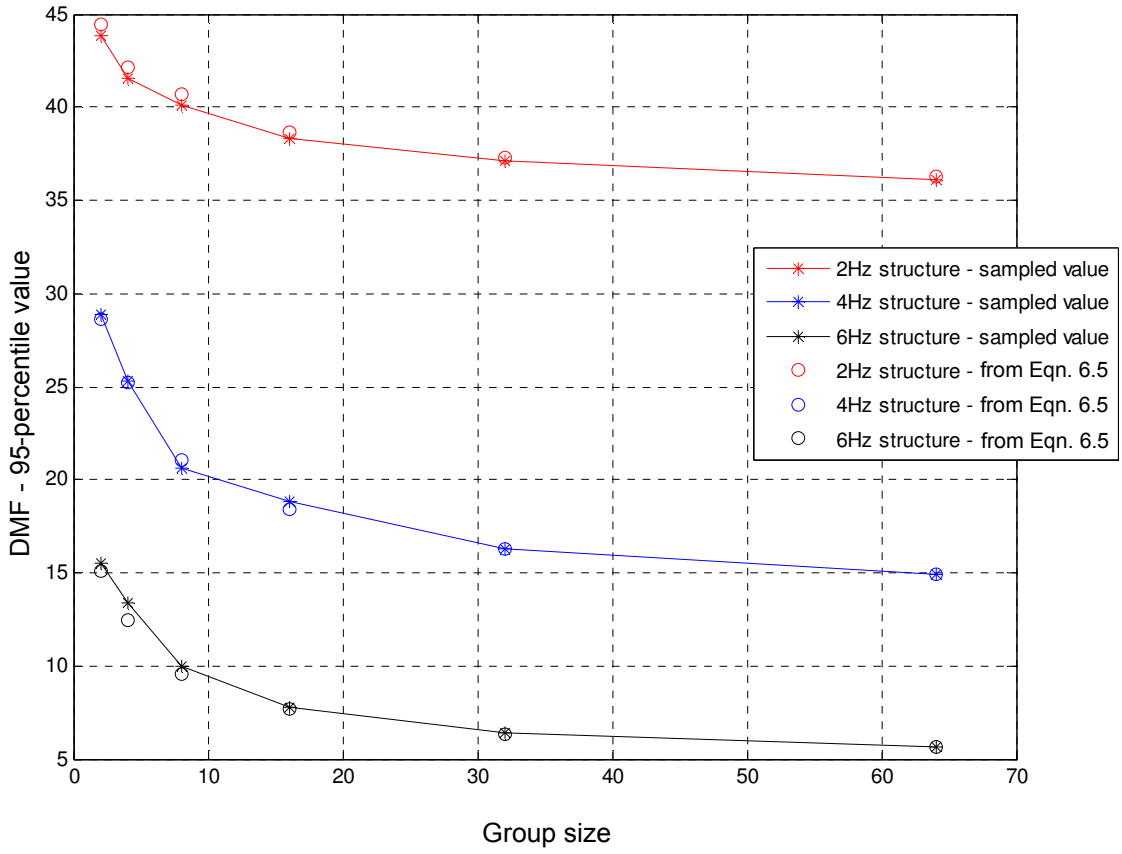

Figure 6.10: Comparison of the DMF 95-percentile value between sampled and calculated values using Eqn. 6.5 for group sizes from 2 to 64.

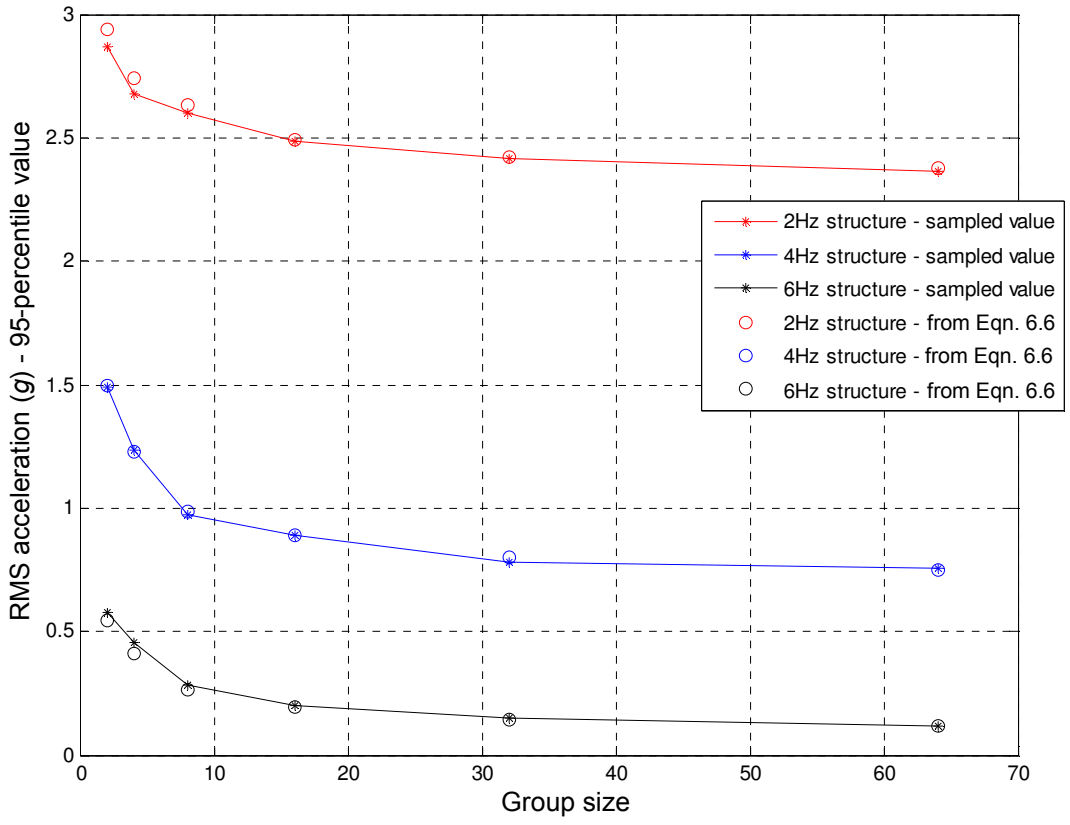

Figure 6.11: Comparison of the RMS acceleration 95-percentile value between sampled and calculated values using Eqn. 6.6 for group sizes from 2 to 64.

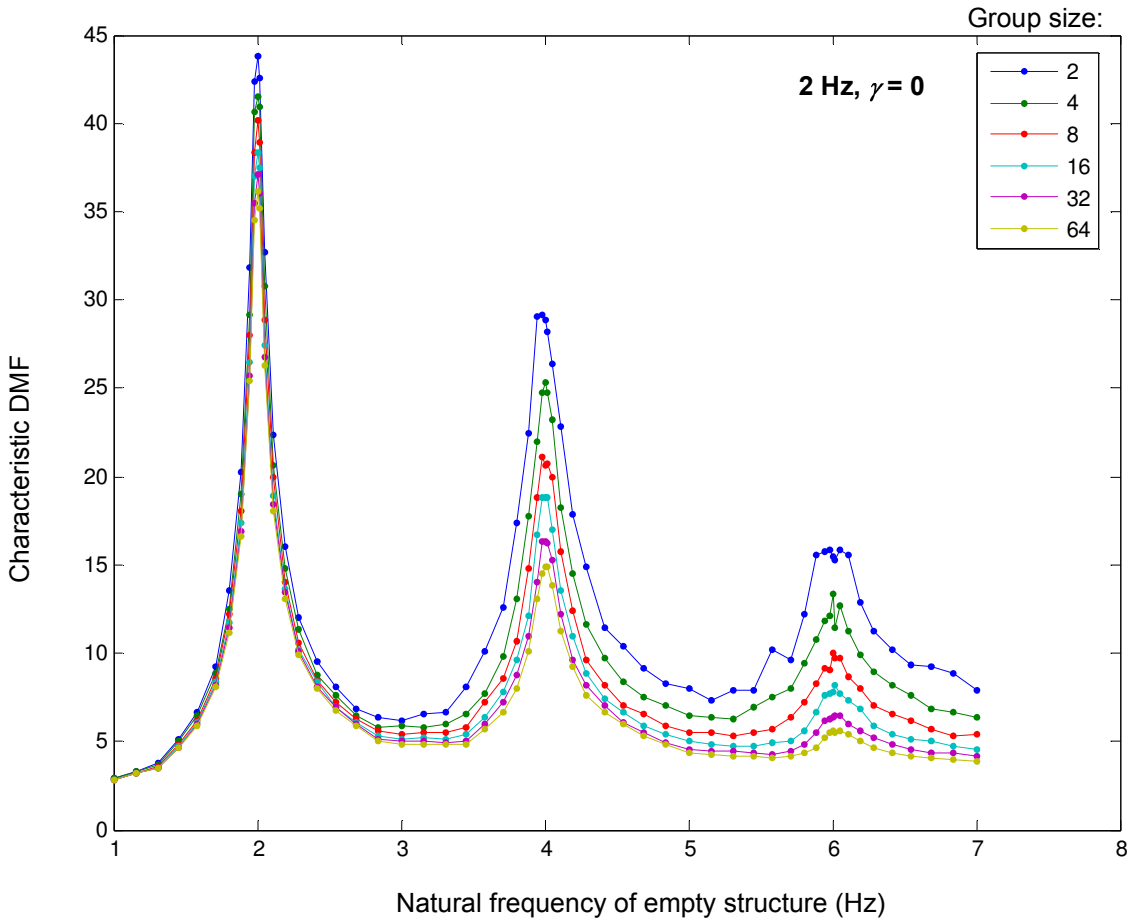

Figure 6.12: Variation of characteristic DMF with natural frequency of empty structure and group size for jumping loads at 2 Hz and $\gamma = 0$.

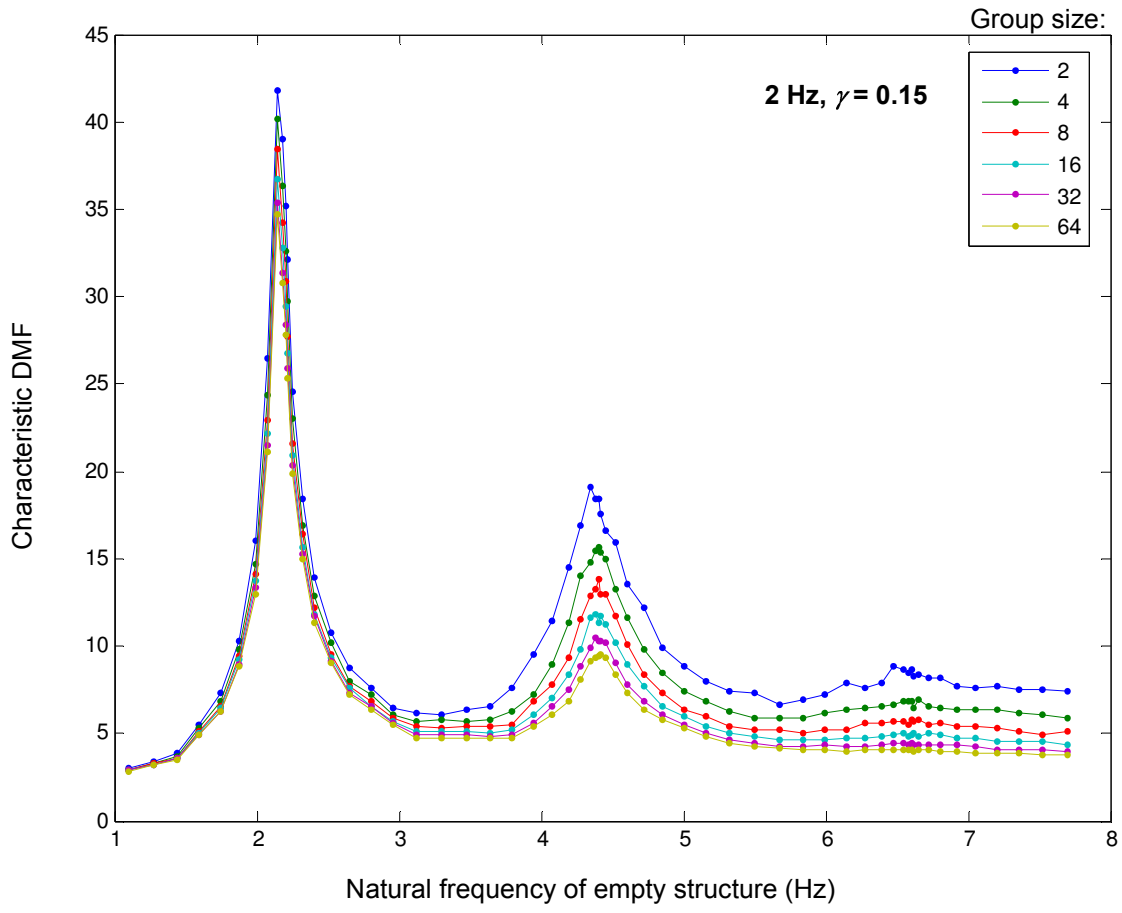

Figure 6.13: Variation of characteristic DMF with natural frequency of empty structure and group size for jumping loads at 2 Hz and $\gamma = 0.15$.

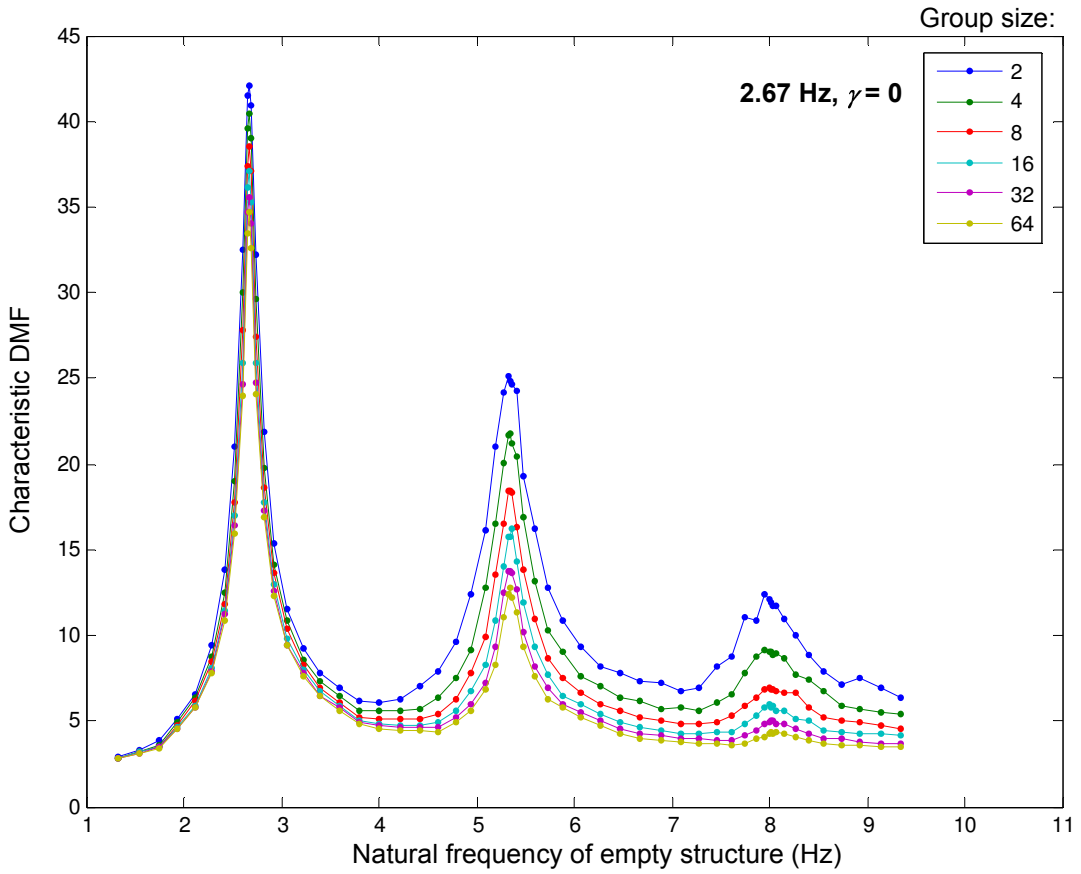

Figure 6.14: Variation of characteristic DMF with natural frequency of empty structure and group size for jumping loads at 2.67 Hz and $\gamma = 0$.

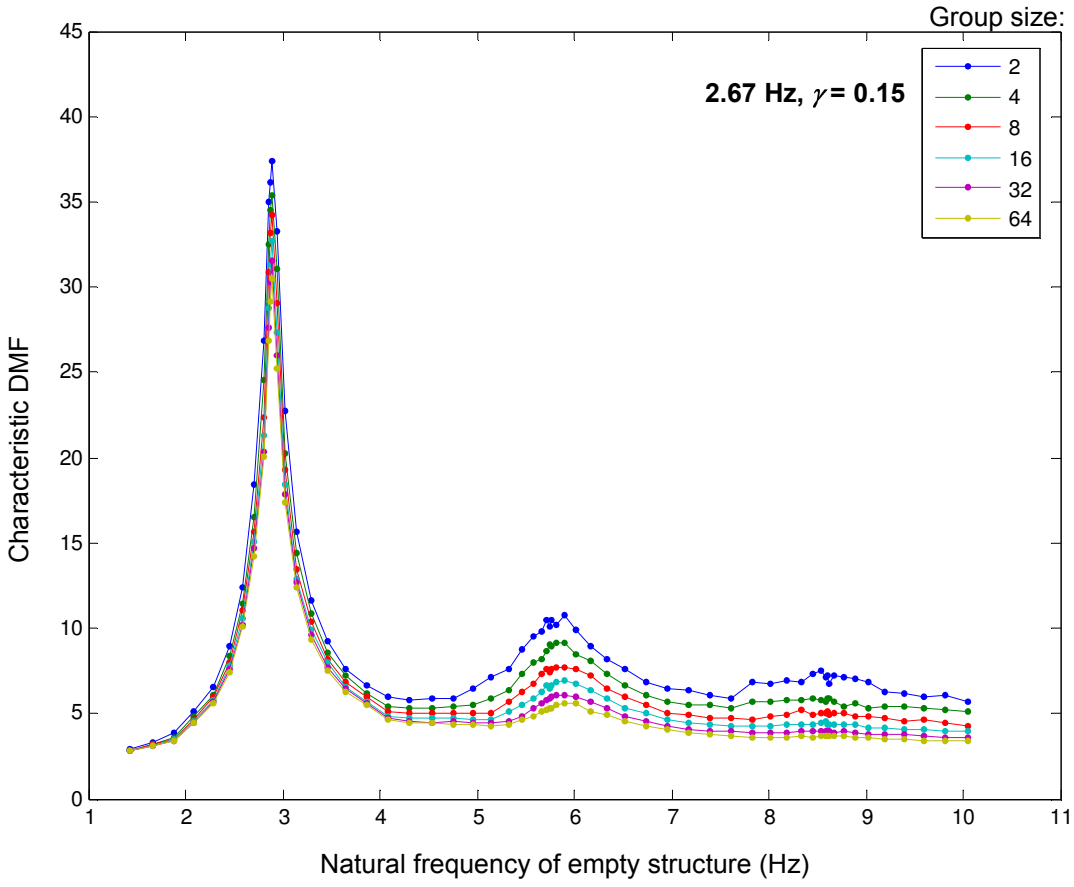

Figure 6.15: Variation of characteristic DMF with natural frequency of empty structure and group size for jumping loads at 2.67 Hz and $\gamma = 0.15$.

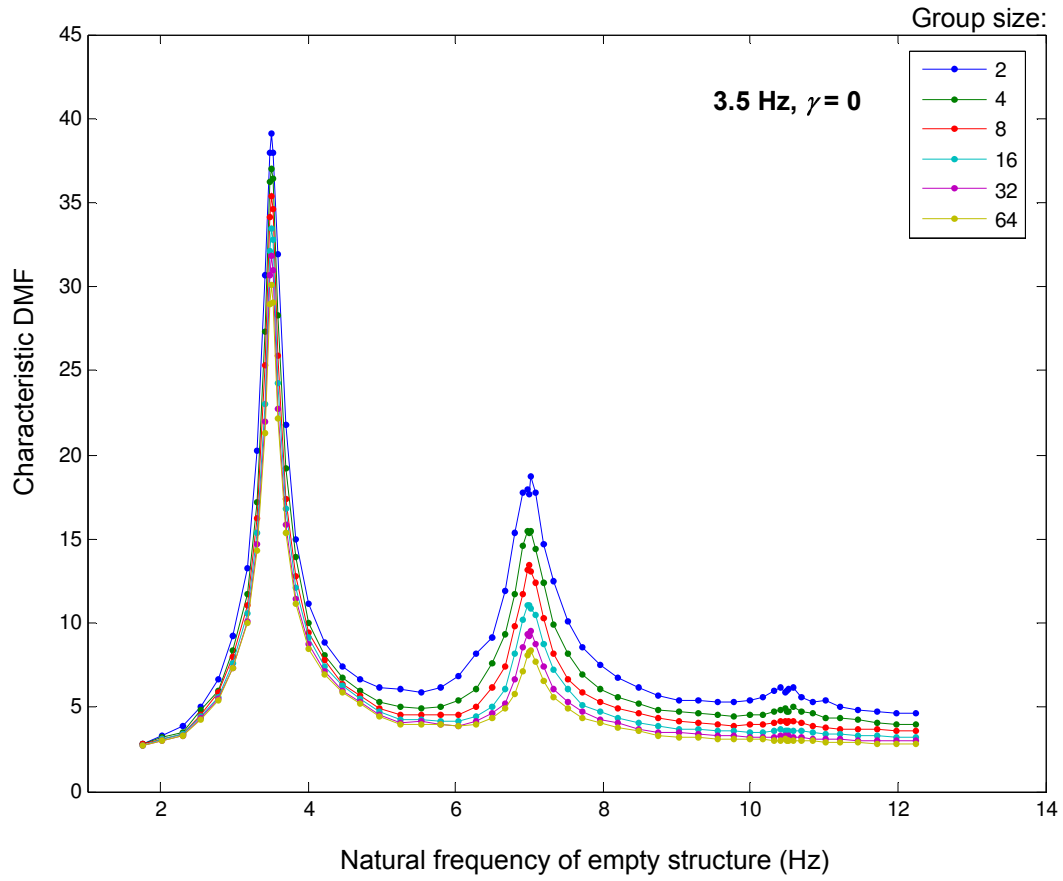

Figure 6.16: Variation of characteristic DMF with natural frequency of empty structure and group size for jumping loads at 3.5 Hz and $\gamma = 0$.

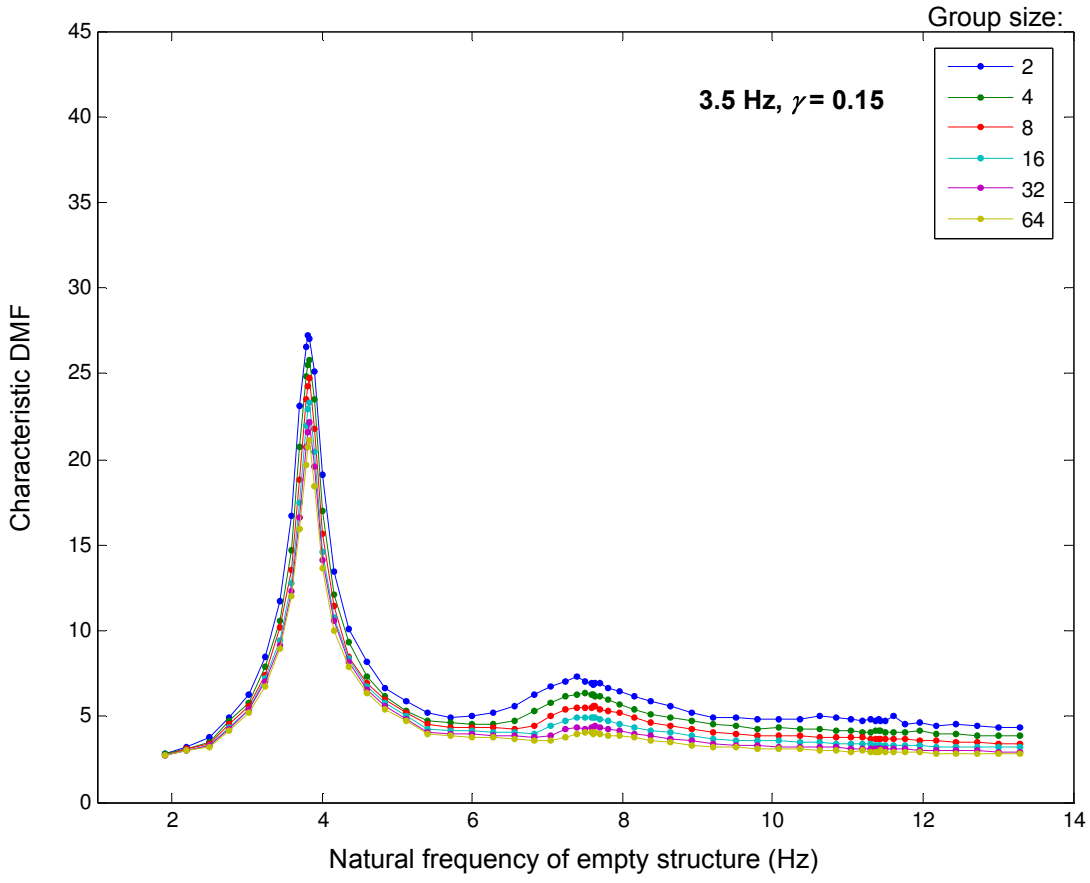

Figure 6.17: Variation of characteristic DMF with natural frequency of empty structure and group size for jumping loads at 3.5 Hz and $\gamma = 0.15$.

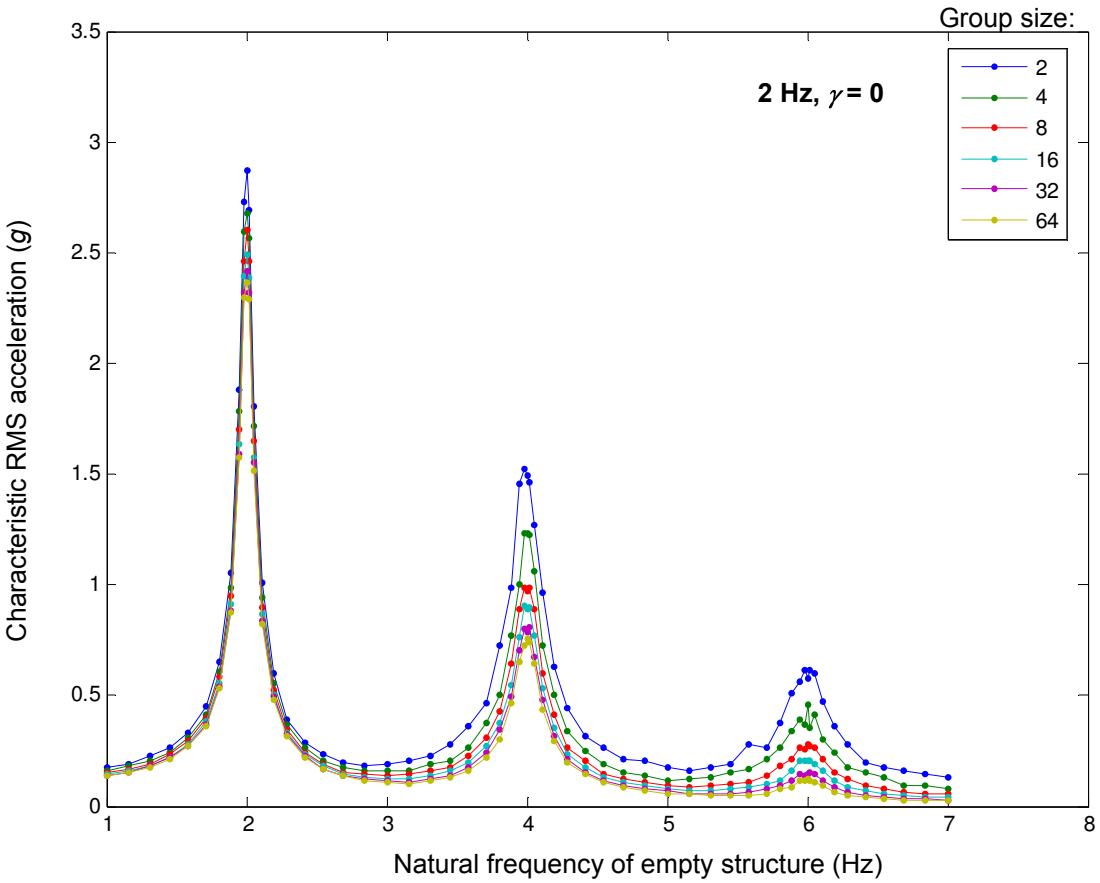

Figure 6.18: Variation of characteristic RMS acceleration with natural frequency of empty structure and group size for jumping loads at 2 Hz and $\gamma = 0$.

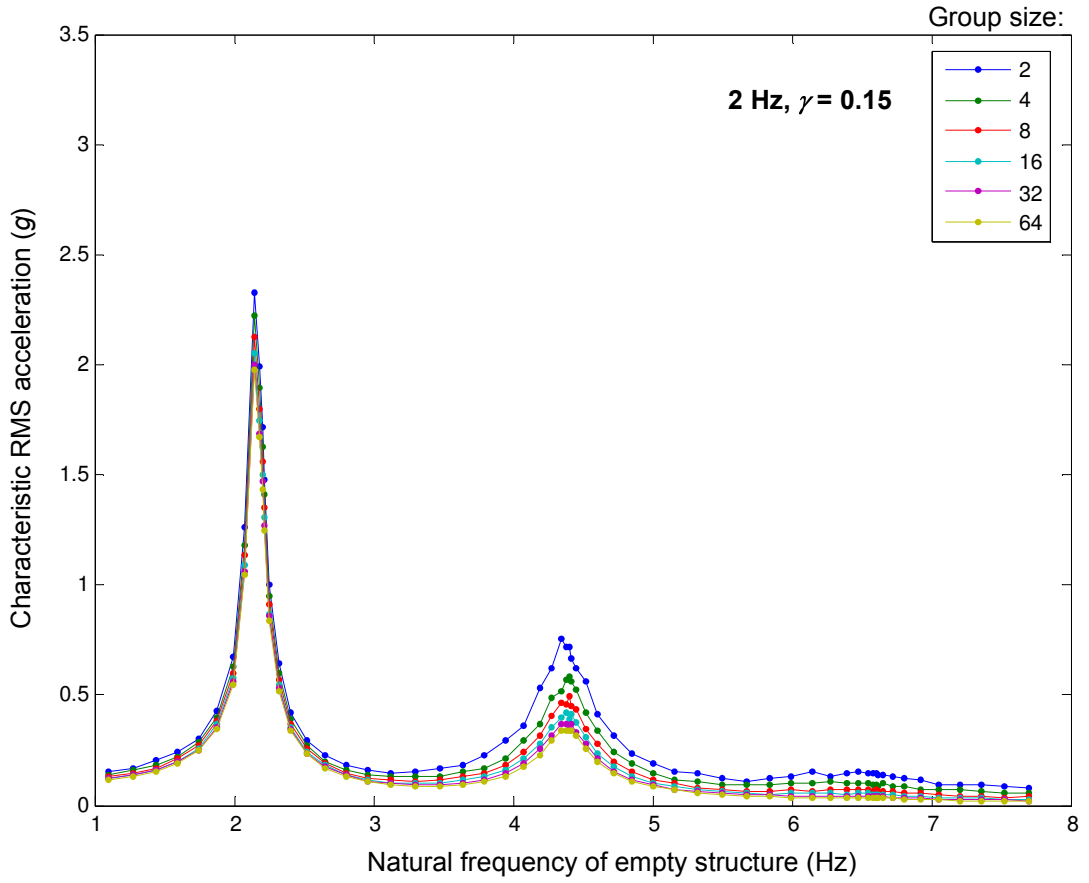

Figure 6.19: Variation of characteristic RMS acceleration with natural frequency of empty structure and group size for jumping loads at 2 Hz and $\gamma = 0.15$.

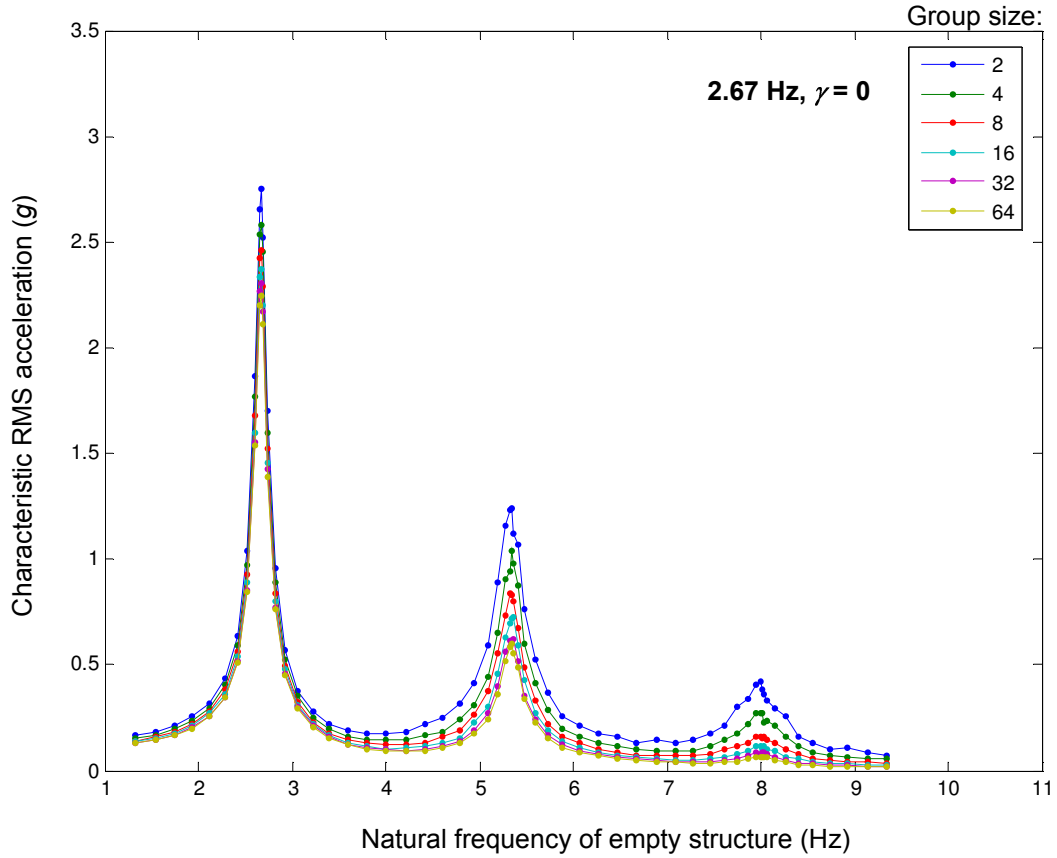

Figure 6.20: Variation of characteristic RMS acceleration with natural frequency of empty structure and group size for jumping loads at 2.67 Hz and $\gamma = 0$.

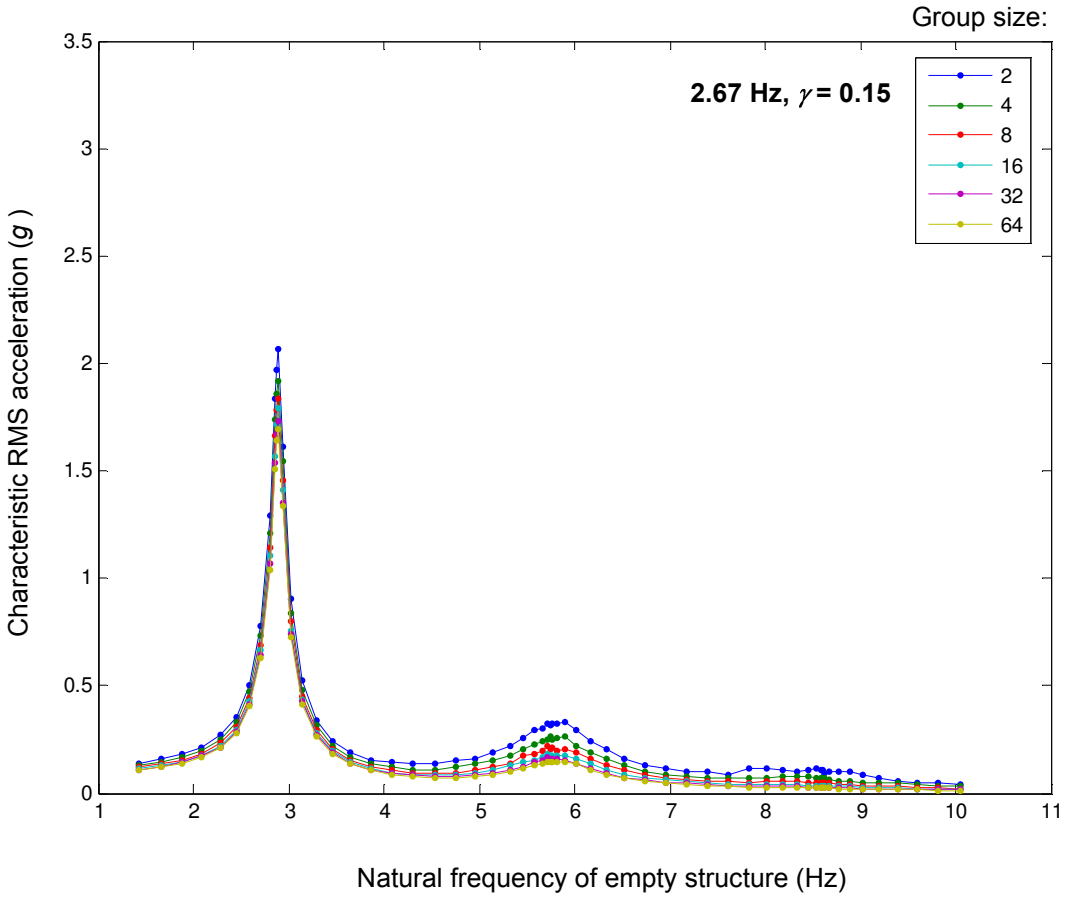

Figure 6.21: Variation of characteristic RMS acceleration with natural frequency of empty structure and group size for jumping loads at 2.67 Hz and $\gamma = 0.15$.

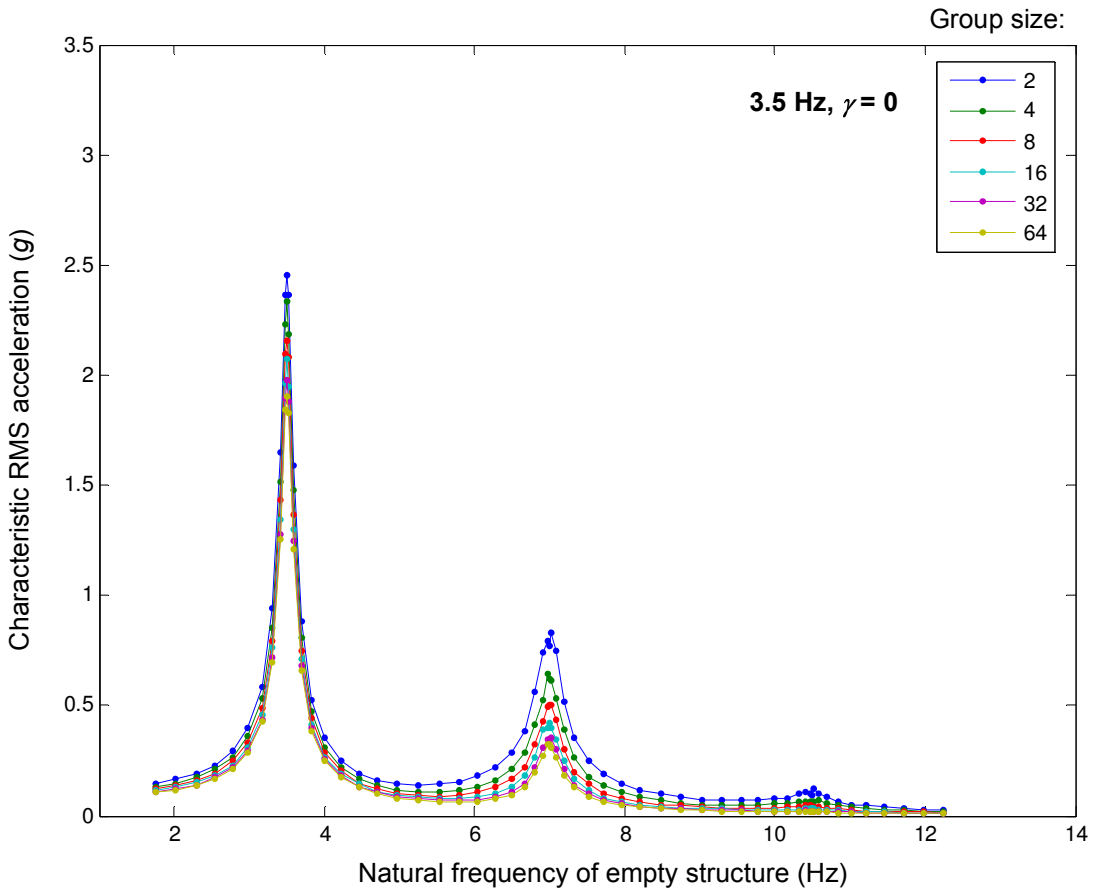

Figure 6.22: Variation of characteristic RMS acceleration with natural frequency of empty structure and group size for jumping loads at 3.5 Hz and $\gamma = 0$.

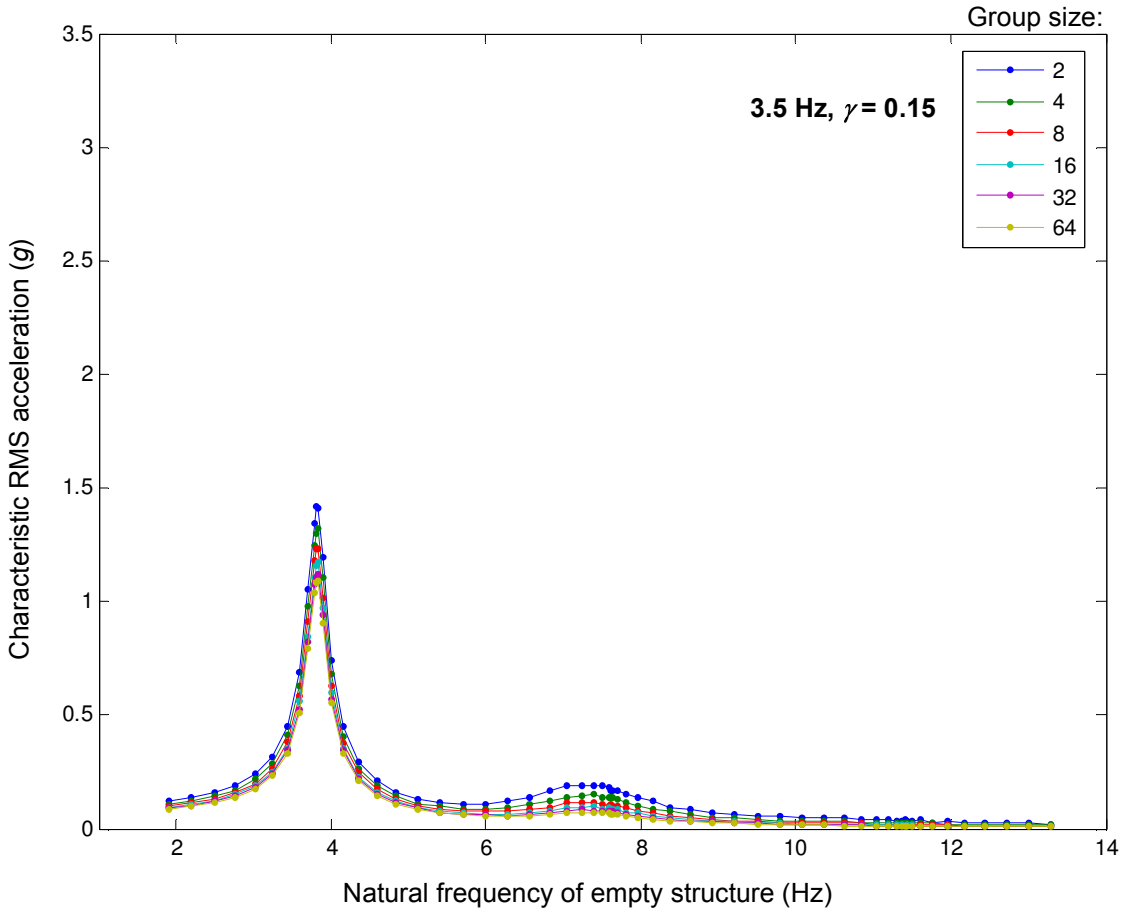

Figure 6.23: Variation of characteristic RMS acceleration with natural frequency of empty structure and group size for jumping loads at 3.5 Hz and $\gamma = 0.15$.

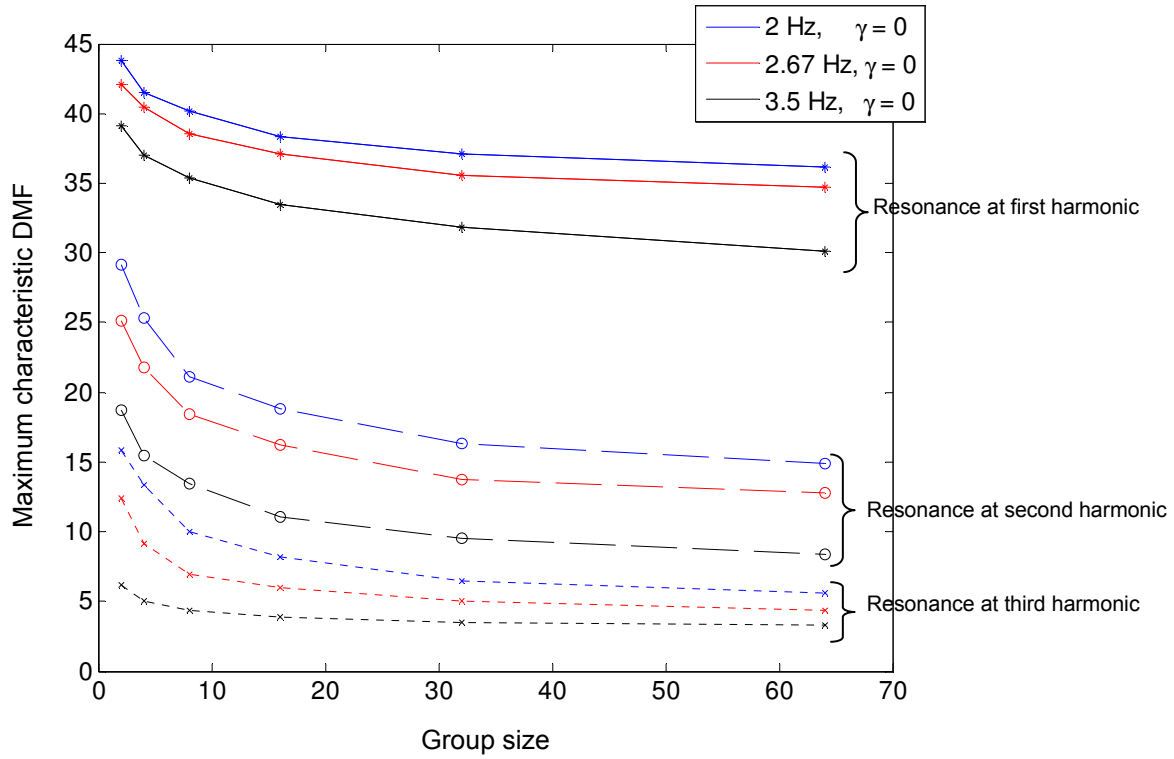

Figure 6.24: Variation of maximum characteristic DMF with group size for resonance at first three harmonics and $\gamma = 0$.

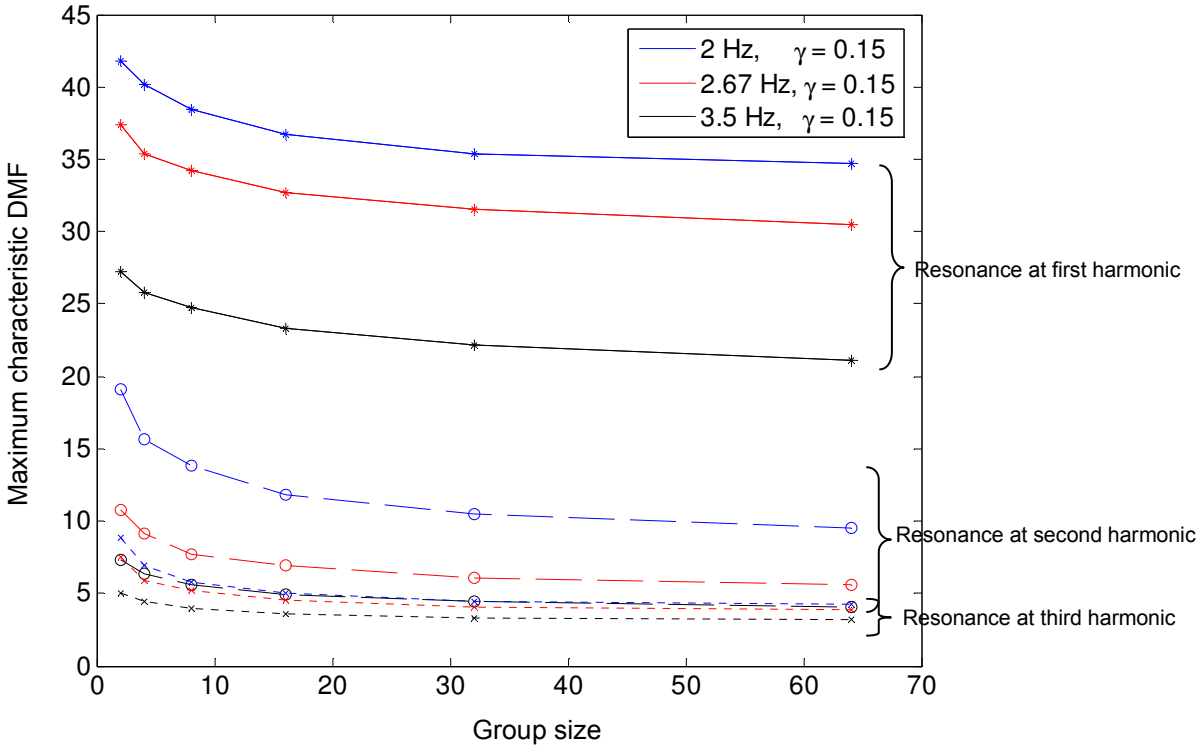

Figure 6.25: Variation of maximum characteristic DMF with group size for resonance at first three harmonics and $\gamma = 0.15$.

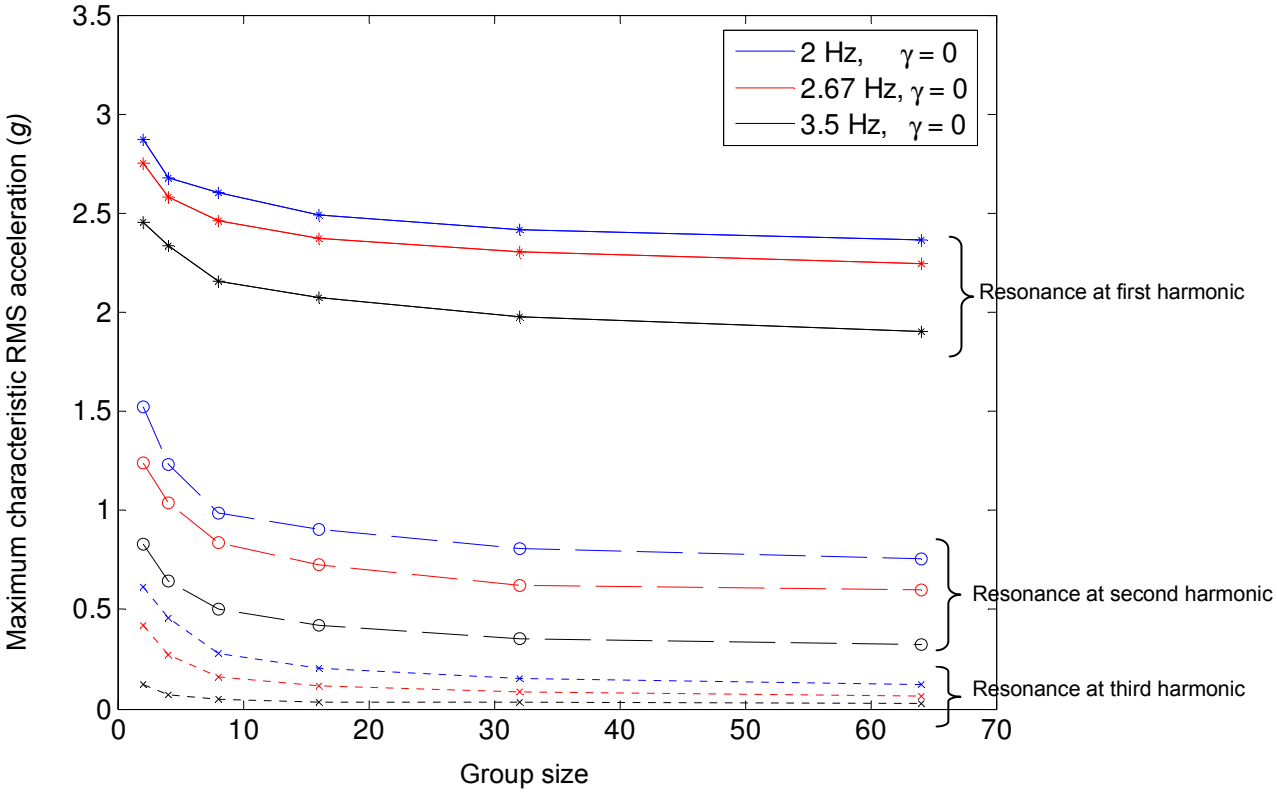

Figure 6.26: Variation of maximum characteristic RMS acceleration with group size for resonance at first three harmonics and $\gamma = 0$.

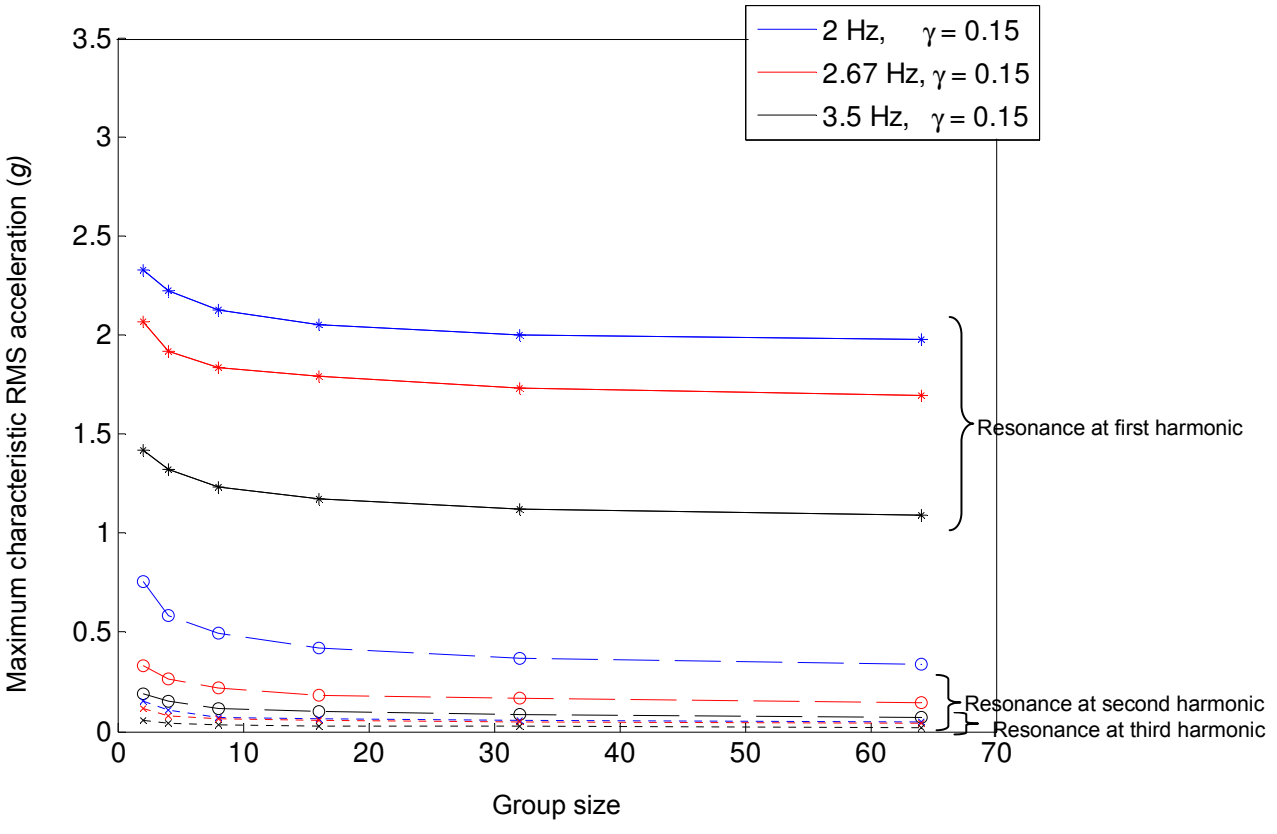

Figure 6.27: Variation of maximum characteristic RMS acceleration with group size for resonance at first three harmonics and $\gamma = 0.15$.

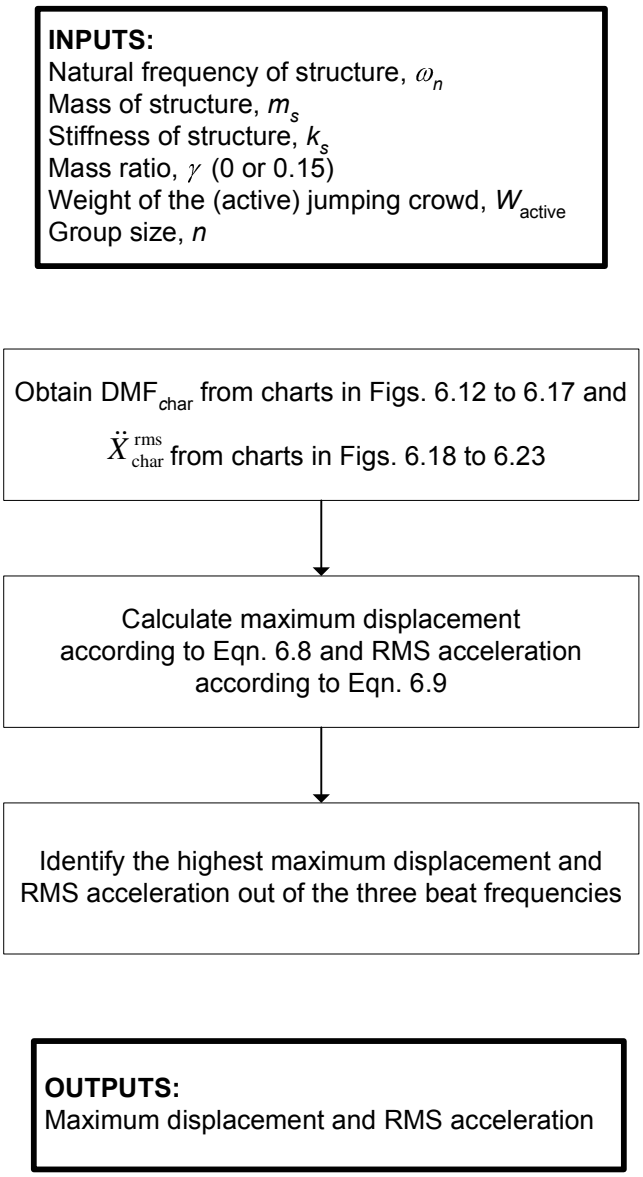

Figure 6.28: Flow chart for estimating the maximum displacement and RMS acceleration of a SDOF system with γ= 0 or 0.15 and ζ= 2%, using charts in Figs. 6.12 to 6.23.

Figure 7.1: Photo showing one test subject on the force platform.

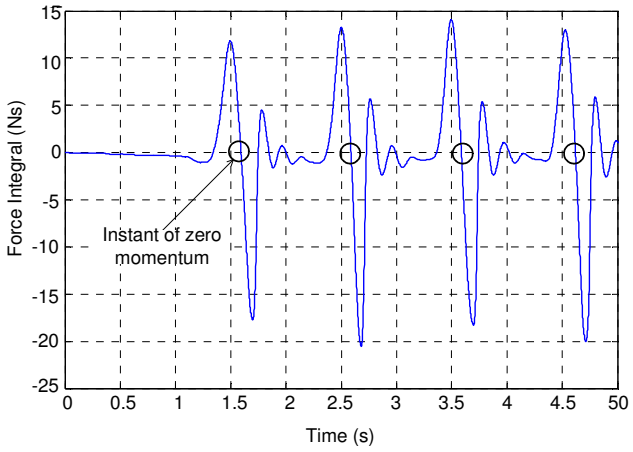

Figure 7.2: Separating individual bobbing impulses at instants of zero momentum.

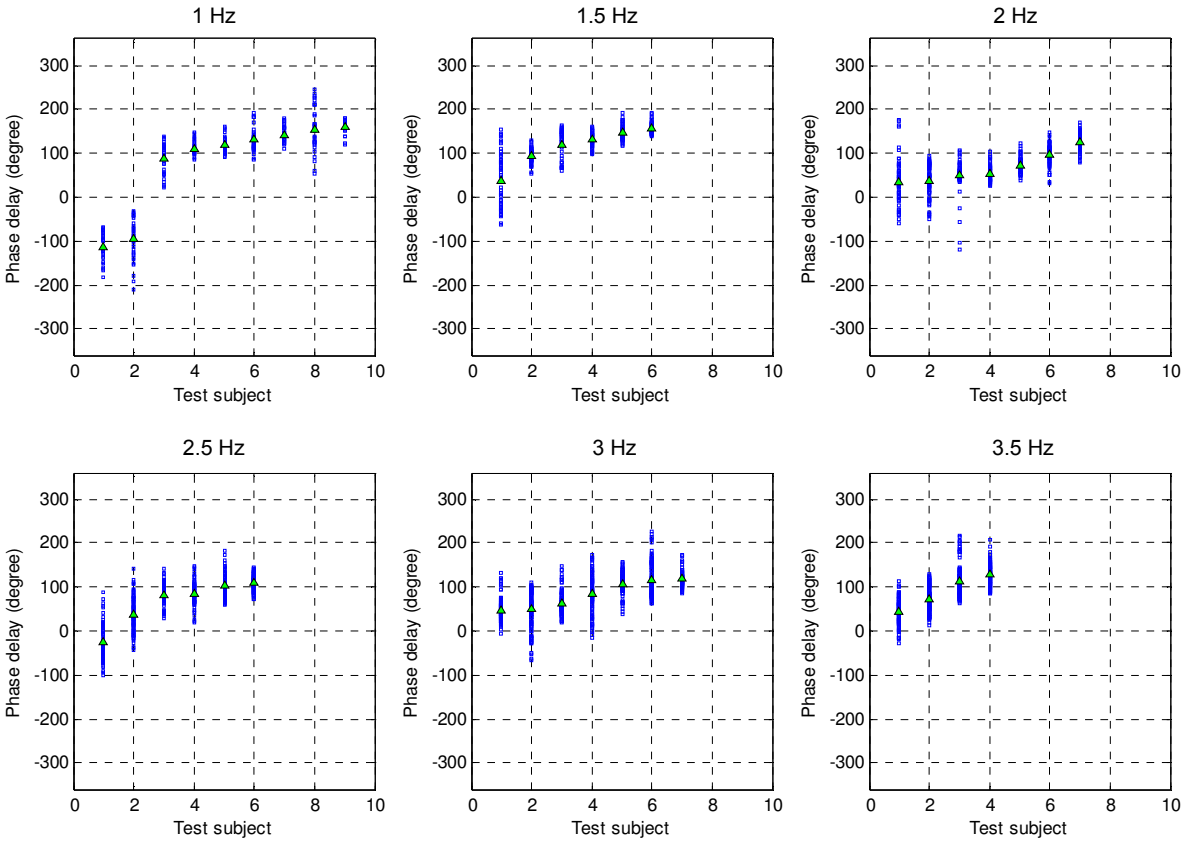

Figure 7.3: Phase delays for all synchronised jumps.

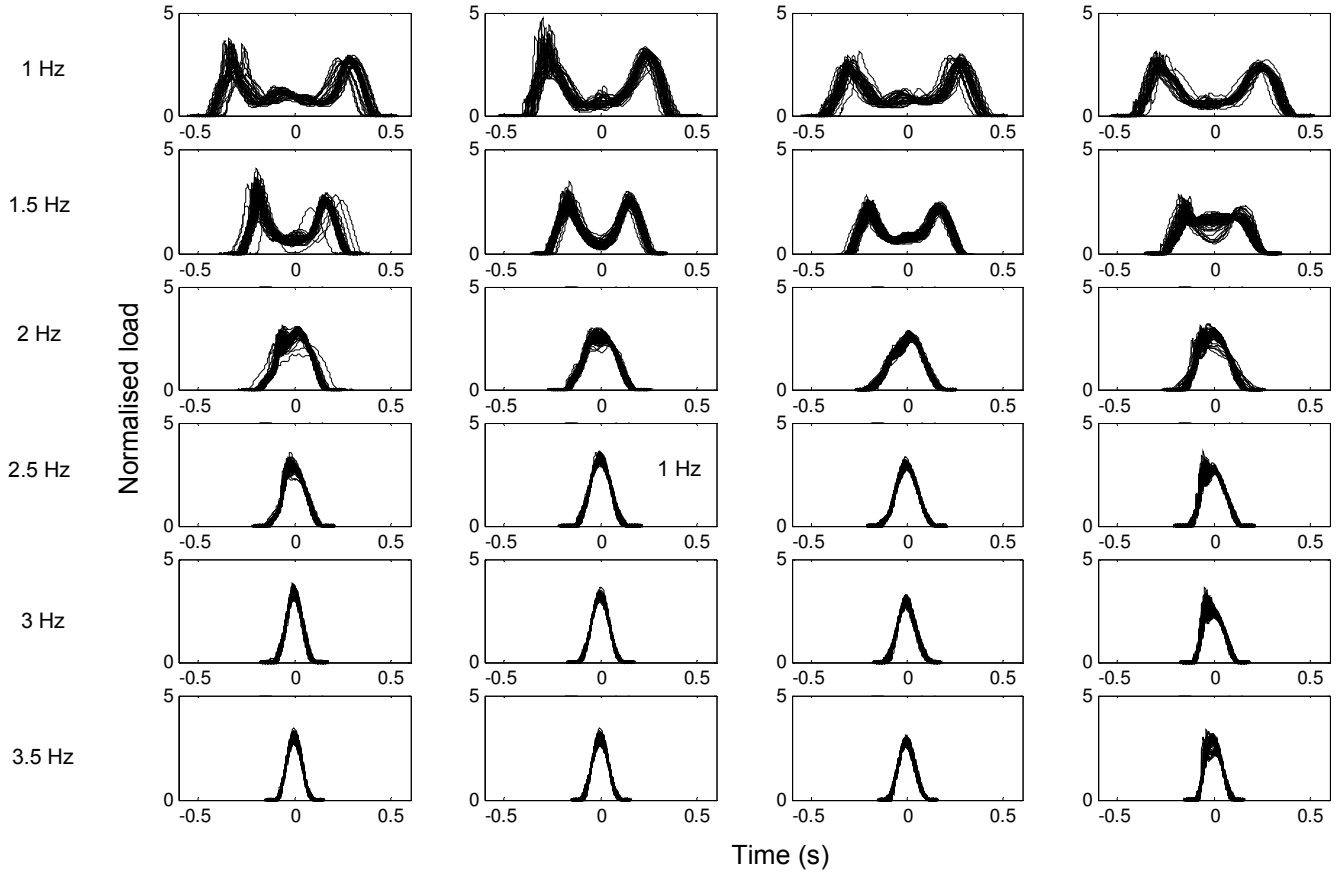

Figure 7.4: Jumping impulses for four subjects at six beat frequencies.

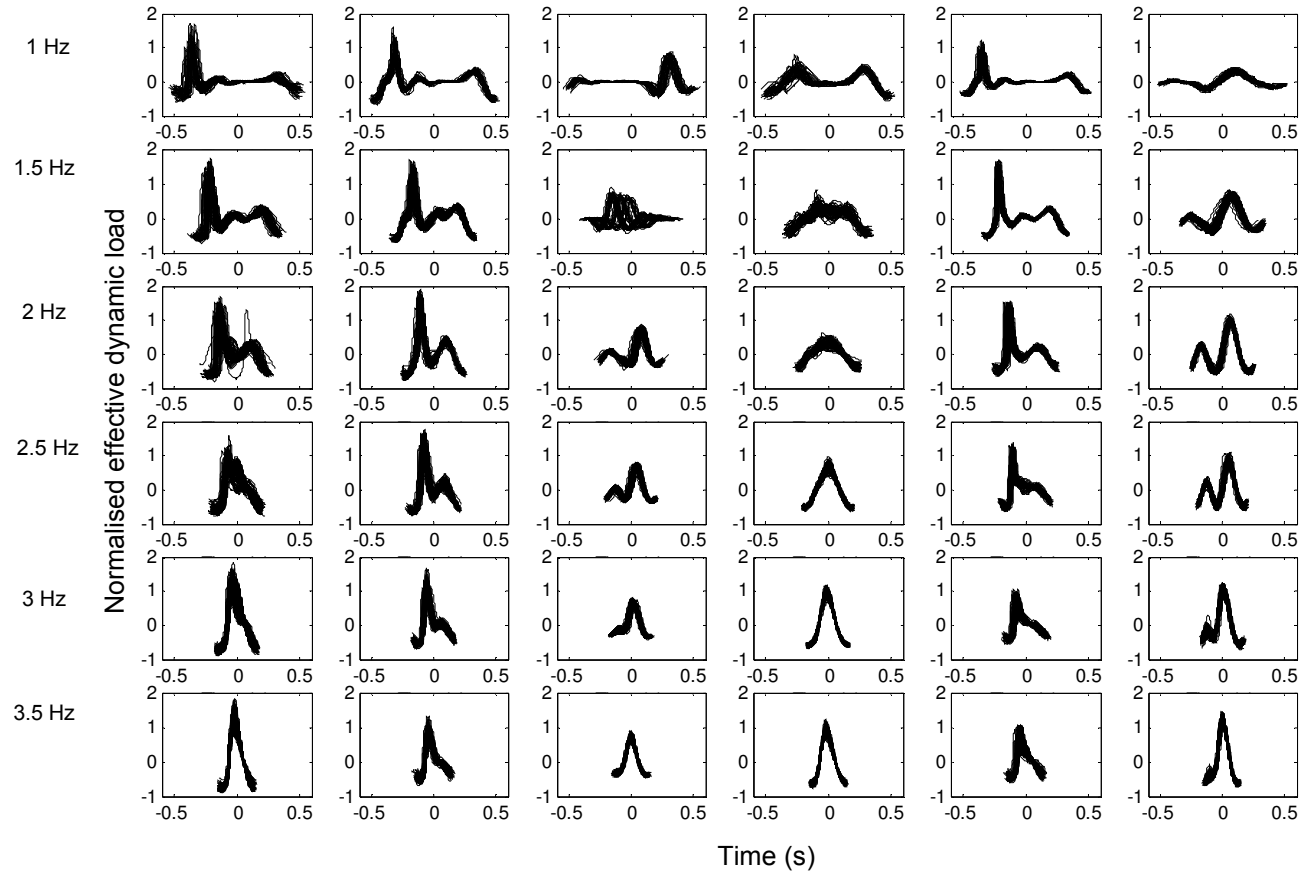

Figure 7.5: Bobbing impulses for six subjects at six beat frequencies.

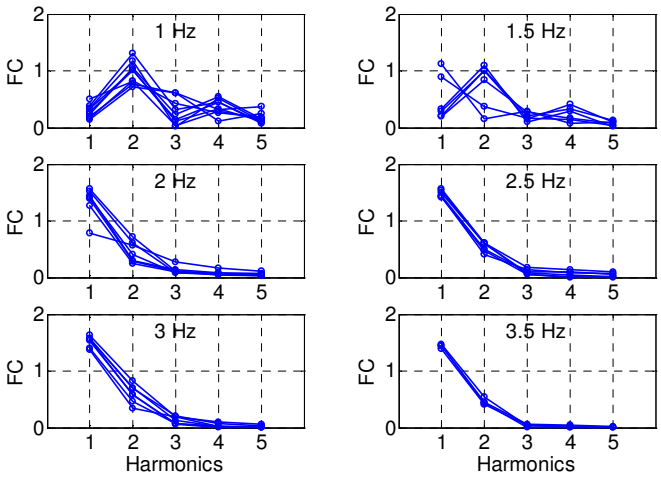

Figure 7.6: Fourier coefficients of average jumping impulse for six beat frequencies.

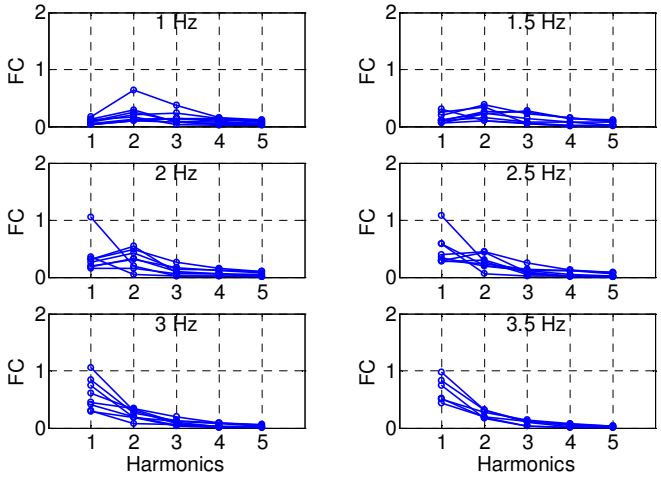

Figure 7.7: Fourier coefficients of average bobbing impulse for six beat frequencies.

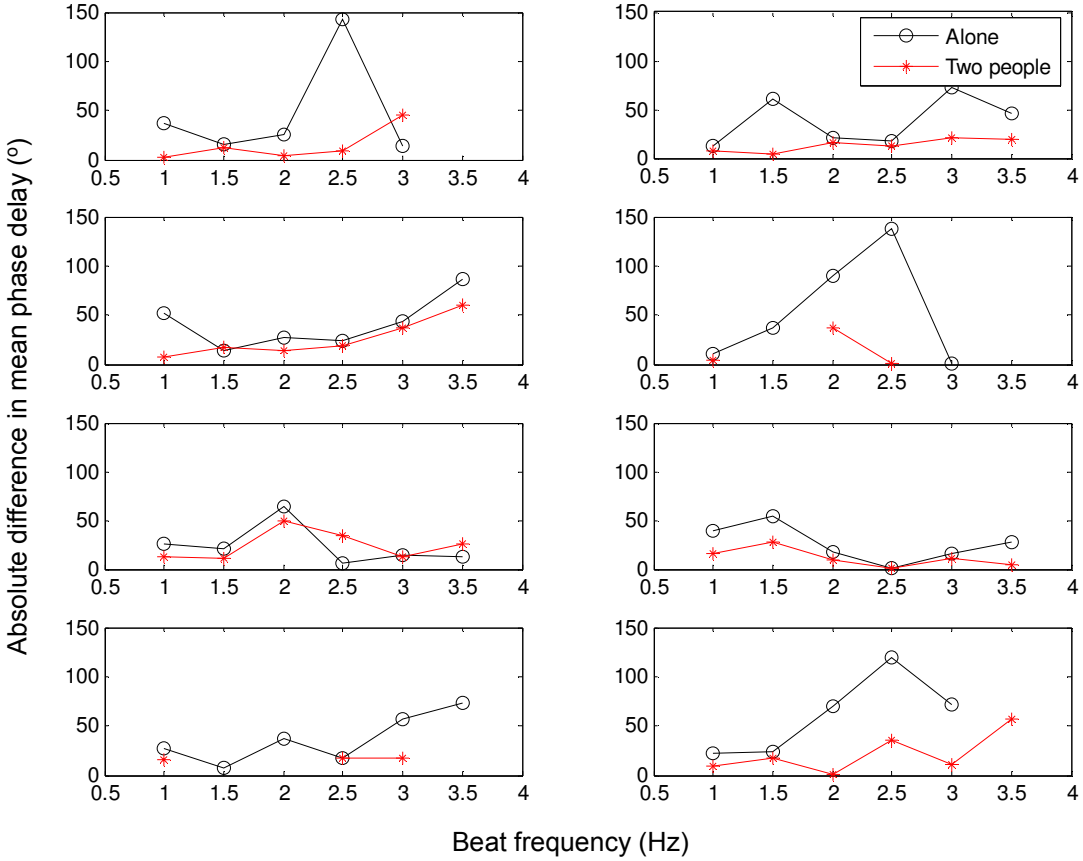

Figure 7.8: Absolute difference in mean phase delay for two subjects when jumping separately and together at six beat frequencies.

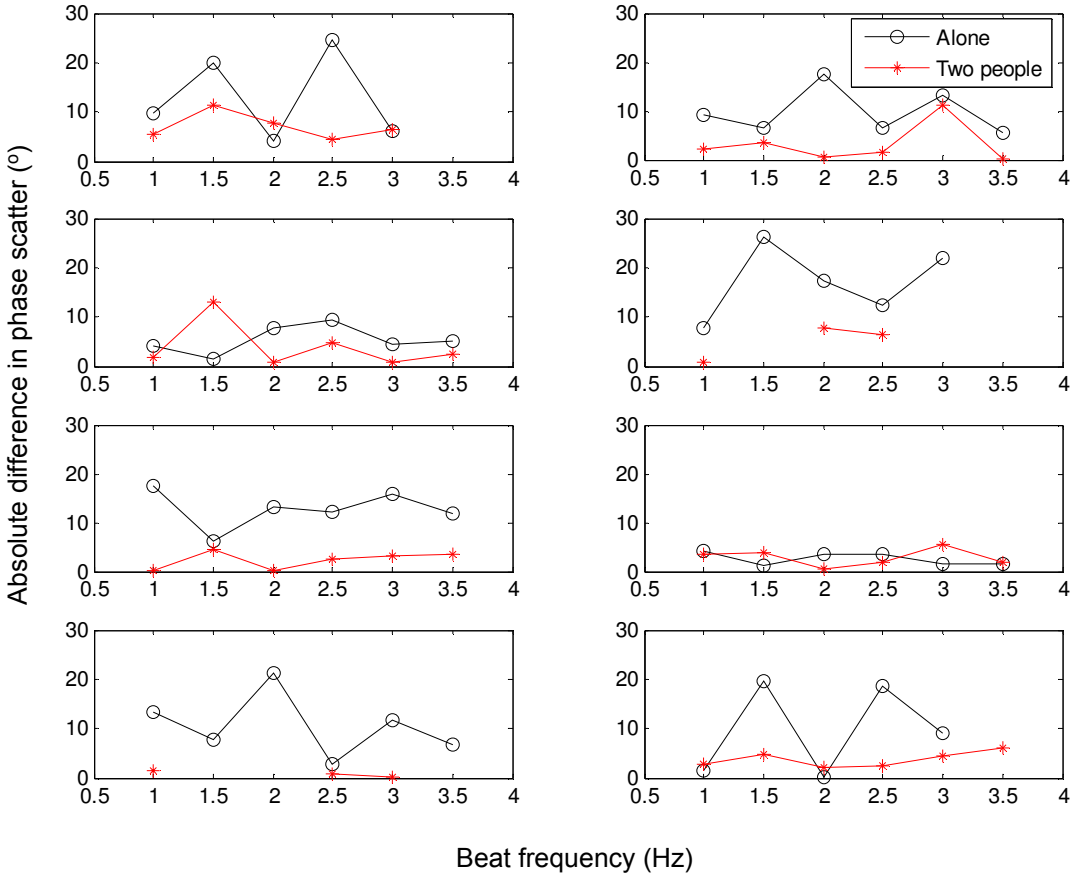

Figure 7.9: Absolute difference in phase scatter for two subjects when jumping separately and together at six beat frequencies.

APPENDIX C

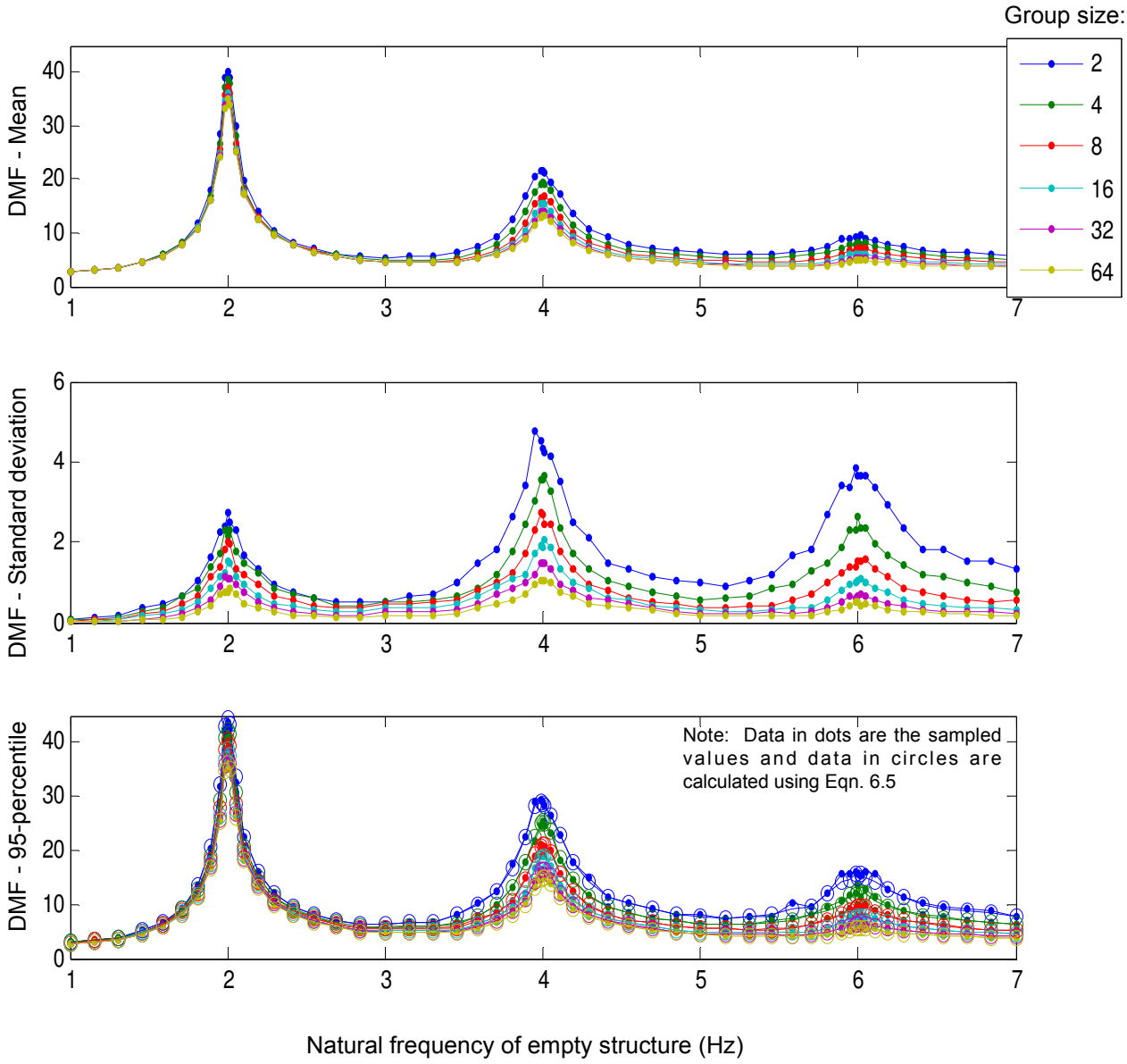

Figure C1: Variation of DMF (mean, standard deviation and 95-percentile value) with natural frequency of the structure and sample size for jumping loads at 2 Hz and $\gamma = 0$.

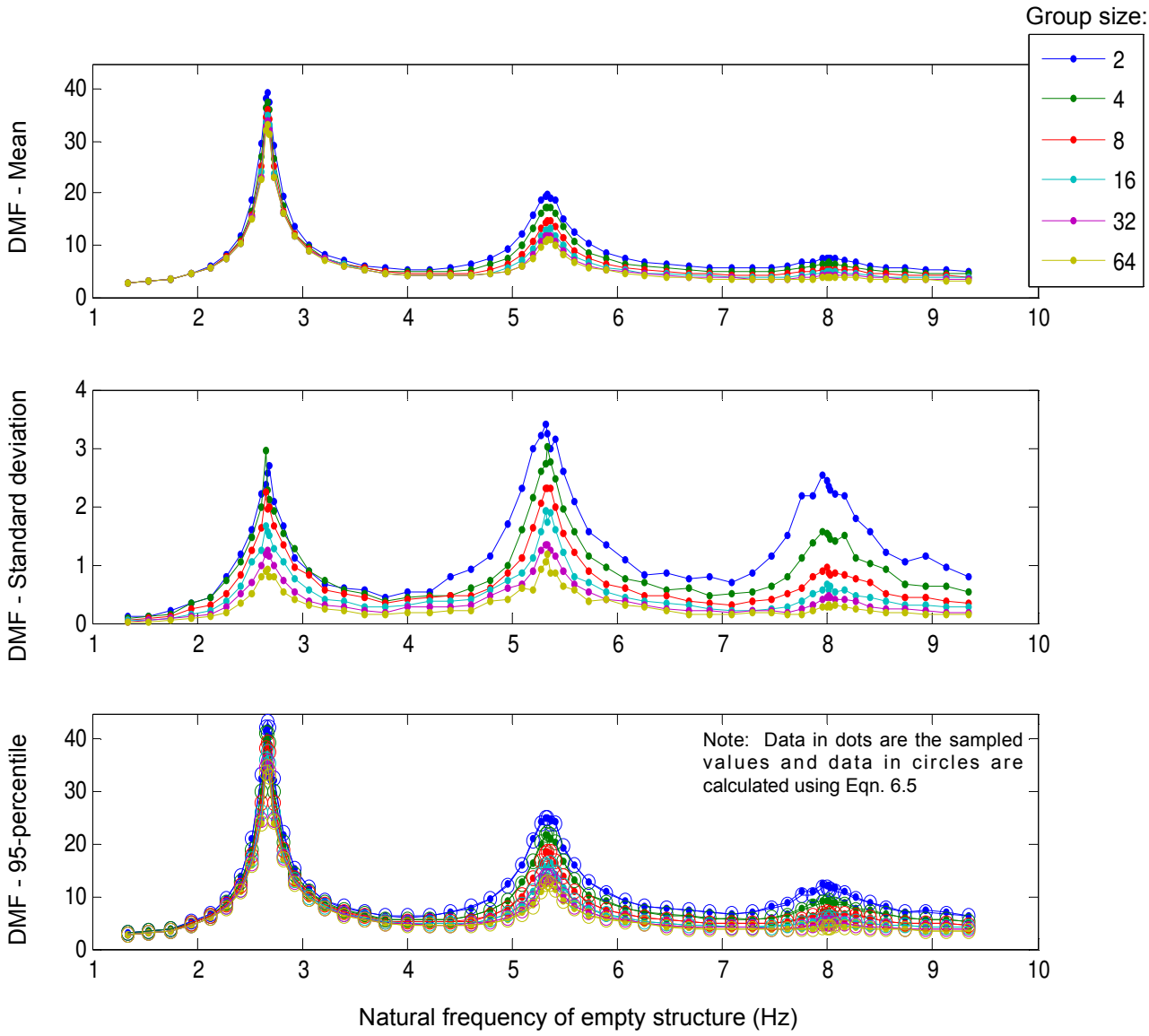

Figure C2: Variation of DMF (mean, standard deviation and 95-percentile value) with natural frequency of the structure and sample size for jumping loads at 2.67 Hz and $\gamma = 0$.

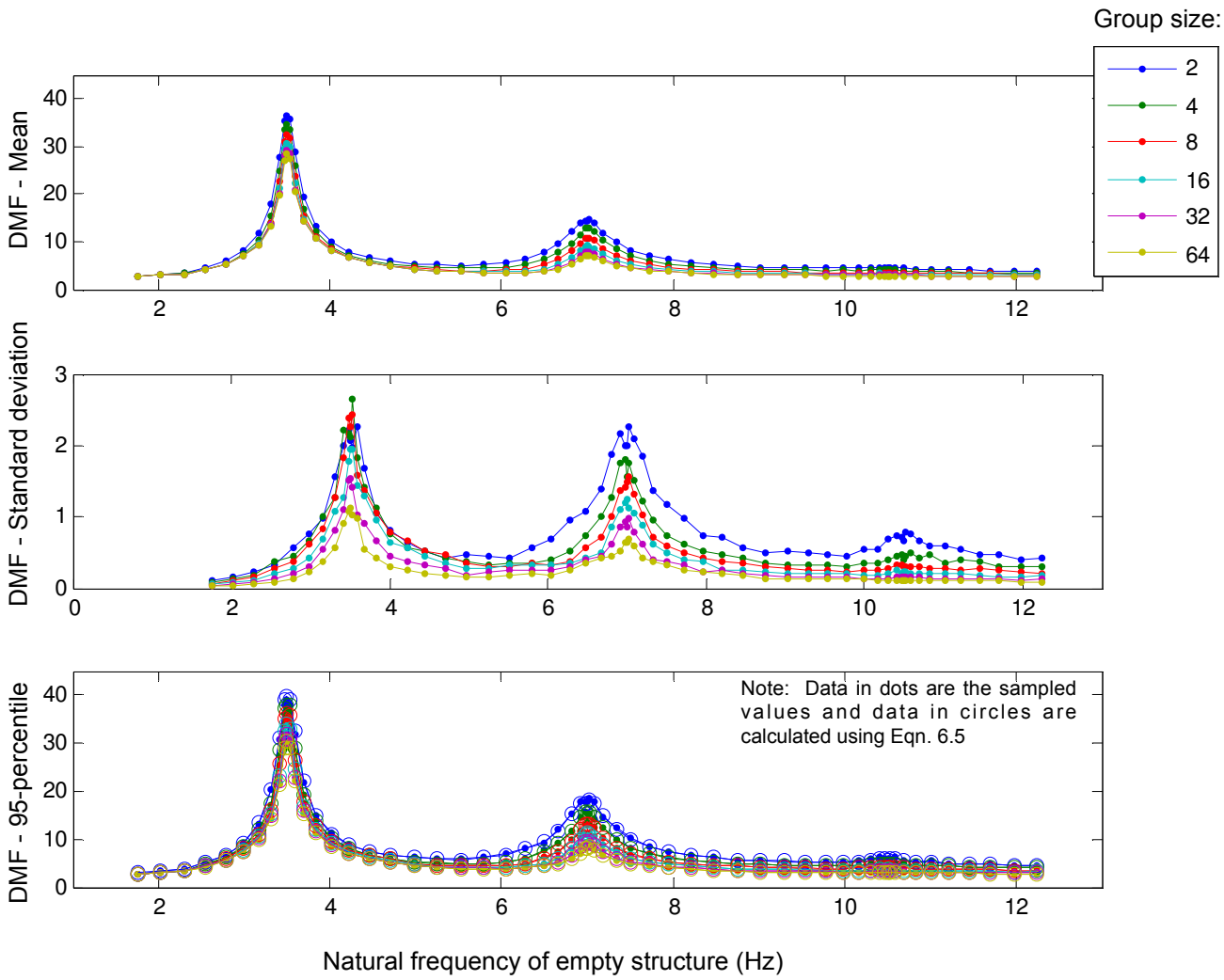

Figure C3: Variation of DMF (mean, standard deviation and 95-percentile value) with natural frequency of the structure and sample size for jumping loads at 3.5 Hz and $\gamma = 0$.

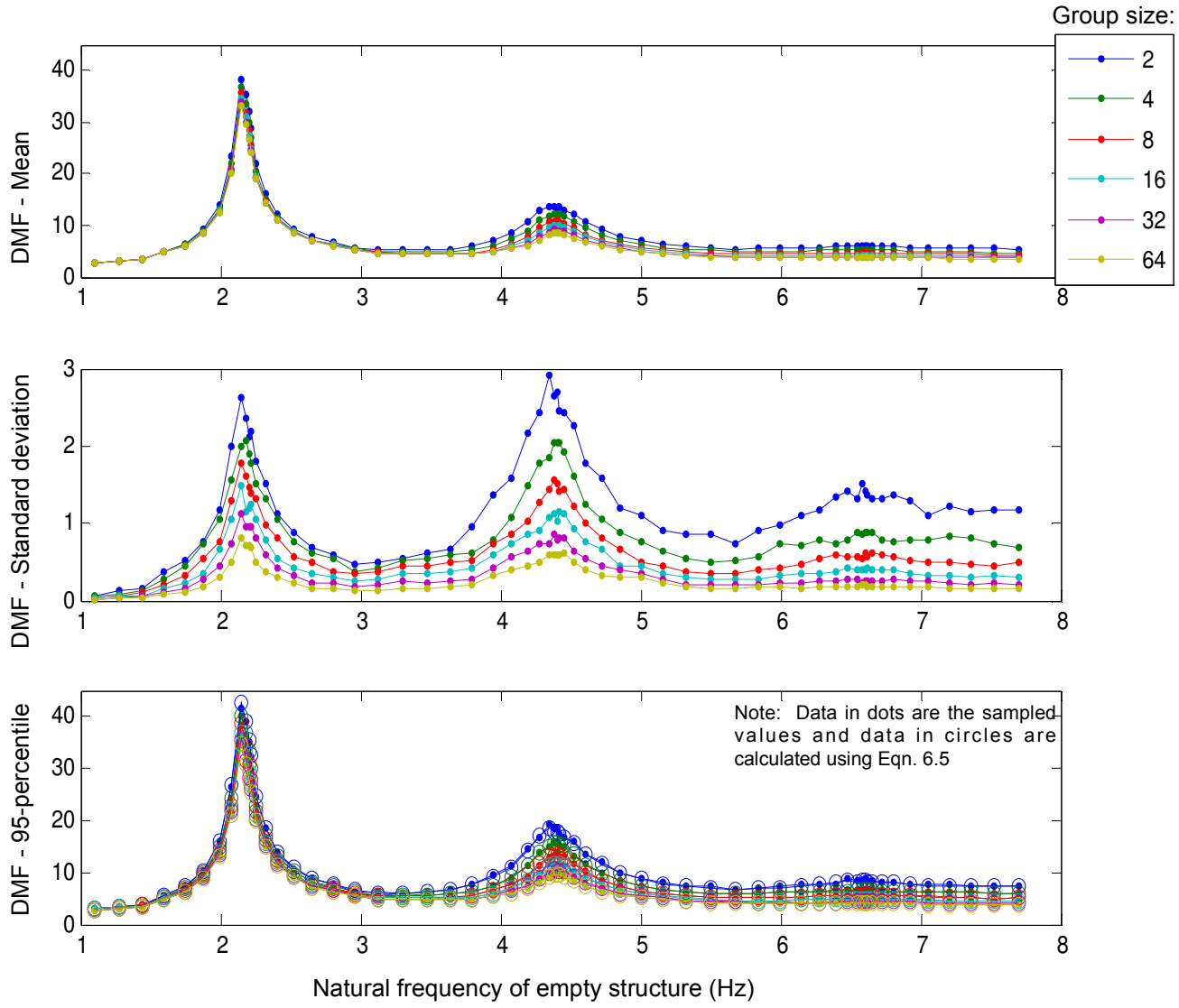

Figure C4: Variation of DMF (mean, standard deviation and 95-percentile value) with natural frequency of the structure and sample size for jumping loads at 2 Hz and $\gamma = 0.15$.

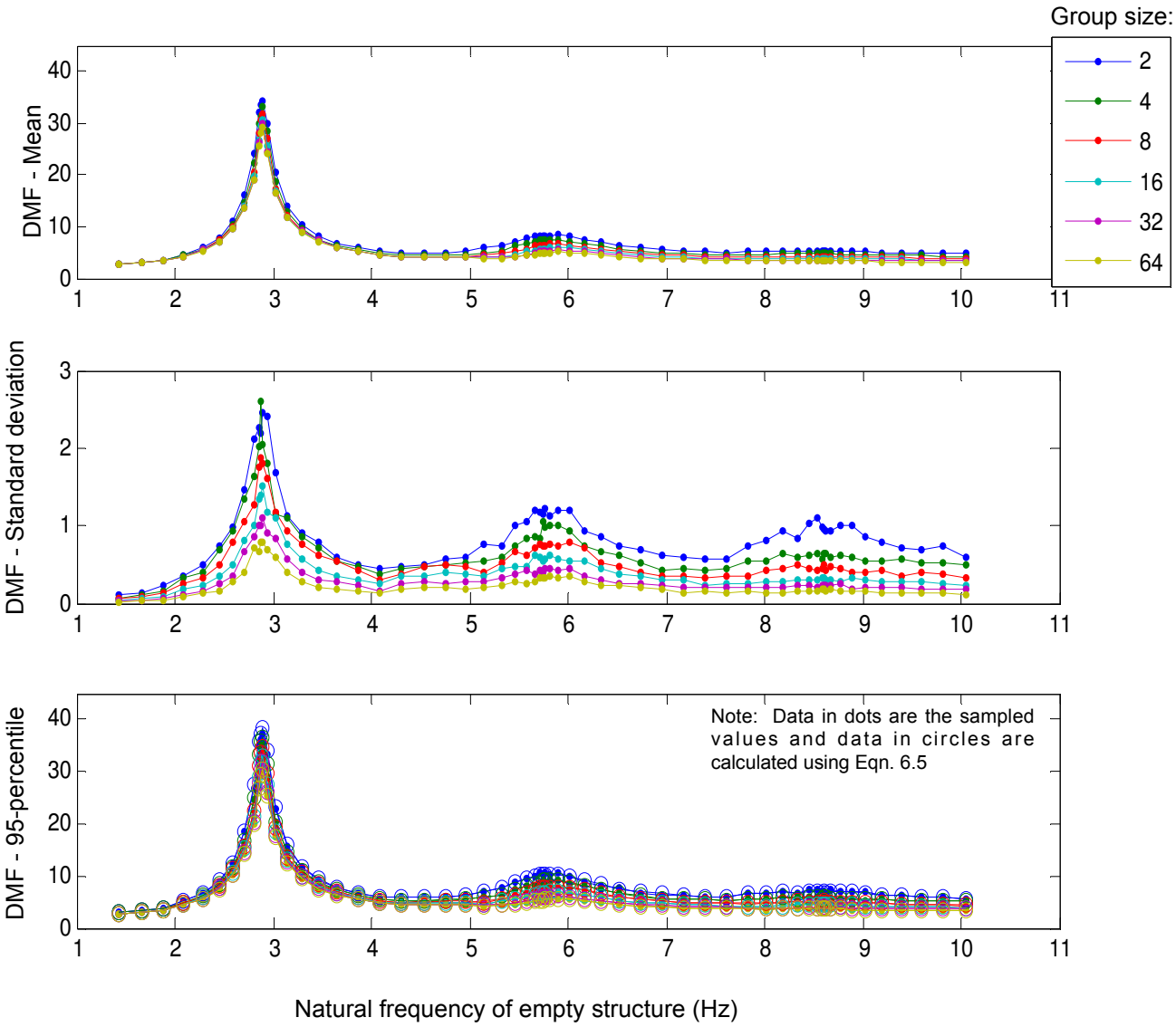

Figure C5: Variation of DMF (mean, standard deviation and 95-percentile value) with natural frequency of the structure and sample size for jumping loads at 2.67 Hz and $\gamma = 0.15$.

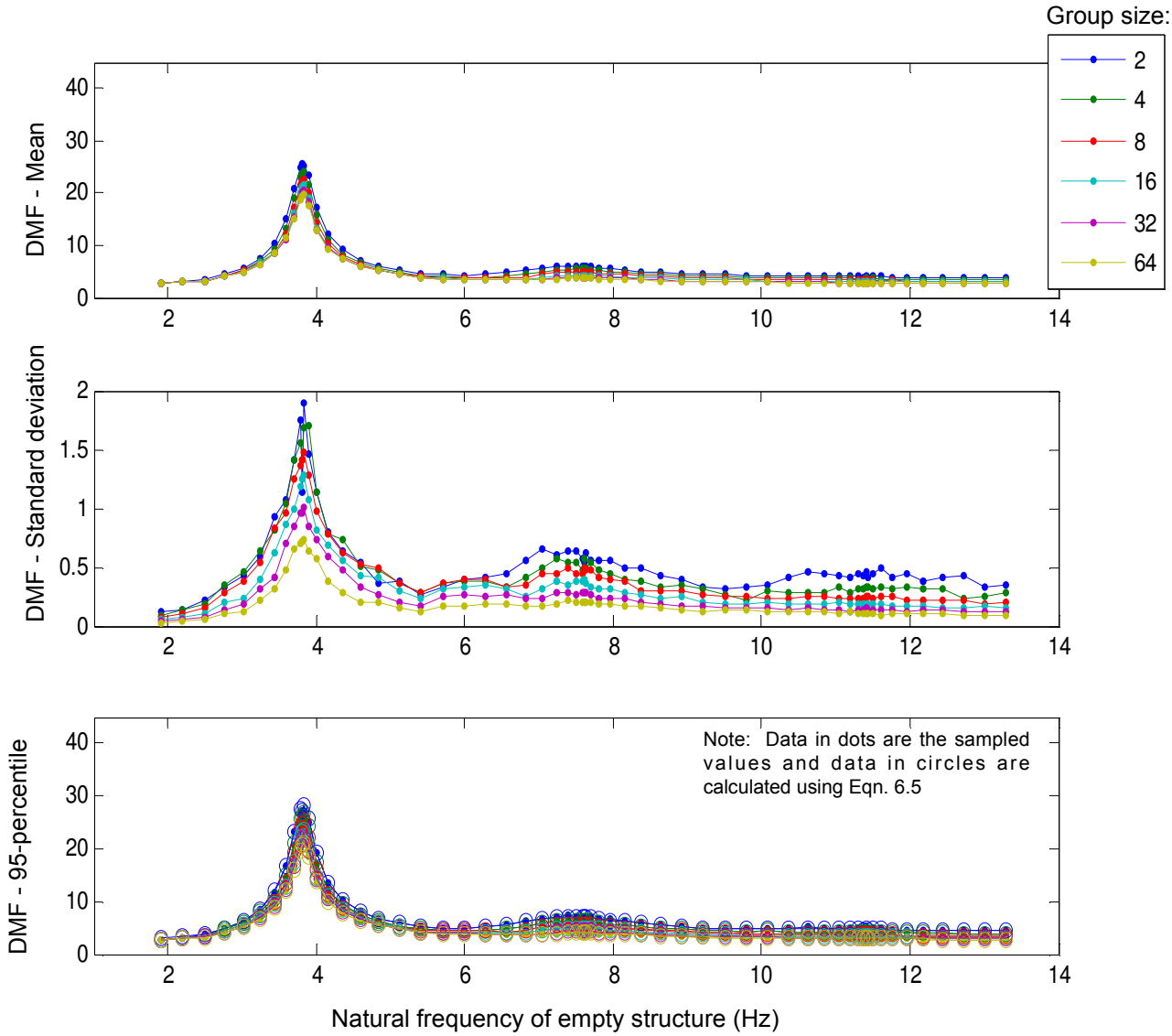

Figure C6: Variation of DMF (mean, standard deviation and 95-percentile value) with natural frequency of the structure and sample size for jumping loads at 3.5 Hz and $\gamma = 0.15$.

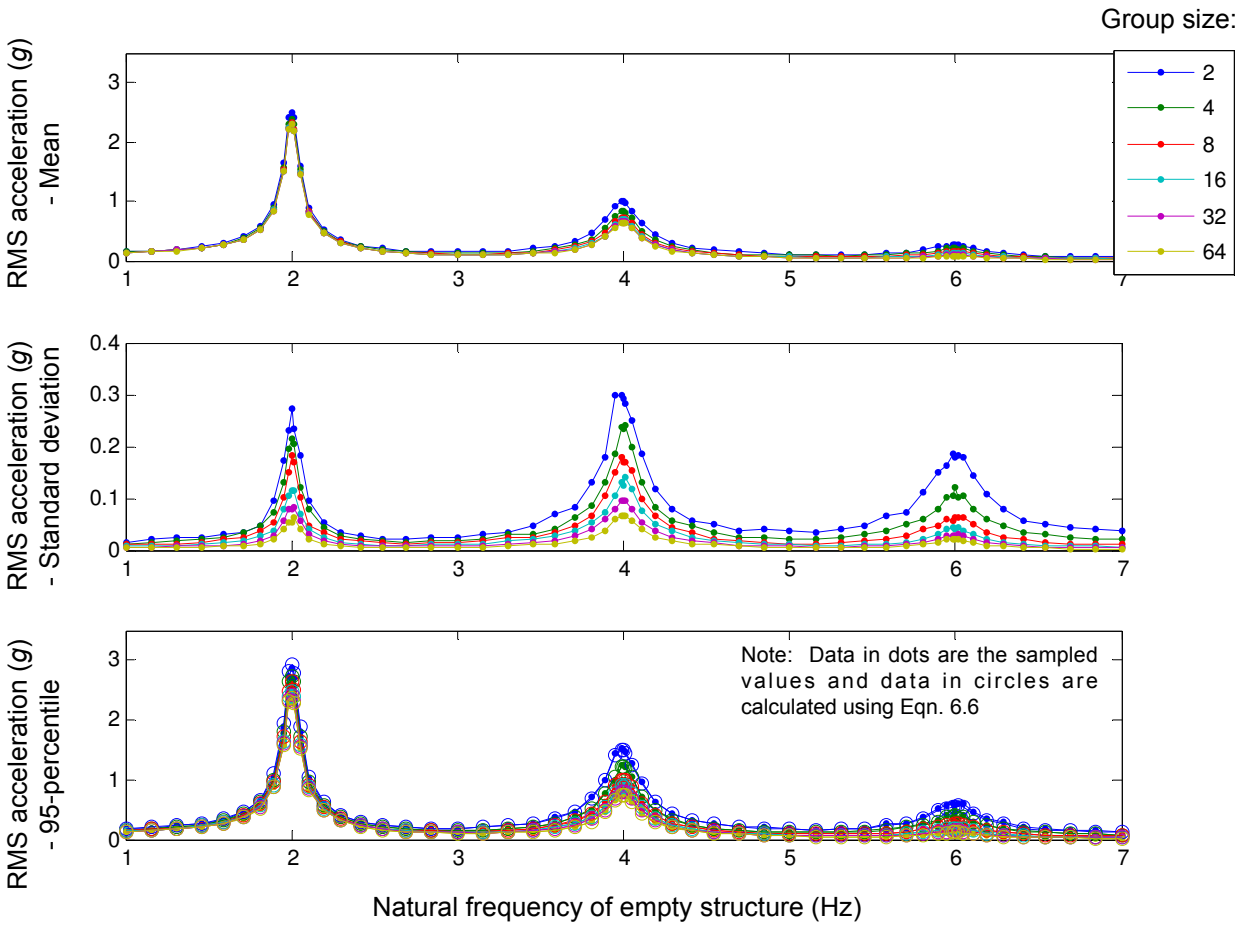

Figure C7: Variation of RMS acceleration (mean, standard deviation and 95-percentile value) with natural frequency of the structure and sample size for jumping loads at 2 Hz and $\gamma = 0$.

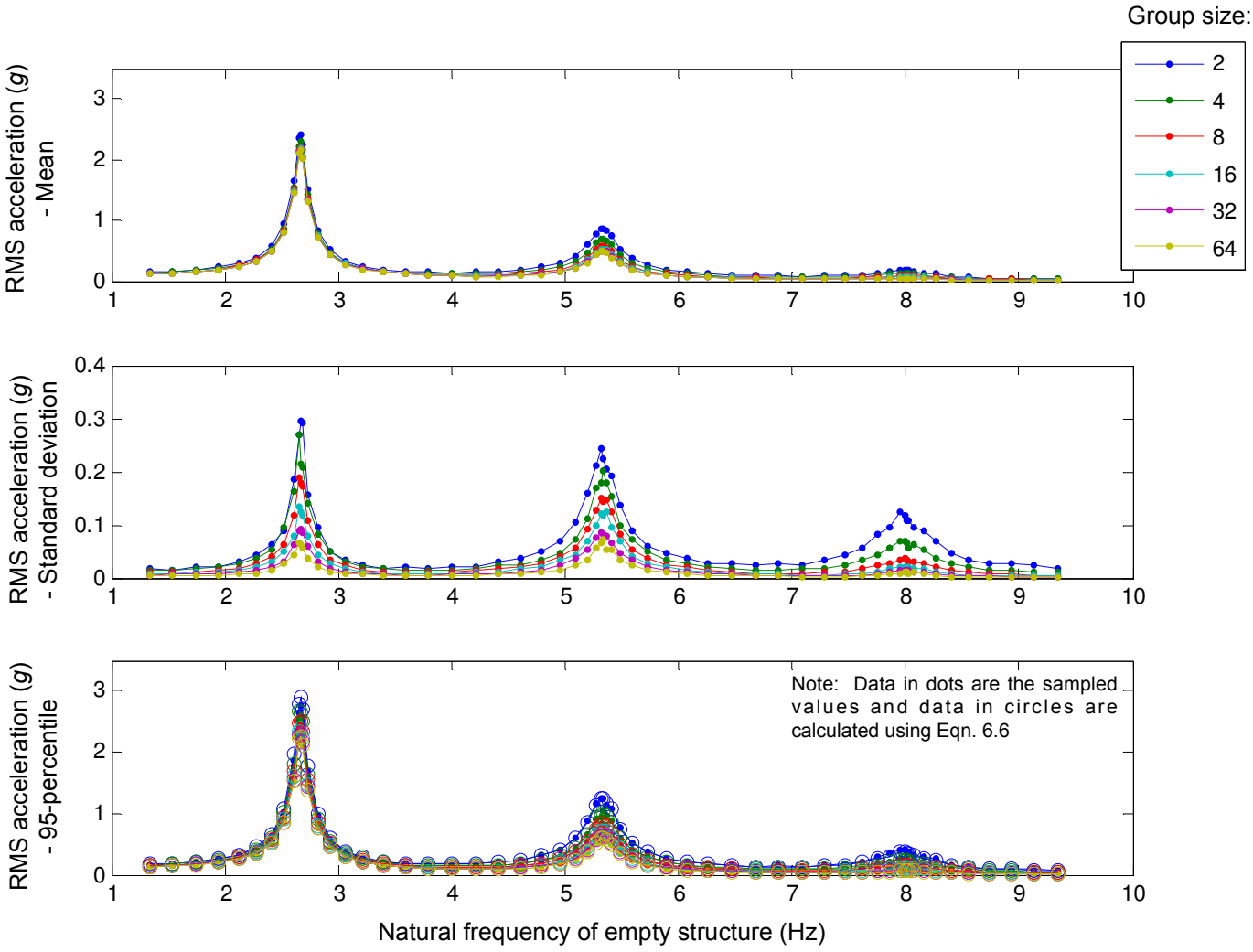

Figure C8: Variation of RMS acceleration (mean, standard deviation and 95-percentile value) with natural frequency of the structure and sample size for jumping loads at 2.67 Hz and $\gamma = 0$.

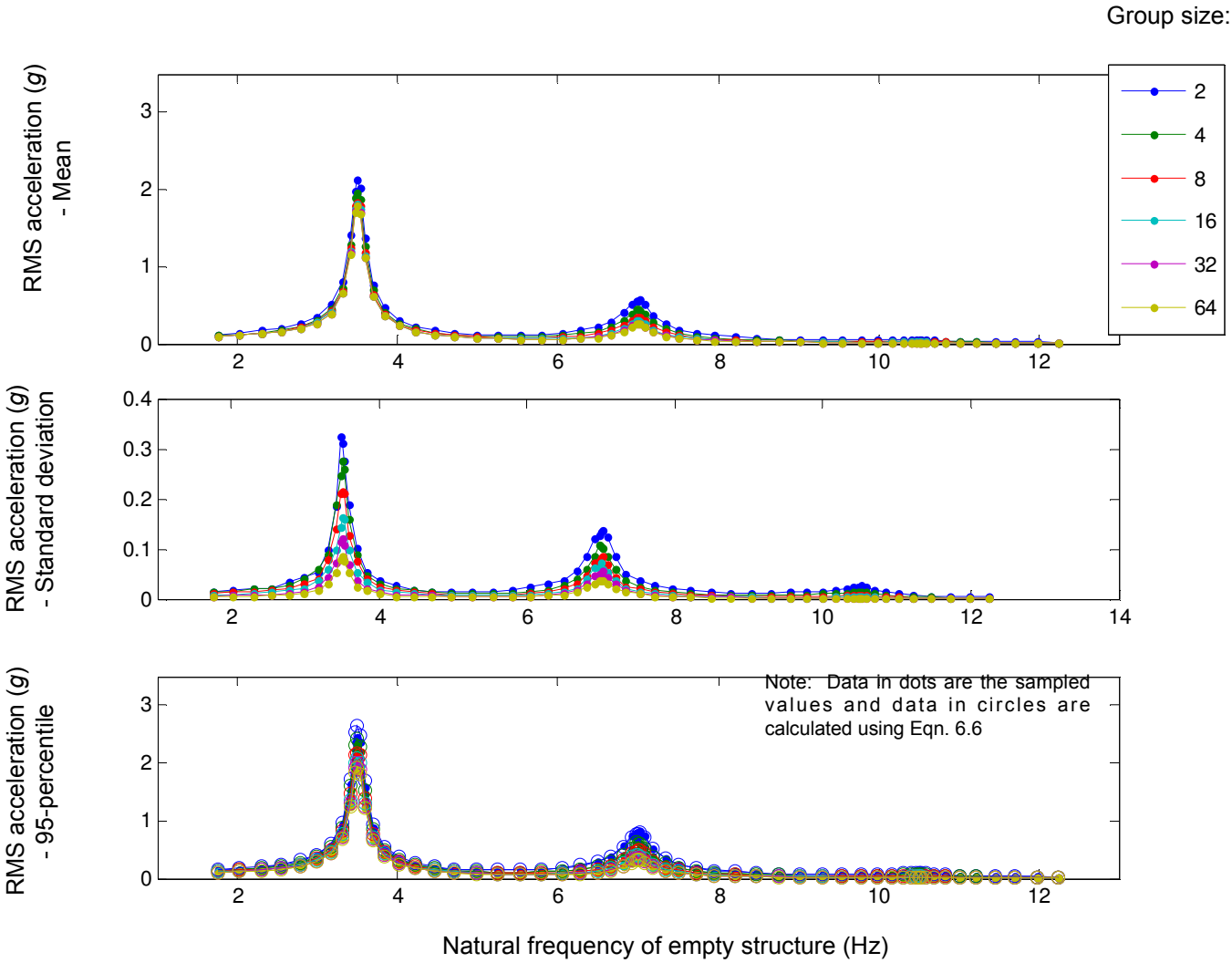

Figure C9: Variation of RMS acceleration (mean, standard deviation and 95-percentile value) with natural frequency of the structure and sample size for jumping loads at 3.5 Hz and $\gamma = 0$.

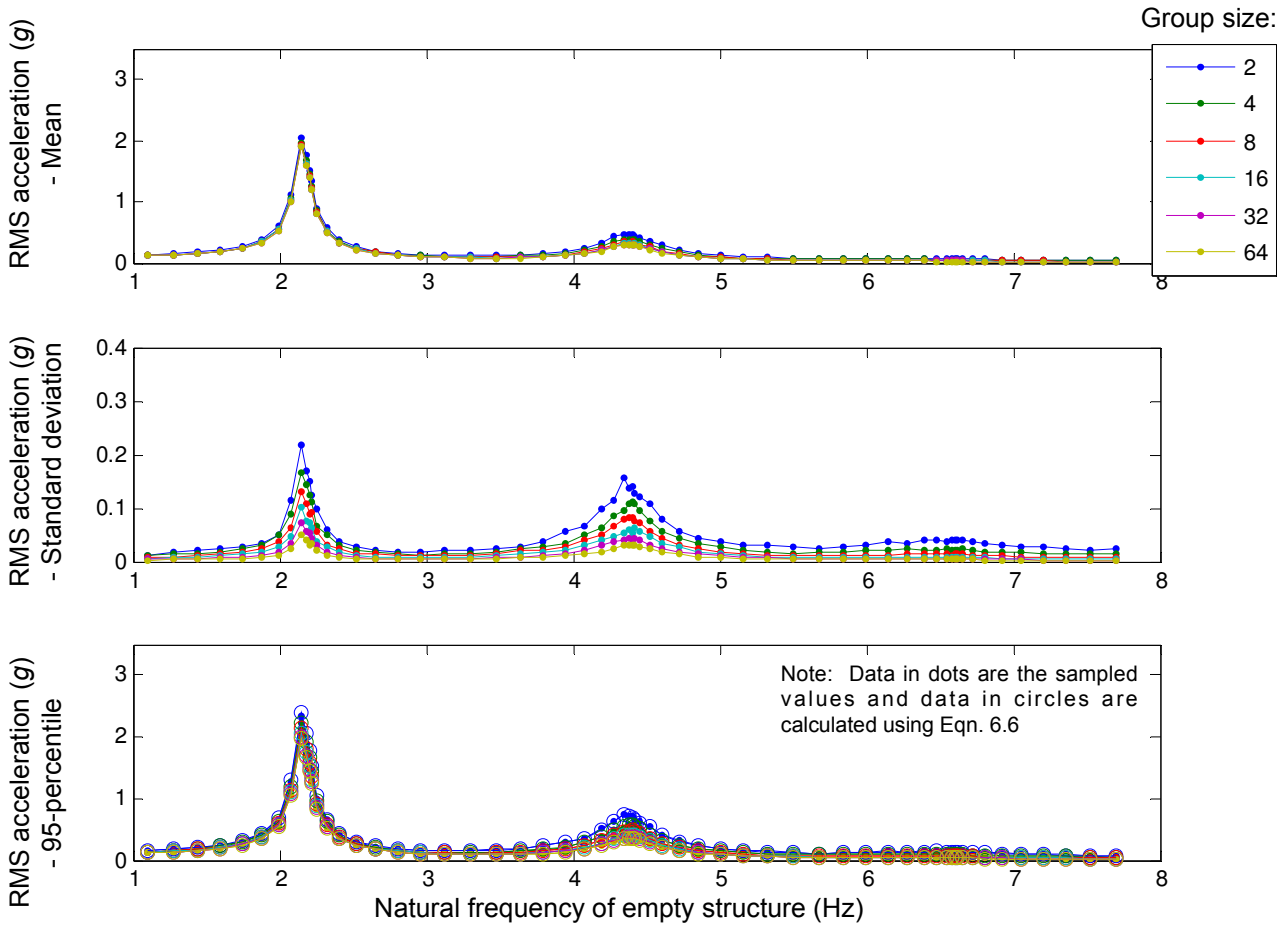

Figure C10: Variation of RMS acceleration (mean, standard deviation and 95-percentile value) fwith natural frequency of the structure and sample size or jumping loads at 2 Hz and $\gamma = 0.15$.

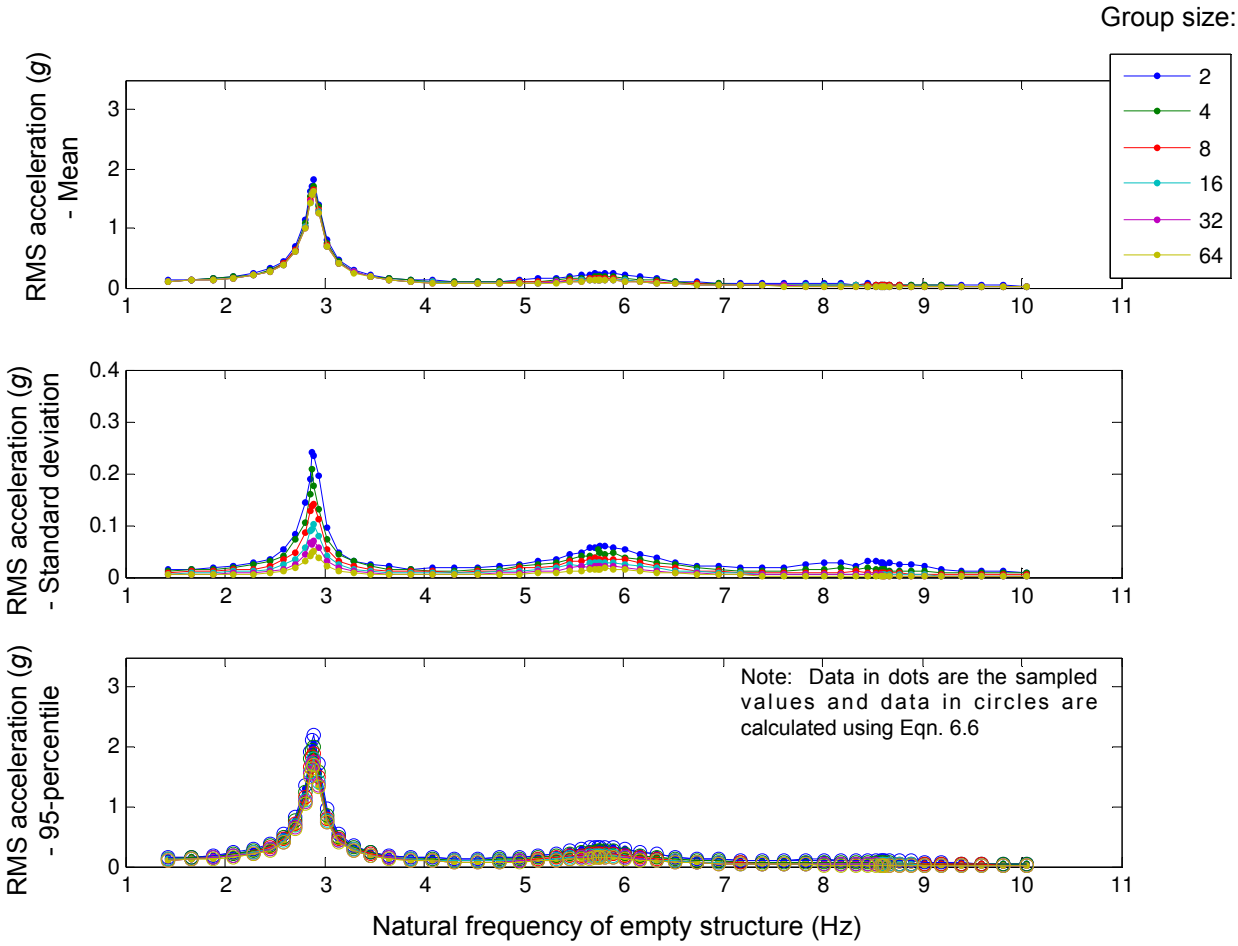

Figure C11: Variation of RMS acceleration (mean, standard deviation and 95-percentile value) with natural frequency of the structure and sample size for jumping loads at 2.67 Hz and $\gamma = 0.15$.

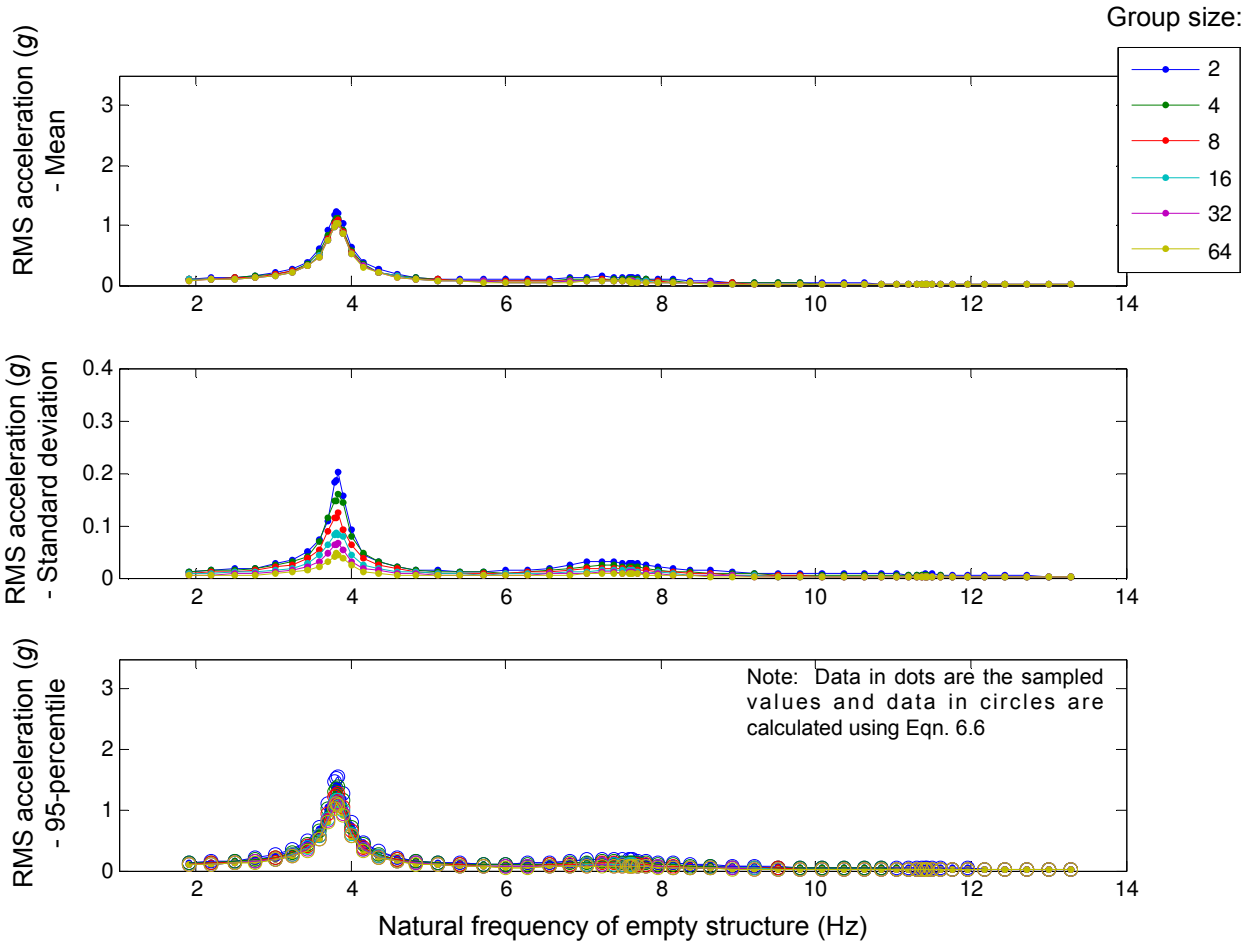

Figure C12: Variation of RMS acceleration (mean, standard deviation and 95-percentile value) with natural frequency of the structure and sample size for jumping loads at 3.5 Hz and $\gamma = 0.15$.